

2009-03-06

Thermodynamic and Kinetic Investigation of Reactions of Low-Valent Group 6 Complexes with N-Donor Ligands

George Charles Fortman
University of Miami, gcfortman@yahoo.com

Follow this and additional works at: https://scholarlyrepository.miami.edu/oa_dissertations

Recommended Citation

Fortman, George Charles, "Thermodynamic and Kinetic Investigation of Reactions of Low-Valent Group 6 Complexes with N-Donor Ligands" (2009). *Open Access Dissertations*. 198.
https://scholarlyrepository.miami.edu/oa_dissertations/198

This Open access is brought to you for free and open access by the Electronic Theses and Dissertations at Scholarly Repository. It has been accepted for inclusion in Open Access Dissertations by an authorized administrator of Scholarly Repository. For more information, please contact repository.library@miami.edu.

UNIVERSITY OF MIAMI

THERMODYNAMIC AND KINETIC INVESTIGATION OF REACTIONS OF LOW-
VALENT GROUP 6 COMPLEXES WITH N-DONOR LIGANDS

By

George C. Fortman

A DISSERTATION

Submitted to the Faculty
of the University of Miami
in partial fulfillment of the requirements for
the degree of Doctor of Philosophy

Coral Gables, Florida

May 2009

©2009
George C. Fortman
All Rights Reserved

UNIVERSITY OF MIAMI

A dissertation submitted in partial fulfillment of
the requirements for the degree of
Doctor of Philosophy

THERMODYNAMIC AND KINETIC INVESTIGATION OF REACTIONS OF LOW-
VALENT GROUP 6 COMPLEXES WITH N-DONOR LIGANDS

George C. Fortman

Approved:

Carl D. Hoff, Ph.D.
Professor of Chemistry

Terri A. Scandura, Ph.D.
Dean of the Graduate School

Angel Kaifer, Ph.D.
Professor of Chemistry

Burjor Captain, Ph.D.
Professor of Chemistry

Steven P. Nolan, Ph.D.
Professor of Chemistry
University of St. Andrews

FORTMAN, GEORGE C.

(Ph.D., Chemistry)

Thermodynamic and Kinetic Investigation
of Reactions of Low-Valent Group 6 Complexes
with N-donor Ligands

(May 2009)

Abstract of a dissertation at the University of Miami.

Dissertation supervised by Professor Carl D. Hoff.

No. of pages in text. (157)

The reactivities of several electron rich, low-valent group 6 complexes with a series of N-donor ligands were explored in order to gain information about the nature of M-N binding. Reactions of trimethylsilyl diazomethane ($\text{N}=\text{N}=\text{CHSiMe}_3$) and 1-adamantyl azide ($\text{N}=\text{N}=\text{N}-\text{Ad}$) with the organometallic complexes $[\text{Cr}(\text{CO})_3(\text{C}_5\text{R}_5)]_2$ ($\text{R} = \text{H}, \text{Me}$) and $\text{HMo}(\text{CO})_3(\text{C}_5\text{R}_5)$ ($\text{R} = \text{H}, \text{CH}_3$) were studied from both a kinetic and thermodynamic aspect. Ultimately, this information was used to propose plausible mechanisms by which the reactions take place. Furthermore, reactions of $\text{M}(\text{P}^i\text{Pr}_3)_2(\text{CO})_3$ ($\text{M} = \text{Mo}, \text{W}$; $^i\text{Pr} = \text{isopropyl}$) with N_2 , trimethylsilyl diazomethane, 1-adamantyl azide, a series of nitriles, and a choice group of N-heterocyclic compounds were studied. The use of the coordinatively unsaturated but sterically hindered $\text{M}(\text{P}^i\text{Pr}_3)_2(\text{CO})_3$ complex was used to evaluate the importance of σ and π bonding in these complexes.

Acknowledgements

Most importantly, I would like to thank my family for making this possible. Without their constant support there is no way that I would be where I am today. My parents (Sue and Bruce) have encouraged me to get to this point from day one. Just as importantly, I would like to thank Carl Hoff. I consider myself very lucky to have had the opportunity to have been taught by a man who possesses such a seemingly infinite knowledge of chemistry and boundless amount of ingenuity. There were many times that I can remember talking to Carl about an experiment and thinking to myself, “You want to measure what!? Good luck my friend.” And after all the duct tape and JB Weld not only were his creations adequate, they typically surpassed all expectation. So the only thing I think I can say at this point is that the Old Man’s still got it! I consider it a true honor to be his “scientific son.”

I would also like to thank the people that I have shared the lab with during my time at UM: Eric McDonough, Derek Isrow, Manuel Temprado and Cai Xiaochen. Furthermore, I would like to thank the numerous collaborators that have helped make this work possible. This is especially true of Burjor Captain. I am very appreciative of hours of time he has spent on many of the crystal structures that were part of my various research projects. Other collaborators whom I have had the pleasure to work with include Bruce King, Tamas Kégl, Ferenc Ungváry Etsuko Fujita, James Muckerman, Quian-Shu Li, Xiuhui Zhang, Paul von Ragué Schleyer, Henry Schaefer, Joshua Telsler, Brian Scott and their respective research groups.

Finally I would like to thank the University of Miami for its financial support and such a wonderful graduate experience.

TABLE OF CONTENTS

	Page
LIST OF FIGURES	vi
LIST OF SCHEMES.....	xi
LIST OF TABLES.....	xiii
 CHAPTER 1: The Organometallic Chemistry of Diazos, Azides and Nitrile Ligands.	
1.1 Introduction	1
1.2 Diazo Chemistry	2
1.3 Nitrile Chemistry	4
1.4 Azide Chemistry	6
1.5 Statement of Purpose	8
 CHAPTER 2: Spectroscopic Detection and Theoretical Confirmation of the Role of $\text{Cr}_2(\text{CO})_5(\text{C}_5\text{R}_5)_2$ and $\bullet\text{Cr}(\text{CO})_2(\eta^2\text{-OCCHSiMe}_3)(\text{C}_5\text{R}_5)$ as Intermediates in Carbonylation of $\text{N}_2\text{CHSiMe}_3$ to OCCHSiMe_3 by $\bullet\text{Cr}(\text{CO})_3(\text{C}_5\text{R}_5)$ ($\text{R} = \text{H}, \text{CH}_3$).	
2.1 Background.....	9
2.2 Results and Discussion	10
2.3 Conclusions.....	33
2.4 Experimental.....	34
 CHAPTER 3: Kinetic and Thermodynamic Studies of the Reactivity of Trimethylsilyldiazomethane with $\text{HMo}(\text{CO})_3(\text{C}_5\text{R}_5)$ ($\text{R} = \text{H}, \text{Me}$).	
3.1 Background.....	41

3.2 Results and Discussion	45
3.3 Conclusions.....	66
3.4 Experimental.....	67
CHAPTER 4: Experimental and Computational Studies of Enthalpies of Binding of Dinitrogen, Nitriles, Azides, Diazoalkanes, Pyridine and Pyrazines to Mo(PⁱPr₃)₂(CO)₃.	
4.1 Background.....	75
4.2 Results.....	76
4.3 Discussion.....	87
4.4 Conclusions.....	103
4.5 Experimental.....	104
CHAPTER 5: Conversion of 1- Adamantyl Azide to 1-Adamantyl Isocyanate by [Cr(CO)₃Cp]₂, Hydrogenation to 1-Adamantyl Amine by HMo(CO)₃Cp and Reaction with Mo(CO)₃(PⁱPr₃)₂ to Form Mo(κ²-ⁱPr₃P=N-N=N-Ad)(CO)₃(PⁱPr₃).	
5.1 Background.....	112
5.2 Results and Discussion	112
5.3 Conclusions.....	123
5.4 Experimental.....	123
APPENDIX A: Supporting Information for Chapter 2.....	128
APPENDIX B: Supporting Information for Chapter 3.....	132
APPENDIX C: Supporting Information for Chapter 4.....	135
APPENDIX D: Supporting Information for Chapter 5.....	144
REFERENCES.....	147

LIST OF FIGURES

CHAPTER 1

Figure 1.1	Resonance structures of diazo compounds.	3
Figure 1.2	Resonance structures of azides.	7

CHAPTER 2

Figure 2.1	FTIR spectral data during initial stage of the reaction of $\bullet\text{Cr}(\text{CO})_3\text{Cp}^*$ with $\text{N}_2\text{CHSiMe}_3$ at 25 °C in toluene under an argon atmosphere.	13
Figure 2.2	FTIR spectral data during second stage of the reaction of $\bullet\text{Cr}(\text{CO})_3\text{Cp}^*$ with $\text{N}_2\text{CHSiMe}_3$ at 25 °C in toluene under an argon atmosphere.	13
Figure 2.3	Absorbance versus time plots for key species in reaction of $\bullet\text{Cr}(\text{CO})_3(\text{C}_5\text{Me}_5)$ with $\text{N}_2\text{CHSiMe}_3$ at 25°C in toluene under Ar and CO at 1.6 atm of pressure.	15
Figure 2.4.	(a) Natural Abundance ESR Spectra of the ESR active intermediate $\bullet\text{Cr}(\text{ketene})(\text{CO})_2(\text{C}_5\text{Me}_5)$ (b) Stacked plot of integrated ESR data showing growth and decay of EPR signal during reaction of $\bullet\text{Cr}(\text{CO})_3(\text{C}_5\text{Me}_5)$ and $\text{N}_2\text{CHSiMe}_3$	18
Figure 2.5	Intensity of EPR signals of $\bullet\text{Cr}(\text{CO})_2(\eta^2\text{-O=C=CHSiMe}_3)(\text{C}_5\text{R}_5)$ for R = H (Cp) and R = CH ₃ (Cp*).	19
Figure 2.6	Experimental and simulated room temperature X-band (9.807 GHz) ESR spectra for $\bullet\text{Cr}(\text{}^{13}\text{CO})_2(\eta^2\text{-O=C}^{13}\text{=CHSiMe}_3)(\text{C}_5\text{Me}_5)$	19
Figure 2.7	FTIR spectral data during initial stage of reaction of $\bullet\text{Cr}(\text{CO})_3\text{Cp}$ with $\text{N}_2\text{CHSiMe}_3$ at 25 °C in toluene under an argon atmosphere.	22
Figure 2.8	Drawing of the calculated SOMO for $\bullet\text{Cr}(\text{CO})_2(\text{N}_2\text{CH}_2)(\text{C}_5\text{H}_5)$	28
Figure 2.9	Calculated structure of $(\text{C}_5\text{H}_5)(\text{CO})_2\text{Cr-N}\equiv\text{N-CH}_2\text{-Cr}(\text{C}_5\text{H}_5)(\text{CO})_3$	29
Figure 2.10	Computed transition state for step 5-ii in the mechanism in Scheme 2.1.	30

Figure 2.11	Calculated minimum energy structures for C,C and C,O bonded tautomers of $\bullet\text{Cr}(\text{CO})_2(\eta^2\text{-O=C=CH}_2)(\text{C}_5\text{H}_5)$	32
-------------	--	----

CHAPTER 3

Figure 3.1	First order plots of $\ln(A-A_{\text{inf}})$ versus time for the reaction of $\text{HMo}(\text{CO})_3\text{Cp}$ (0.01 M) with $\text{N}_2\text{CHSiMe}_3$ (0.056 M) in heptane, toluene, and THF at 0°C	48
Figure 3.2	Rates of reaction of HMp (0.0057M) and DMp with $\text{N}_2\text{CHSiMe}_3$, (isotopic enrichment $85 \pm 10\%$) at 286 K and 301 K in heptane showing nearly identical rates of reaction.	49
Figure 3.3	Typical sequential FTIR spectra for the reaction of $\text{Mo}(\text{CO})_3\text{Cp}$ with $\text{N}_2\text{CHSiMe}_3$. Reaction was carried out in heptane at 273 K.....	51
Figure 3.4	Enhanced view of FTIR spectral changes due to the increase of the alkyl side product $\text{Mo}(\text{CHSiMe}_3)(\text{CO})_3\text{Cp}$ and the decay of the intermediate complex.....	52
Figure 3.5	Plot of Absorbance at 2017 cm^{-1} of proposed intermediate versus Absorbance at 2030 cm^{-1} of $\text{HMo}(\text{CO})_3\text{Cp}$ for data in Figure 3.3 showing approximate linear relationship between these two bands over the reaction time.	52
Figure 3.6	ORTEP drawing of $\text{W}(\text{CO})_2(\text{N}_2\text{CH}_2\text{SiMe}_3)\text{Cp}$ with ellipsoids at 35% probability.....	54
Figure 3.7	Computed structure of $\text{Mo}(\text{CO})_2(\text{N}_2\text{CH}_2\text{SiMe}_3)\text{Cp}$ and $\text{W}(\text{CO})_2(\text{N}_2\text{CH}_2\text{SiMe}_3)\text{Cp}$	54
Figure 3.8	Theoretically calculated structure for the intermediate containing a loose Mo-N bond following the initial proton transfer.....	57

CHAPTER 4

Figure 4.1	Van't Hoff plot for the formation of $\text{Mo}(\text{P}^i\text{Pr}_3)_2(\text{CO})_3(\text{C}_4\text{H}_4\text{N}_2)$	78
Figure 4.2	Van't Hoff plot for the binding of N_2 to $\text{Mo}(\text{P}^i\text{Pr}_3)_2(\text{CO})_3$	79

Figure 4.3	Colors of the Mo(P^iPr_3) ₂ (CO) ₃ (RCN) complexes studied (R = Ad; 4-NMe ₂ C ₆ H ₄ ; 2,4,6-Me ₃ C ₆ H ₂ ; C ₆ H ₅ ; 2,6-F ₂ C ₆ H ₃ ; 4-CF ₃ C ₆ H ₄ ; F ₅ C ₆).....	81
Figure 4.4	ORTEP diagram of W(P^iPr_3) ₂ (CO) ₃ (NCNMe ₂) showing 35 % probability thermal ellipsoids.	83
Figure 4.5	ORTEP diagram of W(P^iPr_3) ₂ (CO) ₃ (2,6-Me ₂ C ₄ H ₂ N ₂) showing 35 % probability thermal ellipsoids.	84
Figure 4.6	ORTEP diagram of W(P^iPr_3) ₂ (CO) ₃ (2,4,6-Me ₃ C ₆ H ₂ CN) showing 35 % probability thermal ellipsoids.	84
Figure 4.7	Plot of calculated vs. experimental N-binding enthalpies.	88
Figure 4.8	Solution phase binding to Mo(P^iPr_3) ₂ (CO) ₃ measured in the present work vs. literature gas phase proton affinities.	89
Figure 4.9	Ligand substitution viewed as carbene transfer	91

CHAPTER 5

Figure 5.1	FTIR of first phase of the reaction of [Cr(CO) ₃ Cp] ₂ with N ₃ Ad in toluene under an Ar atmosphere.....	113
Figure 5.2	FTIR of second phase of the reaction of [Cr(CO) ₃ Cp] ₂ with N ₃ Ad in toluene under an Ar atmosphere.....	114
Figure 5.3	FTIR of the reaction of [Cr(CO) ₃ Cp] ₂ with N ₃ Ad in toluene under a CO atmosphere.....	114
Figure 5.4	Sequential ESR (approximately every 50 seconds) of reaction of [Cr(CO) ₃ Cp] ₂ with N ₃ Ad.	115
Figure 5.5	ESR of the paramagnetic intermediate involved in the reaction of N ₃ Ad with [Cr(¹³ CO) ₃ Cp] ₂	116
Figure 5.6	ORTEP diagram of (λ^2 - ⁱ Pr ₃ PN ₃ Ad)Mo(P^iPr_3) ₂ (CO) ₃ with ellipsoids drawn at 35% probability	120
Figure 5.7	FTIR of the reaction of Mo(P^iPr_3) ₂ (CO) ₃ with ⁱ Pr ₃ P=N ₃ -Ad under an atmosphere of 1.7 atm N ₂ in toluene at 295 K.....	121

Appendix A

Figure A.1	Drawing of the calculated SOMO for $\bullet\text{Cr}(\text{CO})_2(\text{NNCH}_2)(\text{C}_5\text{H}_5)$ and (b) $\bullet\text{Cr}(\text{CO})_3(\text{C}_5\text{H}_5)$	128
Figure A.2	Reaction of $\bullet\text{Cr}({}^{13}\text{CO})_3(\text{C}_5\text{Me}_5)$ and $\text{N}_2\text{CHSiMe}_3$ run under conditions comparable to those shown in Figures 2.1 and 2.2 for $\bullet\text{Cr}({}^{12}\text{CO})_3(\text{C}_5\text{Me}_5)$ and $\text{N}_2\text{CHSiMe}_3$	128
Figure A.3	Spectra run in phase two of reaction shown in Figure 2.7 of text.	129
Figure A.4	Normalized spectra showing product distribution of intermediate complex as a function of CO pressure	129
Figure A.5	Kinetic plots as a function of time for decay of $\text{Cp}_2\text{Cr}_2(\text{CO})_5$, showing first order rate constants of 0.0011 s^{-1} at 15°C , 0.0069 s^{-1} at 25°C , and 0.0158 s^{-1} at 35°C	130
Figure A.6	${}^1\text{H}$ NMR showing growth of signal due to $\text{Cr}_2(\text{CO})_4\text{Cp}_2$ "from nowhere" due to absence of an NMR signal due to $\text{Cr}_2(\text{CO})_5\text{Cp}_2$	130

Appendix B

Figure B.1	Eyring plot for the reaction of $\text{HMo}(\text{CO})_3\text{Cp}$ with $\text{N}_2\text{CHSiMe}_3$ in heptane	132
Figure B.2	${}^1\text{H}$ NMR data showing peaks near 2.92 ppm assigned to $\text{Mo}(\text{CO})_2(\text{N}_2\text{C}(\text{H})_2\text{SiMe}_3)\text{Cp}$ and at 2.90 ppm assigned to $\text{Mo}(\text{CO})_2(\text{N}_2\text{C}(\text{H})\text{DSiMe}_3)\text{Cp}$	132

Appendix C

Figure C.1	Variable temperature FTIR data on reaction of $\text{Mo}(\text{P}^i\text{Pr}_3)_2(\text{CO})_3 + \text{N}_2 \rightarrow \text{Mo}(\text{P}^i\text{Pr}_3)_2(\text{CO})_3(\text{N}_2)$	135
Figure C.2	Variable temperature FTIR data on reaction $(\mu\text{-C}_4\text{H}_4\text{N}_2)[\text{Mo}(\text{P}^i\text{Pr}_3)_2(\text{CO})_3]_2 + \text{pyrazine} \rightarrow 2(\text{C}_4\text{H}_4\text{N}_2)\text{Mo}(\text{P}^i\text{Pr}_3)_2(\text{CO})_3$	135
Figure C.3	ORTEP diagram of $\text{Mo}(\text{P}^i\text{Pr}_3)_2(\text{CO})_3(\text{CNAd})$ showing 35 % probability thermal ellipsoids	136

Figure C.4	ORTEP diagram of $W(P^iPr_3)_2(CO)_3(CNAd)$ showing 35 % probability thermal ellipsoids	136
Figure C.5	ORTEP diagram of $Mo(P^iPr_3)_2(CO)_3(NCAd)$ showing 35 % probability thermal ellipsoids	137
Figure C.6	ORTEP diagram of $W(P^iPr_3)_2(CO)_3(NCAd)$ showing 35 % probability thermal ellipsoids	137
Figure C.7	ORTEP diagram of $W(P^iPr_3)_2(CO)_3(2,6-F_2C_6H_2CN)$ showing 35 % probability thermal ellipsoids	138
Figure C.8	TD-DFT calculated HOMO and LUMO orbitals of $Mo(P^iPr_3)_2(CO)_3$	139
 Appendix D		
Figure D.1	Comparison of the reaction of the consumption of $[Cr(CO)_3Cp]_2$ in the reaction with N_3Ad under CO and Ar Atmospheres	144
Figure D.2	ORTEP diagram of Cy_3PN_3Ad showing 35% probability thermal ellipsoids	144

LIST OF SCHEMES

CHAPTER 2

- Scheme 2.1 Proposed Reaction Scheme for reaction of $\bullet\text{Cr}(\text{CO})_3(\text{C}_5\text{R}_5)$
(R = Me, H) with $\text{N}_2\text{CHSiMe}_3$ 27

CHAPTER 3

- Scheme 3.1 CO insertion into the Mo-CH₃ bond..... 43
- Scheme 3.2 N₂ insertion into the Mo-CH₃ bond..... 44
- Scheme 3.3 Proposed mechanism for the reaction of $\text{HMo}(\text{CO})\text{Cp}$
with $\text{N}_2\text{CHSiMe}_3$ producing diazo, alkyl, and metal-metal dimer
products..... 56
- Scheme 3.4 Thermochemical cycle used to calculate the enthalpy of the
homolytic bond formation between $\bullet\text{Mo}(\text{CO})_3\text{Cp}$ and
 $\bullet\text{N}_2\text{CHSiMe}_3$ 60
- Scheme 3.5 Thermochemical cycle used to estimate the enthalpy of insertion
of molecular nitrogen into the Mo-R bond of $\text{Mo}(\text{CO})_3(\text{CH}_3)\text{Cp}$ 61
- Scheme 3.6 Computed energies {B3LYP/6-311+G**} relevant to
thermochemical cycle for hydrogenation of $\text{N}_2\text{CHSiMe}_3$ 64
- Scheme 3.7 Proposed steps in catalytic hydrogenation of $\text{N}_2\text{CHSiMe}_3$ by
 $\text{HMo}(\text{CO})_3\text{Cp}$ in the presence of $\text{Mo}(\text{CO})_3(\text{P}^i\text{Pr}_3)_2$ 65

CHAPTER 4

- Scheme 4.1 Thermodynamic cycle determining the enthalpy of dissociation
of $\mu\text{-(N}_2\text{C}_4\text{H}_4\text{)[Mo(P}^i\text{Pr}_3)_2(\text{CO})_3]_2$ to $\text{Mo(P}^i\text{Pr}_3)_2(\text{CO})_3(\text{N}_2\text{C}_4\text{H}_4)$ +
 $\text{Mo(P}^i\text{Pr}_3)_2(\text{CO})_3$ in toluene solution..... 78
- Scheme 4.2 Thermodynamic cycle determining the enthalpy of dissociation of
 $\mu\text{-(N}_2\text{)[Mo(P}^i\text{Pr}_3)_2(\text{CO})_3]_2$ to $\text{Mo(P}^i\text{Pr}_3)_2(\text{CO})_3(\text{N}_2)$ + $\text{Mo(P}^i\text{Pr}_3)_2(\text{CO})_3$
in toluene solution..... 80

CHAPTER 5

Scheme 5.1	Proposed initial phase of reaction of $\bullet\text{Cr}(\text{CO})_3\text{Cp}$ with N_3Ad	117
Scheme 5.2	Proposed mechanism for formation of the κ^2 -phosphazide ligand....	122

LIST OF TABLES

CHAPTER 3

Table 3.1	Relative product distribution based on solvent for the reaction of $\text{HMo}(\text{CO})_3\text{Cp}$ with $\text{N}_2\text{CHSiMe}_3$	46
Table 3.2	Rate constants for reaction of metal hydrides and trimethylsilyldiazomethane.....	48

CHAPTER 4

Table 4.1	Binding enthalpies of ligands determined by means of ligand displacement by AdNC (eqn 4.2).....	77
Table 4.2	Binding enthalpies determined by reaction of $\text{Mo}(\text{P}^i\text{Pr}_3)_2(\text{CO})_3(\text{AdCN})$ with benzonitriles	81
Table 4.3	Selected bond distances from X-ray crystal structures and theoretically calculated structures of $\text{M}(\text{P}^i\text{Pr}_3)_2(\text{CO})_3\text{L}$	85
Table 4.4	Selected bond angles from X-ray crystal structures and theoretically calculated structures of $\text{M}(\text{P}^i\text{Pr}_3)_2(\text{CO})_3\text{L}$	86
Table 4.5	Computed and experimental binding enthalpies of NNX ligands in toluene solution.....	90
Table 4.6	Experimental stretching frequencies of Mo-NNX complexes in toluene solution.....	91
Table 4.7	Experimental and computed binding enthalpies of NCR ligands in toluene solution.....	93
Table 4.8	Experimental (UV-vis and FTIR) data on nitrile complexes.....	93
Table 4.9	Computed and experimental binding enthalpies of pyrazine-like ligands in toluene solution	96
Table 4.10	Experimental ν_{CO} stretching frequencies of N-heterocyclic complexes, in toluene solution.....	97
Table 4.11	Experimental and computational enthalpies of binding of N-donor ligands to $\text{Mo}(\text{P}^i\text{Pr}_3)(\text{CO})_3$ (in toluene) and experimental heats of binding for N-donor ligands to $[\text{Ru}(\text{NH}_3)_5(\text{H}_2\text{O})]^{2+}$ in aqueous solution.....	101

CHAPTER 5

Table 5.1	Selected bond length and angles for the single crystal x-ray structure of (κ^2 - i -Pr ₃ PN ₃ Ad)Mo(P ^{<i>i</i>} Pr ₃) ₂ (CO) ₃	119
-----------	--	-----

Appendix A

Table A.1	FTIR data for selected compounds and intermediates in toluene solution.....	131
-----------	---	-----

Appendix B

Table B.1	Infrared data for complexes in different solvents	133
Table B.2	Crystal data and structure refinement for CpW(CO) ₂ (N ₂ CHSiMe ₃)	134

Appendix C

Table C.1	Table of experimentally and theoretically determined ΔH of binding to Mo(P ^{<i>i</i>} Pr ₃) ₂ (CO) ₃	140
Table C.2	Computed and experimental λ_{\max} of bound benzonitriles Mo(P ^{<i>i</i>} Pr ₃) ₂ (CO) ₃ (L).....	141
Table C.3	FTIR ν_{CO} of Mo(P ^{<i>i</i>} Pr ₃) ₂ (CO) ₃ (L).....	141
Table C.4	Crystallographic data for compounds Mo(P ^{<i>i</i>} Pr ₃) ₂ (CO) ₃ (AdNC), Mo(P ^{<i>i</i>} Pr ₃) ₂ (CO) ₃ (AdCN) and W(P ^{<i>i</i>} Pr ₃) ₂ (CO) ₃ (AdNC).....	142
Table C.5	Crystallographic data for compounds W(P ^{<i>i</i>} Pr ₃) ₂ (CO) ₃ (2,6-(CH ₃) ₂ C ₄ H ₂ N ₂), W(P ^{<i>i</i>} Pr ₃) ₂ (CO) ₃ (2,4,6-(CH ₃) ₃ C ₆ H ₂ CN) and W(P ^{<i>i</i>} Pr ₃) ₂ (CO) ₃ (2,6-F ₂ C ₆ H ₂ CN).....	143

Appendix D

Table D.1	Identifying FTIR ν_{CO} stretches for species studied	145
Table D.2	Crystallographic data for Mo(κ^2 - i -Pr ₃ PN ₃ Ad) (CO) ₃ (P ^{<i>i</i>} Pr ₃).....	146

CHAPTER 1: The Organometallic Chemistry of Diazos, Azides and Nitrile Ligands.

1.1 Introduction

In spite of years of work, the factors controlling binding of N_2 , which is intrinsically inferior to CO both as a σ donor and as a π acceptor, are not fully understood. It has been concluded that:

N_2 is an exceedingly poor electron donor, even toward strong electrophiles, where it is much feebler than the weakest known ligands, e.g., CH_2Cl_2 . The complete lack of binding to $([Mn(CO)_3(PCy_3)_2][B[C_6H_3(3,5-CF_3)_2]_4])$ and other electron-poor cationic complexes indicates that N_2 apparently can only be stabilized on a metal center by a high degree of π -back-donation, even in actinide complexes.¹

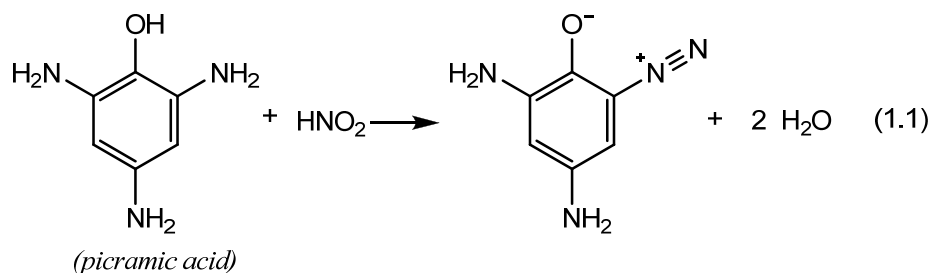
Due to the importance of N_2 binding, this thesis reports data on reactions of N_2 and “ N_2 mimics” such as nitriles, azides, and diazoalkanes with organometallic complexes to gain information about the nature of the M-NX interaction as a function of X for the complexes $[Cr(CO)_3(C_5R_5)]_2$ (R = H, Me), $HMo(CO)_3(C_5R_5)$ (R = H, CH_3) and $M(P^iPr_3)_2(CO)_3$ (M = Mo, W; iPr = isopropyl).

As with all organometallic chemistry, before understanding a reaction of a ligand with a metal complex one must possess a comprehensive knowledge of that ligand. The following sections of this chapter will first present a highlighted background of diazos, nitriles and azides not as ligands, but as stable and complete molecules in their own right. Once a familiarity with these ligands is established the discussion will then move on to

examples of some of the more prominent reactions involving metal complexes and these aforementioned “N₂ mimics.”

1.2 Diazo Chemistry

The chemistry of diazo (N=N=CR₂) compounds has been studied for over 140 years. In 1858 Griess successfully identified and characterized the first aromatic diazo compound.² The method of synthesis employed by Griess was to pass nitrous gases, prepared by the reduction of nitric acid with starch or arsenious acid, into an alcoholic solution of picramic acid (eqn. 1.1). The chemistry started by Griess would later be expanded upon by Ilosvay. Their combined work would later be labeled as the Griess-Ilosvay’s reagent which was ultimately used analytically for the detection of nitrates after their reduction with zinc to nitrites.



The chemistry of diazos was further expanded upon by numerous chemists.³ The interest in these compounds stems predominately from how versatile they are in reactions. Diazos are susceptible to attack by nucleophiles at the terminal nitrogen,⁴ attack by electrophiles at the α carbon,⁵ loss of N₂ to form reactive carbenes,⁶ cycloaddition to multiple bonds⁷ and attack by free radicals.⁸ This plethora of reactions comes from the unsaturation of the N=N=C component of the molecule which has the resonance structures shown in Figure 1.1.

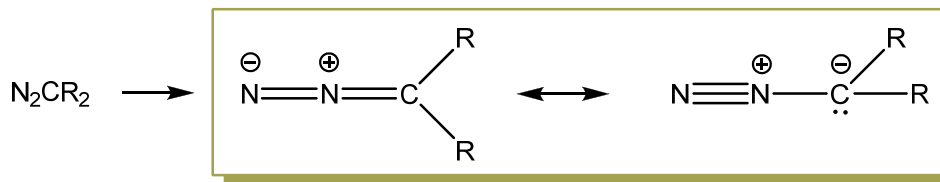
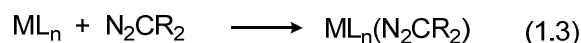
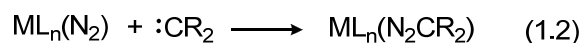
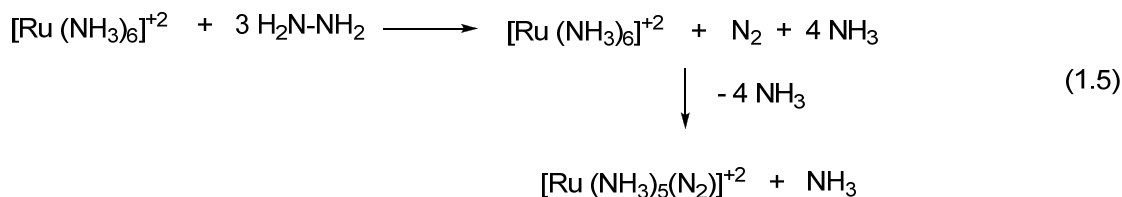
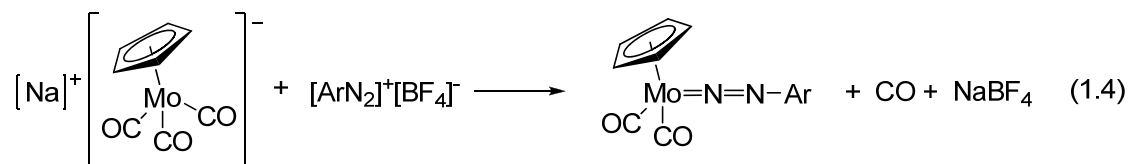


Figure 1.1. Resonance structures of diazo compounds.

Another interesting aspect of the chemistry of diazos is its various reactions with organometallic complexes. Numerous reviews have been written upon just this topic.⁹ The main interest stems from the similarities of activated bound N_2 and a bound diazo, N_2R as shown in eqns. 1.2 and 1.3.



In fact, the first bound diazo compound and the first bound molecular nitrogen compound were discovered within a very close time of one another. King and Bissett isolated¹⁰ and characterized the first arenediazonium ion containing metal complex (eqn. 1.4) and within the same year Allen and Senoff discovered¹¹ the first transition metal complex containing dinitrogen as a ligand (eqn. 1.5).



Since these discoveries scientist have continued to make nearly countless such organometallic diazo compounds. Sutton's review,^{9b} which is not meant to be comprehensive contains over 260 references, contains examples of organometallic diazo

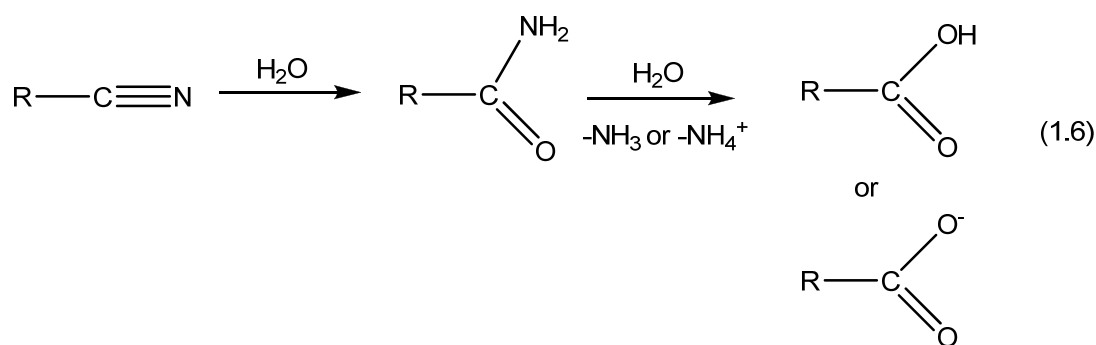
complexes of nearly all transition metals and was written over 15 years ago! Chapters 2 and Chapter 3 will add to the current reservoir of knowledge of organometallic diazo complexes by discussing the mechanism of reactions of trimethylsilyl diazomethane ($\text{N}_2\text{CHSiMe}_3$) with various group 6 metal complexes.

1.3 Nitrile Chemistry

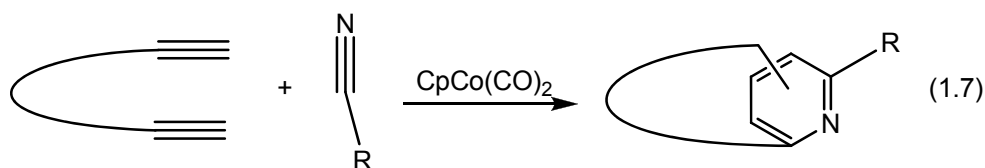
The chemistry of nitriles ($\text{N}\equiv\text{C-R}$) has long been a focal point in both industry and academia. In industry nitriles are used as solvents, in the production of plastics and in insecticides. In the laboratory, the importance of this class of compounds comes from the reactivity of the $\text{N}\equiv\text{C}$ moiety of the molecule. This triple bond serves as a site for addition of nucleophiles at the carbon, electrophiles at the nitrogen or asymmetric cycloaddition which can result in the formation of new C-C, C-N, C-O and C-S bonds.¹²

The simplest of nitriles, hydrogen cyanide was first synthesized by Scheele in 1782.¹³ Scheele was later killed while trying to isolate the anhydrous product.¹² Many significant advances were made over the next 100 plus years (including the synthesis of benzonitrile)¹⁴ but a large increase in nitriles research was seen during and after World War I.

Acid or base catalyzed hydrolysis of nitriles is a common method for the synthesis of carboxylic acids.¹⁵ The general reaction proceeds as shown in eqn. 1.6.



Unfortunately the acid/base catalysis generally leads to salt formation which can make purification of the product difficult. Aldehydes can be synthesized from nitriles by using SnCl_2 and HCl to first create an iminium salt $[\text{R}-\text{CH}=\text{NH}_2]\text{Cl}$ followed by reaction with water to form the desired $\text{RC}(=\text{O})\text{H}$.¹⁶ Nitriles can also be used in cycloaddition reactions such as the one shown in eqn. 1.7 in which bis-alkynes with nitriles were reported to under go cyclization to pyridine-cyclophanes.¹⁷



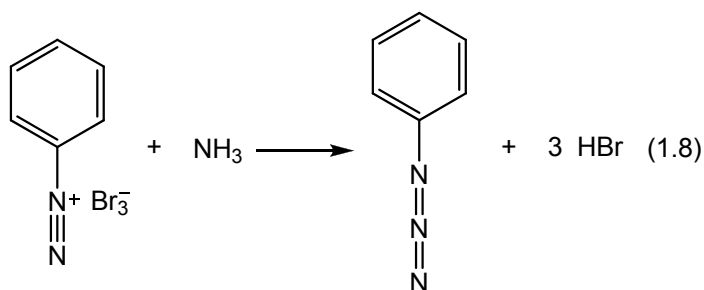
Reactions of nitriles with organometallic compounds are numerous. In synthesis, nitriles (such as acetonitrile) are commonly used as stepping stones to more complex compounds. Nitriles as ligands are usually labile due to their relatively weak σ donating and π back bonding abilities. Commonly they tend to bond low valent, electron rich metals with strong π basicities.

Also of interest is the fact that nitriles are isoelectronic with ligands such as N_2 and CO . Such similarities can be used as a probe to investigate the nature of the metal-nitrogen bond. Chapter 4 will discuss just this topic, in which a series of nitriles $\text{N}\equiv\text{CR}$

will be used to investigate the back bonding from the complex $M(\text{CO})_3\text{P}^i\text{Pr}_3$ ($M = \text{Mo}, \text{W}$) to the nitrile as a function of R.

1.4 Azide Chemistry

Similar to diazos, Peter Griess also reported the first synthesis of an azide.¹⁸ In 1864 Griess reported the synthesis of phenyl azide from the reaction of benzenediazonium perbromide with ammonia as shown in eqn. 1.8. Since their discovery azides have been used extensively in industry. Predominantly they are used for their intrinsic explosive properties such as in detonators and airbags. Biomedical applications include azidonucleosides which have been used in the treatment of HIV.¹⁹ Azides have also been used in the vulcanization of rubber, as broad spectrum herbicides, as dyes and in many other applications.²⁰



Similar to the two functionalities previously discussed, azides, being an unsaturated system, possess an incredibly diverse range of reaction possibilities.²¹ Shown in Figure 1.2 are the resonance structures that give rise to this multiplex of reactivities. Among the copious reactions of azides some of the more common include: reduction to amines;²² rearrangement of acyl azides to isocyanates (Curtius rearrangement); reaction of azides with alkenes²³ or alkynes²⁴ which leads to a 1,3 cycloaddition and the formation of a 5 membered 1,2,3 triazole (Huisgen reaction); the reaction of azides with

tertiary phosphine to form phosphazenes (Staudinger reaction),²⁵ and thermal or photochemical decomposition of azides to nitrenes.²⁶

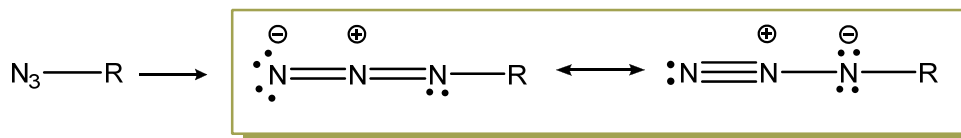
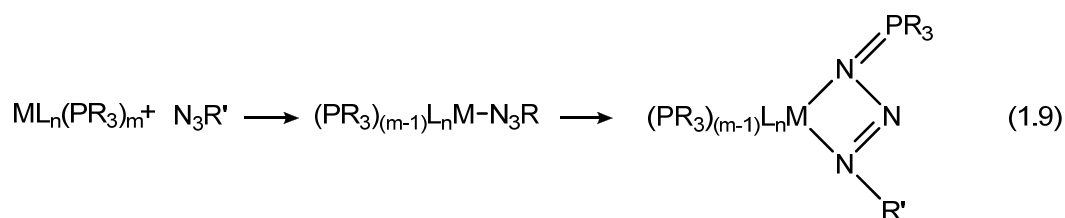


Figure 1.2. Resonance structures of azides.

Organometallic complexes with azido ligands are quite diverse. However, in contrast to both the organometallic azides and cyanides discussed previously, very few examples of terminally bound η^1 -azido complexes have been characterized crystallographically. Typically they thermally decompose via the elimination of N_2 to form the imido complex ($\text{L}_n\text{M}=\text{NR}$).²⁷ Photochemical excitation of azide organometallic compounds can result in nitrene generation or the nitrido complexes ($\text{L}_n\text{M}\equiv\text{N}$).²⁸ Also coordination of azides to metal complexes containing tertiary phosphines can result in the formation of a bound phosphazide (see eqn 1.9).²⁹



Chapter 5 will discuss the investigational results of three reactions of metal complexes with the alkyl azide, 1-adamantyl azide (N_3Ad). In the first reaction N_3Ad is hydrogenated by $\text{HMo}(\text{CO})_3\text{Cp}$ to form adamantyl amine. In the second reaction, N_3Ad and CO are catalytically transformed by $[\text{Cr}(\text{CO})_3\text{Cp}]_2$ to the isocyanate, OCNAd , and N_2 . The final reaction discussed is the reaction of $\text{Mo}(\text{CO})_3(\text{P}^i\text{Pr}_3)$ with N_3Ad in which

the azide is initially bound and slowly rearranges to a κ^2 -chelating phosphazide similar to that shown in eqn. 1.9.

1.5 Statement of Purpose

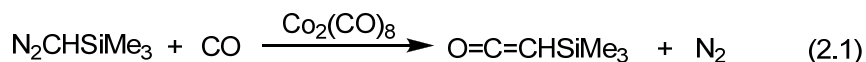
The following chapters will discuss the reaction of nitrogen donor ligands with low valent group 6 transition metal complexes. Kinetic, thermodynamic and computationalⁱ data will be presented and then utilized to construct plausible mechanisms for the reactions and/or to deduce information on the nature of the new bonds formed at the expense of the bonds broken. The goal of this work is to expand the knowledge about N-donor binding and inter-conversion of organic compounds which may be of use in the design of catalytic syntheses in the future.

ⁱ Theoretical calculations presented throughout the manuscript were performed by various collaborators. These calculations are included in this manuscript due to the fact that they assist in the conclusions presented in each chapter.

CHAPTER 2: Spectroscopic Detection and Theoretical Confirmation of the Role of $\text{Cr}_2(\text{CO})_5(\text{C}_5\text{R}_5)_2$ and $\bullet\text{Cr}(\text{CO})_2(\eta^2\text{-OCCHSiMe}_3)(\text{C}_5\text{R}_5)$ as Intermediates in Carbonylation of $\text{N}_2\text{CHSiMe}_3$ to OCCHSiMe_3 by $\bullet\text{Cr}(\text{CO})_3(\text{C}_5\text{R}_5)$ ($\text{R} = \text{H}, \text{CH}_3$).

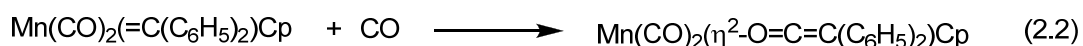
2.1 Background

The generation of ketenes ($\text{R}_2\text{C}=\text{C}=\text{O}$) is important because of their prominent role in organic synthesis.³⁰ In this connection diazoalkanes ($\text{R}_2\text{C}=\text{N}=\text{N}$) can serve as ketene sources by their thermal or photochemical reaction with CO. Ungváry and coworkers have recently shown that carbonylation of (trimethylsilyl)diazomethane is catalyzed by $\text{Co}_2(\text{CO})_8$ and selectively produces (trimethylsilyl)ketene.³¹



Such methods provide an attractive route to the *in situ* generation of ketenes. However, the mechanism of the metal catalyzed conversion of diazoalkanes to ketenes is not fully understood even though the coordination chemistry of both diazoalkanes and ketenes has been extensively investigated.³²

A number of fascinating aspects of ketene coordination chemistry have been discovered. Grotjahn and coworkers have demonstrated coordination of ketenes by both C,C- and C,O-bonding modes to *trans*- $\text{ClIr}[\text{P}(\text{iPr})_3]_2$.³³ Related Ir(I) complexes containing chelating phosphines were shown to split bound ketene ligands to CO and carbene units in reversible reactions.³⁴ Hermann and coworkers reported the synthesis and structures of η^2 -ketene complexes by slow high pressure carbonylation of metallocarbenes as shown in eqn. 2.2.³⁵



The stability of the η^2 -ketene bonding mode was indicated by the ability of such metal complexes to withstand high pressures of CO without undergoing ligand displacement.

Related η^2 -ketene complexes have also been prepared by the reaction of photogenerated $(\eta^5\text{-C}_5\text{H}_5)\text{Mn}(\text{CO})_2(\text{THF})$, $(\eta^5\text{-C}_5\text{R}'_5)\text{Mn}(\text{CO})_3$, and diazoalkanes. This surprising reaction was proposed to occur by direct transfer of a carbene to a bound carbonyl ligand.

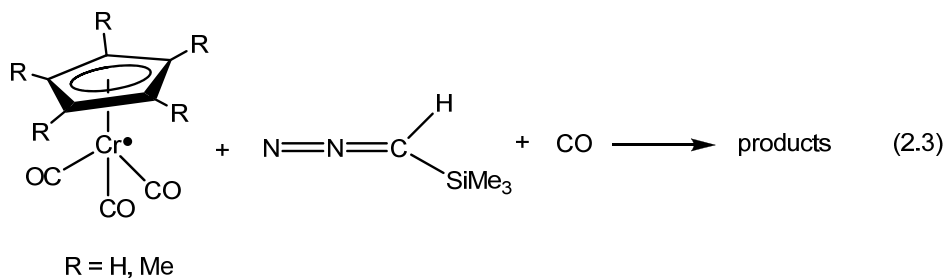
This chapter reports the investigation of eqn. 2.1 using $[\text{Cr}(\text{CO})_3(\text{C}_5\text{R}_5)]_2$ ($\text{R} = \text{H}, \text{CH}_3$) instead of $\text{Co}_2(\text{CO})_8$. Compared to Co, the Cr complexes show a greater tendency to dissociate and yield reactive monomeric $17e^-$ radical species by homolytic cleavage of the weak Cr–Cr bond.³⁶ An additional difference in the Cr system is the presence of the highly stable Cr \equiv Cr complexes $[\text{Cr}(\text{CO})_2(\text{C}_5\text{R}_5)]_2$ for which there is no known stable counterpart in cobalt carbonyl chemistry.

In recent years methods based on density functional theory (DFT) have had great impact on organotransition metal chemistry.^{37,38,39,40,41,42,43,44,45} For example, recent work on metal-metal bonded complexes of first row transition metals has yielded quantitative predictions regarding structure and stability.^{46,47,48,49} This chapter reports the convergence of theory^{ii,50} and experiment to study the mechanism of activation of a diazo compound by concerted attack of two metal radicals.

2.2 Results and Discussion

Qualitative and kinetic studies. Eqn. 2.3 presented a number of surprises as well as difficulties in its study:

ⁱⁱ Calculations were performed by three separate research groups: Tamas Kégl from the University of Pannonia; Henry F. Schaefer III, Yaoming Xie and R. Bruce King from the University of Georgia; Quian-Shu Li and Xiuhui Zhang from the Beijing Institute of Technology. (see ref. 50 for full computational details)

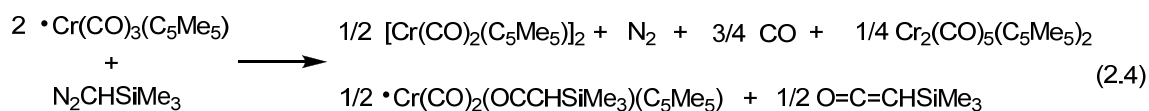


The yield and nature of the products were found to depend on the concentration of virtually every reactant and product in the equation.ⁱⁱⁱ Furthermore, the precursor complexes $[\text{Cr}(\text{CO})_3(\text{C}_5\text{R}_5)]_2$ (R = H, CH₃) dissociate to radicals to varying degrees depending on the temperature and nature of the R group. The third order rate laws often found³⁶ for $\bullet\text{Cr}(\text{CO})_3(\text{C}_5\text{Me}_5)$ also implicate a strong dependence on the absolute concentration of the metal. This section summarizes key aspects of this reaction studied under conditions designed to simplify and isolate given types of reactivity. The focus is on the reactions that occur at relatively high concentrations (typically from 1 to 20 mM) of metal complex and ratios of Cr/diazo of 2/1 and 1/1, under CO, Ar, and N₂ atmospheres.

Reaction of 2 $\bullet\text{Cr}(\text{CO})_3(\text{C}_5\text{Me}_5)$ with $\text{N}_2\text{CHSiMe}_3$ under Ar or N₂. With a 2/1 Cr/diazoalkane mole ratio under Ar or N₂, the reaction is best viewed as occurring in two

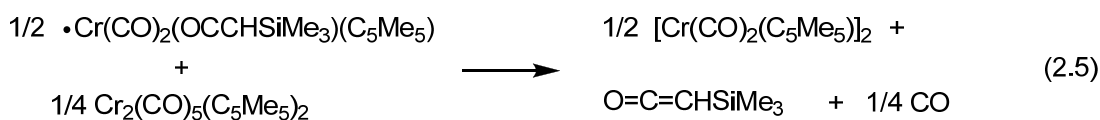
ⁱⁱⁱ Several intermediate complexes are either detected or proposed to be present in reactions studied at relatively low concentrations of diazoalkane. Attempts to extend these studies to regimes of high diazoalkane concentration produced unknown products. It seems plausible that these resulted from radical intermediates already containing a bound diazoalkane or ketene moiety reacting further with additional equivalents of free diazoalkane to produce oligomeric products. Catalytic conversion of diazoalkane to ketene could be achieved by repeated injections of small amounts of diazoalkane. However "flooding" the system with a high concentration of diazoalkane was found to produce side products of unknown and presumably oligomeric nature.

stages. The observed reactivity during "stage one"^{iv} corresponds roughly to the approximate stoichiometry shown in eqn. 2.4 below:



During this phase of the reaction (Figure 2.1) most of the chromium radical reacts and produces ketene, the Cr≡Cr triple bonded product $[\text{Cr}(\text{CO})_2(\text{C}_5\text{Me}_5)]_2$ as well as intermediate products. Infrared bands assigned to the two proposed intermediate complexes $\cdot\text{Cr}(\text{CO})_2(\text{OCCHSiMe}_3)(\text{C}_5\text{Me}_5)$ and $\text{Cr}_2(\text{CO})_5(\text{C}_5\text{Me}_5)_2$ are observed to increase during this first stage of the reaction.

During the second stage of the reaction, bands assigned to the two intermediate complexes are observed to decay according to the approximate stoichiometry shown in eqn. 2.5:



Spectroscopic data during the later stage of reaction is shown in Figure 2.2. During this time the bands assigned to intermediates have reached a maximum and begin to decay liberating additional ketene and producing additional triple bonded product. The clean nature of the reaction under these conditions is shown by the presence of an isobestic point clearly visible at approximately 1810 cm^{-1} (see Figure 2.2.) The fact that a significant amount of free ketene is liberated during this phase, in spite of low levels of

^{iv} Separation of the reaction into two phases is somewhat artificial and is meant to show the qualitative nature of the two periods. In the first phase intermediates build up and in the second they decay. In terms of reaction kinetics there is of course one continuous process, and particularly in the middle where the "two phases" overlap there is no clear distinction. Nevertheless the very beginning and ending parts of the reaction approach the limiting stoichiometries discussed.

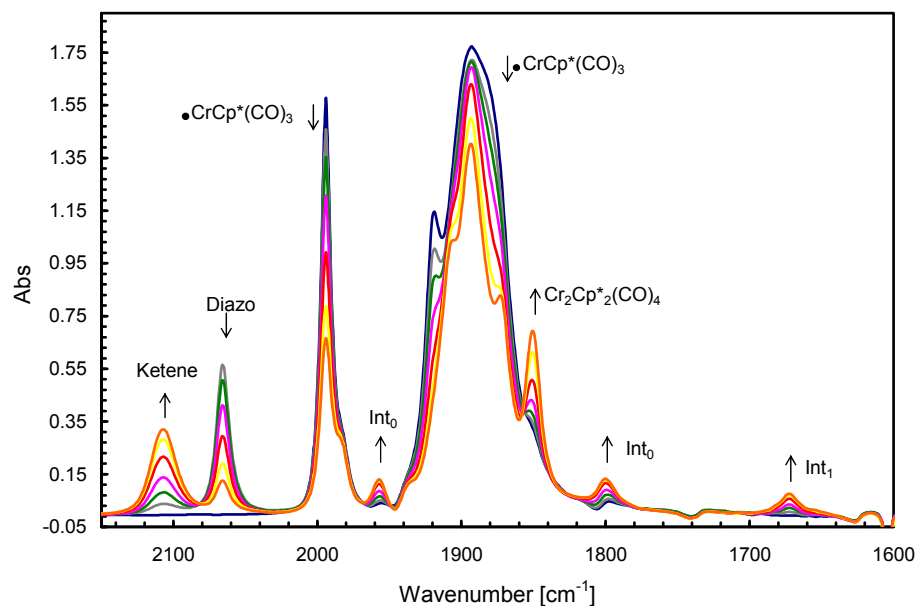


Figure 2.1. FTIR spectral data during initial stage of the reaction of $\bullet\text{Cr}(\text{CO})_3\text{Cp}^*$ (≈ 0.033 M) with $\text{N}_2\text{CHSiMe}_3$ (≈ 0.0165 M) at 25°C in toluene under an argon atmosphere. Bands assigned to $\text{int}_0 = \text{Cr}_2(\text{CO})_5(\text{C}_5\text{Me}_5)_2$ are at 1957, 1894, 1799 cm^{-1} and bands assigned to $\text{int}_1 = \bullet\text{Cr}(\text{CO})_2(\text{ketene})(\text{C}_5\text{Me}_5)$ occur at 1984, 1908, 1672 cm^{-1} . In the text and figures the common abbreviations $\text{Cp} = \text{C}_5\text{H}_5$ and $\text{Cp}^* = \text{C}_5\text{Me}_5$ are used interchangeably. For complete band assignments see Appendix A Table A.1.

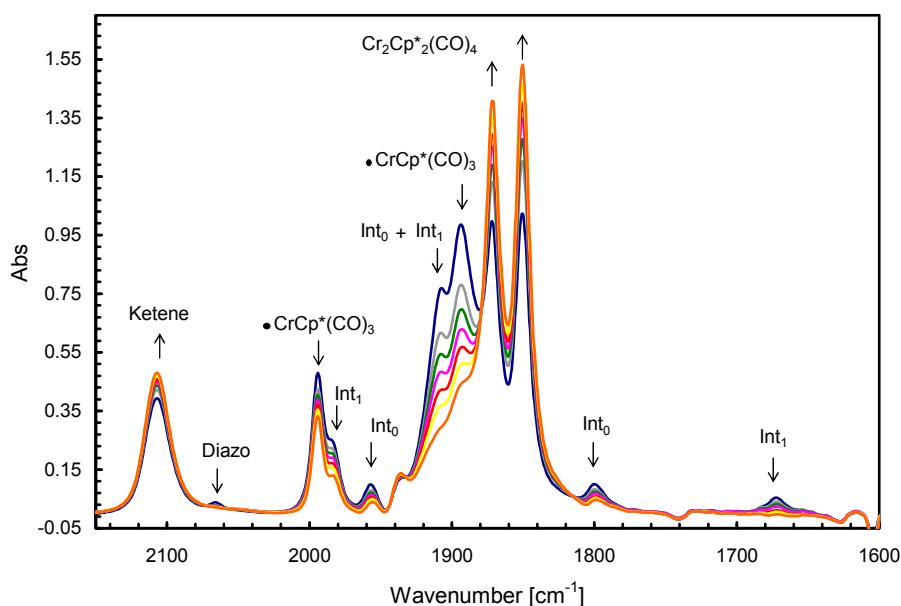


Figure 2.2. Second stage of reaction showing decay of the intermediate complexes formed during the first stage of the reaction shown in Figure 2.1 to produce primarily free ketene and $[\text{Cr}(\text{CO})_2(\text{C}_5\text{Me}_5)]_2$. For complete band assignments see Appendix A Table A.1.

free diazo present in solution, indicates that at least one of the intermediates contains a bound form of ketene or a precursor to it.

Reactions performed under an N₂ atmosphere were studied in an attempt to see if either rate or product distribution differed significantly from reactions under Ar atmosphere. No significant differences were observed implying that reversible dissociation of N₂ was not a rate determining step in the overall mechanism.

Reaction of 2 •Cr(CO)₃(C₅Me₅) with N₂CHSiMe₃ under CO. Reaction of 2 •Cr(CO)₃(C₅Me₅) with N₂CHSiMe₃ under 1.6 atm of CO showed several distinctive differences compared to reaction under argon. The first is a markedly slower rate of reaction. The second is that less [Cr(CO)₂(C₅Me₅)]₂ is produced and less •Cr(CO)₃(C₅Me₅) is consumed during ketene production. This implies that it is CO gas that is utilized to produce ketene rather than the organometallic complex being decarbonylated by the diazoalkane. In addition, the level of detectable intermediates under CO at a 2/1 Cr/diazoalkane mole ratio is lower than what is observed under argon. Finally, as shown in Figure 2.3 the reaction shows a characteristic "S" shape curve for production of ketene, consistent with an induction period followed by a relatively rapid reaction. The "S" shape is more pronounced under Ar atmosphere compared to CO.

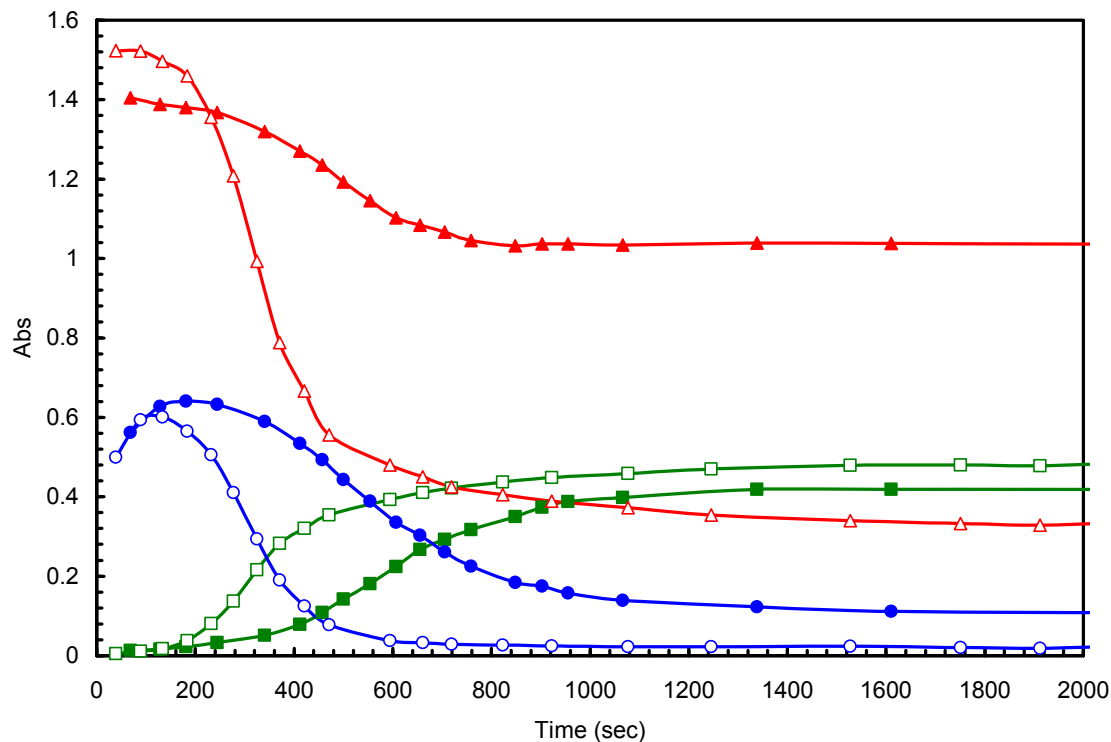


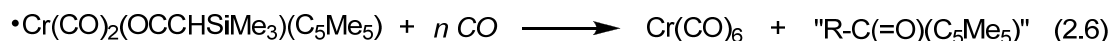
Figure 2.3. Absorbance versus time plots for key species in reaction of $\bullet\text{Cr}(\text{CO})_3(\text{C}_5\text{Me}_5)$ ($\approx .033 \text{ M}$) with $\text{N}=\text{N}=\text{CHSiMe}_3$ ($\approx 0.0165 \text{ M}$) at 25°C in toluene under Ar and CO at 1.6 atm of pressure. Absorbance bands used for quantification of key species: $\text{N}_2\text{CHSiMe}_3 = 2066 \text{ cm}^{-1}$; $\text{OCCHSiMe}_3 = 2107 \text{ cm}^{-1}$; $\bullet\text{Cr}(\text{CO})_3(\text{C}_5\text{Me}_5) = 1994 \text{ cm}^{-1}$. [● $\text{N}_2\text{CHSiMe}_3$ (CO); ○ $\text{N}_2\text{CHSiMe}_3$ (Ar); ■ OCCHSiMe_3 (CO); □ OCCHSiMe_3 (CO); ▲ $\bullet\text{Cr}(\text{CO})_3(\text{C}_5\text{Me}_5)$ (CO); △ $\bullet\text{Cr}(\text{CO})_3(\text{C}_5\text{Me}_5)$ (Ar)]

FTIR and ESR studies of the reaction of $\bullet\text{Cr}(\text{CO})_3(\text{C}_5\text{Me}_5)$ and $\bullet\text{Cr}^{13}\text{CO}_3(\text{C}_5\text{Me}_5)$ with $\text{N}_2\text{CHSiMe}_3$. Reaction of $\bullet\text{Cr}(\text{CO})_3(\text{C}_5\text{Me}_5)$ with $\text{N}_2\text{CHSiMe}_3$ in a 1/1 ratio was found to show significant differences from those studied at a 2/1 molar ratio. This is presumably because the reductive elimination step is dinuclear and the presence of excess diazo in solution generates $\bullet\text{Cr}(\text{CO})_2(\text{ketene})(\text{C}_5\text{Me}_5)$ more quickly than it is consumed. In addition it was found that under a CO atmosphere^v the intermediate complex $\text{Cr}_2(\text{CO})_5(\text{C}_5\text{Me}_5)_2$ is

^v In addition to external gas pressure utilized in the reaction, the shape of the reaction container and how it is stirred can also play a role in terms of how quickly any CO

carbonylated but $\bullet\text{Cr}(\text{CO})_2(\text{ketene})(\text{C}_5\text{Me}_5)$ reacts only extremely slowly with CO. The net result is that significant quantities of the radical ketene complex buildup. This increase can be seen in both the IR and ESR spectra.

FTIR studies of the reaction of $\bullet\text{Cr}(\text{CO})_3(\text{C}_5\text{Me}_5)$ with $\text{N}_2\text{CHSiMe}_3$ at a 1/1 molar ratio were studied under CO pressures of 10–700 psi. Under higher pressures the reaction is slow and may take up to week to go to completion at room temperature. The principal product under these conditions is the intermediate complex formulated as $\bullet\text{Cr}(\text{CO})_2(\text{ketene})(\text{C}_5\text{Me}_5)$. Attempts to obtain crystals of this highly air sensitive complex were unsuccessful in spite of repeated attempts. During these long reactions under high CO pressure, slow buildup of $\text{Cr}(\text{CO})_6$, identified by its characteristic IR spectrum, and an unknown organic carbonyl compound were observed to be formed, presumably from eqn. 2.6.^{vi,51}



The formulation of the intermediate as $\bullet\text{Cr}(\text{CO})_2(\text{ketene})(\text{C}_5\text{Me}_5)$ is based on its vibrational spectrum (Appendix A, Table A.1), observed release of ketene upon reaction

released in solution can escape to the gas phase. In the narrow confines of a sealed ESR tube, for example, even reactions run initially under argon may soon buildup significant CO concentrations serving to quench the reaction as well as alter the product distribution. For that reason ESR studies described are primarily qualitative in nature.

^{vi} Production of $\text{Mo}(\text{CO})_6$ from $\text{RMo}(\text{CO})_3(\text{C}_5\text{R}_5)$ under CO pressure has been shown to yield $\text{R-C(=O)-C}_5\text{R}_5$ as described in reference 51. The complex $\bullet\text{Cr}(\text{CO})_2(\eta^2\text{-ketene})(\text{C}_5\text{Me}_5)$ is resistant to carbonylation. It seems possible that this is due to an unfavorable pre-equilibrium to generate $\bullet\text{Cr}(\text{CO})_3(\eta^1\text{-ketene})(\text{C}_5\text{Me}_5)$. Once formed, this radical complex, rather than liberate ketene may form a C-C bonded complex in which the $(\eta^1\text{-ketene})$ moiety migrates to the cyclopentadienyl ring and then adds further CO yielding ultimately $\text{Cr}(\text{CO})_6$ and some complex organic carbonyl. The growth of a broad band near 1700 cm^{-1} in these experiments is in keeping with hypothesis that but no attempt was made to further characterize this side product.

with $\bullet\text{Cr}(\text{CO})_3(\text{C}_5\text{Me}_5)$ or $\text{Cr}_2(\text{CO})_5(\text{C}_5\text{Me}_5)_2$, as well as ESR spectroscopy. Study of the reactions of $\bullet\text{Cr}(\text{CO})_3(\text{C}_5\text{R}_5)$ ($\text{R} = \text{H}, \text{CH}_3$) with $\text{N}_2\text{CHSiMe}_3$ by ESR spectroscopy showed the presence of a radical species that built up and then decayed in rough accord with the FTIR spectroscopic studies discussed above. Representative spectroscopic data illustrating the buildup and slow decay of this complex, as well as the spectrum of the natural isotope abundance species are shown in Figure 2.4.

Reaction studies using analogous ESR techniques to those shown for $\bullet\text{Cr}(\text{CO})_3(\text{C}_5\text{Me}_5)$ were also performed for reactions of $\bullet\text{Cr}(\text{CO})_3(\text{C}_5\text{H}_5)$ and $\text{Co}_2(\text{CO})_8$. As shown in Figure 2.5 the overall level of radical concentration is approximately twenty five times lower for the Cp compared to the Cp* chromium systems. The reaction of $\text{Co}_2(\text{CO})_8$ with diazo showed no detectable signal above background noise. Radical species in the cobalt system were estimated to be present at levels at least six orders of magnitude lower than for the chromium systems under comparable conditions.

The ^{13}CO labeled radical $\bullet\text{Cr}(^{13}\text{CO})_3(\text{C}_5\text{Me}_5)$ complex was prepared and allowed to react with $\text{N}_2\text{CHSiMe}_3$ to prepare *in situ* the isotopically labeled complex $\bullet\text{Cr}(^{13}\text{CO})_2(\eta^2\text{-O}=\text{C}=\text{CHSiMe}_3)(\text{C}_5\text{Me}_5)$. ESR spectra for this complex and a computer simulation are shown in Figure 2.6. The computer simulation was prepared by Joshua Telsner from Roosevelt University. Both display a coupling to ^{13}CO not present in the natural abundance spectrum shown in Figure 2.4. The spectrum of the ^{13}CO labeled complex consists essentially of a triplet of doublets centered at $g = 2.007$, with low intensity satellites due to ^{53}Cr ($I = 3/2$, 9.5% abundant). The largest hyperfine coupling is

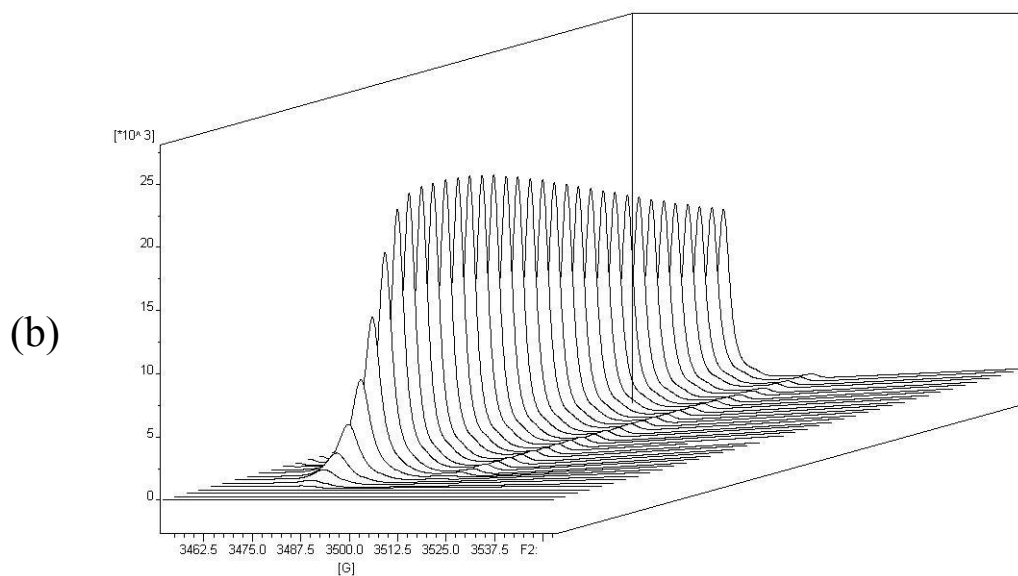
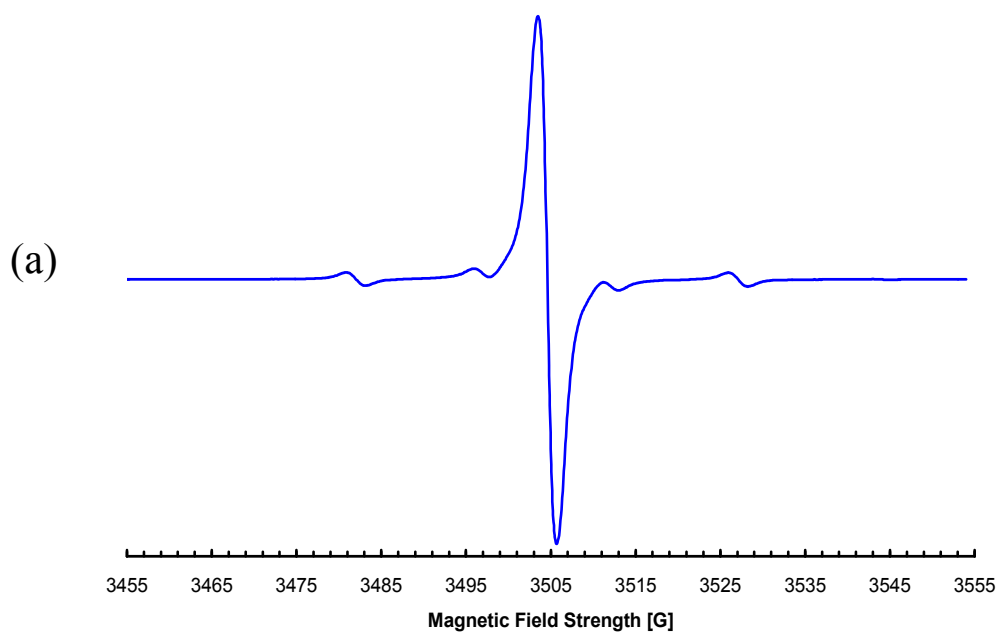


Figure 2.4. (a) Natural Abundance ESR Spectra of the ESR active intermediate $\bullet\text{Cr}(\text{ketene})(\text{CO})_2(\text{C}_5\text{Me}_5)$ (b) Stacked plot of integrated ESR data showing growth and decay of EPR signal during reaction of $\bullet\text{Cr}(\text{CO})_3(\text{C}_5\text{Me}_5)$ and $\text{N}_2\text{CHSiMe}_3$. Spectra acquired under initial argon atmosphere with isotopes at natural abundance at a time interval of 30 seconds between spectra.

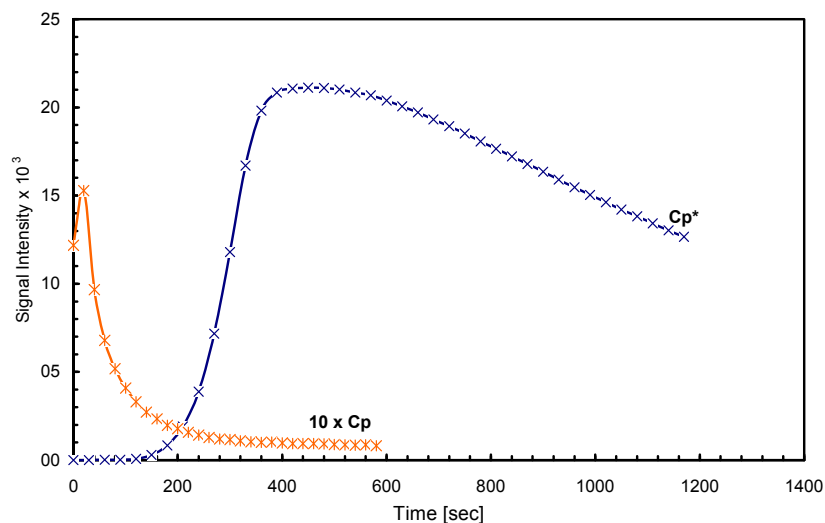


Figure 2.5. Intensity of EPR signals of $\bullet\text{Cr}(\text{CO})_2(\eta^2\text{-O}=\text{C}=\text{CHSiMe}_3)(\text{C}_5\text{R}_5)$ for $\text{R} = \text{H}$ (Cp) and $\text{R} = \text{CH}_3$ (Cp*). Note that the intensity of the Cp signal should be divided by ten. This illustrates not only the lower level of this radical species in the Cp system, but also its more rapid growth and decay. Analogous studies with $\text{Co}_2(\text{CO})_8$ showed no detectable radical species above background noise.

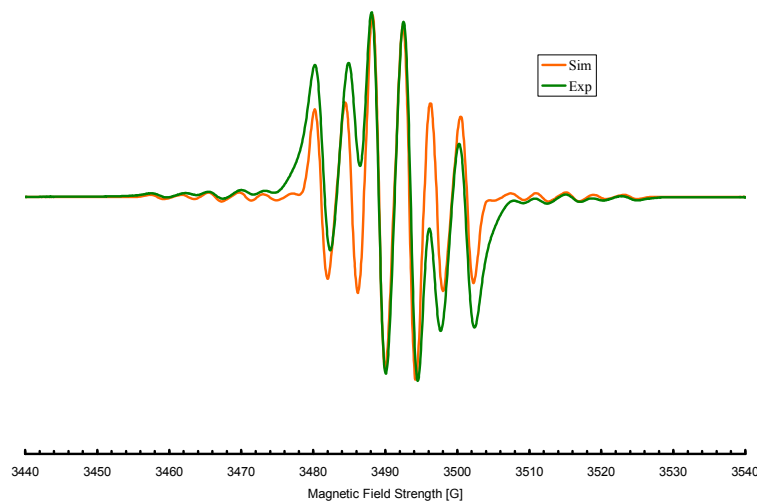


Figure 2.6. Experimental and simulated room temperature X-band (9.807 GHz) ESR spectra for $\bullet\text{Cr}(\text{C}^{13}\text{CO})_2(\eta^2\text{-O}=\text{C}^{13}=\text{CHSiMe}_3)(\text{C}_5\text{Me}_5)$. Simulated data are fit assuming 95% isotopic substitution in ^{13}C and natural abundance in ^{53}Cr and the following parameters: $g_{\text{iso}} = 2.007$; $A_{\text{iso}}(^{53}\text{Cr}) = 42.5$ MHz; $A_{\text{iso}}(^{13}\text{C a})_2 = 22.5$ MHz; $A_{\text{iso}}(^{13}\text{C b})_1 = 12.0$ MHz; 3 MHz Gaussian line widths.

to the metal, $A(^{53}\text{Cr}) = 42.5$ MHz, with additional hyperfine splitting assigned as 22.5 MHz for the two equivalent ^{13}CO ligands and 12.0 MHz for $\eta^2\text{-O}=\text{}^{13}\text{C}=\text{CHSiMe}_3$. No hyperfine splitting is assignable to ^1H , as indicated by the simple ESR spectra of the natural abundance spectrum shown in Figure 2.4a.

It can not be excluded that low levels of other radical species may be present in solution, but the dominant pattern seen in a number of experiments was reproducible and the fit of computed and experimental data are good. The growth and decay of the peaks assigned to this intermediate as followed by ESR were also observed in FTIR studies done in parallel reactions.

These ESR results can be compared with those for other organochromium radicals.^{52,53} The value for isotropic ^{53}Cr hyperfine coupling, 42.5 MHz, is comparable, but larger than that seen for $\bullet\text{Cr}(\text{CO})_3(\text{C}_5\text{H}_5)$ ($a_{\text{iso}}(^{53}\text{Cr}) = 23$ MHz, based on measurements at low temperatures in doped single crystals of the diamagnetic host, $\text{CpMn}(\text{CO})_3$),^{53b} which indicates the significant Cr(I) character of $\bullet\text{Cr}(\text{CO})_2(\eta^2\text{-O}=\text{C}=\text{CHSiMe}_3)(\text{C}_5\text{Me}_5)$. The complex $\bullet\text{Cr}(\text{CO})_3(\text{C}_5\text{H}_5)$ also exhibited hyperfine coupling from the carbonyl ligands (detected in natural isotopic abundance) with $a_{\text{iso}}(^{13}\text{C}) = 25$ MHz,^{53b} quite close to the value observed here (the author is unaware of any relevant data for the ketene-based ^{13}C hyperfine coupling).

An interesting difference, however, is that the symmetrical parent radical, as well as related derivatives $\bullet\text{Cr}(\text{CO})_3(\text{C}_5\text{R}_5)$ ($\text{R} = \text{H}, \text{CH}_3, \text{Ph}$) are known to display **no** solution phase ESR spectra at room temperature.⁵² However, for species of lower effective symmetry such as $\bullet\text{Cr}(\text{CO})_2(\text{L})(\text{C}_5\text{Me}_5)$,⁵³ $[\bullet\text{Cr}(\text{CO})_2(\text{RC}\equiv\text{CR})(\text{C}_6\text{Me}_6)]^+$,⁵⁴ and $\bullet\text{Cr}(\text{CO})_2(\eta^3\text{-tris(pyrazolylborato)})(\text{PMe}_3)$ ⁵⁵ solution phase spectra are reported even

at ambient temperature. These arguments support assignment of the radical species in solution as $\bullet\text{Cr}(\text{CO})_2(\eta^2\text{-O=C=CHSiMe}_3)(\text{C}_5\text{Me}_5)$, which likewise has lower effective symmetry. Computed SOMO and spin density data are shown in Appendix A Figure A.1 and also support a highly delocalized radical which is predominantly metal based. Similar conclusions were made for the cationic acetylene complexes $[\bullet\text{Cr}(\text{CO})_2(\text{RC}\equiv\text{CR})(\text{C}_6\text{Me}_6)]^+$ which are probably closest in nature to the proposed intermediate ketene radical complex reported here.⁵⁴

Reaction of $\bullet\text{Cr}(\text{}^{13}\text{CO})_3(\text{C}_5\text{Me}_5)$ with $\text{N}_2\text{CHSiMe}_3$ was also investigated by FTIR spectroscopy as shown in Appendix A Figure A.2. A shift in the assigned vibrational bands of all assigned bands was observed (see Appendix A, Table A.1). However of principal interest was the shift in ν_{CO} of the assigned band of the coordinated ketene from 1672 cm^{-1} to 1637 cm^{-1} for $\bullet\text{Cr}(\text{}^{13}\text{CO})_2(\eta^2\text{-O}=\text{}^{13}\text{C=CHSiMe}_3)(\text{C}_5\text{Me}_5)$. This is strong evidence that loss of N_2 occurs previous to the formation of this intermediate.

Reaction of $[\text{Cr}(\text{CO})_3(\text{C}_5\text{H}_5)]_2$ with $\text{N}_2\text{CHSiMe}_3$. Reaction of $[\text{Cr}(\text{CO})_3\text{Cp}]_2$ with $\text{N}_2\text{CHSiMe}_3$ in a 1.5/1 stoichiometric ratio {a 3/1 ratio based on the monomeric radical $\bullet\text{Cr}(\text{CO})_3(\text{C}_5\text{H}_5)$ } under argon was found to occur more rapidly for the C_5H_5 than the C_5Me_5 system. That is in spite of the fact that lower concentrations of radical species are present in the Cp system. Production of ketene was nearly complete following a short induction period as shown in Figure 2.7. The initial organometallic products are an intermediate complex with major bands near 1922 and 1832 cm^{-1} and a minor band near 2006 cm^{-1} as well as small quantities of the known triple bonded complete $[\text{Cr}(\text{CO})_2(\text{C}_5\text{H}_5)]_2$. As discussed later, the ν_{CO} frequencies are in good agreement with

formulation of the previously unreported product as $\text{Cr}_2(\text{CO})_5(\text{C}_5\text{H}_5)_2$ based on high level density functional theory.

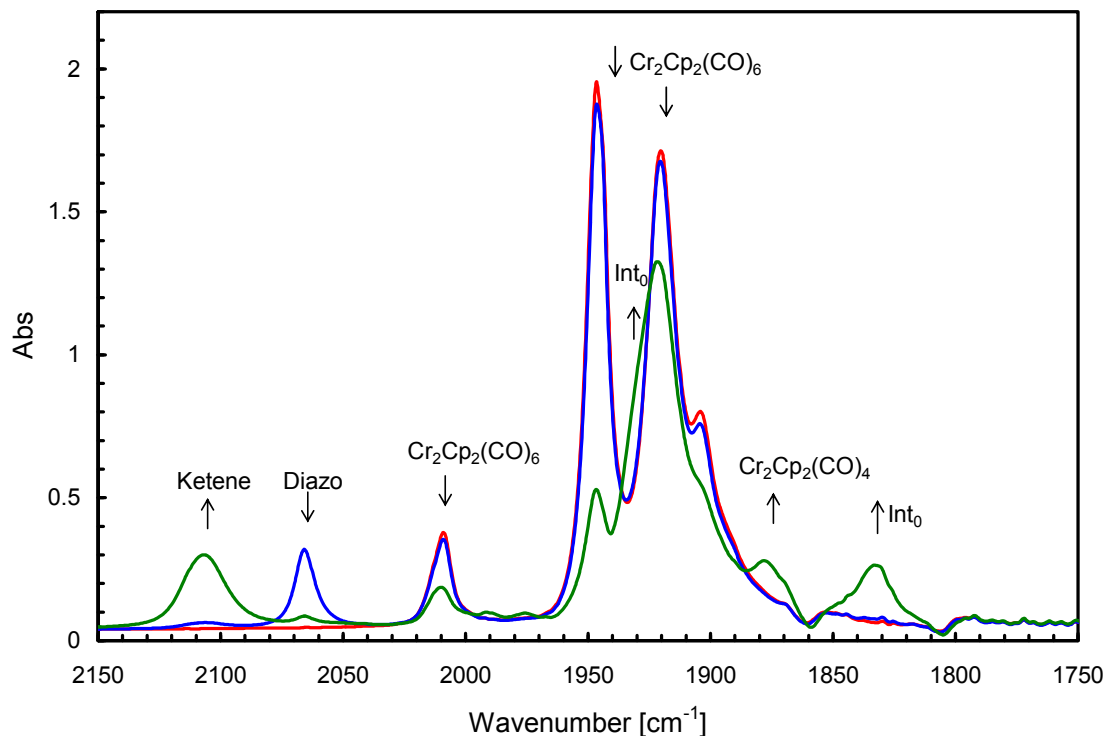
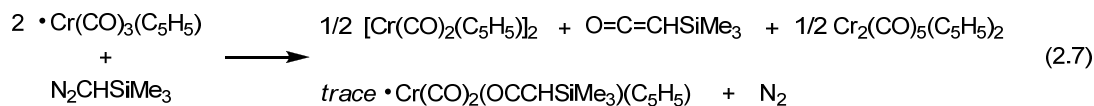


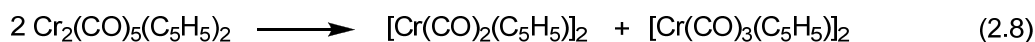
Figure 2.7. Stock solution of $[\text{Cr}(\text{CO})_3\text{Cp}]_2$ (0.0163 M) in toluene under argon prior to addition of $\text{N}_2\text{CHSiMe}_3$ (0.0108 M) in a 1.5/1 molar ratio at 25°C (red spectrum), $t \approx 30$ sec following addition of $\text{N}_2\text{CHSiMe}_3$ (blue spectrum) and $t \approx 60$ sec (green spectrum). Little reaction occurs during the initial induction period as shown in the blue spectrum. The green spectrum shows rapid growth in free ketene, nearly complete reaction of initial diazo and $[\text{Cr}(\text{CO})_3\text{Cp}]_2$, minor buildup of $[\text{Cr}(\text{CO})_2\text{Cp}]_2$ and the presence of an intermediate complex. For band positions see Table A.1.

Thus the first stage of the reaction of $[\text{Cr}(\text{CO})_3(\text{C}_5\text{H}_5)]_2$ with $\text{N}_2\text{CHSiMe}_3$ is considered to occur in a manner similar to that for $2 \cdot \text{Cr}(\text{CO})_3(\text{C}_5\text{Me}_5)$ but with a only trace amounts of the bound ketene radical and a much greater amount of $\text{Cr}_2(\text{CO})_5(\text{C}_5\text{H}_5)_2$.



A very small band near 1700 cm^{-1} can be detected and is tentatively assigned to small amounts of $\bullet\text{Cr}(\text{CO})_2(\text{ketene})(\text{C}_5\text{H}_5)$ by comparison with the band near 1672 cm^{-1} assigned to $\bullet\text{Cr}(\text{CO})_2(\text{ketene})(\text{C}_5\text{Me}_5)$. In addition, ESR measurements for the Cp system show the presence of a rapidly decaying radical species in low concentration as discussed above. Reactions done with a greater excess of $[\text{Cr}(\text{CO})_3(\text{C}_5\text{H}_5)]_2$ such that the Cr/diazo mole ratio was $> 3/1$ were found to produce the bands assigned to $\text{Cr}_2(\text{CO})_5(\text{C}_5\text{H}_5)_2$ more rapidly with the near absence of initially produced $[\text{Cr}(\text{CO})_2(\text{C}_5\text{H}_5)]_2$.

The second stage of reaction under an argon atmosphere (Appendix A Figure A.3) was initially interpreted as a disproportionation reaction:



However, decay of $\text{Cr}_2(\text{CO})_5(\text{C}_5\text{H}_5)_2$ is best described by independent reactions (2.9) and (2.10).



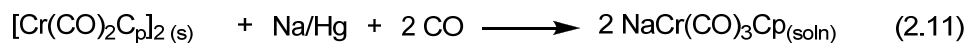
The product ratio observed in decomposition of $\text{Cr}_2(\text{CO})_5(\text{C}_5\text{H}_5)_2$ was found to depend on CO pressure. At high CO pressures predominantly $[\text{Cr}(\text{CO})_3(\text{C}_5\text{H}_5)]_2$ is produced, and at very low CO pressures $[\text{Cr}(\text{CO})_2(\text{C}_5\text{H}_5)]_2$ is the major product as shown in Appendix A Figure A.4.

Kinetic studies of the rate of decay of $\text{Cr}_2(\text{CO})_5(\text{C}_5\text{H}_5)_2$ as a function of temperature and CO pressure were performed. First order plots of the rate of decay of $\text{Cr}_2(\text{CO})_5(\text{C}_5\text{H}_5)_2$ under argon as a function of temperature, producing primarily $[\text{Cr}(\text{CO})_2(\text{C}_5\text{H}_5)]_2$ are shown in Appendix A Figure A.5. The measurements led to an estimated activation parameters of $\Delta H^\ddagger = 23\text{ kcal mol}^{-1}$, $\Delta S^\ddagger = 55\text{ cal mol}^{-1}\text{ K}^{-1}$ for eqn.

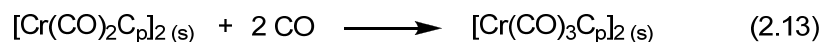
2.9. The product branching ratio between eqns. 2.9 and 2.10 was observed to depend on CO pressure, but for a fixed CO pressure the selectivity showed little temperature variation between experiments done at 15, 25, and 35 °C. This implies a similar enthalpy of activation for both loss of CO as well as addition of CO to $\text{Cr}_2(\text{CO})_5(\text{C}_5\text{H}_5)_2$.

The relatively slow rate of eqns. 2.9 and 2.10, as well as the B3LYP and BP86 DFT calculations prepared by R. Bruce King, Henry F. Schaefer III and Yamoming Xie in a collaborative effort, suggested that $\text{Cr}_2(\text{CO})_5(\text{C}_5\text{H}_5)_2$ might be a ground state triplet, and as such not display a detectable NMR signal (nor ambient temperature ESR). Reaction of $[\text{Cr}(\text{CO})_3(\text{C}_5\text{H}_5)]_2$ with $\text{N}_2\text{CHSiMe}_3$ was therefore studied by NMR spectroscopy in C_6D_6 at 15 °C. The first NMR spectrum was taken approximately 240 seconds after initiating reaction. At that time, complete conversion of the diazo to ketene had occurred, in keeping with earlier FTIR studies. A very small broad peak due to $[\text{Cr}(\text{CO})_3(\text{C}_5\text{H}_5)]_2$ was detected near 5.3 ppm and underwent only minor changes during the reaction. The only major change seen in the NMR spectra was the appearance "out of nowhere" of a steadily increasing signal near 4.2 ppm due to $[\text{Cr}(\text{CO})_2(\text{C}_5\text{H}_5)]_2$ as shown in Appendix A Figure A.6. These studies strongly support the formulation of the intermediate as $\text{Cr}_2(\text{CO})_5(\text{C}_5\text{H}_5)_2$.

Calorimetric study of enthalpies of reduction of $[\text{Cr}(\text{CO})_2(\text{C}_5\text{H}_5)]_2$ and $[\text{Cr}(\text{CO})_3(\text{C}_5\text{H}_5)]_2$ by Na/Hg under CO. In order to make an estimate of the $\text{Cr}\equiv\text{Cr}$ bond strength in $[\text{Cr}(\text{CO})_2(\text{C}_5\text{H}_5)]_2$ the energies of eqns. 2.11 [$\Delta E = -94.9 \pm 0.8 \text{ kcal mol}^{-1}$] and 2.12 [$\Delta E = -80.7 \pm 1.3 \text{ kcal mol}^{-1}$] were measured by solution calorimetry in THF solution.



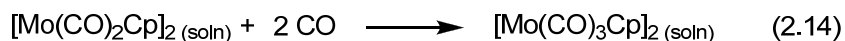
The difference between eqns. 2.11 and 2.12 yield a value for eqn. 2.13 of $\Delta E = -14.2 \pm 2.1 \text{ kcal mol}^{-1}$ since all other terms cancel.



The computed energy change is based on reactions of the solids as shown in eqn. 2.13.

Conversion of the value for ΔE_{solids} to ΔH_{solns} however results in no significant change in the value of $-14.2 \text{ kcal mol}^{-1}$ for the enthalpy of eqn. 2.13 with all species in solution.^{vii}

Measurements of the enthalpy of eqn. 2.14 ($\Delta H = -40.3 \text{ kcal mol}^{-1}$) have been reported.⁵⁶



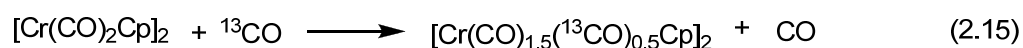
The considerably more exothermic reaction of the $\text{Mo}\equiv\text{Mo}$ complex as shown in eqn. 2.14 is in keeping with its generally much greater reactivity compared to the relatively inert $\text{Cr}\equiv\text{Cr}$ complex.⁵⁷ The difference between the enthalpies of eqns. 2.13 and 2.14 ($\sim -26 \text{ kcal mol}^{-1}$) implies that while the Cr-Cr single bond is much weaker than the Mo-Mo single bond, that situation does not extend to the triple bonded complexes.^{viii}

^{vii} The value for the enthalpy of eqn. 13 as measured from solid to solid should require little adjustment for reaction in toluene solution. Measurement of the enthalpy of solution of $[\text{Cr}(\text{CO})_3\text{Cp}]_2$ presents problems owing to its dissociation to radicals. However experiments with the corresponding molybdenum complexes (which undergo no such dissociation) suggest that the enthalpy of solution of $[\text{Cr}(\text{CO})_3\text{Cp}]_2$ in toluene is approximately $1.2 \text{ kcal mol}^{-1}$ more endothermic than for $[\text{Cr}(\text{CO})_2\text{Cp}]_2$. However, the actual calorimetric measurements are for ΔE and not ΔH in the closed system. Since $\Delta H = \Delta E + \Delta PV$, and correction for the two moles of gas absorbed in the reaction ($RT\Delta n$ of $\sim 1.2 \text{ kcal mol}^{-1}$) will essentially cancel the difference in the estimated enthalpies of solution.

^{viii} The Cr-Cr single bond strength is on the order of 15 kcal mol^{-1} and the Mo-Mo bond strength is on the order of $32.5 \text{ kcal mol}^{-1}$. This difference ($17.5 \text{ kcal mol}^{-1}$) alone would make the enthalpy of eqn. 2.14 exothermic by that amount. The Mo-CO bond

In fact, use of a value of Cr-CO = 37 kcal mol⁻¹⁵⁸ leads to an estimate of the Cr≡Cr bond strength of 74 kcal mol⁻¹, slightly larger than the previous reported estimate of the Mo≡Mo bond strength of 69 kcal mol⁻¹.

Attempted ¹³CO exchange in [Cr(CO)₂Cp]₂. Investigation as to the reversibility of eqn. 2.9 showed that CO did not readily add at pressures up to ~10 atm at room temperature. Wrighton and coworkers have reported slow carbonylation at pressures in excess of 100 atm.⁵⁹ That reaction involves addition of two moles of CO presumably through intermediate Cp₂Cr₂(CO)₅. In order to test this possibility we studied eqn. 2.15



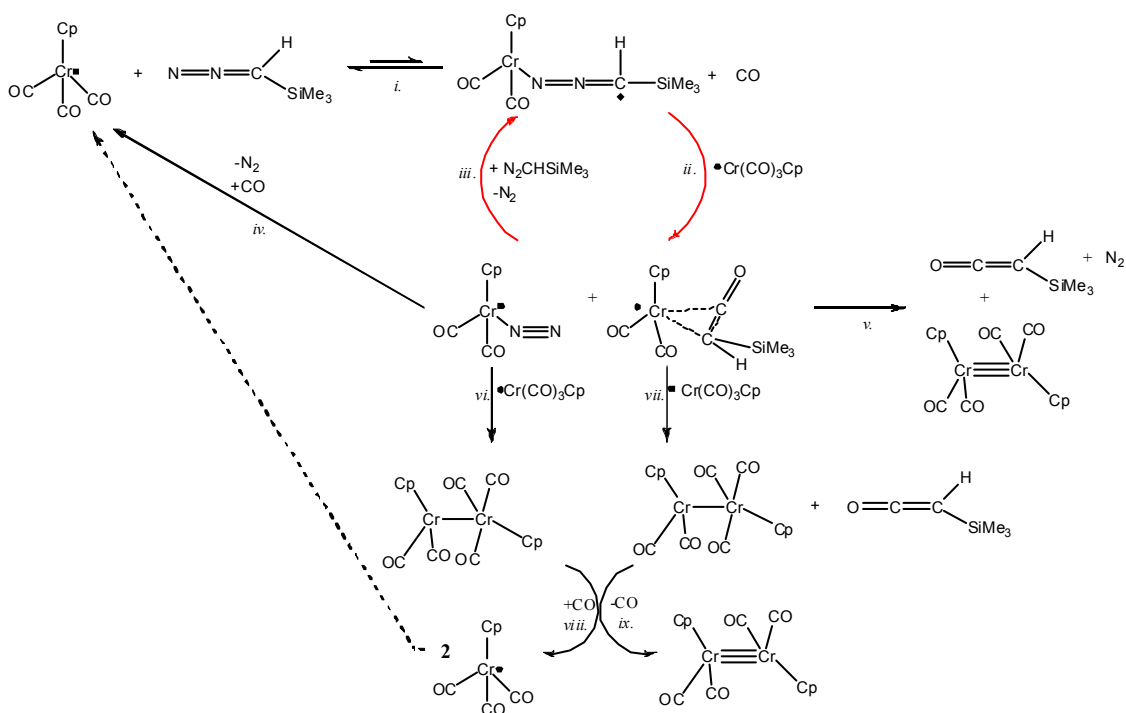
At ¹³CO pressure of ~10 atm and at temperatures up to ~50 °C no real sign of incorporation of ¹³CO label in [Cr(CO)₂Cp]₂ was observed. This was taken to indicate that there was little if any formation of Cp₂Cr₂(CO)₄(¹³CO) from [Cr(CO)₂Cp]₂ by direct addition under these conditions. Since carbonylation of [Cr(CO)₂Cp]₂ by 2 CO is known to occur⁵⁹ albeit slowly, and since Cr₂(CO)₅Cp₂ adds CO at roughly the same rate as it loses it we conclude that addition of CO to ¹[Cr(CO)₂Cp]₂ is slow to the combination of both spin state and geometric changes occurring in eqn. 2.15.^{60,ix}

strength is typically viewed as being ~ 4 kcal mol⁻¹ greater than the Cr-CO bond strength. Since two CO bonds are transferred that would make an estimate of $\Delta H \cong -17.5 + 2 \times -4 = -25.5$ kcal mol⁻¹. This is close to the measured difference and implies that the Cr≡Cr and Mo≡Mo bond strengths are roughly comparable in terms of the reaction: Cp(CO)₂M≡M(CO)₂Cp → 2 MCp(CO)₂ as a definition of the BDE reaction. It is apparently the case that the weak nature of the Cr-Cr single bond does not carry over to the triple bond, at least in comparison to corresponding Mo complexes.

^{ix} Theoretical treatment of the role of spin state changes in organometallic reactions for mononuclear species is still evolving (see ref 60). The author is not aware of

Proposed reaction pathways for carbonylation of $\text{N}_2\text{CHSiMe}_3$ by $\bullet\text{Cr}(\text{CO})_3(\text{C}_5\text{R}_5)$ $\text{R} = \text{H}, \text{CH}_3$. A general mechanism in keeping with experimental studies described previously and computational results is presented in Scheme 2.1. The first step, *i*, is consistent with both the inhibiting effect of CO as well as the observed induction period and "S" shaped curve. This step consists of the slow loss of CO to form the radical diazo complex $\bullet\text{Cr}(\text{CO})_2(\text{N}=\text{N}=\text{CHSiMe}_3)(\text{C}_5\text{R}_5)$. DFT calculations performed by Tamás Kégl at the University of Pannonia of this initial associative ligand displacement reaction (using the model molecule N_2CH_2) showed the net reaction free energy of this elementary step is $+3.6 \text{ kcal mol}^{-1}$. A molecular orbital calculation of the SOMO of the simplified model of this radical complex is shown in Figure 2.8

Scheme 2.1. Proposed Reaction Scheme for reaction of $\bullet\text{Cr}(\text{CO})_3(\text{C}_5\text{R}_5)$ ($\text{R} = \text{Me}, \text{H}$) with $\text{N}_2\text{CHSiMe}_3$.



theoretical analysis of concomitant spin state/geometric changes being reported for metal-metal bonded systems similar to this one.

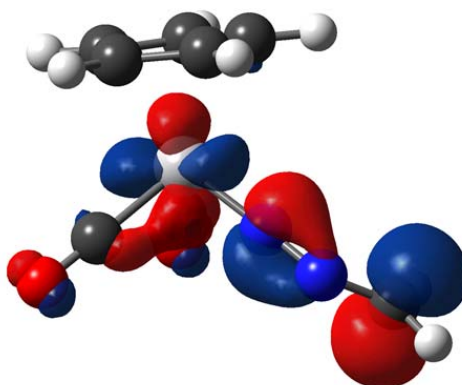
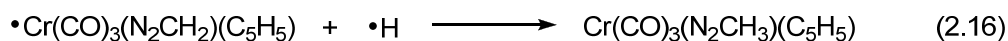


Figure 2.8. Drawing prepared by Tamás Kégl at the University of Pannonia of the calculated SOMO for $\bullet\text{Cr}(\text{CO})_2(\text{N}_2\text{CH}_2)(\text{C}_5\text{H}_5)$.

Significant spin density appears resident on the terminal C of the diazo ligand of this radical. Addition of an H atom to the proposed intermediate shown in Figure 2.8 would yield a methyldiazenido complex $\text{Cr}(\text{CO})_2(\text{N}_2\text{CH}_3)(\text{C}_5\text{H}_5)$ as shown in eqn. 2.16:



Analogous diazenido complexes of Mo and W are known.^{61,62} Formation of the diazenido complex, which is isoelectronic with the highly stable nitrosyl complex $\text{Cr}(\text{CO})_2(\text{NO})(\text{C}_5\text{H}_5)$, would be expected to be highly favorable. Such a radical combination would be expected to be rapid^{x,63} and the structure of a key reaction intermediate during step *ii* of Scheme 2.1 is proposed to be the addition of $\bullet\text{Cr}(\text{CO})_3\text{C}_5\text{H}_5$ rather than $\bullet\text{H}$ to yield an intermediate complex $(\text{C}_5\text{H}_5)(\text{CO})_2\text{Cr}-\text{N}\equiv\text{N}-\text{CH}_2-\text{Cr}(\text{C}_5\text{H}_5)(\text{CO})_3$. The computed structure for this proposed intermediate is shown in Figure 2.9. This intermediate complex is poised for formation of a C-C bond by migration of the Cr-C bond to a coordinated terminal CO.

^x In addition to rapid radical-radical combination reactions, studies of ultrafast disproportionation reactions of the photochemically generated radical $\bullet\text{W}(\text{CO})_3(\text{C}_5\text{H}_5)$ have recently been reported. (see ref. 63)

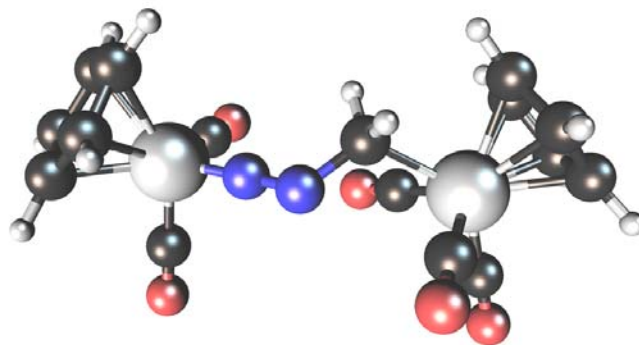


Figure 2.9. Calculated structure of $(C_5H_5)(CO)_2Cr-N\equiv N-CH_2-Cr(C_5H_5)(CO)_3$ prepared by Tamás Kégl at the University of Pannonia.

A second critical step is proposed to be migration of an alkyl radical in the bridging dinuclear intermediate, shown in Figure 2.10, from chromium to a carbonyl group in a manner analogous to CO insertion. As this occurs, the driving force to form ketene and N_2 provides the needed energy to split the complex to the two intermediate radicals $\bullet Cr(CO)_2(ketene)(C_5R_5)$ and $\bullet Cr(CO)_2(N_2)(C_5R_5)$ as shown in step *ii* of Scheme 2.1. The reaction was calculated to be exothermic with a free energy difference of $-9.3 \text{ kcal mol}^{-1}$ and was calculated to proceed with a free energy barrier of $21.3 \text{ kcal mol}^{-1}$. Harmonic vibrational frequency calculation confirmed that **TS1** is indeed a transition state which goes on to produce $\bullet Cr(CO)_2(ketene)(C_5R_5)$ and $\bullet Cr(CO)_2(N_2)(C_5R_5)$ by cleavage of the C-N bond.

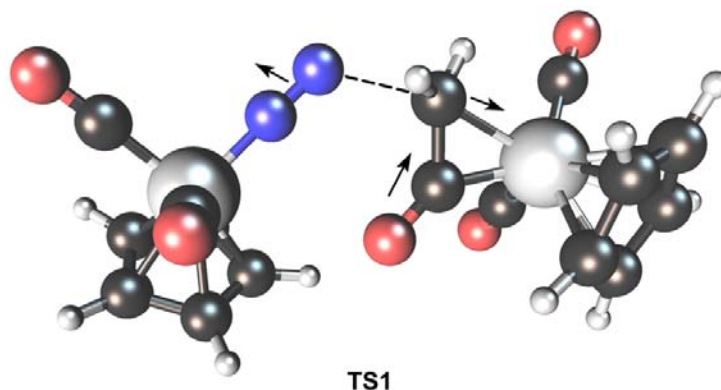


Figure 2.10. Computed transition state for step *ii* in the mechanism in Scheme 2.1 prepared by Tamás Kégl at the University of Pannonia.

One possible reaction of $\bullet\text{Cr}(\text{CO})_2(\text{ketene})(\text{C}_5\text{R}_5)$ and $\bullet\text{Cr}(\text{CO})_2(\text{N}_2)(\text{C}_5\text{R}_5)$ is proposed to be recombination to reform a Cr-Cr bond and eliminate N_2 , ketene, and form $\text{Cr}_2(\text{CO})_4\text{Cp}_2$. However, as shown in Figure 2.10, the geometry of cleaving the C-N bond appears to present an initially unfavorable steric orientation to radical combination to form a Cr-Cr bond along this trajectory. Therefore it is proposed (especially for the experimentally studied complex which has a pendant SiMe_3 on the diazo carbon) that the radicals predominantly diffuse into solution rather than combine directly to form N_2 , ketene, and $[\text{Cr}(\text{CO})_2\text{Cp}]_2$ in a single step as shown in step *v.* of Scheme 2.1. This diffusion process is also in accord with spectroscopic data which shows the buildup of other intermediate complexes rather than direct formation of products.

One of the products of this reaction, $\bullet\text{Cr}(\text{CO})_2(\text{ketene})(\text{C}_5\text{R}_5)$ is detectable by ESR spectroscopy, however the second product of step *ii*, $\bullet\text{Cr}(\text{CO})_2(\text{N}_2)(\text{C}_5\text{R}_5)$ is undetected and presumed to be highly reactive owing to the expected weak nature of the Cr- N_2 bond.^{xi,64} Step *iii* involves associative displacement of N_2 from

^{xi} (a) The labile nature of the Cr- N_2 compared to the Cr-CO bond is illustrated by the fact that the complex $\text{Cr}(\text{CO})_5(\text{N}_2)$ is stable enough to be detected by fast infrared

$\bullet\text{Cr}(\text{CO})_2(\text{N}_2)(\text{C}_5\text{R}_5)$ by free $\text{N}_2\text{CHSiMe}_3$ to reform $\bullet\text{Cr}(\text{CO})_2(\text{N}_2\text{CHSiMe}_3)(\text{C}_5\text{R}_5)$. This is part of a reaction cycle (shown in red in Scheme 2.1) which accounts for the "S" shaped nature of the reaction.

Step *vi*, radical combination of $\bullet\text{Cr}(\text{CO})_2(\text{N}_2)(\text{C}_5\text{R}_5)$ with $\bullet\text{Cr}(\text{CO})_3(\text{C}_5\text{R}_5)$, is proposed as a major route leading ultimately to $\text{Cr}_2(\text{CO})_5(\text{C}_5\text{R}_5)_2$. Of key importance to this study was the calculation that the most stable state of $\text{Cr}_2(\text{CO})_5(\text{C}_5\text{R}_5)$ is a triplet which is calculated to lie 10.4 (B3LYP) or 4.9 (BP86) kcal mol⁻¹ lower than the lowest lying singlet state. These data are in complete accord with experimental data which showed no NMR signal detectable for the intermediate complex formulated as $\text{Cp}_2\text{Cr}_2(\text{CO})_5$ based on its observed disproportionation to $[\text{Cr}(\text{CO})_2\text{Cp}]_2$ and $[\text{Cr}(\text{CO})_3\text{Cp}]_2$. Once formed, $\text{Cr}_2(\text{CO})_5(\text{C}_5\text{R}_5)_2$ can either eliminate or add CO as shown in steps *viii* and *ix*. Finally, dinuclear elimination of ketene from $\bullet\text{Cr}(\text{CO})_2(\text{ketene})(\text{C}_5\text{R}_5)$ and $\bullet\text{Cr}(\text{CO})_3(\text{C}_5\text{R}_5)$ is postulated in step *vii*.

Structure of the $\bullet\text{Cr}(\text{CO})_2(\eta^2\text{-O=C=CH}_2)(\text{C}_5\text{R}_5)$ intermediate. Computation of the minimum energy configuration of the intermediate complex formulated as $\bullet\text{Cr}(\text{CO})_2(\eta^2\text{-ketene})(\text{C}_5\text{R}_5)$ yielded two tautomeric structures; a C,C bonded and a C,O bonded form as shown in Figure 2.11.

spectroscopy but decays with a first order rate constant of 1.7 s⁻¹ (see ref 64a). This is presumably a dissociative displacement of bound N₂. In the system studied here, the Cr-N₂ absolute bond strength might be somewhat stronger, but associative displacement in the 17 e⁻ radical would also make it more labile to ligand displacement by any stronger ligand. The L_nM-CO bond is typically 15-20 kcal mol⁻¹ stronger than the L_nM-N₂ bond for low valent complexes (see ref. 64b). In addition, 18 e⁻ complexes $\text{Cr}(\text{CO})_2(\text{N}_2)(\text{Arene})$ have been photochemically prepared (see ref 64c). These observations all point to expected thermochemical stability for $\bullet\text{Cr}(\text{CO})_2(\text{N}_2)\text{C}_5\text{Me}_5$ but rapid kinetic lability. In spite of the reasonable nature of its postulation as a reactive intermediate in this process, there is to the author's knowledge no experimental data regarding $\bullet\text{Cr}(\text{CO})_2(\text{N}_2)(\text{C}_5\text{Me}_5)$.

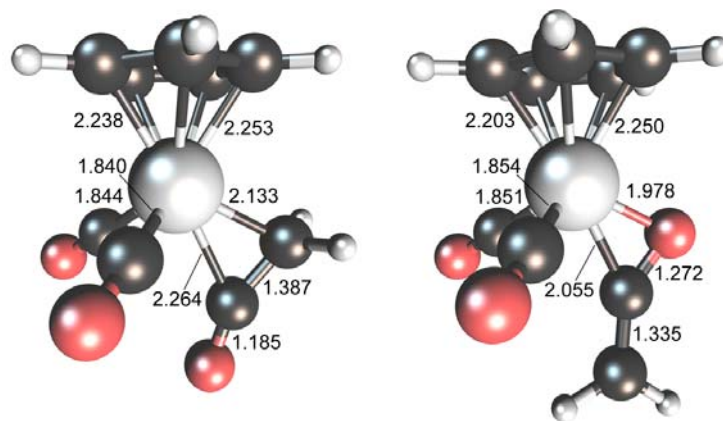


Figure 2.11. Calculated minimum energy structures for C,C and C,O bonded tautomers of $\bullet\text{Cr}(\text{CO})_2(\eta^2\text{-O}=\text{C}=\text{CH}_2)(\text{C}_5\text{H}_5)$ prepared by Tamás Kégl at the University of Pannonia. Selected bond lengths are given in Å .

The computed energies of the C,C and C,O tautomers are quite close, with the C,O tautomer being lower in energy by $1.3 \text{ kcal mol}^{-1}$. The $\text{Mn}(\text{CO})_2(\text{ketene})\text{Cp}$ complexes prepared by Herrmann and coworkers exhibit the C,C bonded form of the ketene.³⁵ Work of Grotjahn has shown there is a fine balance that governs bonding in the C,C ketene, C,O ketene, and carbene + CO, and other bonding motifs available in the $\text{R}_2\text{C}=\text{C}=\text{O}$ system.^{33a} Infrared and ESR data do not allow for conclusive^{xii} assignment of which of the two binding modes shown in Figure 2.11 best fits experimental data. The relatively

^{xii} Grotjahn and coworker (see ref. 33a) have shown that for coordination to the $\text{IrCl}(\text{P}^i\text{Pr}_3)_2$ fragment $\text{Ph}_2\text{C}=\text{C}=\text{O}$ coordinates in an $\eta^2\text{-C,O}$ form with $\nu_{\text{CO}} = 1632 \text{ cm}^{-1}$, but that $\text{Ph}(\text{H})\text{C}=\text{C}=\text{O}$ coordinates in an $\eta^2\text{-C,C}$ form with $\nu_{\text{CO}} = 1752 \text{ cm}^{-1}$. The Cr radical complex reported here has $\nu_{\text{CO}} = 1672 \text{ cm}^{-1}$ which is somewhat closer to the C,O tautomer for Ir. However the electronic differences between the Cr and Ir complexes are large enough that no conclusion can be made at this time. Both the $\eta^2\text{-C,O}$ form and $\eta^2\text{-C,C}$ form have two approximately symmetry equivalent CO ligands. The ESR data showing hyperfine splitting from two equivalent ^{13}C nuclei derived from ^{13}CO cannot distinguish between the two forms. Use of ^{13}C labeled diazoalkane might be helpful in identifying possible coordination by this carbon (in the $\eta^2\text{-C,C}$ form), but is synthetically beyond the scope of the present study.

strong analogy to the manganese carbonyl complex suggests that the C,C form is the more likely structure, as well as the most likely transition state leading to the bound form of ketene as shown in Figure 2.11 suggests the C,C tautomer. At this point, no firm conclusion can be made regarding whether $\bullet\text{Cr}(\text{CO})_2(\eta^2\text{-ketene})(\text{C}_5\text{H}_5)$ is a C,C or C,O bonded.

2.3 Conclusions

A combination of theoretical and experimental approaches was used to propose a radical based complex reaction mechanism for the seemingly simple conversion of a diazoalkane and CO to the corresponding ketene and N_2 . Two key paramagnetic complexes were observed spectroscopically (triplet not actually observed directly) and supported by DFT studies, namely $\text{Cr}_2(\text{CO})_5(\text{C}_5\text{R}_5)_2$ and $\bullet\text{Cr}(\text{CO})_2(\eta^2\text{-O=C=CHSiMe}_3)(\text{C}_5\text{R}_5)$. The rate determining step is attributed to formation of the undetected radical diazoalkane complex $\bullet\text{Cr}(\text{CO})_2(\eta^1\text{-N=N=CHSiMe}_3)(\text{C}_5\text{R}_5)$ which is then trapped by a second mole of $\bullet\text{Cr}(\text{CO})_3(\text{C}_5\text{R}_5)$ to form $(\text{C}_5\text{H}_5)(\text{CO})_2\text{Cr-N}\equiv\text{N-C(H)(SiMe}_3)\text{-Cr}(\text{C}_5\text{H}_5)(\text{CO})_3$ and subsequently leads to products as outlined in Scheme 2.1. Mechanisms can not be proven; however, the reasonable accord between theory and experiment presented here supports a concerted mechanism of this type and represents our best understanding of the complicated sequence of reactions in this system. The mechanism of carbonylation of diazoalkanes by $[\text{Cr}(\text{CO})_3(\text{C}_5\text{R}_5)]_2$ reported here appears to be quite different from that for $\text{Co}_2(\text{CO})_8$ studied by Ungváry and coworkers.³¹ Even in the well-developed field of organometallic chemistry of transition metals such as

chromium and cobalt, interesting new complexes, reaction mechanisms, and theoretical understanding remain a source of surprise.

2.4 Experimental

General procedures. Unless stated otherwise, all operations were performed in a Vacuum Atmospheres glove box under an atmosphere of purified argon or utilizing standard Schlenk tube techniques under argon. Toluene and THF were purified by distillation under argon from sodium benzophenone ketyl into flame dried glassware. $[\text{Cr}(\text{CO})_3(\text{C}_5\text{R}_5)]_2$ was prepared as described in earlier publications.^{36e} Solutions of $\text{N}=\text{N}=\text{CHSiMe}_3$ (2.0 M in hexanes) were obtained from Sigma-Aldrich and used without further purification. FTIR data were obtained on a Perkin Elmer system 2000 spectrometer. FTIR spectra for kinetic measurements were taken using a closed system FTIR cell that has been described in previous publications.⁶⁵ NMR spectra were obtained on a Bruker AVANCE 500 MHz spectrometer. ESR spectra were taken with a Bruker EMX ESR Spectrometer.

Qualitative studies of reaction of $[\text{Cr}(\text{CO})_3(\text{C}_5\text{R}_5)]_2$ ($\text{R} = \text{H}, \text{Me}$) and $\text{N}_2\text{CHSiMe}_3$. Qualitative studies of reactions of $[\text{Cr}(\text{CO})_3(\text{C}_5\text{R}_5)]_2$ ($\text{R} = \text{H}, \text{CH}_3$) and $\text{N}_2\text{CHSiMe}_3$ were performed using standard Schlenk techniques. Reaction products were analyzed in terms of the bands shown in the Appendix A Table A.1 for the known complexes utilized. Approximate percent conversions were made based on band shape analysis using standard procedures.

Kinetic studies of reaction of $[\text{Cr}(\text{CO})_3(\text{C}_5\text{R}_5)]_2$ ($\text{R} = \text{H}, \text{Me}$) and $\text{N}_2\text{CHSiMe}_3$ under low pressures of Ar, CO, and N_2 . In a typical procedure, a solution

of 0.1360 g $[\text{Cr}(\text{CO})_3(\text{C}_5\text{Me}_5)]_2$ in 15 mL toluene was prepared in a Schlenk tube under argon to make a 0.0167 M solution (.0334 M solution in radical). The Cr radical solution was then stirred for about 20 minutes to allow the compound to dissolve completely. In the glovebox the solution was loaded into a Hamilton gas tight syringe fitted with a syringe filter. Outside the glovebox the $[\text{Cr}(\text{CO})_3(\text{C}_5\text{Me}_5)]_2$ solution was filtered into the closed system IR cell via syringe. The cell had been previously placed under an atmosphere of 9 psi of CO. The sample was shaken vigorously to ensure that the maximum amount of CO was dissolved into the solution. The IR cell was then attached to a constant temperature bath and allowed to reach thermal equilibrium at 298 K. The initial IR spectrum was then taken. A Hamilton gas tight syringe was filled with 0.125 mL of a 2.0 M solution of $\text{N}_2\text{CHSiMe}_3$ in hexanes. Simultaneously the diazo solution was added and the timer was started. The sample was then shaken vigorously to ensure thorough mixing. IR spectra were taken on an average of every 60 seconds. Similar procedures were used to study the reaction of $[\text{Cr}(\text{CO})_3(\text{C}_5\text{R}_5)]_2$ ($\text{R} = \text{H}, \text{Me}$) and $\text{N}_2\text{CHSiMe}_3$ over a range of temperatures ($T = 278 - 308 \text{ K}$) and pressures of Ar, CO and N_2 ($p = 1 - 4.5 \text{ atm}$).

Kinetic studies of reaction of $[\text{Cr}(\text{CO})_3(\text{C}_5\text{Me}_5)]_2$ and $\text{N}_2\text{CHSiMe}_3$ at 12.7 atm CO. In a typical procedure, a solution of 0.1936 g $[\text{Cr}(\text{CO})_3(\text{C}_5\text{Me}_5)]_2$ in 20 mL toluene was prepared in a Schlenk tube under argon to make a 0.0179 M solution. The solution was then mixed for about 20 minutes to allow the compound to dissolve. In the glovebox the solution was loaded into a Hamilton gas tight syringe fitted with a syringe filter. Outside the glovebox the $[\text{Cr}(\text{CO})_3(\text{C}_5\text{Me}_5)]_2$ solution was filtered into the closed system IR cell via syringe using Schlenk techniques under Ar. The cell was then

connected to a tank of CO. A Hamilton gas tight syringe was used to add 0.180 mL of a 2.0 M solution of $\text{N}_2\text{CHSiMe}_3$ in hexanes to the cell after which the cell was immediately pressured up to a total of 173 psi. The reaction was thermostated at 290 K. IR spectra were taken as the reaction proceeded over the next week. Slow build up of the $\bullet\text{Cr}(\text{CO})_2(\text{ketene})\text{C}_5\text{Me}_5$ was monitored by IR peaks at 1672, 1908 and 1984 cm^{-1} . Other side products that were seen during the course of the reaction include a slow build up of both $\text{Cr}(\text{CO})_6$ (1981 cm^{-1}) and an unknown organic carbonyl near 1700 cm^{-1} which overlapped the broad band at 1672 cm^{-1} peak of the ketene complex.

ESR measurements of the reaction of $[\text{Cr}(\text{CO})_3(\text{C}_5\text{R}_5)]_2$ ($\text{R} = \text{H}, \text{Me}$) and $\text{Co}_2(\text{CO})_8$. In a representative experiment a 0.0162 M $[\text{Cr}(\text{CO})_3(\text{C}_5\text{R}_5)]_2$ ($\text{R} = \text{H}, \text{Me}$) solution was prepared under Schlenk techniques. The $[\text{Cr}(\text{CO})_3(\text{C}_5\text{R}_5)]_2$ solution (1.5 mL) was syringe filtered into a Pyrex NMR tube.^{xiii} The end of the NMR tube was sealed and taken for ESR analysis. To the tube 0.5 eq of $\text{N}_2\text{CH}(\text{SiMe}_3)$ (12 μL of 2.0 M in hexanes) was added. The tube was inverted several times to ensure proper mixing. The ESR spectrum was then taken. The reaction of $[\text{Cr}(\text{CO})_3(\text{C}_5\text{Me}_5)]_2$ with diazoalkane leads to an intense signal at $g = 2.007$. The reaction of $[\text{Cr}(\text{CO})_3(\text{C}_5\text{H}_5)]_2$ with diazoalkane leads to a small signal at $g = 2.005$. No signal was detected for the reaction of $\text{Co}_2(\text{CO})_8$ with the diazoalkane. Experimental conditions: T , 298 K; microwave power, 0.630 mW; microwave frequency, 9.840 GHz; modulation amplitude, 1.37 G.

Preparations of ^{13}CO labeled $[\text{Cr}(\text{CO})_3(\text{C}_5\text{R}_5)]_2$ ($\text{R} = \text{H}, \text{Me}$). In the glovebox 0.2146 g of $[\text{Cr}(\text{CO})_3(\text{C}_5\text{Me}_5)]_2$ was dissolved in 25 mL of toluene (0.016 M) with

^{xiii} Initial studies were made using quartz ESR tubes. It was found that 5mm screw cap NMR tube fitted with a Teflon coated silicone septum showed no significant signal that overlapped with the signal for the Cr complex for these concentrated solutions.

stirring for approximately 20 minutes. Using Schlenk techniques the solution was then syringe filtered into the closed system IR cell which in turn was pressurized to 230 psi with ^{13}CO (99 atom % obtained from ISOTECH). CO exchange was allowed to occur overnight. The next morning the ^{13}CO in the cell was evacuated and replaced by 193 psi of fresh ^{13}CO . FTIR of the sample led to the conclusion that this yielded approximately 96% $[\text{Cr}(^{13}\text{CO})_3(\text{C}_5\text{Me}_5)]_2$ with the remaining 4% primarily consisting of $[\text{Cr}(^{13}\text{CO})_2(^{12}\text{CO})(\text{C}_5\text{Me}_5)]_2$.

ESR of $[\text{Cr}(^{13}\text{CO})_3(\text{C}_5\text{R}_5)]_2$ ($\text{R} = \text{H}, \text{Me}$). In a representative experiment 1.5 mL of a 0.2146 M $[\text{Cr}(^{13}\text{CO})_3(\text{C}_5\text{Me}_5)]_2$ solution prepared as described above was syringe filtered into the a 5 mm pyrex NMR/ESR tube fitted with a screw cap and teflon coated silicone septum. The NMR/ESR tube had been purged with argon prior to addition. An ESR spectrum run prior to injection of $\text{N}_2\text{CHSiMe}_3$ showed no significant signal in keeping with the previously reported observation that in solution $\bullet\text{Cr}(\text{CO})_3(\text{C}_5\text{Me}_5)$ does not produce an observable ESR spectrum.⁵² To the ESR tube 3.3 eq. of $\text{N}_2\text{CHSiMe}_3$ (20 μL of 2.0 M in hexanes) was added. The tube was inverted several times to ensure proper mixing and the ESR spectrum was taken. As in the experiments with natural isotopic abundance complexes, the reaction of $[\text{Cr}(^{13}\text{CO})_3(\text{C}_5\text{Me}_5)]_2$ with diazoalkane led to an intense signal at $g_{iso} = 2.007$ and the reaction of $[\text{Cr}(^{13}\text{CO})_3(\text{C}_5\text{H}_5)]_2$ with diazo led to a small signal at $g_{iso} = 2.005$. An additional small signal seen in the spectrum for $[\text{Cr}(^{13}\text{CO})_3\text{C}_5\text{H}_5]_2$ was attributed to an unknown organic radical. Experimental conditions: T , 298 K; microwave power, 0.630 mW; microwave frequency, 9.807 GHz; modulation amplitude, 1.00 G.

NMR studies of reaction of $[\text{Cr}(\text{CO})_3(\text{C}_5\text{H}_5)]_2$ and $\text{N}_2\text{CHSiMe}_3$. In a typical experiment 0.0321 g of $[\text{Cr}(\text{CO})_3(\text{C}_5\text{H}_5)]_2$ was dissolved in 5 mL C_6D_6 . One milliliter was then syringe filtered into an argon purged 5 mm Pyrex NMR tube fitted with a screw cap and septum. The sample was placed in the 500 MHz Bruker AVANCE 500 MHz NMR spectrometer. It was left in the NMR at 288 K for about 15 minutes in order to reach thermal equilibrium. The tube was then quickly ejected, loaded with 0.5 eq. of $\text{N}_2\text{CHSiMe}_3$ (12.0 μL of 2 M in hexanes), mixed and placed back in the NMR. Spectra were run starting at about 240 seconds and successively run roughly every 80 seconds. In the Cp region (3.0-6.0 ppm) the only significant peak detected was a signal at ~ 4.21 ppm attributed to $[\text{Cr}(\text{CO})_2\text{C}_5\text{H}_5]_2$ which grew in steadily during the course of the reaction. The reaction was confirmed by the FTIR spectra that were taken following the conclusion of the NMR experiment. The contents of the final solution included OCCHSiMe_3 (2107 cm^{-1}), traces of unreacted $[\text{Cr}(\text{CO})_3(\text{C}_5\text{H}_5)]_2$ (2009, 1946, 1920 cm^{-1}) and $[\text{Cr}(\text{CO})_2(\text{C}_5\text{H}_5)]_2$ (1901, 1878 cm^{-1}). NMR spectra were referenced to C_6HD_5 in the C_6D_6 at 7.15 ppm.

Calvet calorimetric measurement of heat of reaction of $[\text{Cr}_2(\text{CO})_2(\text{C}_5\text{H}_5)]_2$ and $[\text{Cr}(\text{CO})_3(\text{C}_5\text{H}_5)]_2$ with 1% Na/Hg. These experiments represent a modification of experimental procedures used in a previous report on enthalpies of reduction of organometallic compounds.^{66,xiv} In the glove box 0.5 mL of 1% Na/Hg was loaded into

^{xiv} Data obtained here for reduction of $[\text{Cr}(\text{CO})_3(\text{C}_5\text{H}_5)]_2$ using Na/Hg in THF under CO was found to be similar to previous measurements of the same reaction under Ar. Initial attempts at measuring the enthalpy of reduction utilized $\text{Na}^+\text{Benzophenone}^-$ as has been described previously. (see ref. 66) During the course of these investigations it was found that due to pinacol coupling type reactions that occur in some systems involving $\text{Na}^+\text{Benzophenone}^-$ the Na/Hg reactions are more accurate. The purpose of the current work was to generate reliable enthalpies of reduction for $[\text{Cr}(\text{CO})_2\text{Cp}]_2$.

the cell of the Setaram-C-80 Calvet microcalorimeter under an atmosphere of CO. Subsequently added to the cell was 4.5 ml of THF that had been shaken and stored in the glovebox over the 1% Na/Hg and under a CO atmosphere. The solid-containing compartment of the calorimeter was loaded with 0.0132 g of $[\text{Cr}(\text{CO})_2(\text{C}_5\text{H}_5)]_2$ which had been recently recrystallized from heptane and methylene chloride. The calorimeter cell was assembled and sealed under a CO atmosphere and taken from the glove box and loaded into the calorimeter. After reaching temperature equilibration the reaction was initiated. The thermogram indicated a rapid reaction which returned cleanly to baseline with no thermal signal indicative of any substantial secondary reactions occurring.

Following return to baseline, the cell was taken back into the glove box. A sample analyzed by FTIR spectroscopy showed the presence of $\text{Na}^+[\text{Cr}(\text{CO})_3(\text{C}_5\text{H}_5)]^-$ as the sole organometallic product. The calorimetric signal was integrated and the average value for reduction of solid $[\text{Cr}(\text{CO})_2(\text{C}_5\text{H}_5)]_2$ to yield a THF solution of $\text{Na}^+[\text{Cr}(\text{CO})_3(\text{C}_5\text{H}_5)]^-$ was $-94.6 \pm 0.75 \text{ kcal mol}^{-1}$. The above procedure was also followed for the reaction of $[\text{Cr}(\text{CO})_3(\text{C}_5\text{H}_5)]_2$ with 1% Na/Hg. An average value of $-80.7 \pm 1.3 \text{ kcal mol}^{-1}$ was obtained for the reduction of this solid to $\text{Na}^+[\text{Cr}(\text{CO})_3(\text{C}_5\text{H}_5)]^-$ in THF solution. Spectral data for the formation of $\text{Na}^+[\text{Cr}(\text{CO})_3(\text{C}_5\text{H}_5)]^-$ were identical for reductions starting from solid $[\text{Cr}(\text{CO})_2(\text{C}_5\text{H}_5)]_2$ and $[\text{Cr}(\text{CO})_3(\text{C}_5\text{H}_5)]_2$. Heats of solution for both complexes are assumed to be very similar. Spectral data for all relevant compounds are listed in the Appendix A, Table A.1.

To the authors knowledge the reaction itself has not been previously reported. Reduction of $\text{Cr}_2(\text{CO})_n(\text{C}_5\text{H}_5)_2$ ($n = 2,3$) was measured by both methods $\text{Na}^+\text{Benzophenone}^-$ and Na/Hg reduction. The *differences* between enthalpies of reduction (for $n = 2, 3$) were similar. Due to pinacol coupling like reactions only the Na/Hg measurements are considered reliable and reported here.

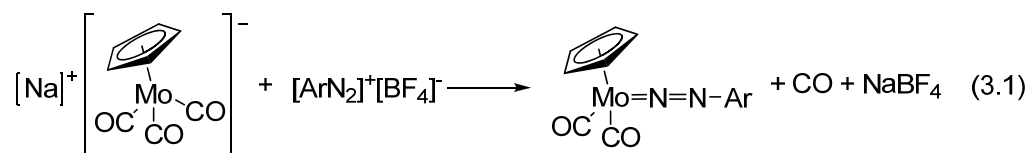
CO exchange of $[\text{Cr}(\text{CO})_2(\text{C}_5\text{H}_5)]_2$ with ^{13}CO . Under Schlenk techniques 0.055 mmol of $[\text{Cr}(\text{CO})_2(\text{C}_5\text{H}_5)]_2$ was dissolved in 10 mL toluene. Under argon the solution was then transferred to the closed system FTIR cell via Hamilton gas tight syringe. An initial FTIR spectrum was taken. The cell was then pressurized to 112 psi of ^{13}CO and thermostated at 295 K for 1 hour. No change was observed. In addition the temperature was increased from 295 to 310 K for an hour and finally to 323 K for 2 hours. No significant change was seen. The sample was left at room temperature overnight and again no significant change was seen.

Computational results. Calculations of the structures and energies of $\text{Cr}_2(\text{CO})_5\text{Cp}_2$ using DZP basis sets at the B3LYP and BP86 levels and were prepared by Henry F. Schaefer III, Yaoming Xie and R. Bruce King from the University of Georgia and Quian-Shu Li and Xiuhui Zhang from the Beijing Institute of Technology. Calculations of the structures and energies of $\bullet\text{Cr}(\text{CO})_2(\text{N}_2\text{CH}_2)(\text{C}_5\text{H}_5)$, $(\text{C}_5\text{H}_5)(\text{CO})_2\text{Cr}-\text{N}\equiv\text{N}-\text{CH}_2-\text{Cr}(\text{C}_5\text{H}_5)(\text{CO})_3$, the transition state $[\text{Cr}(\text{CO})_2(\text{N}_2)\text{Cp}][\text{Cr}(\text{CO})_2(\eta^2-\text{OCCH}_2)\text{Cp}]$ (TS1) and the C,C and C,O bonded tautomers of $\bullet\text{Cr}(\text{CO})_2(\eta^2-\text{O}=\text{C}=\text{CH}_2)\text{Cp}$ were calculated using the SDD basis set with the corresponding effective core potential for chromium and the 6-311G(d,p) basis set for all the other atoms by Tamás Kégl from the University of Pannonia. A more detailed discussion of these calculations is presented in the recently published article.⁵⁰

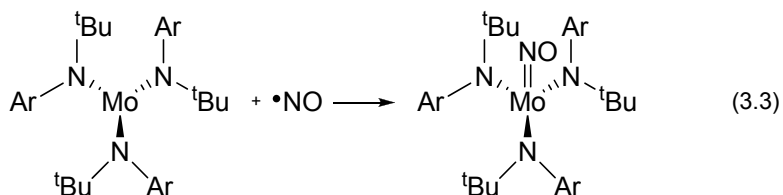
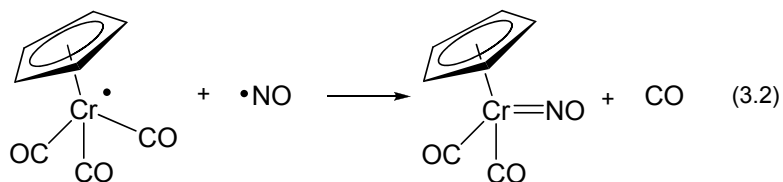
CHAPTER 3: Kinetic and Thermodynamic Studies of the Reactivity of Trimethylsilyldiazomethane with $\text{HMo}(\text{CO})_3(\text{C}_5\text{R}_5)$, ($\text{R} = \text{H}, \text{Me}$).

3.1 Background

The first transition metal complex containing a bound diazo group was prepared according to eqn. 3.1 by Bisette and King more than forty years ago.¹⁰



At that time the authors noted that the relationship between $\text{Mo}(\text{CO})_2(\text{NO})\text{Cp}$ and $\text{Mo}(p\text{-N}_2\text{C}_6\text{H}_4\text{OCH}_3)(\text{CO})_2\text{Cp}$ ($\text{Cp} = \eta^5\text{-C}_5\text{H}_5$) "appears to be especially close." This statement first highlighted the similarity of the $\bullet\text{NO}$ and $\bullet\text{NNR}$ ligands' binding properties to metal complexes. Quantitative estimates of the bond strength between metal centers and the 3-electron donor, $\bullet\text{NNR}$, have not been reported. In fact there are relatively few reports for the enthalpy of binding of $\bullet\text{NO}$ to metal complexes. The enthalpies of the reactions shown in eqns. 3.2 and 3.3 have been measured and yield estimates of the $\text{Cr}-\text{NO}$ and $\text{Mo}-\text{NO}$ bond strengths as 70 and 83 kcal mol^{-1} respectively.⁶⁷

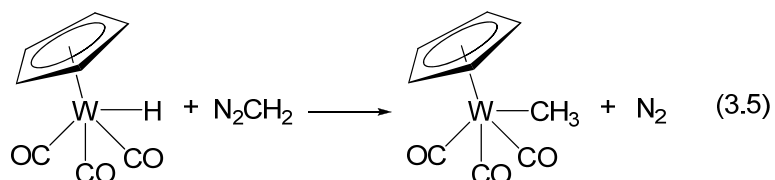
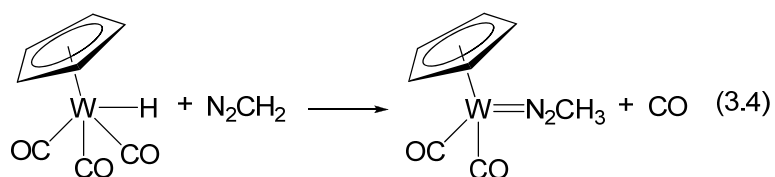


These data show the high strength of the formal 3-electron bond between a metal and $\bullet\text{NO}$. Comparison of bond strengths between $\bullet\text{NO}$ and $\bullet\text{NNR}$ with metal complexes is of

relevance to conversion of dinitrogen to amines since a possible first step in any such scheme may be formation of L_nM-NNR .

Unfortunately $\bullet N\equiv NR$ is unstable with respect to loss of $\bullet R$, and thus direct calorimetric measurements such as those made with $\bullet N\equiv O$ cannot be made. To circumvent this problem, the reaction of metal hydrides with diazoalkanes could be used to evaluate the thermochemistry of the formal insertion of N_2 into the $Mo-R$ bond to form a metal diazo complex provided that the reaction is sufficiently clean to allow for a thermochemical study.

Herrmann reported that $HW(CO)_3Cp$ reacts with diazomethane to produce the diazo complex shown in eqn. 3.4 as the major reaction product.⁶⁸ A minor reaction pathway, however, produced a metal alkyl as shown in eqn. 3.5.



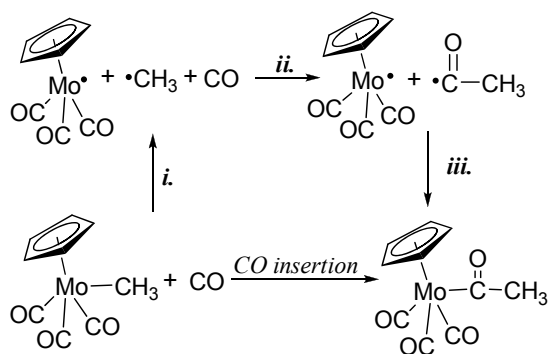
If conditions could be found such that the enthalpy of eqn. 3.4 could be measured, it would provide, in principle, an inroad to estimating the strength of the $W-(NNCH_3)$ bond in $W(CO)_2(N_2CH_3)Cp$. Furthermore, the difference between eqns. 3.4 and 3.5 results in the reaction shown in eqn. 3.6. This reaction corresponds to the formal insertion of N_2 into the metal-alkyl bond to form a diazenido complex which is also accompanied with the elimination of CO .



The energetics of reactions such as that shown in eqn. 3.6 are of clear relevance to catalytic and photochemical attempts to incorporate N_2 into the production of organic amines or other organo-nitrogen compounds.

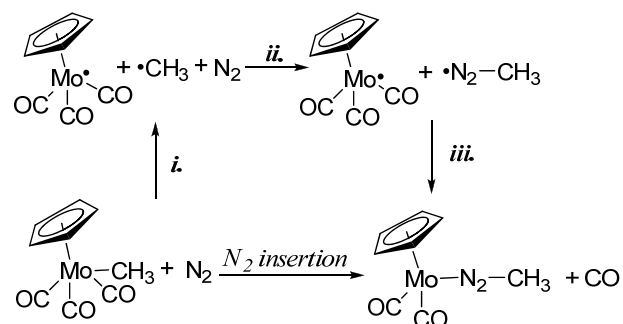
Analysis of the CO insertion reaction has previously been reported utilizing the thermochemical cycle shown in Scheme 3.1.⁶⁹

Scheme 3.1. CO insertion into the Mo-CH₃ bond.



The enthalpy of carbonyl insertion was dominated by the organic radical addition (step 3.1.*ii.*), which is exothermic by $\approx 12 \text{ kcal mol}^{-1}$ and corresponds closely to the observed net enthalpy of reaction. The M-C bond strengths for the alkyl and acyl derivatives (steps 3.1.*i.* and 3.1.*iii.*) roughly cancel.

A corresponding scheme for analysis of N_2 insertion is shown in Scheme 3.2. In spite of the isoelectronic nature of CO and N_2 , both the energetics and the structure of the products are different for these two cycles. Formation of the acyl radical $\bullet C(=O)CH_3$ is exothermic and its stability can be experimentally determined. Diazenido radicals such as $\bullet NNCH_3$ are unstable and are best analyzed computationally. Another salient difference between Schemes 3.1 and 3.2 is that the enthalpies of steps 3.1.*i.* and 3.1.*iii.* were found to largely cancel while the same cannot be expected for steps 3.2.*i.* and 3.2.*iii.*

Scheme 3.2. N₂ insertion into the Mo-CH₃ bond.

One other obstacle in the task of evaluating the thermochemistry of organometallic diazo complexes is the uncertainties in experimental data on the enthalpy of formation of diazomethane itself. Recent computational results suggest an enthalpy of formation of $\approx 65 \text{ kcal mol}^{-1}$ for $\text{CH}_2\text{N}_2(\text{g})$.⁷⁰ This is considerably different than existing experimental data of $\approx 50 \text{ kcal mol}^{-1}$.⁷¹

For practical organometallic chemistry $\text{N}_2\text{CHSiMe}_3$ provides a useful starting material and an alternative to the more hazardous diazomethane. Based on the process pioneered by Seyferth and coworkers,⁷² heptane solutions of $\text{N}_2\text{CHSiMe}_3$ are commercially available and stable for long periods of time. Reactions analogous to that shown in eqn. 3.4 were originally reported by Lappert for the trimethylsilyl derivative.⁷³ A stable $\text{N}_2\text{CHSiMe}_3$ adduct of Co(I) was recently reported by Caulton and coworkers,⁷⁴ while the structure and reactions of $\text{Cp}^*_2\text{Ti}(\eta^2\text{-N}_2\text{CHSiMe}_3)$ ($\text{Cp}^* = \eta^5\text{-C}_5\text{Me}_5$) were investigated by Bergman and coworkers.⁷⁵ The catalytic conversion of trimethylsilyl diazomethane to the corresponding ketene by dicobalt octacarbonyl was recently reported.⁷⁶

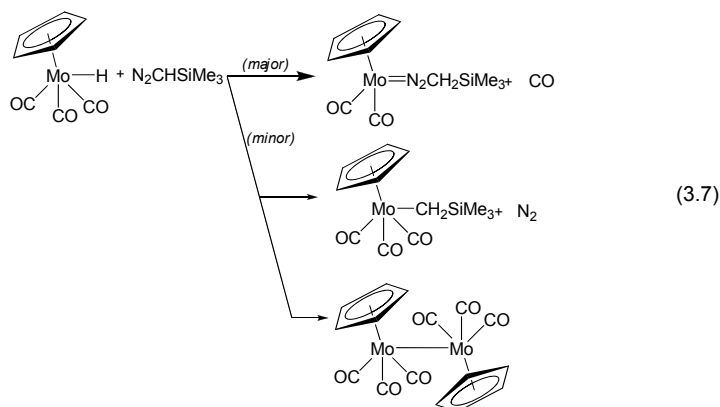
This chapter reports thermodynamic, kinetic, and computational data^{xv, 77} for the reaction of $\text{HMo}(\text{CO})_3\text{Cp}$ (HMP) with $\text{N}_2\text{CHSiMe}_3$ to yield $\text{Mo}(\text{CO})_2(\text{N}_2\text{CH}_2\text{SiMe}_3)_3\text{Cp}$ and CO. Also reported is a catalytic reaction in which $\text{N}_2\text{CHSiMe}_3$ is coordinated to $\text{M}(\text{CO})_3(\text{PR}_3)_2$ ($\text{M} = \text{Mo}, \text{W}$; $\text{R} = \text{Cy}, \text{}^i\text{Pr}$) and subsequently reacts with 2 equivalents of $\text{HMo}(\text{CO})_3\text{Cp}$. The bound diazo ligand is hydrogenated to form molecular nitrogen and TMS ($\text{TMS} = \text{Si}(\text{CH}_3)_4$) while the molybdenum hydride compound is converted to the dimer $[\text{Mo}(\text{CO})_3\text{Cp}]_2$ (Mp_2). In addition to probing the mechanisms of these reactions, reaction energetics relative to insertion of dinitrogen into the metal-alkyl bond are investigated from both theoretical and experimental vantages. Finally crystallographic structure data is reported for the complex $\text{W}(\text{CO})_2(\text{N}_2\text{CH}_2\text{SiMe}_3)\text{Cp}$.

3.2 Results and Discussion

One goal of this work was to determine the thermochemical barriers to N_2 insertion as shown in Scheme 3.2 comparable to those already reported for CO insertion as shown in Scheme 3.1. In addition it was sought to compare the bonding capabilities of NO and N_2R as ligands. For N_2 insertion to be favorable, a strong bond between the metal and the N_2R fragment is required. As discussed later, unlike $\bullet\text{C}(\text{O})\text{R}$ or $\bullet\text{NO}$, the $\bullet\text{N}_2\text{R}$ fragment itself is unstable. A blend of theory and experiment is required to analyze the bonding. In order to start investigations in this area we initially sought conditions to achieve a clean reaction of $\text{HMo}(\text{CO})_3\text{Cp}$ with $\text{N}_2\text{CHSiMe}_3$ to yield a single product.

^{xv} Computational results were provided by Paul von Ragué Schleyer and Henry F. Schaefer III from the University of Georgia and by Tamas Kégl and Ferenc Ungváry from the University of Pannonia. (see ref 77 for full details)

Kinetics of the reaction of $\text{N}_2\text{CHSiMe}_3$ with $\text{HM}(\text{CO})_3(\text{C}_5\text{R}_5)$ ($\text{M} = \text{Mo}, \text{W}$; $\text{R} = \text{H}, \text{CH}_3$). Reaction of $\text{HMo}(\text{CO})_3\text{Cp}$ with excess $\text{N}_2\text{CHSiMe}_3$ resulted in complete consumption of metal hydride. The reactions were readily followed by quantitative FTIR spectroscopic study.^{xvi}



The product distribution of the reaction of $\text{HMo}(\text{CO})_3\text{Cp}$ with $\text{N}_2\text{CHSiMe}_3$ was found to depend mainly on the solvent in which the reaction was carried out. This relationship between product distribution and solvent is shown below in Table 3.1.

Table 3.1. Relative product distribution based on solvent for the reaction of $\text{HMo}(\text{CO})_3\text{Cp}$ with $\text{N}_2\text{CHSiMe}_3$.

Solvent	$\text{Mo-N}_2\text{CH}_2\text{SiMe}_3^a$	$\text{Mp-CH}_2\text{SiMe}_3^b$	$[\text{Mo}(\text{CO})_3\text{Cp}]_2$
Heptane	80%	10%	10%
Toluene	95%	5%	0%
THF	100%	0%	0%
$\text{Mo}(\text{PR}_3)_2(\text{CO})_3/\text{tol}^c$	0%	0%	100%

^a $\text{Mo} = \text{Mo}(\text{CO})_2\text{Cp}$. ^b $\text{Mp} = \text{Mo}(\text{CO})_3\text{Cp}$. ^c $\text{R} = \text{}^i\text{Pr}$, Cy ($\text{}^i\text{Pr} = \text{CH}(\text{CH}_3)_2$; $\text{Cy} = \text{C}_6\text{H}_{11}$.)

^{xvi} Products were identified qualitatively and quantitatively by FTIR bands as assigned in Appendix B Table B.1 and verified by comparison to authentic samples of recrystallized $[\text{Mo}(\text{CO})_3\text{Cp}]_2$ and $\text{Mo}(\text{CH}_2\text{SiMe}_3)(\text{CO})_2\text{Cp}$ (independently prepared by reaction of $\text{NaMo}(\text{CO})_3\text{Cp}$ and $\text{Cl-CH}_2\text{SiMe}_3$). Peak positions assigned to the diazo compounds are in agreement with those originally reported by Lappert and Poland (see ref. 73.)

The reaction of $\text{HMo}(\text{CO})_3\text{Cp}$ with $\text{N}_2\text{CHSiMe}_3$ was found to be first order in metal complex in all three solvents studied. Under pseudo first order conditions^{xvii} with excess $\text{N}_2\text{CHSiMe}_3$ the rates were also seen to have a solvent dependence as shown in Figure 3.1. The plots of $\ln [A-A_\infty]$ versus time were linear through at least two half lives. The rate of reaction in toluene was roughly 17 times faster while the reaction in THF was observed to be approximately 59 times faster than the measured rate in heptane. As shown in Table 3.1 the reaction also produces more diazo complex as product in going from heptane to toluene to THF. No significant perturbation of the reaction rate was observed when the reaction was performed under an atmosphere of CO (as opposed to an atmosphere of Ar). The expected first order dependence on $\text{N}_2\text{CHSiMe}_3$ was confirmed in heptane solution where pseudo first order reactions at different $[\text{N}_2\text{CHSiMe}_3]$ (0.056 and 0.385 M) yielded the same derived rate constants within $\approx 10\%$ experimental error. The rates of reaction of $\text{HMo}(\text{CO})_3\text{Cp}$ and $\text{DMo}(\text{CO})_3\text{Cp}$ in heptane were also found to be the same within experimental error. As discussed later, this is attributed to H/D exchange between $\text{DMo}(\text{CO})_3\text{Cp}$ and the diazoalkane. The rates of reaction of $\text{HMo}(\text{CO})_3\text{Cp}^*$ and $\text{HW}(\text{CO})_3\text{Cp}$ were found to be slower than the reaction of $\text{HMo}(\text{CO})_3\text{Cp}$. Derived rate constants for eqn. 3.7 are summarized in Table 3.2. An Eyring plot of the data in heptane

^{xvii} The pseudo first order conditions were typically in the range of 5.7 to 10 fold excess of $\text{N}_2\text{CHSiMe}_3$ and the average concentration during the run was utilized. For a 5.75 fold excess, during two half lives the final $\text{N}_2\text{CHSiMe}_3$ will drop to 5.0. The average of 5.38 will thus vary by $\approx .38/5.38 \approx 7\%$ during the course of the run. Somewhat surprisingly this did not show up as a systematic deviation in fitting data to a straight line in $\ln [A-A_\infty]$ versus time compared to reactions in which a 10 fold excess of ligand was used. The lower amounts were used to slow down the reaction and also conserve the amount of diazoalkane used.

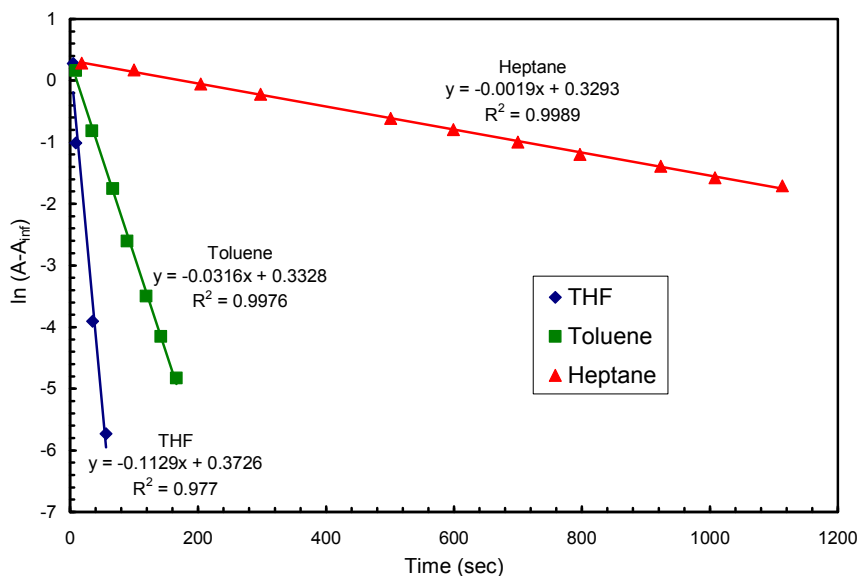


Figure 3.1. First order plots of $\ln(A - A_{\text{inf}})$ versus time for the reaction of $\text{HMo}(\text{CO})_3\text{Cp}$ (0.01 M) with $\text{N}_2\text{CHSiMe}_3$ (0.056 M) in heptane, toluene, and THF at 0°C .

Table 3.2. Rate constants for reaction of metal hydrides and trimethylsilyldiazomethane.^a

HML_n	T ($^\circ\text{C}$)	Solvent	k ($\text{M}^{-1}\text{s}^{-1}$)
$\text{HMo}(\text{CO})_3\text{Cp}$	0	Heptane	0.034 ± 0.002
$\text{HMo}(\text{CO})_3\text{Cp}$	0	Toluene	0.56 ± 0.02
$\text{HMo}(\text{CO})_3\text{Cp}$	0	THF	2.0 ± 0.3
$\text{HMo}(\text{CO})_3\text{Cp}$	13	Heptane	0.085 ± 0.007
$\text{DMo}(\text{CO})_3\text{Cp}$	13	Heptane	0.082 ± 0.005
$\text{HMo}(\text{CO})_3\text{Cp}$	28	Heptane	0.22 ± 0.01
$\text{HMo}(\text{CO})_3\text{Cp}^*$	28	Heptane	0.011 ± 0.001
$\text{HW}(\text{CO})_3\text{Cp}$	28	Heptane	0.0039 ± 0.0002

^a Reactions were performed under pseudo-first order conditions with $\text{N}_2\text{CHSiMe}_3$ in excess and obey the rate law $-\text{d}[\text{HML}_n]/\text{dt} = k[\text{HML}_n][\text{N}_2\text{CHSiMe}_3]$. First order dependence on the metal-hydride complex was found for all data. First order dependence in $\text{N}_2\text{CHSiMe}_3$ was confirmed for $\text{HMo}(\text{CO})_3\text{Cp}$ in heptane only; other metal-hydride data are for comparative purposes.

solution is shown in Appendix B Figure B.1 ($\Delta H^\ddagger = + 10.1 \pm 2.0 \text{ kcal mol}^{-1}$; $\Delta S^\ddagger = - 19.3 \pm 3.0 \text{ cal mol}^{-1} \text{ K}^{-1}$.)

Reaction of $\text{DMo}(\text{CO})_3\text{Cp}$ with $\text{N}_2\text{CHSiMe}_3$. Attempts were made to probe the kinetic isotope effect by investigating reactions of $\text{HMo}(\text{CO})_3\text{Cp}$ and $\text{DMo}(\text{CO})_3\text{Cp}$ (85 ± 10 isotopic enrichment) under comparable conditions. As shown in Figure 3.2, these data yielded virtually identical rates and appeared to show no kinetic isotope effect within experimental error.

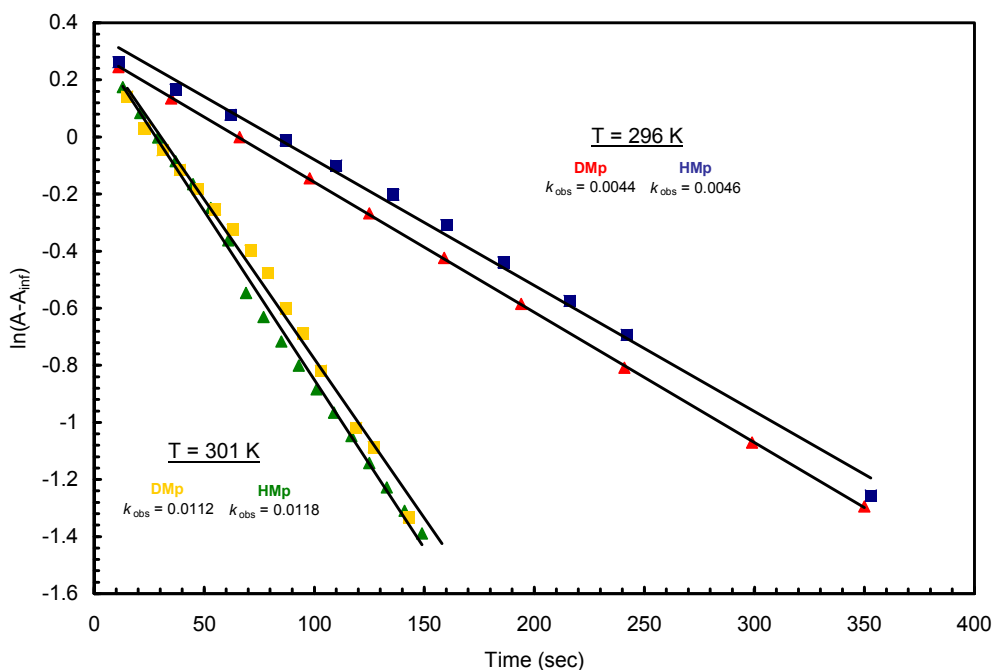
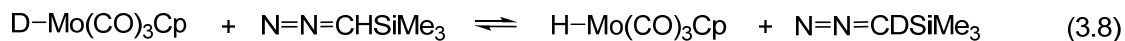
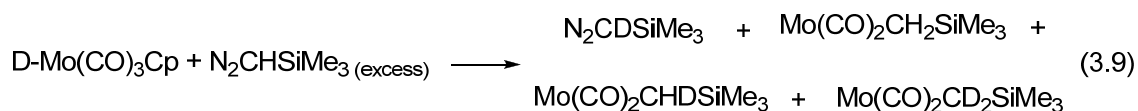


Figure 3.2. Rates of reaction of $\text{HMo}(\text{CO})_3\text{Cp}$ (0.0057M) and $\text{DMo}(\text{CO})_3\text{Cp}$ (0.0057 M) with $\text{N}=\text{N}=\text{CHSiMe}_3$ (0.056 M), isotopic enrichment $85 \pm 10\%$) at 286 K and 301 K in heptane showing nearly identical rates of reaction; $k(\text{H})/k(\text{D}) = 1.04 \pm 0.05$ ($\text{HMP} = \text{HMo}(\text{CO})_3\text{Cp}$; $\text{DMp} = \text{DMo}(\text{CO})_3\text{Cp}$)

The negligible value of the kinetic isotope effect $k(\text{H})/k(\text{D}) = 1.04 \pm 0.05$ prompted NMR investigations of the reaction to see if H/D exchange occurred as shown in eqn. 3.8.



In the limiting case that H/D exchange was slow compared to the rate of eqn. 3.8, the use of $\text{DMo}(\text{CO})_3\text{Cp}$ with 85 % labeling would produce the $\text{Mo}(\text{N}_2\text{CHDSiMe}_3)(\text{CO})_2\text{Cp}$ complex in the ratio of 85:15 (HD to HH). That is, the product distribution would be independent of the presence of excess $\text{N}_2\text{CHSiMe}_3$ and conversely, solely dependent upon the extent to which the $\text{HMo}(\text{CO})_3\text{Cp}$ was isotopically labeled as $\text{DMo}(\text{CO})_3\text{Cp}$. However if the H/D exchange is extremely rapid compared to the rate of eqn. 3.7 then full randomization of H/D would be expected. This would result in a statistical mixture of products as shown in eqn. 3.9.



Control experiments showed that once formed the diazo complex did not undergo exchange with $\text{DMo}(\text{CO})_3\text{Cp}$. Experiments were performed in heptane at 286 K by the addition of varying ratios of $\text{N}_2\text{CHSiMe}_3$ to $\text{DMo}(\text{CO})_3\text{Cp}$, allowing the reaction to go to completion and then evacuating the reaction solution to dryness.^{xviii,78} Samples were then redissolved in C_6D_6 and analyzed by ^1H NMR and FTIR spectroscopy. The ratio of (H,H):(H,D):(D,D) products were found to depend upon the relative concentrations of the reagents (see Appendix B, Figure B.2), implying that exchange as shown in eqn. 3.9 was in fact competitive with the overall reaction itself. More detailed analyses of these data

^{xviii} (a) The complex $\text{Mo}(\text{CO})_2(\text{N}_2\text{CH}_2\text{SiMe}_3)\text{Cp}$ shows a singlet at 2.92 ppm and the complex $\text{Mo}(\text{CO})_2(\text{N}_2\text{C}(\text{H})(\text{D})\text{SiMe}_3)\text{Cp}$ shows a broad unresolved triplet at 2.90 ppm (in C_6D_6). However, analysis of these data required evacuation which led to some side products. Since $\text{N}_2\text{CHSiMe}_3$ was added in hexane and the reaction done in heptane, NMR analysis required evacuation to dryness and reconstituted in C_6D_6 . During concentration some decomposition was observed to occur, particularly for $\text{Mo}(\text{CO})_3(\text{CH}_2\text{SiMe}_3)\text{Cp}$. The alkyl product can react further with $\text{HMo}(\text{CO})_3\text{Cp}$ (see: ref 78).

(including both kinetic and equilibrium isotope effects)⁷⁹ were not attempted beyond the mechanistic observation of more rapid H/D exchange than overall reaction.

Spectroscopic detection of an intermediate complex in heptane solution.

Typical spectroscopic data for the overall reaction in heptane solution are shown in Figure 3.3. These data show a smooth decay in the bands assigned to $\text{HMo}(\text{CO})_3\text{Cp}$ and concomitant buildup of bands of the major product $\text{Mo}(\text{CO})_2(\text{N}_2\text{CH}_2\text{SiMe}_3)\text{Cp}$, as well as the minor products $\text{Mo}(\text{CO})_3(\text{CH}_2\text{SiMe}_3)\text{Cp}$ and $[\text{Mo}(\text{CO})_3\text{Cp}]_2$. Expansion of the spectroscopic data during reaction in heptane at low temperature reveals bands at 2017 and 1930 cm^{-1} assigned to an intermediate complex (see Figure 3.4).

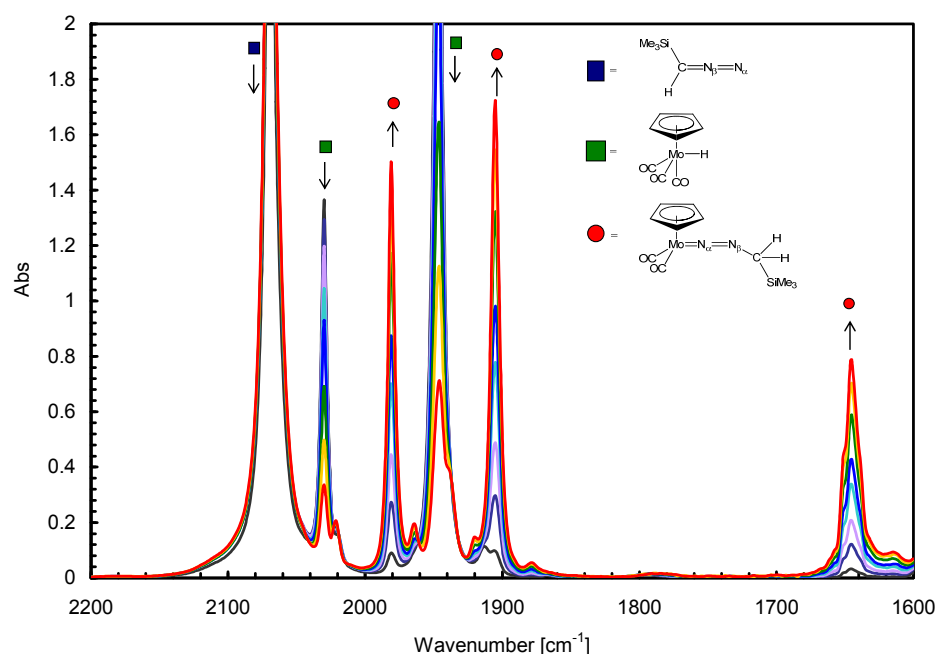


Figure 3.3. Typical sequential FTIR spectra for the reaction of $\text{Mo}(\text{CO})_3\text{Cp}$ with $\text{N}_2\text{CHSiMe}_3$. Reaction was carried out in heptane at 273 K. (See Appendix B Table B.1 for band assignments)

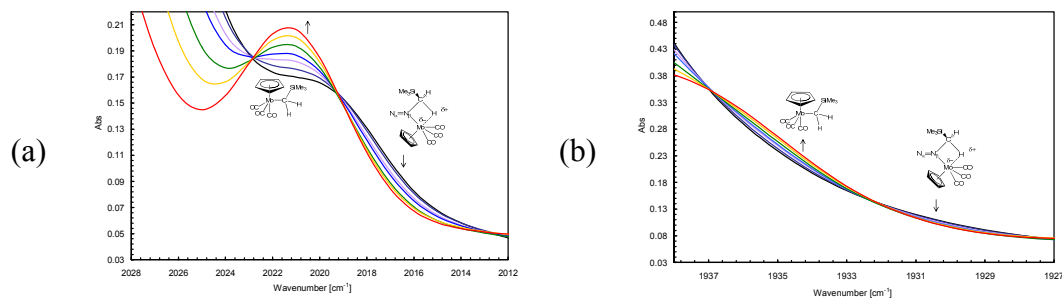


Figure 3.4. Enhanced view of FTIR spectral changes due to the increase of the alkyl side product $\text{Mo}(\text{CHSiMe}_3)(\text{CO})_3\text{Cp}$ and the decay of the intermediate complex.

Following a rise time during the first spectrum, the bands near 2017 and 1930 cm^{-1} reach a maximum and then decay during the course of the reaction. A plot of the absorbance at 2017 cm^{-1} for the intermediate versus 2030 cm^{-1} for $\text{HMo}(\text{CO})_3\text{Cp}$ showed reasonable linear behavior over the course of the reaction as shown in Figure 3.5.

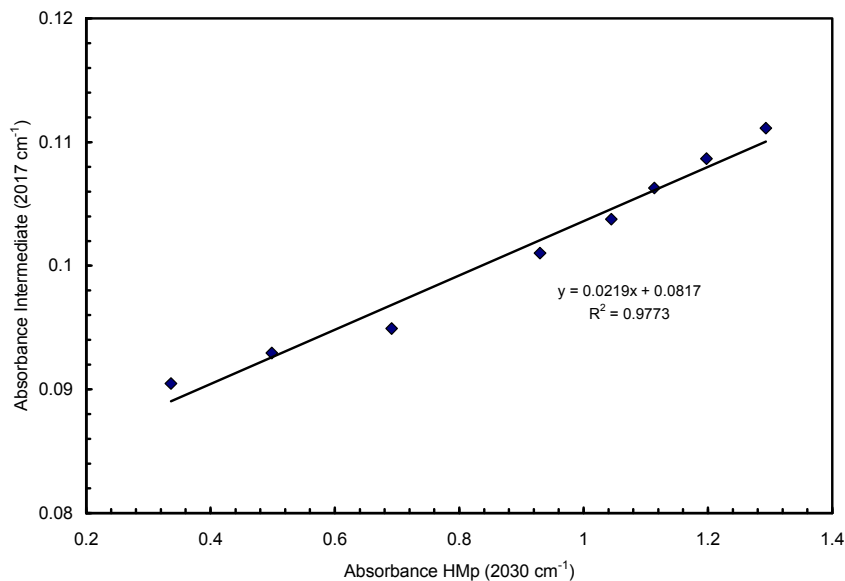
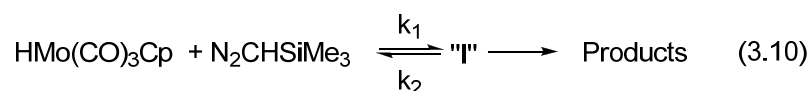


Figure 3.5. Plot of Absorbance at 2017 cm^{-1} of proposed intermediate versus Absorbance at 2030 cm^{-1} of $\text{HMo}(\text{CO})_3\text{Cp}$ for data in Figure 3.3 showing approximate linear relationship between these two bands over the reaction time.

At higher concentrations of $\text{N}_2\text{CHSiMe}_3$ the bands assigned to the intermediate were observed to increase. These data are in keeping with formation of a pre-equilibrium complex between $\text{N}_2\text{CHSiMe}_3$ and $\text{HMo}(\text{CO})_3\text{Cp}$ which goes on to products as shown in eqn. 3.10:



The intermediate, "I", is formulated as $[\text{Me}_3\text{SiCH}_2\text{-N}_\beta\text{=N}_\alpha^{\delta+}][\delta^-\text{Mo}(\text{CO})_3\text{Cp}]$ (*vide infra.*)

Experimentally and Computationally determined structure of $\text{W}(\text{CO})_2(\text{N}_2\text{CH}_2\text{SiMe}_3)\text{Cp}$. The structure of $\text{W}(\text{CO})_2(\text{N}_2\text{CH}_3)\text{Cp}$ has been reported by Hillhouse and Herrmann.⁸⁰ Determination of the structure of the analogous trimethylsilyl substituted derivative was of interest to see if any significant differences occurred which might be indicative of bond strength differences. Within experimental error there are no significant differences. Single crystals of this complex were grown by slow recrystallization from heptane. The structure is shown in Figure 3.6 (full structural data is provided in Appendix B Table B.2). The W-N(1)-N(2) angle of 174.3° and the N(1)-N(2)-C(8) angle of 117.4° are consistent with sp and sp^2 hybridizations on N(1) and N(2) respectively and are consistent with the formulation $\text{W}=\text{N}=\text{N}-\text{CH}_2\text{SiMe}_3$.

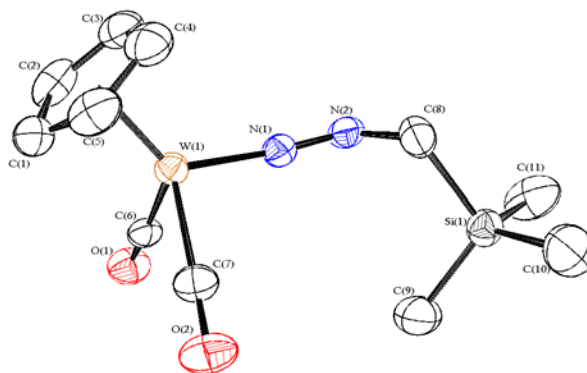


Figure 3.6. ORTEP drawing of $W(CO)_2(N_2CH_2SiMe_3)Cp$ with ellipsoids at 35% probability. Selected bond distances (Å) and angles (deg): W-N1 1.862(4), N1-N2 (1.207(6), N2-C8 1.471(7), C8-Si1 1.898(6), W1-N1-N2 174.3(4), N1-N2-C8 117.4(5), N2-C8-Si 1110.6(4). Structural data collected and interpreted by Brian Scott from Los Alamos National Laboratory.

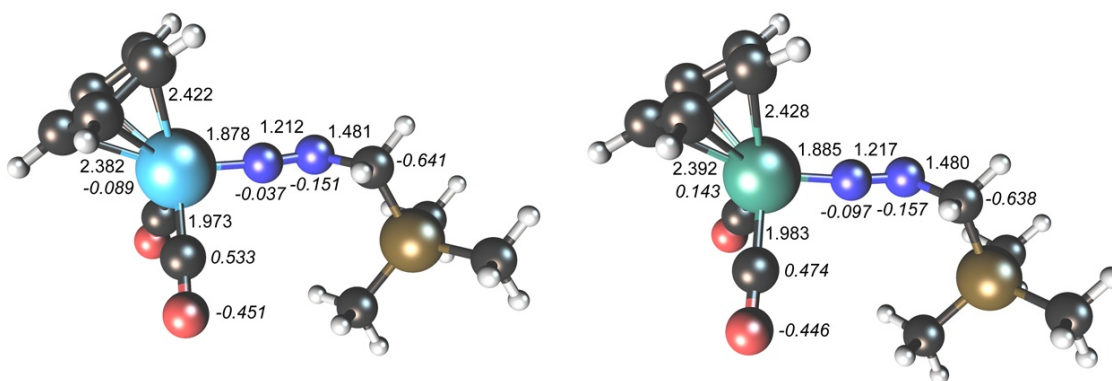
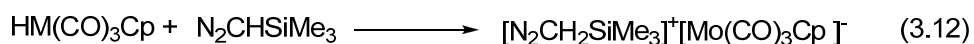


Figure 3.7. Computed structure of $Mo(CO)_2(N_2CH_2SiMe_3)Cp$ (left) and $W(CO)_2(N_2CH_2SiMe_3)Cp$ (right). Bond lengths are given in angstrom, natural charges are written in italics. Computations involving these structures were performed by Ferenc Ungaváry and Tamás Kégl

Computed structures at the BP86 level for $M(CO)_2(N_2CH_2SiMe_3)Cp$ ($M = Mo, W$) at the BP86 level are shown in Figure 3.7. The structures were computed at the BP86 level by Ferenc Ungaváry and Tamás Kégl. The theoretical bond lengths for the W complex are in good agreement with the solid state structure shown in Figure 3.6. The computed geometries of $Mo(CO)_2(N_2CH_2SiMe_3)Cp$ and $W(CO)_2(N_2CH_2SiMe_3)Cp$ are very similar. Conversely, the charge distribution shows a notable difference between

them as molybdenum carries a negative charge and tungsten carries a partial positive charge in the analogous complex. Accordingly, NBO analysis reveals some difference in the metal-nitrogen bond polarization: the bond is 56% polarized towards nitrogen in $\text{Mo}(\text{CO})_2(\text{N}_2\text{CH}_2\text{SiMe}_3)\text{Cp}$ and 59% polarized towards nitrogen in $\text{W}(\text{CO})_2(\text{N}_2\text{CH}_2\text{SiMe}_3)\text{Cp}$. The largest contributions in the metal-nitrogen NBOs involve the valence d_{xz} natural atomic orbitals (NAOs) of the transition metals and the $2p_z$ NAOs of nitrogen. The Wiberg bond indices are 1.295 for $\text{Mo}(\text{CO})_2(\text{N}_2\text{CH}_2\text{SiMe}_3)\text{Cp}$ and 1.325 for $\text{W}(\text{CO})_2(\text{N}_2\text{CH}_2\text{SiMe}_3)\text{Cp}$.

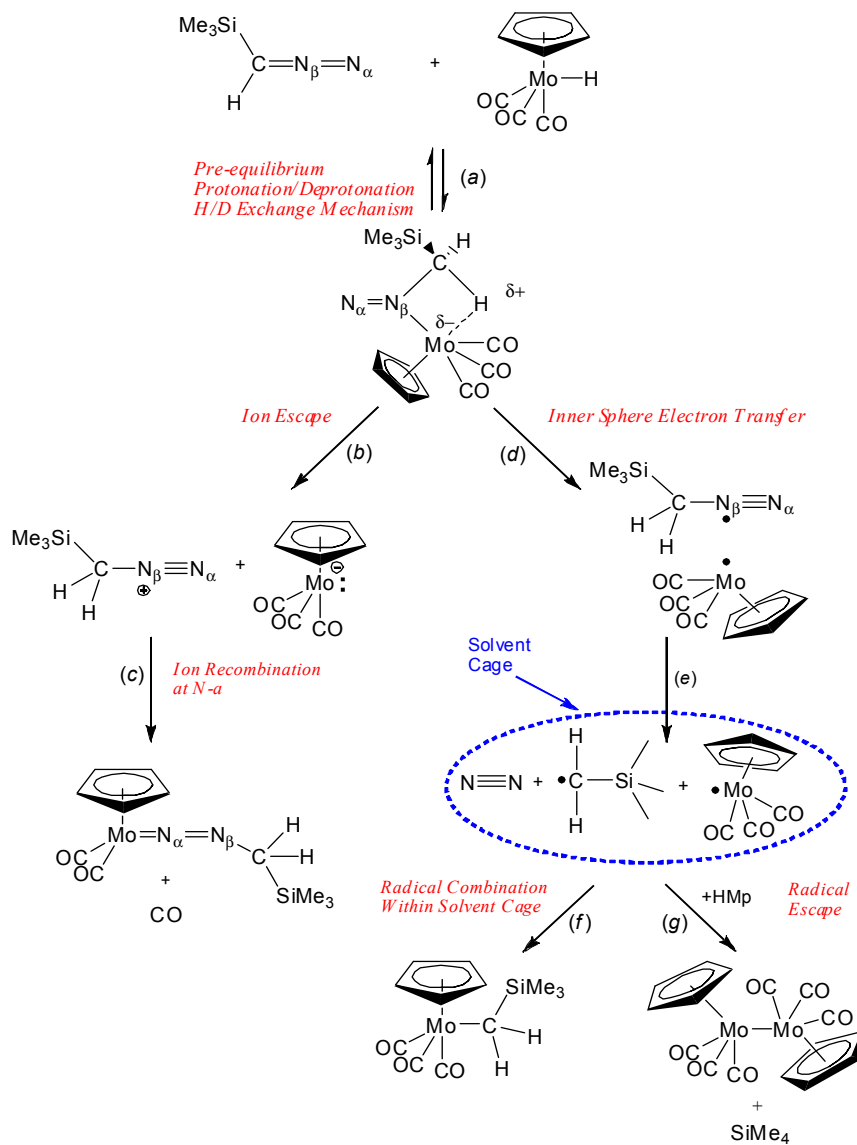
Proposed mechanism for reaction of $\text{HMo}(\text{CO})_3\text{Cp}$ with $\text{N}_2\text{CHSiMe}_3$. The lack of an inhibiting influence of CO on the rate of reaction discounted steps involving ligand displacement of carbon monoxide by diazo. However, it does suggest either H atom transfer as shown in eqn. 3.11 or proton transfer as shown in eqn. 3.12 as the initial step of the reaction.



Theoretical calculations^{xix} at the B3LYP level showed that the C–H bond strength formed in $\cdot\text{N}_2\text{CH}_2\text{SiMe}_3$ (+53 kcal mol⁻¹) is weaker than the bond broken in $\text{H–Mo}(\text{CO})_3\text{Cp}$ (+66 kcal mol⁻¹)⁸¹ by ≈ 13 kcal mol⁻¹. The experimentally observed enthalpy of activation of $+10.1 \pm 2.0$ kcal mol⁻¹ is lower than this value but is still similar enough that the hydrogen atom transfer shown in eqn. 3.11 cannot be ruled out.

^{xix} Computational results were provided by Paul von Ragué Schleyer and Henry F. Schaefer III from the University of Georgia (see ref 77 for full details)

Scheme 3.3. Proposed mechanism for the reaction of $\text{HMo}(\text{CO})_3\text{Cp}$ with $\text{N}_2\text{CHSiMe}_3$ producing diazo, alkyl, and metal-metal dimer products.



Key findings were that the H/D exchange was faster than the overall reaction itself and that both the rate and product distribution were solvent dependent. A plausible mechanism consistent these observations in addition to the other previously discussed observations is shown in Scheme 3.3.

The first step involves formation of an initial adduct by rapid proton transfer from the metal hydride to the carbene carbon⁸² and formation of the proposed key intermediate

complex. The intermediate can be viewed either as a tight ion pair or as an η^1 -diazo complex bonded to N_β . The reversible nature of the protonation/deprotonation step accounts for the H/D scrambling that is observed. The computed structure, provided by Tamas Kégl and Ferenc Ungváry, for this intermediate is shown in Figure 3.8.

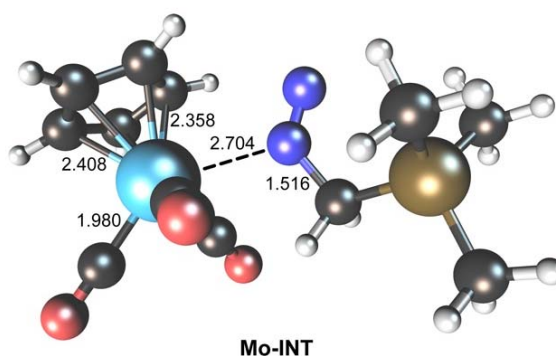


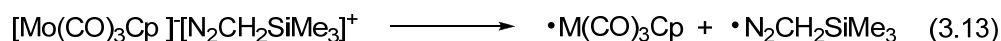
Figure 3.8. Theoretically calculated structure for the intermediate containing a loose Mo-N bond following the initial proton transfer. (All values given in Å.)

Separation of the ion pair and recombination at N_α would result in formation of the diazo complex which is the major reaction product. This corresponds roughly to the reaction shown in eqn. 3.1 but in which the arenediazonium salt is replaced with the alkyl diazonium cation formed by protonation of trimethylsilyldiazomethane. The increased tendency to dissociate to ion pairs as more coordinating solvents are used is in keeping with the fact that in going from heptane to toluene to THF the reaction becomes both faster and shows fewer side products.

The products of diazoalkane protonations have long been postulated to depend on the rate of escape from the solvent cage of initial ion pairs formed. In studies of the reactions in alcohol of diazoalkanes with benzoic acid, the product ratio has been interpreted in terms of the relative rates of escape of the ions from the initial ion pair, with ester product arising from a tight ion pair and ether product from escape.⁸³ This

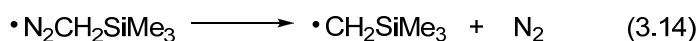
ratio was found to not be temperature dependent but to depend critically on solvent polarity. The role of cage effects in photochemical reactions of $[\text{W}(\text{CO})_3\text{Cp}]_2$ and PR_3 ligands has also recently been studied.⁸⁴

Retention of the initial ion pair (favored in more non-polar solvents), however, could result in electron transfer to yield radical products as shown in eqn. 3.13 (step 3.3.e).



This corresponds to the net reaction for H atom transfer and is kinetically indistinguishable from eqn. 3.11 occurring directly. The fact that the computed activation energy for H atom transfer in eqn. 3.11 is only marginally higher than the observed activation energy supports the close balance between these two processes.

Computational studies performed by Schleyer and Schaefer suggested that formation of a free $\bullet\text{N}_2\text{CH}_2\text{SiMe}_3$ radical would be expected to result in rapid expulsion of N_2 , as shown in eqn. 3.14. (step 3.3.d)

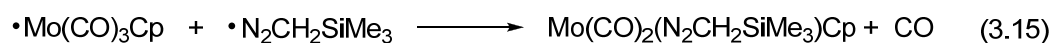


The radicals $\bullet\text{CH}_2\text{SiMe}_3$ and $\bullet\text{Mo}(\text{CO})_3\text{Cp}$ would then be free to form the alkyl product if they combine directly. Reaction of $\bullet\text{CH}_2\text{SiMe}_3$ and $\text{HMo}(\text{CO})_3\text{Cp}$ in solution would be expected⁸⁵ to rapidly form SiMe_4 and $\bullet\text{Mo}(\text{CO})_3\text{Cp}$. Combination of two $\bullet\text{Mo}(\text{CO})_3\text{Cp}$ radicals will rapidly form $[\text{Mo}(\text{CO})_3\text{Cp}]_2$. The solvent dependence on reaction products as well as spectroscopic detection of an intermediate appears to be in accord with these observations.

The mechanism in Scheme 3.3 is proposed to involve a polar addition of H^+ in a reversible first step. This might be expected to depend on the pK_a of the metal hydride.

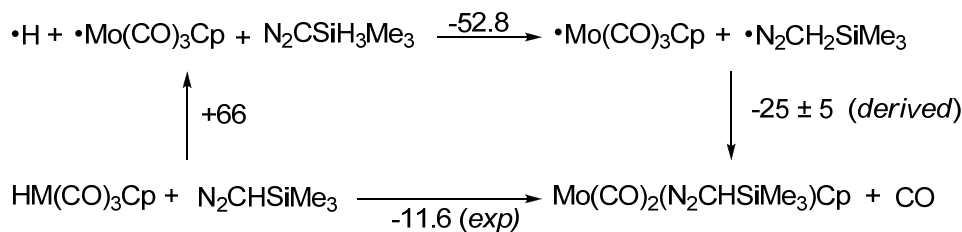
Compared to $\text{HMo}(\text{CO})_3\text{Cp}$ ($\text{pK}_a = 6.4$; H_2O), $\text{HMo}(\text{CO})_3\text{Cp}^*$ ($\text{pK}_a = 9.6$; H_2O) and $\text{HW}(\text{CO})_3\text{Cp}$ ($\text{pK}_a = 8.6$; H_2O) are both weaker acids.⁸⁶ Investigations of these two other hydrides showed they reacted more slowly. At $T = 28\text{ }^\circ\text{C}$ $\text{HMo}(\text{CO})_3\text{Cp}^*$ was found to react approximately 20 times more slowly and $\text{HW}(\text{CO})_3\text{Cp}$ approximately 56 times more slowly than $\text{HMo}(\text{CO})_3\text{Cp}$. It is worth noting that in reactions of $\text{HMo}(\text{CO})_3\text{Cp}^*$ both alkyl and metal-metal dimer side products are formed as was the case for $\text{HMo}(\text{CO})_3\text{Cp}$. However, reactions of $\text{HW}(\text{CO})_3\text{Cp}$ with $\text{N}_2\text{CHSiMe}_3$ in heptane produced exclusively $\text{W}(\text{CO})_3(\text{CH}_2\text{SiMe}_3)\text{Cp}$ as a side product. $[\text{W}(\text{CO})_3\text{Cp}]_2$ was not produced in any detectable amount.

Thermochemistry of the formation of $\text{Mo}(\text{CO})_2(\text{N}_2\text{CH}_2\text{SiMe}_3)\text{Cp}$. The enthalpy of the reaction of $\text{HMo}(\text{CO})_3\text{Cp}$ with $\text{N}_2\text{CHSiMe}_3$ was measured in THF solution by solution calorimetry at 272 K. The resultant value of $-9.5 \pm 1.1\text{ kcal mol}^{-1}$ based on solid $\text{HMo}(\text{CO})_3\text{Cp}$ yields a value with all species in solution of $-11.6 \pm 1.2\text{ kcal mol}^{-1}$. Estimated data in toluene solution were found to be in agreement with this value.



The heat of reaction was in turn used to estimate the enthalpy of eqn. 3.15. This value was calculated using the thermochemical cycle shown in Scheme 3.4. The combination of the Mo-H bond strength in $\text{HMo}(\text{CO})_3\text{Cp}$ of 66 kcal mol^{-1} ,⁸¹ the enthalpy of $\bullet\text{H}$ addition to $\text{N}_2\text{CHSiMe}_3$ of $-52.8\text{ kcal mol}^{-1}$, with the experimental net enthalpy of reaction of $-11.6 \pm 1.2\text{ kcal mol}^{-1}$ allowed for the estimation of the enthalpy of displacement of CO by $\bullet\text{N}_2\text{CH}_2\text{SiMe}_3$. A derived value of $\Delta H_{\text{rxn}} = 25.5 \pm 5\text{ kcal mol}^{-1}$ for was determined for eqn 3.15.

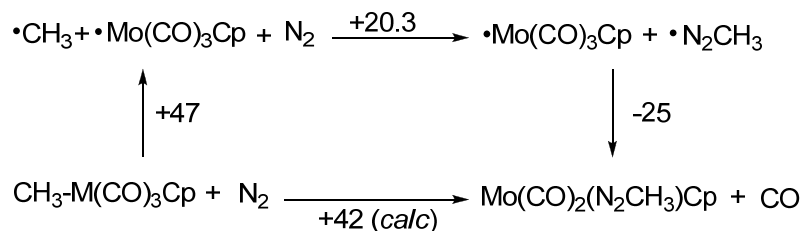
Scheme 3.4. Thermochemical cycle used to calculate the enthalpy of the homolytic bond formation between $\bullet\text{Mo}(\text{CO})_3\text{Cp}$ and $\bullet\text{N}_2\text{CHSiMe}_3$ (all values in kcal mol^{-1} .)



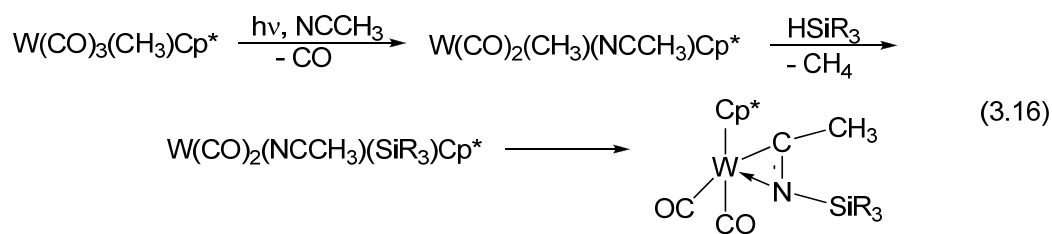
This value overlapped within experimental error with the value that was computed independently by Kégl and Ungváry for the difference between the Mo-CO and Mo=N₂CHSiMe₃ (22.3 kcal mol^{-1} .) Additionally, this value can also be compared to data for eqn. (3.2) ($\Delta\text{H} = -33.2 \pm 1.8 \text{ kcal mol}^{-1}$) where an $\bullet\text{N}=\text{O}$ radical displaces CO in the corresponding $\bullet\text{Cr}(\text{CO})_3\text{Cp}^*$ complex. There is a larger energy gap between $\bullet\text{N}=\text{O}$ and CO for Cr than between $\bullet\text{N}_2\text{CH}_2\text{SiMe}_3$ and CO for Mo. Work is in progress in our laboratory to expand data in this series to allow more accurate assessment of bond strength trends in these and related complexes.

The data generated here can be further used to estimate the energy required for N₂ insertion into the Mo-R bond for R-Mo(CO)₃Cp as shown previously in Scheme 3.2. In spite of the strong Mo-diazo bond formed, the insertion is predicted to be uphill by $\approx 42 \pm 5 \text{ kcal mol}^{-1}$ (Scheme 3.5.) This estimate was made using the H₃C-Mo BDE of 47 kcal mol^{-1} in Mo(CO)₃(CH₃)Cp,⁸⁷ and the computed endothermic addition of an alkyl radical to N₂ of 20 kcal mol^{-1} (*vide infra*), together with the value of $-25 \pm 5 \text{ kcal mol}^{-1}$ estimated from Scheme 3.4 for the enthalpy of displacement of CO by $\bullet\text{N}_2\text{CH}_2\text{SiMe}_3$.

Scheme 3.5. Thermochemical cycle used to estimate the enthalpy of insertion of molecular nitrogen into the Mo-R bond of $\text{Mo}(\text{CO})_3(\text{CH}_3)\text{Cp}$ (all values in kcal mol^{-1} .)

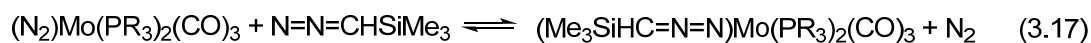


This suggests that prior photochemical loss of CO from $\text{R-Mo}(\text{CO})_3\text{Cp}$ would result in a nearly thermoneutral reaction since the Mo-CO bond is $\approx 40 \text{ kcal mol}^{-1}$.⁵⁶ In this regard, nitrile insertion has been recently reported to occur in the photochemical/thermal reaction sequence shown in eqn 3.16.⁸⁸

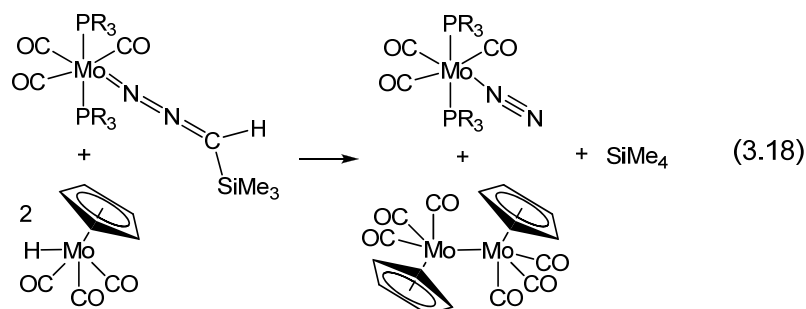


The observed $\text{N}\equiv\text{CR}$ insertion in this photochemically generated nitrile complex provides hope that the goal of analogous photochemical $\text{N}\equiv\text{N}$ insertion may not be out of reach. In the case of N_2 insertion, the final product would presumably be an η^1 -diazo complex rather than the η^2 binding motif observed for the nitrile product in eqn. 3.16.

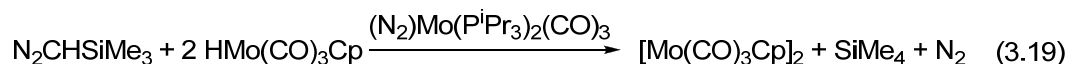
Reaction of 2 $\text{HMo}(\text{CO})_3\text{Cp}$ with $\text{N}_2\text{CHSiMe}_3$ in the presence of $\text{M}(\text{PR}_3)_2(\text{CO})_3$ ($\text{M} = \text{Mo}, \text{W}$; $\text{R} = \text{Cy}, \text{}^i\text{Pr}$): catalytic hydrogenation to SiMe_4 and $[\text{Mo}(\text{CO})_3\text{Cp}]_2$. Coordination of $\text{N}_2\text{CHSiMe}_3$ to $\text{M}(\text{PR}_3)_2(\text{CO})_3$ ($\text{M} = \text{Mo}, \text{W}$; $\text{R} = \text{Cy}, \text{}^i\text{Pr}$) was investigated. $\text{N}_2\text{CHSiMe}_3$ was found to be a better donor ligand than dinitrogen in terms of the equilibrium shown in eqn. 3.17 (see Chapter 4)



The relatively strong binding of $\text{N}_2\text{CHSiMe}_3$ to this complex prompted an investigation of how this would alter the nature of reactivity of $\text{N}_2\text{CHSiMe}_3$ with $\text{HMo}(\text{CO})_3\text{Cp}$. Surprisingly, the reaction occurred rapidly according to eqn. 3.18.

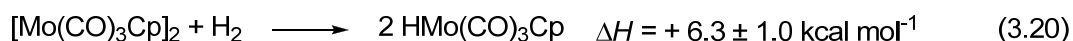


In stoichiometric reactions, the dinitrogen complex is observed as the final product of eqn. 3.18. However, since this is readily displaced by the stronger ligand $\text{N}_2\text{CHSiMe}_3$ reactions in which excess $\text{N}_2\text{CHSiMe}_3$ and $\text{HMo}(\text{CO})_3\text{Cp}$ are combined in the presence of trace amounts of $\text{M}(\text{PR}_3)_2(\text{CO})_3$ to yield the catalytic hydrogen transfer reaction shown in eqn. 3.19.



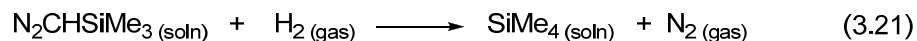
Such catalysis was also observed for other coordinatively unsaturated complexes of formula $\text{M}(\text{PR}_3)_2(\text{CO})_3$ ($\text{M} = \text{Mo}, \text{W}$; $\text{R} = \text{Cy}, ^i\text{Pr}$).

Enthalpy of hydrogenation of $\text{N}_2\text{CHSiMe}_3$. The reaction shown in eqn. 3.19 provided a means to determine the enthalpy of formation of $\text{N}_2\text{CHSiMe}_3$. This is possible due to the fact that the enthalpy of eqn. 3.20 has previously been reported.⁸¹



Pure $\text{HMo}(\text{CO})_3\text{Cp}$ was used as the limiting reagent in the solution calorimetric studies. The selective nature of the catalysis by $\text{M}(\text{P}^i\text{Pr}_3)_2(\text{CO})_3$ ($\text{M} = \text{Mo}, \text{W}$) was verified in that quantitative conversion to only $[\text{Mo}(\text{CO})_3\text{Cp}]_2$ and SiMe_4 was observed. Production of

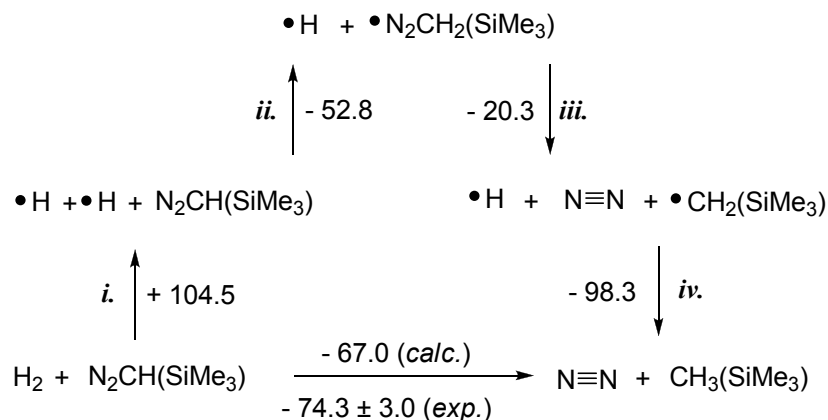
these products was confirmed by NMR spectroscopy. Values for the enthalpy of reaction were independent of whether the Mo or W analog was used as a catalyst. Adding the measured enthalpy of the reaction shown in eqn. 3.19, $-80.6 \pm 2.0 \text{ kcal mol}^{-1}$ to the reaction in eqn. 3.20 yields the enthalpy of the reaction in eqn. 3.21 to be equal to $-74.3 \pm 3.0 \text{ kcal mol}^{-1}$.



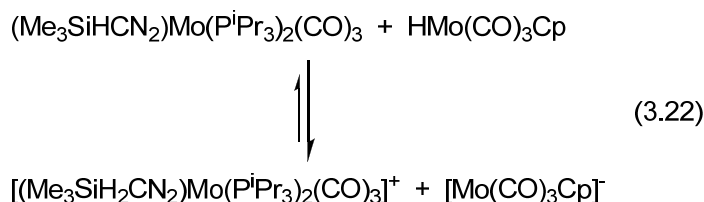
The enthalpies of mixing of both $\text{N}_2\text{CHSiMe}_3$ and SiMe_4 in toluene are expected to be less than 1 kcal mol^{-1} and largely cancel. The enthalpy of formation of $\text{N}_2\text{CHSiMe}_3$ is calculated as $5.8 \pm 3.0 \text{ kcal mol}^{-1}$ based on the standard enthalpy of formation of SiMe_4 of $-68.5 \text{ kcal mol}^{-1}$.⁸⁹

Computed enthalpy of hydrogenation of $\text{N}_2\text{CHSiMe}_3$. The experimental value for ΔH of eqn. 3.21 in solution phase ($-74.3 \pm 3.0 \text{ kcal mol}^{-1}$) can be compared to the computational result provided by Paul von Ragué Schleyer and Henry F. Schaefer III from the University of Georgia. A gas phase value of $-67 \text{ kcal mol}^{-1}$ was derived from B3LYP/6-311+G** level calculations. The elementary steps are shown in Scheme 3.6 below. Step *i.* in this scheme is simple dissociation of H_2 , and step *ii.* is addition of $\bullet\text{H}$ to $\text{N}=\text{N}=\text{C}(\text{H})\text{SiMe}_3$ to yield $\bullet\text{N}=\text{N}=\text{CH}_2\text{SiMe}_3$. Step *iii.* is a key step since it shows that dissociation of $\bullet\text{CH}_2\text{SiMe}_3$ from $\bullet\text{N}=\text{N}-\text{CH}_2\text{SiMe}_3$ is considerably more exothermic than that computed for loss of $\bullet\text{H}$ from $\bullet\text{N}=\text{N}-\text{H}$ for which values of -3.8 and -8 kcal mol^{-1} have been reported.⁹⁰

Scheme 3.6. Computed energies {B3LYP/6-311+G**} relevant to thermochemical cycle for hydrogenation of N₂CHSiMe₃ (all values in kcal mol⁻¹).



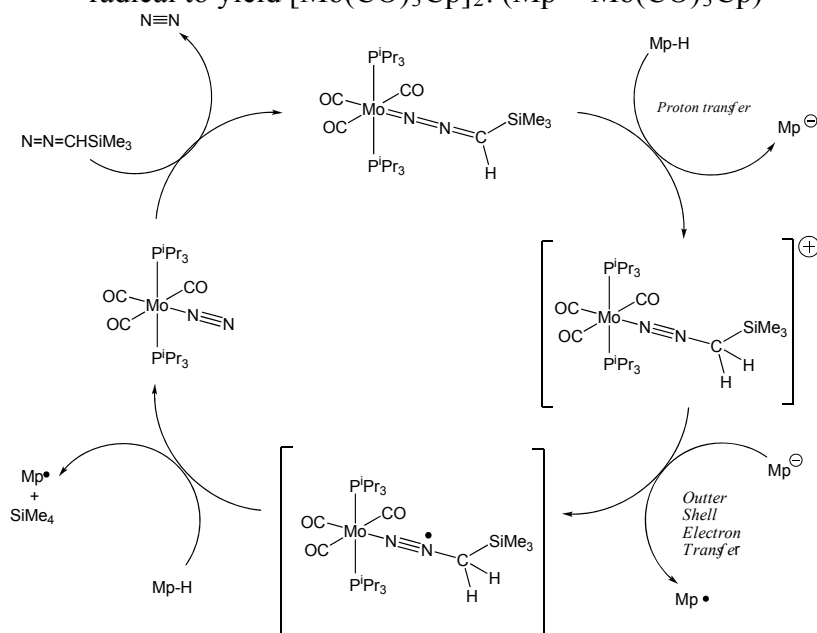
Proposed mechanism for the reaction of HMo(CO)₃Cp and N₂CHSiMe₃ in the presence of Mo(PⁱPr₃)₂(CO)₃, M = Mo,W). A plausible proposed mechanism for the catalytic process is summarized in Scheme 3.7. The reaction of Mo(CO)₃Cp with N₂CHSiMe₃ was observed to be much more rapid in the presence of M(PⁱPr₃)₂(CO)₃ in spite of the new steric barriers presented by the M(PⁱPr₃)₂(CO)₃ fragment surrounding the N₂CHSiMe₃. The observed increased rate of reaction may be due to the coordination of the N₂CHSiMe₃ to the electron rich metal center which in turn could shift the proposed initial protonation/deprotonation of the diazo as shown in eqn 3.22.



Increased basicity of coordinated diazoalkanes has been reported by Eisenberg.⁹¹ The strong π basicity of Mo(PⁱPr₃)₂(CO)₃ has been demonstrated by Kaim and coworkers,⁹² where the methylpyrazine cation was found to form a stable complex. Thus it is plausible that the methyldiazonium cation would remain bound to the complex Mo(PⁱPr₃)₂(CO)₃

and that this protonation/deprotonation equilibrium is first, rapidly established and second, more favorable for the bound diazo relative to the free.

Scheme 3.7. Proposed steps in catalytic hydrogenation of $\text{N}_2\text{CHSiMe}_3$ by $\text{HMo}(\text{CO})_3\text{Cp}$ in the presence of $\text{Mo}(\text{CO})_3(\text{P}^i\text{Pr}_3)_2$. A step not shown is combination of 2 $\bullet\text{Mo}(\text{CO})_3\text{Cp}$ radical to yield $[\text{Mo}(\text{CO})_3\text{Cp}]_2$. ($\text{Mp} = \text{Mo}(\text{CO})_3\text{Cp}$)



Due to the steric factors, the reaction channel involving migration from N_β to N_α which leads to the diazo complex as shown in Scheme 3.3 would be blocked when the diazoalkane is coordinated. Donation of a second hydrogen atom from another $\text{HMo}(\text{CO})_3\text{Cp}$ would then produce the TMS leaving N_2 bound to the $\text{Mo}(\text{CO})_3(\text{P}^i\text{Pr}_3)_2$ complex. The catalytic cycle is then closed when a second mole of $\text{N}_2\text{CHSiMe}_3$ replaces the bound N_2 .

The resulting $\bullet\text{Mo}(\text{CO})_3\text{Cp}$ pair up to form the stable dimer $[\text{Mo}(\text{CO})_3\text{Cp}]_2$. A second reaction that occurs upon “flooding” of the system with $\text{N}_2\text{CHSiMe}_3$ is the reaction of the diazo with the metal hydride $\text{HMo}(\text{CO})_3\text{Cp}$. As discussed earlier the resultant products are $\text{HMo}(\text{N}_2\text{CH}_2\text{SiMe}_3)(\text{CO})_2\text{Cp}$ and CO . The carbon monoxide

readily reacts with the catalyst $\text{Mo}(\text{CO})_3(\text{P}^i\text{Pr}_3)_2$ to form the unreactive tetracarbonyl complex $\text{Mo}(\text{CO})_4(\text{P}^i\text{Pr}_3)_2$. Thus too much diazo poisons the catalyst and shuts down the cycle.

3.3 Conclusions

Both experimental and theoretical chemistry were collectively utilized to gain insight into the reaction mechanism of the alkyl diazo, $\text{N}_2\text{CHSiMe}_3$ with the metal hydride, $\text{HMo}(\text{CO})_3\text{Cp}$. The initial step of the reaction was observed to be the result of an equilibrium process in which a proton was rapidly exchanged between the reactants. A dependency upon the reaction solvent was seen to significantly effect the product distribution and reaction rate. Thermodynamic study of this reaction led to an estimate for heat of insertion of N_2 into the Mo-CH_3 bond of $\approx +42 \pm 5 \text{ kcal mol}^{-1}$.

The catalytic hydrogenation of $\text{N}_2\text{CHSiMe}_3$ by $\text{HMo}(\text{CO})_3\text{Cp}$ outlined in Scheme 3.7 allowed reasonably accurate determination of the enthalpy of formation of this reactive diazo compound in solution to be $+5.8 \pm 3.0 \text{ kcal mol}^{-1}$. Key aspects of this measurement was that the determination relied on the purified organometallic reagent $\text{HMo}(\text{CO})_3\text{Cp}$ and that the catalysis by $\text{Mo}(\text{P}^i\text{Pr}_3)_2(\text{CO})_3$ cleanly led to the products SiMe_4 and $[\text{Mo}(\text{CO})_3\text{Cp}]_2$. This line of approach, in which an organic compound too reactive to be isolated in neat form, can be addressed by its reaction with organometallic reagents of known thermochemistry which are easier to purify and characterize thermochemically, may find an increased use in the future.

3.4 Experimental

General procedures Unless stated otherwise, all operations were performed in a Vacuum Atmospheres glove box under an atmosphere of purified argon or utilizing standard Schlenk tube techniques under argon. THF, toluene and heptane were purified by distillation under argon from sodium benzophenone ketyl into flame dried glassware and then degassed. Solutions of trimethylsilyldiazomethane in hexanes (2.0 M) were purchased from Aldrich and used without further purification. $\text{HMo}(\text{CO})_3\text{Cp}$,⁹³ $\text{HW}(\text{CO})_3\text{Cp}$,⁹³ $\text{HMo}(\text{CO})_3\text{Cp}^*$,⁹⁴ and $\text{M}(\text{PPR}_3)_2(\text{CO})_3$ ($\text{M} = \text{Mo}, \text{W}$; $\text{R} = \text{iPr}, \text{Cy}$)⁹⁵ were prepared by standard literary procedures. The metal hydrides were further purified by sublimation at c.a. 60 °C and 10^{-2} torr. The complexes $\text{M}(\text{CO})_2\text{N}_2\text{CH}_2\text{SiMe}_3\text{Cp}$ ($\text{M} = \text{Mo}, \text{W}$) were characterized by FTIR, NMR and Mass spectroscopy as well as x-ray crystallography for $\text{M} = \text{W}$. FTIR and NMR data were found to be in agreement with those originally reported by Lappert and Poland.⁷³ A sample of $\text{Mo}(\text{CH}_2\text{SiMe}_3)(\text{CO})_3\text{Cp}$ was prepared by reaction of $\text{NaMo}(\text{CO})_3\text{Cp}$ and $\text{Cl-CH}_2\text{SiMe}_3$) and shown to have identical spectroscopic properties to those detected in solution phase studies. FTIR data were obtained on a Perkin Elmer system 2000 spectrometer fitted with a microscope and flow through cell that has been described in detail elsewhere.⁹⁶ ^1H NMR spectra were obtained taken in C_6D_6 ($\delta = 7.16$) on a Bruker AVANCE 400 MHz spectrometer. MS spectra obtained on a VG MASSLAB TRIO-2 using FAB techniques.

Kinetic studies of reaction of $\text{HM}(\text{CO})_3\text{Cp}$ with $\text{N}_2\text{CHSiMe}_3$. In a typical procedure, a solution of 0.1 g $\text{HMo}(\text{CO})_3\text{Cp}$ in 35 mL heptane was prepared in a Schlenk tube under argon to make a 0.0012 M solution. The solution was then loaded into a

syringe in the glove box. A Hamilton gas tight syringe fitted with a valve was filled with 1.00 mL of a 2.0 M solution of $\text{N}_2\text{CHSiMe}_3$ in hexanes. Both syringes were taken from the glove box. The hydride solution was transferred under argon atmosphere to a 50 mL thermostatted glass reactor with magnetic stir rod. The system was connected to a Schlenk line and also to the Perkin Elmer 2000 FTIR microscope system by means of a small diameter teflon tube. Following temperature equilibration approximately 1 mL of the hydride solution was transferred under argon to the FTIR cell and a stock solution spectrum recorded. The reaction was started by injection of the $\text{N}_2\text{CHSiMe}_3$ solution and periodically small samples were removed for analysis by transfer to the flow through cell. Similar procedures under CO atmosphere were performed with careful ventilation.

NMR studies of H/D exchange. In the glove box a Schlenk tube was charged with 0.2057 g $\text{DMo(CO)}_3\text{Cp}$ which was then dissolved in 25.0 mL heptane (0.035 M) under argon. One milliliter of this solution was used for taking an FTIR and to three different Schlenk tubes was added 8.0 mL of this solution. These tubes were removed from the glove box and connected to a Schlenk line. All three Schlenk tubes were placed in an ice bath at 0 °C. After temperature equilibration 1.0 mL of 2.0 M solution $\text{N}_2\text{CHSiMe}_3$ in hexanes was added to one of the tubes. To the other two tubes 0.100 and 0.025 mL of the diazo solution were added respectively. All three flasks were allowed to stand for one hour at 0 °C. At that time the reaction was judged to be complete by FTIR spectra and all volatile material was removed from each flask by vacuum. C_6D_6 (3.0 mL) was added to the solid residue in each flask and the material dissolved with no trace of residual solids. Each solution was analyzed by FTIR and ^1H NMR spectroscopy. In addition to the expected major product $\text{Mo(CO)}_2(\text{N}_2\text{CH}_x\text{D}_{2-x}\text{SiMe}_3)\text{Cp}$, FTIR bands

showed both known $[\text{Mo}(\text{CO})_3\text{Cp}]_2$ and $\text{Me}_3\text{SiCH}_2\text{Mo}(\text{CO})_3\text{Cp}$ and unidentified minor additional products. These unidentified products were attributed to reactions that most likely occurred upon concentration during the evacuation of the sample and were judged to not significantly influence the NMR analysis of the major products ($\text{Mo}(\text{CO})_2(\text{N}_2\text{CH}_x\text{D}_{2-x}\text{SiMe}_3)\text{Cp}$.) ^1H NMR shifts (C_6D_6) (ppm): $\text{MoN}_2\text{CH}_2\text{SiMe}_3$ 5.08 5H(s), 2.92 2H(s), -0.02 9H(s); $\text{MoN}_2\text{C}(\text{H})(\text{D})\text{SiMe}_3$ 5.08 5H(s), 2.90 2H(t), -0.02 9H(s).

Crystal growth of $\text{W}(\text{CO})_2\text{N}_2\text{CH}_2\text{SiMe}_3\text{Cp}$. Crystals of $\text{W}(\text{CO})_2(\text{N}_2\text{CH}_2\text{SiMe}_3)\text{Cp}$ suitable for structure determination were prepared by dissolving of 0.1002 g of $\text{HW}(\text{CO})_3\text{Cp}$ in 10 mL of toluene (0.0030 M.) To this 0.200 mL of a 2.0 M $\text{N}_2\text{CHSiMe}_3$ solution in hexanes was added. After the addition of the $\text{N}_2\text{CHSiMe}_3$ the solution turned from a clear orange to a dark red. The reaction was allowed to continue for a period of approximately 80 minutes and the product was characterized by FTIR spectroscopy. The major product of the reaction was $\text{W}(\text{CO})_2(\text{N}_2\text{CH}_2\text{SiMe}_3)\text{Cp}$. A side reaction also leads to the formation of $\text{W}(\text{CO})_2(\text{CH}_2\text{SiMe}_3)\text{Cp}$. Peak assignments for these compounds can be seen in the Appendix B Table B.1. The solution was then evaporated to dryness and redissolved in 4.0 mL heptane. A portion of the $\text{W}(\text{CO})_2(\text{N}_2\text{CH}_2\text{SiMe}_3)\text{Cp}$ remained undissolved. The solution was removed and filtered into a glass tube under argon. The remaining undissolved portion was dissolved in another 4.0 mL of heptane and used to characterize the product by IR spectroscopy. The glass tube was sealed under vacuum and placed in a freezer (≈ -20 °C) for a period of 2 weeks. The tube was opened in the glove box; the mother liquor removed by syringe and replaced with a small amount of degassed mineral oil. The tube was then sealed again and stored until mounting for structure determination.

Crystal structure determination. Crystal structure determination was performed by Brian Scott at Los Alamos National Laboratory. Due to air sensitivity the crystal was mounted from a pool of mineral oil under argon gas flow. The crystal was placed on a Bruker P4 diffractometer with 1k CCD, and cooled to 203 K using a Bruker LT-2 temperature device. The instrument was equipped with a sealed, graphite monochromatized MoK α X-ray source ($\lambda = 0.71073$ Å). A hemisphere of data was collected using ϕ scans, with 30 second frame exposures and 0.3° frame widths. Data collection and initial indexing and cell refinement were handled using SMART⁹⁷ software. Frame integration, including Lorentz-polarization corrections, and final cell parameter calculations were carried out using SAINT⁹⁸ software. The data were corrected for absorption using the SADABS⁹⁹ program. Decay of reflection intensity was monitored *via* analysis of redundant frames. The structure was solved using Direct methods and difference Fourier techniques. All hydrogen atom positions were idealized, and rode on the atom they were attached to. The final refinement included anisotropic temperature factors on all non-hydrogen atoms. Structure solution, refinement, graphics, and creation of publication materials were performed using SHELXTL.¹⁰⁰

Reaction of HM(CO)₃Cp with N₂CH₂SiMe₃ in presence of M(PR₃)₂(CO)₃ complexes (M = Mo, W; R = ⁱPr₃, Cy). In the glove box 0.2044 g Mo(PCy₃)₂(CO)₃ (0.27 mmol) solid was dissolved in 10.0 mL toluene to which 0.2 mL of a 2.0 M solution of N₂CHSiMe₃ in hexanes (0.4 mmol). An FTIR spectrum was run and showed peaks at 2066 cm⁻¹ due to free N₂CHSiMe₃ (≈ 0.13 mmol) as well as bands at 1948 (w), 1844 (s), 1833(sh) assigned to Mo(PCy₃)₂(CO)₃(N₂CHSiMe₃) (≈ 0.27 mmol). In addition a small band at 1866 cm⁻¹ was present due to the known and unreactive complex

Mo(PCy₃)₂(CO)₄ which is a common contaminant of the air sensitive Mo(PCy₃)₂(CO)₃. In a second Schlenk tube a solution of freshly sublimed HMo(CO)₃Cp (0.0811 g 0.33 mmol) was prepared in 10 ml toluene and then added to the solution of Mo(PCy₃)₂(CO)₃(N₂CHSiMe₃). An FTIR spectrum run within minutes of mixing showed new bands attributed to [Mo(CO)₃Cp]₂. No bands due to HMo(CO)₃Cp, Mo(CO)₂(N₂CH₂SiMe₃)Cp or free N₂CHSiMe₃ were seen. The FTIR data for Mo(PCy₃)₂(CO)₃(N₂CHSiMe₃) was largely unchanged. Bands assigned to the known complexes Mo(PCy₃)₂(CO)₃ and Mo(PCy₃)₂(CO)₃(N₂) were present in keeping with the calculated stoichiometry of reaction: 2 HMp (0.33 mmol) + Mo(PCy₃)₂(CO)₃(N₂CHSiMe₃)(0.27 mmol) + N₂CHSiMe₃(0.13 mmol) → Mp₂ (0.165 mmol) + Mo(PCy₃)₂(CO)₃(N₂CHSiMe₃)(0.235 mmol) + Mo(PCy₃)₂(CO)₃(N₂)/Mo(PCy₃)₂(CO)₃ (0.035 mmol) + N₂ (0.165 mmol) + SiMe₄(0.165 mmol). In separate experiments performed in C₆D₆ the production of SiMe₄ was proven by NMR spectroscopy. Addition of CO to the reaction mixture described above showed IR bands attributable to free N₂CHSiMe₃ generated from Mo(PCy₃)₂(CO)₃(N₂CHSiMe₃) as well as conversion of all other products except Mp₂ and Mo(PCy₃)₂(CO)₄.

Repetition of this reaction at room temperature under varying ratios of reagents showed that both Mo(PCy₃)₂(CO)₃ and Mo(P^{*i*}Pr₃)₂(CO)₃ as well as the corresponding W derivatives produced clean hydrogenation of N₂CHSiMe₃ from HMp in toluene even at ratios of 4/1 of free N₂CHSiMe₃ to bound N₂CHSiMe₃. No detectable amount of Mo(CO)₂(N₂CH₂SiMe₃)Cp was observed in the room temperature reactions.

Calorimetric measurement of the enthalpy of reaction of HMo(CO)₃Cp with N₂CH₂SiMe₃ in THF. In the glove box a solution of 350 mL THF and 10 mL of 2.0 M

$\text{N}_2\text{CHSiMe}_3$ in hexanes was prepared in a Schlenk flask. The solution was transferred to the calorimeter. Also in the glove box a glass ampoule was filled with 0.2204 g of $\text{HMo}(\text{CO})_3\text{Cp}$ (0.90 mmol.) The ampoule was sealed under vacuum. The ampoule was placed inside the calorimeter and allowed to come to thermal equilibrium at 272 K under stirring.

Upon equilibration the calorimeter was electrically calibrated by heating a standardized resistor with a known current for typically 60 sec. The system was then allowed to reestablish thermal equilibrium in a period of (on average) 15 to 20 min. The reaction was then initiated and the thermogram was recorded electronically at 10 sec intervals. The calorimeter was once again left to reach thermal equilibrium. Once equilibrium was reached the calorimeter was electrically calibrated. The average of the two electrical calibrations was used to evaluate the heat given off in the reaction. Six total runs were averaged together to obtain a final value of $-9.5 \pm 1.1 \text{ kcal mol}^{-1}$. Correction for the endothermic enthalpy of solution of solid $\text{HMo}(\text{CO})_3\text{Cp}$ ($+2.1 \pm 0.1 \text{ kcal mol}^{-1}$) yielded a final value with all species in THF solution of $-11.6 \pm 1.2 \text{ kcal mol}^{-1}$.

After all runs were completed the final products of the several runs of calorimetry were verified by FTIR spectroscopy. The main peaks at the end of the experiment were assigned to excess $\text{N}_2\text{CHSiMe}_3$ (2065 cm^{-1}) and the final product of $\text{Mo}(\text{CO})_2(\text{N}_2\text{CH}_2\text{SiMe}_3)\text{Cp}$. Trace amounts of $\text{Mo}(\text{CO})_2(\text{CH}_2\text{SiMe}_3)$ were also seen in the spectrum. Both products' peak assignments can be seen in Table A.1 of the Appendix A. Also, small peaks at 1862 and 1804 cm^{-1} were seen and are believed to be unknown decomposition products.

Calorimetric measurement of the enthalpy of hydrogenation of $\text{N}_2\text{CH}_2\text{SiMe}_3$ by $\text{HMo}(\text{CO})_3\text{Cp}$ in the presence of $\text{W}(\text{CO})_3(\text{P}^i\text{Pr}_3)_2\text{N}_2\text{CHSiMe}_3$. In the glove box a solution of 10.0 mL of toluene and 0.400 mL 2.0 M $\text{N}_2\text{CHSiMe}_3$ in hexane was prepared. To this solution 0.2080g of $\text{W}(\text{CO})_3(\text{P}^i\text{Pr}_3)_2$ (0.36 mmol) was added. One mL of this solution was used for recording an FTIR spectrum, and the 4 mL were loaded under argon into the cell of The Setaram-C-80 Calvet microcalorimeter. The solid-containing compartment of the calorimeter was loaded with 0.0206g of freshly sublimed $\text{HMo}(\text{CO})_3\text{Cp}$. The assembled calorimeter cell was taken from the glove box and loaded into the calorimeter. After reaching temperature equilibration the reaction was initiated and the thermogram indicated a rapid reaction which returned cleanly to baseline with no thermal signal indicative of any substantial secondary reactions occurring.

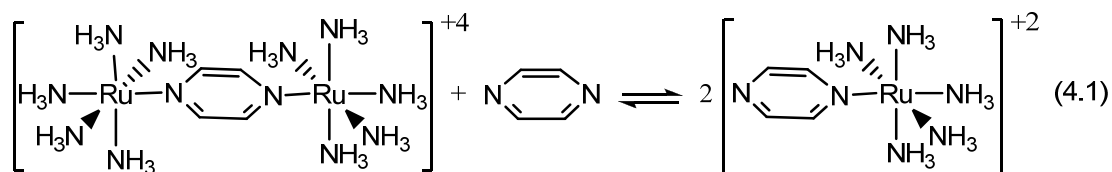
Following return to baseline, the cell was taken back into the glove box and a sample analyzed by FTIR spectroscopy showed the presence of $\text{W}(\text{CO})_3(\text{P}^i\text{Pr}_3)_2(\text{N}_2\text{CHSiMe}_3)$, $\text{N}_2\text{CHSiMe}_3$, $[\text{Mo}(\text{CO})_3\text{Cp}]_2$ and $\text{W}(\text{CO})_4(\text{P}^i\text{Pr}_3)_2$ the latter of which is present whenever handling $\text{W}(\text{CO})_3(\text{P}^i\text{Pr}_3)_2$. The spectral peaks of these compounds are listed in Supplementary Information Table ST-1. The reported enthalpy of reaction is the average of five measurements and yielded an average value based on solid $\text{HMo}(\text{CO})_3\text{Cp}$ of $-37.2 \pm 0.9 \text{ kcal mol}^{-1}$. Correction for the endothermic enthalpy of solution of solid $\text{HMo}(\text{CO})_3\text{Cp}$ ($+3.1 \pm 0.1 \text{ kcal mol}^{-1}$ in THF) yielded a final value with all species in toluene solution of $-40.3 \pm 1.0 \text{ kcal mol}^{-1}$ of reacting $\text{HMo}(\text{CO})_3\text{Cp}$ $-80.6 \pm 2.0 \text{ kcal mol}^{-1}$ of $\text{N}_2\text{CHSiMe}_3$ reacting. The derived enthalpy of reaction was found to be the same when $\text{Mo}(\text{CO})_3(\text{P}^i\text{Pr}_3)_2(\text{N}_2\text{CHSiMe}_3)$ was used in place of $\text{W}(\text{CO})_3(\text{P}^i\text{Pr}_3)_2(\text{N}_2\text{CHSiMe}_3)$ as catalyst for the hydrogenation.

Computational results. Computational results were provided by Paul von Ragué Schleyer and Henry F. Schaefer III from the University of Georgia and by Tamas Kégl and Ferenc Ungváry from the University of Pannonia. All computations were calculated at the BP86 level. For molybdenum and tungsten the valence triple- ζ SDD basis set following the (8s7p6d1f) \rightarrow [6s5p3d1f] contraction pattern is utilized with the corresponding relativistic effective core potential. For the other atoms the 6-311G(d,p) basis set was used. Complete details concerning theoretical calculations can be viewed in the article published as a result of this work.⁷⁷

Chapter 4: Experimental and Computational Studies of Binding of Dinitrogen, Nitriles, Azides, Diazoalkanes, Pyridine and Pyrazines to $M(PR_3)_2(CO)_3$ (M= Mo, W; R = Me, ⁱPr).

4.1 Background

The first compounds characterized to bind hydrogen as a molecule,¹⁰¹ $M(PR_3)_2(CO)_3$ (M = Cr, Mo, W; R = isopropyl, cyclohexyl), were discovered nearly thirty years ago.¹⁰² They are ideal for studying physical aspects of binding and oxidative addition at a sterically-constrained, active metal center.¹⁰³ Taube has been one of the few pioneers in this field of ligand binding to crowded metal centers. He has investigated a range of N donor ligands and their coordination to $[Ru(NH_3)_5(H_2O)]^{2+}$.¹⁰⁴ In these studies it is reported that N_2 prefers to bind in a μ -bridging form by 1.1 ± 2.8 kcal mol⁻¹, while the pyrazine ligand prefers to be mononuclear by 3.0 ± 0.9 kcal mol⁻¹ (in aqueous solution, eqn. 4.1).



Such preferred binding modes can, in principle, illuminate π -back bonding and electron delocalization. Separately, Frenking concluded that differences in the Cr=C bond in $Cr(CO)_5(CHX)$ depend mainly on the π -bonding ability of X, and that the strong bond present when X = H (97.9 kcal mol⁻¹) is nearly 30 kcal mol⁻¹ weaker when X = NH₂ (68.7 kcal mol⁻¹).¹⁰⁵

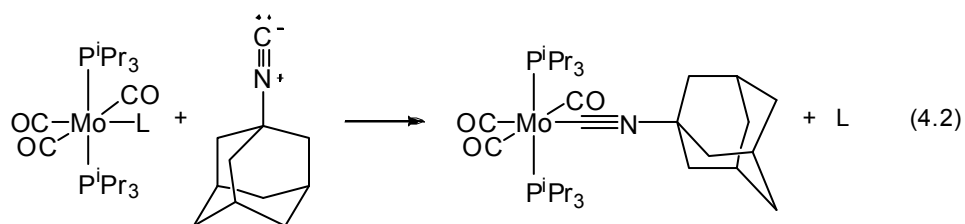
The factors controlling binding of N_2 are not fully understood. Dinitrogen is intrinsically inferior, both as a σ donor and as a π acceptor, to CO (of which it is

isoelectronic with.) Presented in this chapter is the study of the binding of dinitrogen and its mimics: nitriles ($\text{N}\equiv\text{C-R}$), pyridine (NC_5H_{10}), pyrazines ($\text{N}_2\text{C}_4\text{H}_2\text{R}_2$), azides ($\text{N}=\text{N}=\text{N-R}$) and diazos ($\text{N}=\text{N}=\text{CR}_2$) to the coordinatively unsaturated $\text{Mo}(\text{P}^i\text{Pr}_3)_2(\text{CO})_3$ complex. The resultant complexes will be subject to investigation by both experimental and theoretical means. The computational structures and energies presented herein were provided by Patrick Achord and Etsuko Fujita from Brookhaven National Laboratory and James T. Muckerman from Los Alamos National Laboratory as part of a collaborative work. Calculations were carried out at the B3LYP level using LANL2DZ basis sets.

4.2 Results

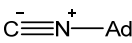
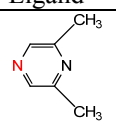
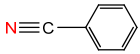
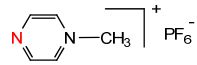
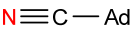
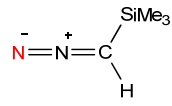
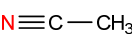
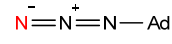
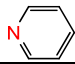
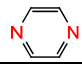
Enthalpies of binding measured by reaction with 1-adamantyl isocyanide.

Binding enthalpies to $\text{M}(\text{PCy}_3)_2(\text{CO})_3$ have been reported ($\text{M} = \text{Cr}, \text{Mo}, \text{W}$).¹⁰⁶ The reference enthalpy of $\text{Mo}(\text{P}^i\text{Pr}_3)_2(\text{CO})_3 + \text{AdNC}$ was found to be $\Delta H = -29.0 \pm 0.3 \text{ kcal mol}^{-1}$ (all species in toluene solution). The majority of calorimetric results were determined by measuring the enthalpy of ligand displacement (eqn. 4.2, Table 4.1).



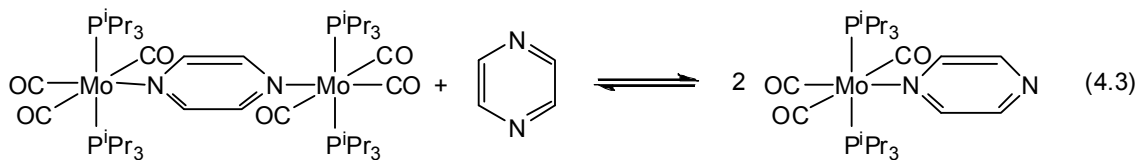
Rationalization for using the displacement reaction for measurements as apposed to the direct oxidative addition of L to $\text{Mo}(\text{P}^i\text{Pr}_3)_2(\text{CO})_3$ stems from the highly air sensitive nature of the unsaturated complex. This helped to reduce unwanted side reactions during calorimetric measurements and thusly ensure results of high quality.

Table 4.1. Binding enthalpies (kcal mol⁻¹) of ligands determined by means of ligand displacement by AdNC (eqn 4.2).

Ligand	$\Delta H_{\text{measured}}^a$	$\Delta H_{\text{binding}}^b$	Ligand	$\Delta H_{\text{measured}}^a$	$\Delta H_{\text{binding}}^b$
	-26.4 ± 0.3 ^c	-29.0 ± 0.3		-11.6 ± 0.5	-14.8 ± 0.6
	-8.8 ± 0.2	-17.6 ± 0.4		-8.9 ± 0.7 ^d	-17.5 ± 0.8
	-9.7 ± 0.5	-16.7 ± 0.6		-12.6 ± 0.4	-13.8 ± 0.5
	-9.8 ± 0.3	-16.6 ± 0.4		-15.2 ± 0.3	-11.2 ± 0.4
	-9.4 ± 0.2	-17.0 ± 0.4		-9.3 ± 0.8	-34.2 ± 1.6 ^d

^a Based on the enthalpy measured with solid AdNC; ^b values with all species in toluene solution; ^c determined from the reaction of Mo(PⁱPr₃)₂(CO)₃ with AdNC; ^d measured in THF for solubility; ^e Enthalpy corresponding to the binding of both nitrogens of pyrazine to form the bridging species

Pyrazine and N₂: mononuclear and bridging forms. Adding pyrazine to Mo(PⁱPr₃)₂(CO)₃ quickly establishes the equilibrium as shown in eqn. 4.3.



The bridging complex is favored; large excesses of pyrazine are required to produce detectable amounts of the mononuclear structure. Variable temperature FTIR studies yielded K_{eq} (Figure 4.1) and thus $\Delta H = +4.4 \pm 0.2$ kcal mol⁻¹ and $\Delta S = +5.8 \pm 0.3$ cal mol⁻¹ K⁻¹. The derived data (Scheme 4.1) for mononuclear binding, $\Delta H = -14.9 \pm 0.9$ kcal mol⁻¹, is very close to the calorimetric value of 2,6-dimethylpyridine, which only binds in a mononuclear fashion.

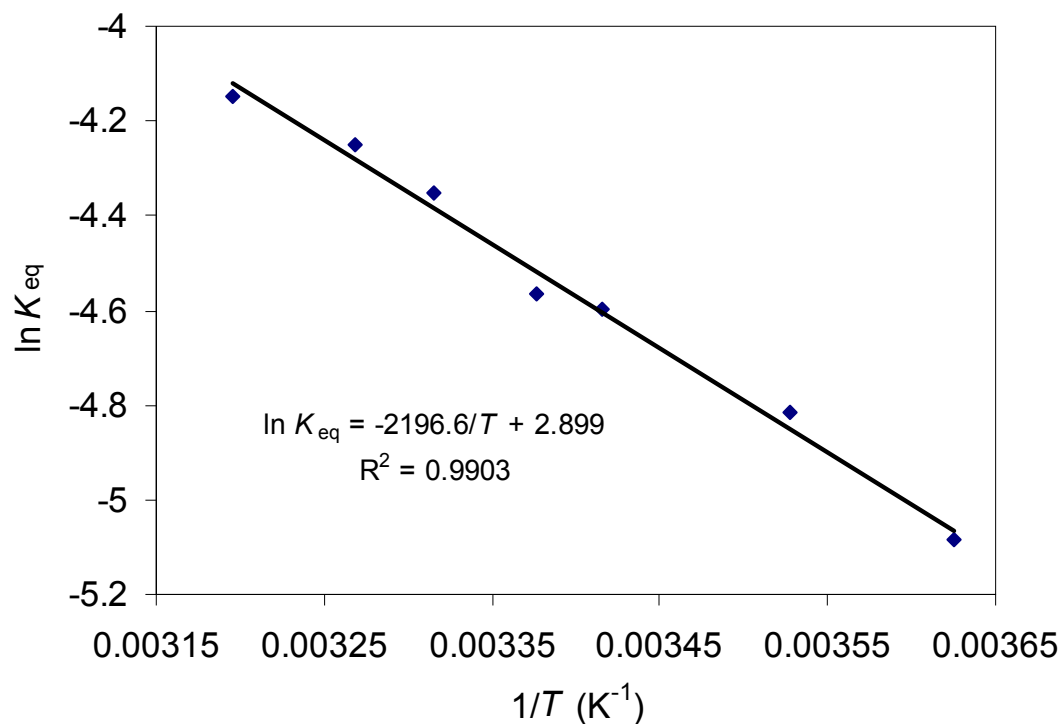
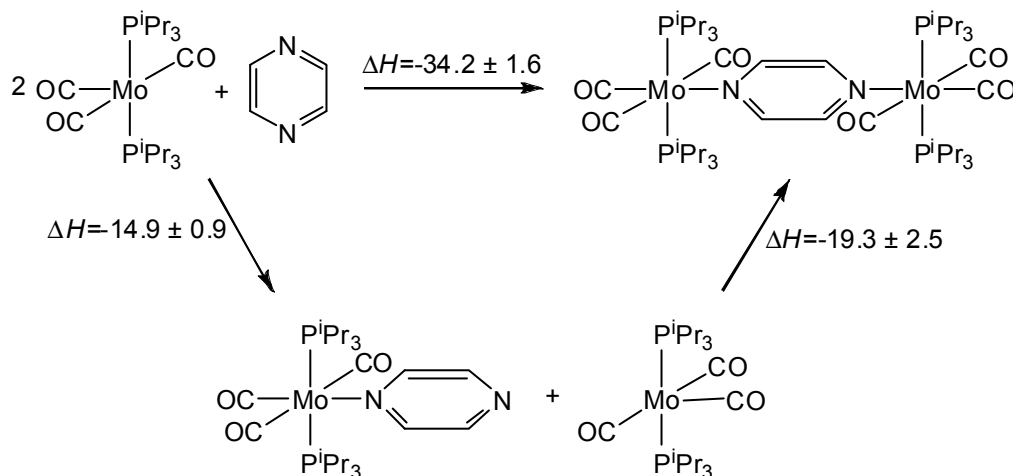
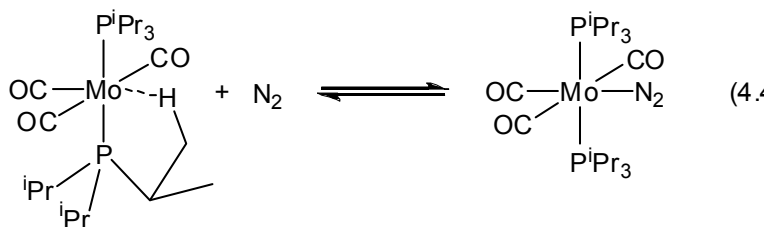


Figure 4.1. Van't Hoff plot for the formation of $\text{Mo}(\text{P}^i\text{Pr}_3)_2(\text{CO})_3(\text{C}_4\text{H}_4\text{N}_2)$. $\Delta H = +4.4 \pm 0.2 \text{ kcal mol}^{-1}$ and $\Delta S = +5.8 \pm 0.3 \text{ cal mol}^{-1} \text{ K}^{-1}$

Scheme 4.1. Thermodynamic cycle determining the enthalpy of dissociation of $\mu\text{-(N}_2\text{C}_4\text{H}_4\text{)}[\text{Mo}(\text{P}^i\text{Pr}_3)_2(\text{CO})_3]_2$ to $\text{Mo}(\text{P}^i\text{Pr}_3)_2(\text{CO})_3(\text{N}_2\text{C}_4\text{H}_4) + \text{Mo}(\text{P}^i\text{Pr}_3)_2(\text{CO})_3$ in toluene solution. (All values in kcal mol^{-1})



Binding of N_2 is not quantitative but in solution the equilibrium shown in eqn 4.4 is rapidly established. FTIR techniques were used to measure this equilibrium.



In spite of experimental scatter in the individually measured values, due in part to the highly air sensitive nature of the solutions, the derived (Figure 4.2) thermodynamic parameters, $\Delta H = -10.3 \pm 0.6 \text{ kcal mol}^{-1}$ and $\Delta S = -32.3 \pm 2.0 \text{ cal mol}^{-1} \text{ K}^{-1}$, are close to those of N_2 to $\text{Mo}(\text{PCy}_3)_2(\text{CO})_3$, $\Delta H = -9.0 \text{ kcal mol}^{-1}$ and $\Delta S = -32.1 \text{ cal mol}^{-1} \text{ K}^{-1}$.¹⁰⁶ The slightly more exothermic binding to the P^iPr_3 complex seems universal, and may be attributable to a stronger Mo-Cyclohexyl agostic bond, and to steric factors.¹⁰⁷

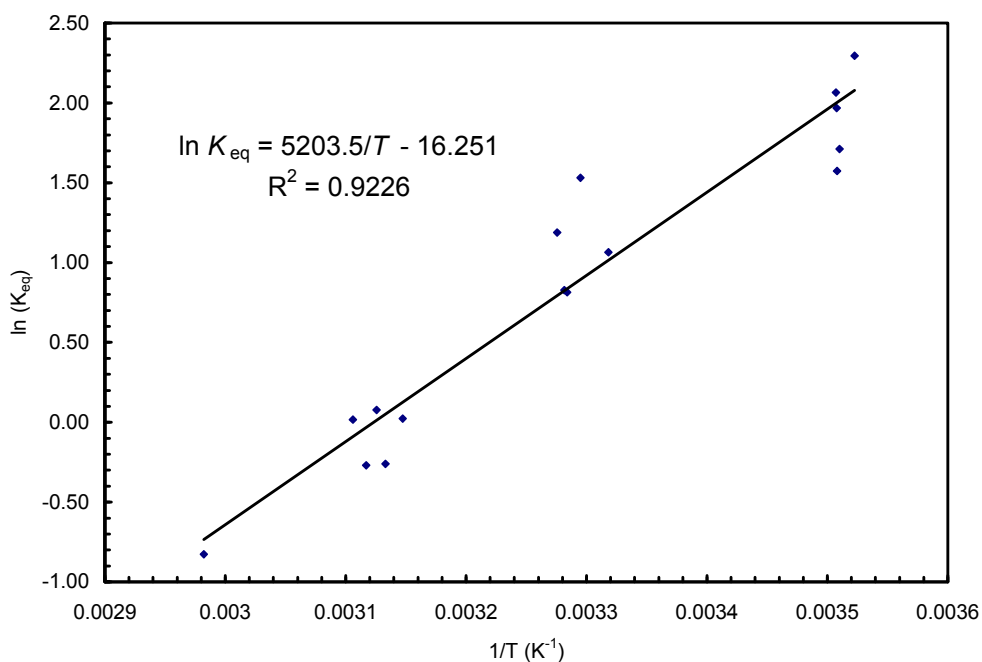
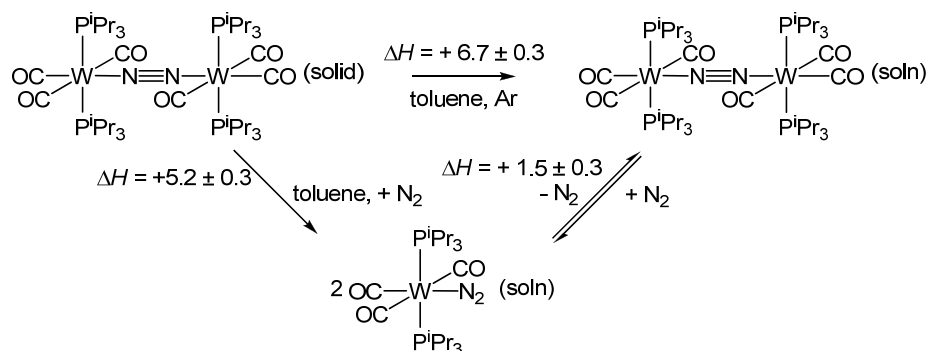


Figure 4.2. Van't Hoff plot for the binding of N_2 to $\text{Mo}(\text{P}^i\text{Pr}_3)_2(\text{CO})_3$. $\Delta H = -10.3 \pm 0.6 \text{ kcal mol}^{-1}$ and $\Delta S = -32.3 \pm 2.0 \text{ cal mol}^{-1} \text{ K}^{-1}$.

Despite the fact that the bridging complex $\mu\text{-(N}_2\text{)[Mo(P}^i\text{Pr}_3\text{)}_2\text{(CO)}_3\text{]}_2$ is stable as a solid, it could not be quantitatively measured in solution. The corresponding W complex revealed that the mononuclear complex is more stable by $+1.5 \pm 0.6 \text{ kcal mol}^{-1}$ (Scheme 4.2). Thus, it is estimated that the binding enthalpy of $\text{Mo(P}^i\text{Pr}_3\text{)}_2\text{(CO)}_3\text{(N}_2\text{)}$ to $\text{Mo(P}^i\text{Pr}_3\text{)CO}_3$ is $-8.8 \pm 1.2 \text{ kcal mol}^{-1}$.^{xx}

Scheme 4.2. Thermodynamic cycle determining the enthalpy of dissociation of $\mu\text{-(N}_2\text{)[Mo(P}^i\text{Pr}_3\text{)}_2\text{(CO)}_3\text{]}_2$ to $\text{Mo(P}^i\text{Pr}_3\text{)}_2\text{(CO)}_3\text{(N}_2\text{)}$ + $\text{Mo(P}^i\text{Pr}_3\text{)}_2\text{(CO)}_3$ + N_2 in toluene solution. (kcal mol^{-1})

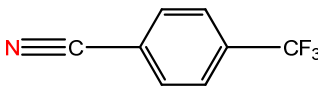
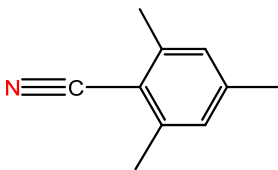
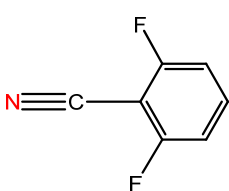
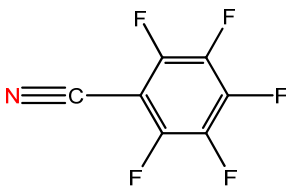
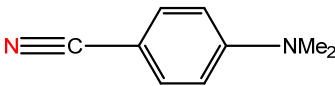


Nitriles: calorimetric and spectroscopic data. The adamantyl nitrile complex is readily crystallized and stable in the solid state for extended periods of time. It thus made a useful starting point. The difference in binding enthalpy of benzonitrile and the alkyl (adamantyl and aceto) nitriles (Table 4.1) is only $1.0 \pm 0.5 \text{ kcal mol}^{-1}$. The enthalpies of substituting any of a set of substituted benzonitriles (4-NMe₂C₆H₄; 2,4,6-Me₃C₆H₂; 2,6-F₂C₆H₃; 4-CF₃C₆H₄; F₅C₆) in place of AdCN were very small (Table 4.2). So small, in fact, that adjustment for enthalpies of dilution of the polar nitriles played a role in the

^{xx} Work on related ligand binding shows that enthalpies of binding of Mo and W closely resemble each other, with binding to Mo being ≈ 0.9 times that of W. Due to the low value of this difference, and the high experimental error, no change was made. Under 1 atm of N₂ pressure we see no evidence for any of the dinuclear complex in solution, only terminal binding and unsaturated complex were detected by FTIR.

calorimetric measurements nearly as significant as the reactions themselves. And yet, the substitutions were accompanied by dramatic color changes (Figure 4.3).

Table 4.2. Binding enthalpies (kcal mol^{-1}) determined by reaction of $\text{Mo}(\text{P}^i\text{Pr}_3)_2(\text{CO})_3(\text{AdCN})$ with benzonitriles

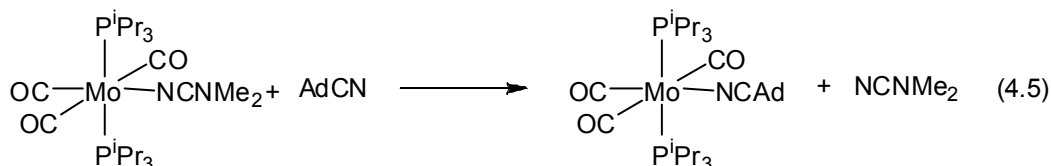
Ligand	$\Delta H_{\text{measured}}$	$\Delta H_{\text{binding}}^{\text{a}}$
	-0.4 ± 0.1	-17.1 ± 0.6
	0.0 ± 0.1	-16.7 ± 0.6
	0.0 ± 0.1	-16.7 ± 0.6
	$+0.3 \pm 0.1$	-16.4 ± 0.6
	$+0.4 \pm 0.1$	-16.3 ± 0.6

^a values with all species in toluene solution.



Figure 4.3. Colors of the $\text{Mo}(\text{P}^i\text{Pr}_3)_2(\text{CO})_3(\text{RCN})$ complexes studied. From left to right: R = Ad; 4- $\text{NMe}_2\text{C}_6\text{H}_4$; 2,4,6- $\text{Me}_3\text{C}_6\text{H}_2$; C_6H_5 ; 2,6- $\text{F}_2\text{C}_6\text{H}_3$; 4- $\text{CF}_3\text{C}_6\text{H}_4$; F_5C_6 .

Dimethylcyanamide. Due to low complex solubility, it was difficult to make reliable calorimetric measurements. Quantitative FTIR studies at room temperature led to an estimate of K_{eq} of 7 ± 2 (Equations 4.5).



This corresponds to ΔG of -1.2 ± 0.3 and -1.0 ± 0.3 kcal mol⁻¹, and implies that Me₂NCN binds 1.2 kcal mol⁻¹ more weakly than does AdCN. The free energy change is attributed to be primarily caused by enthalpic rather than entropic factors, an approximation that is likely valid within experimental error.^{xxi}

Quinuclidine. It is known that primary and secondary amines bind to the Kubas complexes, but tertiary amines do not.¹⁰⁸ This is typically ascribed to steric factors at the sterically crowded metal center which prohibit binding of bulky amines. Even in the presence of a large excess of the quinuclidine, no detectable complex was observed at room temperature.

X-Ray structures. Experimentally and computationally determined selected bond distances and angles of all of the X-ray crystal structures are listed in Tables 4.3 and 4.4. Experimental structures were solved by Burjor Captain from the University of Miami and Brian Scott from Los Alamos National Laboratory. As mentioned previously computational structures were provide by Etsuko Fujita and Patrick Achord from Brookhaven National Laboratory as well as by James T. Muckerman from Brookhaven

^{xxi} Estimation of the entropy of ligand substitution of 4-CF₃C₆H₄C≡N and Mo(PⁱPr₃)₂(CO)₃(4-Me₂NC₆H₄CN) yielded an estimate of $\Delta S^\circ = -5 \pm 2$ cal mol⁻¹ K⁻¹. At room temperature this corresponds to about 1.5 kcal mol⁻¹ in terms of free energy. The error limits on ΔH° derived in this way were increased by this amount.

National laboratory as part of a collaborative work. Crystal structures of $W(P^iPr_3)_2(CO)_3(2,6-Me_2C_4H_2N_2)$, $W(P^iPr_3)_2(CO)_3(2,4,6-Me_3C_6H_2CN)$ and $W(P^iPr_3)_2(CO)_3(NCNMe_2)$ are shown in Figures 4.4-4.6. The rest are shown in Appendix C Figures C.3 (M = Mo; L = AdNC), C.4 (M = W; L = AdNC), C.5 (M = Mo; L = AdCN), C.6 (M = W; L = AdCN) and C.7 (M = W; L = 2,6-F₂C₆H₂CN). In spite of repeated attempts, we were not able to grow crystals of $\mu-(C_4H_4N_2)[M(P^iPr_3)_2(CO)_3]_2$ (M = Mo, W).

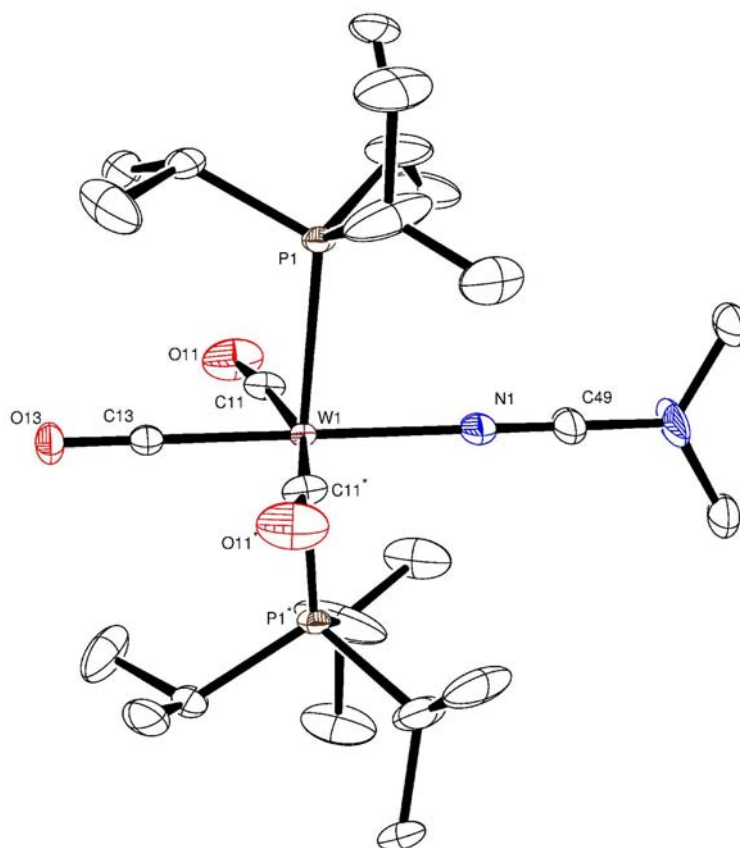


Figure 4.4. ORTEP diagram of $W(P^iPr_3)_2(CO)_3(NCNMe_2)$ showing 35 % probability thermal ellipsoids. Hydrogen atoms are omitted for clarity.

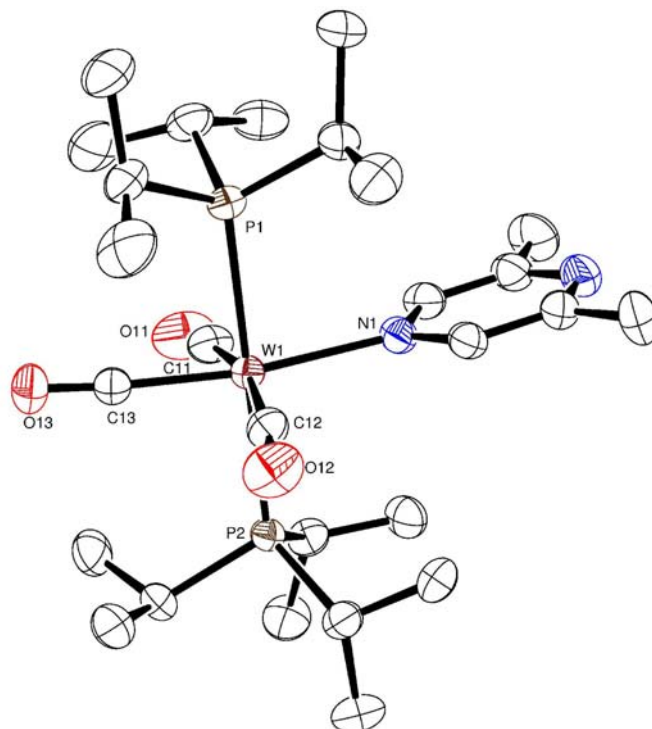


Figure 4.5. ORTEP diagram of $W(P^iPr_3)_2(CO)_3(2,6-Me_2C_4H_2N_2)$ showing 35 % probability thermal ellipsoids. Hydrogen atoms are omitted for clarity.

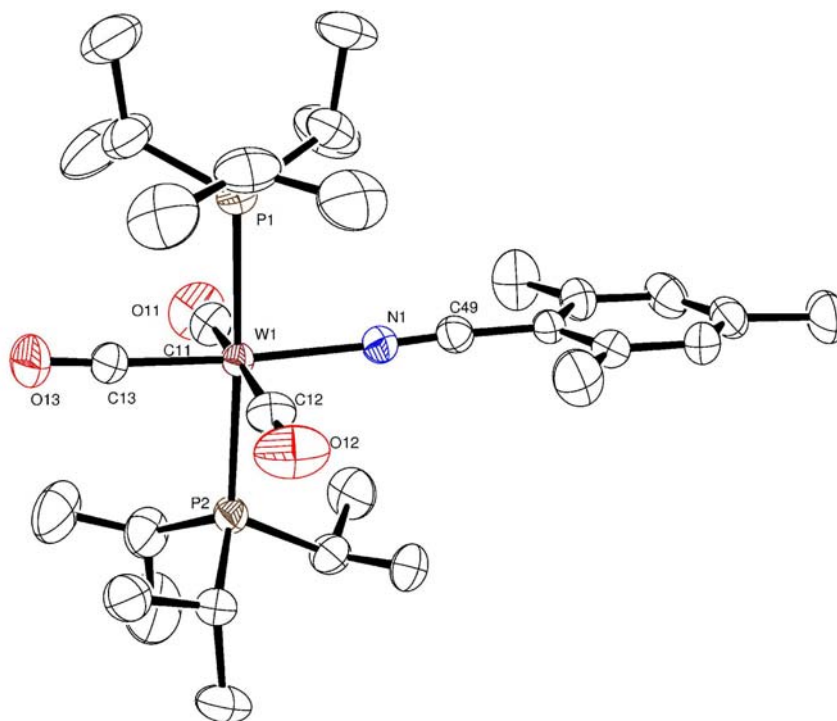


Figure 4.6. ORTEP diagram of $W(P^iPr_3)_2(CO)_3(2,4,6-Me_3C_6H_2CN)$ showing 35 % probability thermal ellipsoids. Hydrogen atoms are omitted for clarity.

Table 4.3. Selected bond distances (Å) from X-ray crystal structures and theoretically calculated structures of $M(\text{P}^i\text{Pr}_3)_2(\text{CO})_3\text{L}$.

		Computational						Experimental					
$\text{Mo}(\text{P}^i\text{Pr}_3)_2\text{CO}_3$	M-C	C-N	C11-O11	C12-O12	C13-O13	M1-C49	C49-N1	C11-O11	C12-O12	C13-O13			
AdNC	2.115	1.193	1.197	1.196	1.204	2.139(3)	1.158(3)	1.147(4)	1.139(3)	1.162(4)			
	M-N	N-C				M1-N1	N1-C49						
AdCN	2.246	1.176	1.198	1.200	1.210	2.220(3)	1.140(4)	1.147(4)	1.144(4)	1.170(4)			
$\text{W}(\text{P}^i\text{Pr}_3)_2\text{CO}_3$	M-C	C-N				M1-C49	C49-N1						
AdNC	2.117	1.195	1.200	1.199	1.207	2.113(6)	1.171(7)	1.159(6)	1.155(6)	1.167(7)			
	M-N	N-C				N1-C49	N1-C49						
AdCN	2.177	1.178	1.202	1.200	1.213	2.195(4)	1.153(6)	1.130(7)	1.177(8)	1.166(8)			
MesitylCN	2.133	1.185	1.200	1.201	1.210	2.166(4)	1.145(6)	1.150(6)	1.168(6)	1.172(6)			
Me_2NCN	2.185	1.187	1.203	1.201	1.215	2.192(5)	1.151(7)	1.178(6)	1.178(6) ^a	1.165(5)			
2,6-F ₂ PhCN						2.130(6)	1.145(9)	1.169(10)	1.146(11)	1.170(10)			
2,6-Me ₂ C ₄ H ₂ N ₂						2.257(4)	n/a	1.155(6)	1.158(6)	1.169(6)			

^a value refers to C11*-O11*

Table 4.4. Selected bond angles ($^{\circ}$) from X-ray crystal structures and theoretically calculated structures of $M(\text{P}^i\text{Pr}_3)_2(\text{CO})_3\text{L}$.

	M1-N1-C49	P1-M1-P2	N1-M1-P1 N1-M1-P2	C11-M1-C12	N1-M1-C11 N1-M1-C12
Mo(P^iPr_3)$_2\text{CO}_3$					
Computation					
AdNC	176.9 ^a	176.5	85.08 ^b 91.59 ^b	172.8	93.09 92.40
AdCN	177.8	174.8	84.77 90.34	171.9	93.96 93.24
W(P^iPr_3)$_2\text{CO}_3$					
AdNC	177.8 ^a	175.9	85.11 ^b 91.13 ^b	172.8	93.00 92.58
AdCN	178.0	174.2	84.44 90.18	171.3	94.62 93.18
2,4,6-Me $_3\text{C}_6\text{H}_2\text{CN}$	176.7	178.4	86.07 95.42	172.1	89.73 90.03
NCNMe $_2$	178.1	174.9	84.61 90.44	170.7	94.13 94.21
Mo(P^iPr_3)$_2\text{CO}_3$					
Experiment					
AdNC	178.0(2) ^a	174.30(2)	89.05(7) ^b 85.33(7) ^b	170.29(12)	94.74(11) 94.93(11)
AdCN	178.4(3)	173.60(3)	88.43(7) 85.24(7)	166.81(16)	96.37(12) 96.82(12)
W(P^iPr_3)$_2\text{CO}_3$					
AdNC	178.1(5) ^a	173.71(5)	88.19(16) ^b 86.12(16) ^b	170.9(2)	96.4(2) 90.6(2)
AdCN	176.9(5)	173.06(5)	86.04(10) 87.20(10)	167.8(3)	98.0(3) 94.2(2)
2,4,6-Me $_3\text{C}_6\text{H}_2\text{CN}$	175.1(4)	182.92(4)	87.49(10) 94.92(9)	172.6(2)	91.50(17) 86.74(18)
NCNMe $_2$	180.000(2)	172.25(4)	86.127(19) 86.127(19) ^c	166.3(2) ^d	96.83(11) 96.83(11) ^c
2,6-F $_2\text{C}_6\text{H}_2\text{CN}$	177.6(7)	174.64(9)	89.15(18) 86.65(18)	170.7(4)	96.8(3) 90.9(4)
2,6-Me $_2\text{C}_4\text{H}_2\text{N}_2$	n/a	179.52(4)	86.43(9) 93.45(9)	167.1(2)	94.36(19) 95.57(17)

^a values correspond to M1-C49-N1. ^b values correspond to C49-M1-P(1/2). ^c value corresponds to N1-M1-P1* ^d value corresponds to C11-W1-C11* ^e value corresponds to N1-W1-C11*

Overall, computational geometries are in good agreement with those that were determined experimentally. Generally mononuclear geometries were slightly distorted octahedra. The ⁱPr groups show two “axial” and one “equatorial” geometry per phosphine. The rotation of such groups, as well as the absolute stereochemistry of each “axial” ⁱPr, is not uniform across the ligand spectrum. This is consistent with the distortions, as complexes must accommodate the ligands and this involves a non-negligible steric component. This is also consistent with the non-binding of quinuclidine; such a ligand is so bulky that its mild σ -donor properties are overwhelmed. As is the case with most low valent Mo and W complexes, derivatives with the same ligand produced nearly identical crystal structures.

3.3 Discussion

Experimentally determined bond strength estimates are combined with B3LYP level calculational values in Figure 4.7 and in Appendix C Table C.1. The calculated binding enthalpies for the complexes with PMe₃ ligands are listed for both the small (LANL2DZ) and large (MWB28 or MWB60 ECP basis for the metal center and 6-311G(d,p) 5d for all other elements) basis sets. The two outliers on the graph correspond to the bridging complexes, and can be explained by poorly-described van der Waals interactions, weak bonding, and/or steric effects. It should be emphasized that while these data correspond to the formal definition of bond strength in solution, the product of ligand dissociation. The Mo(PⁱPr₃)₂(CO)₃ complex is known to contain an agostic bond estimated to be on the order of 6-10 kcal mol⁻¹ in strength. Thus the "absolute" Mo–CNCAd bond strength is not 29 kcal mol⁻¹ since dissociation of AdNC does not yield a

truly coordinatively unsaturated species, but one with a residual agostic bond and so an "absolute" Mo-CNAd bond strength would be on the order of $\sim 35\text{-}39 \text{ kcal mol}^{-1}$.

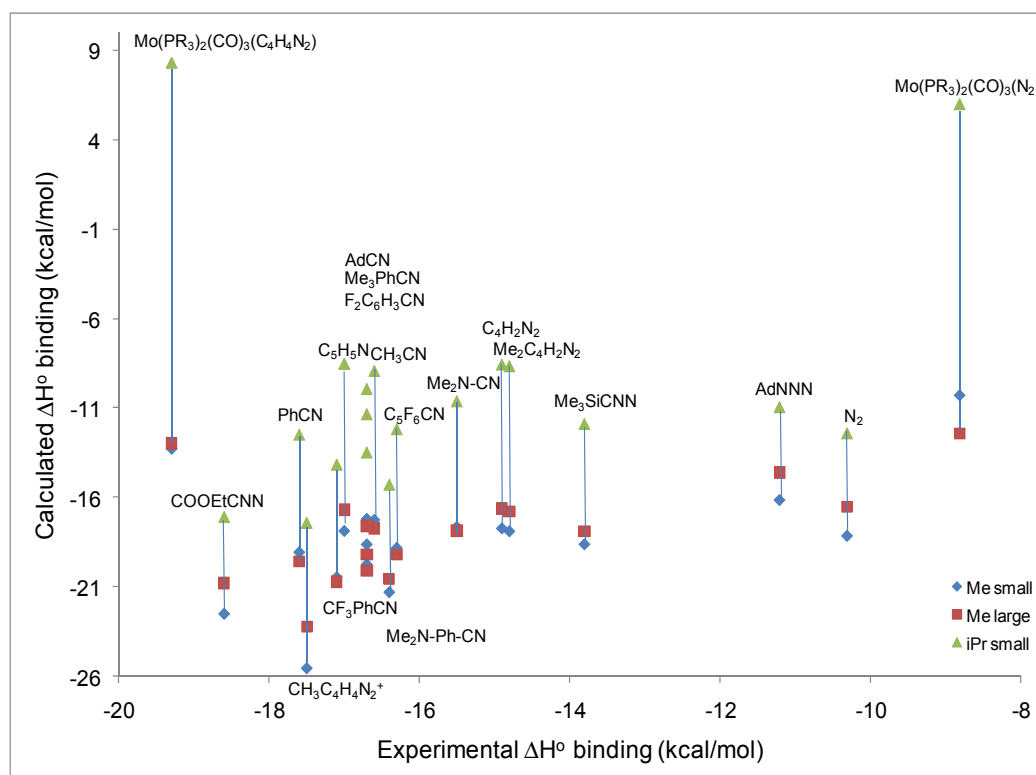


Figure 4.7. Plot of calculated vs. experimental N-binding enthalpies.

Shown in Figure 4.8 is a select plot of binding to $\text{Mo}(\text{P}^i\text{Pr}_3)(\text{CO})_3$ in toluene solution compared to gas-phase ligand protonation enthalpies. There appears to be a somewhat poor correlation. The scatter of the data hints at the roles that sterics and π -back bonding play for binding to the metal center, as a distinct entity from direct ligand σ basicity. The discussion is parsed into the following sections: (i) NNX ligands, (ii) nitrile NCR ligands, (iii) N-heterocyclic ligands, and (iv) comparison with $[\text{Ru}(\text{NH}_3)_5(\text{L})]^{2+}$.

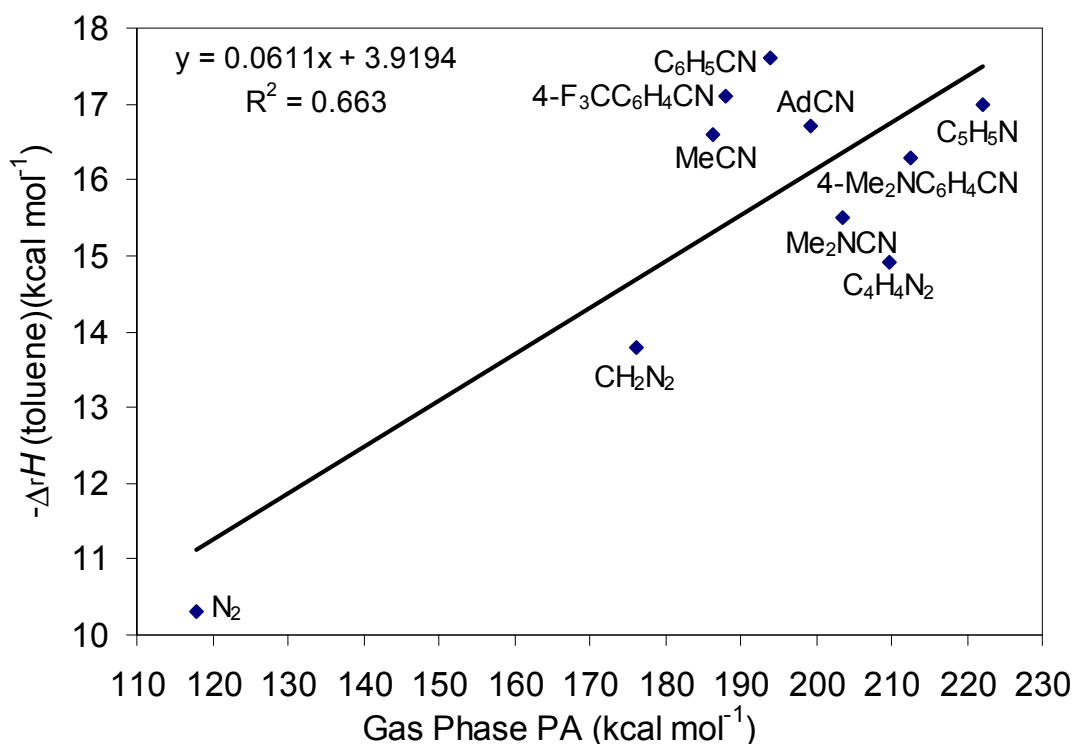

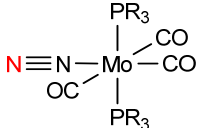
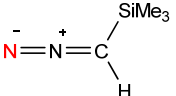
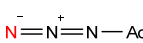


Figure 4.8. Solution phase binding to $\text{Mo}(\text{P}^i\text{Pr}_3)_2(\text{CO})_3$ measured in the present work vs literature gas phase proton affinities.¹⁰⁹ The proton affinity data for CH_2N_2 was taken from a computational study¹¹⁰ and used as a comparison for the experimentally measured $\text{N}_2\text{C}(\text{H})\text{SiMe}_3$ ligand.

NNX ligands. For ligands which contain (in at least one hybrid resonance form) a formal $\text{N}\equiv\text{N}$ bond the experimental binding enthalpies spanned $6.4 \text{ kcal mol}^{-1}$: $\text{Mo}(\text{P}^i\text{Pr}_3)_2(\text{CO})_3(\text{N}_2) < \text{N}_2 < \text{N}_3\text{Ad} < \text{N}_2\text{CHSiMe}_3$ (Table 4.5). Tellingly, the binding enthalpy of $\text{Mo}(\text{PR}_3)_2(\text{CO})_3(\text{N}_2)$ increases strongly upon computational “pruning” of the phosphines, and does so most strongly for the bulkiest structures. This indicates that the steric interactions do have varying effects on the heats of binding and most likely accounts for the instability of the $\mu\text{-(N}_2\text{)[Mo}(\text{P}^i\text{Pr}_3)_2(\text{CO})_3\text{]}_2$ complex.

Table 4.5. Computed and experimental binding enthalpies of NNX ligands (kcal mol⁻¹) in toluene solution.

	ΔH_{BSSE}	$\Delta H_{\text{BSSE, large}}$	ΔH_{BSSE}	ΔH_{Expt}
	Mo(PMe ₃) ₂ (CO) ₃		Mo(P ⁱ Pr ₃) ₂ (CO) ₃	
	-18.1	-16.5	-12.4	-10.3 ± 0.6
	-10.3	-12.5	6.0 ^a	-8.8 ± 1.2
	-18.6	-17.9	-11.9	-13.8 ± 0.5
	-16.1	-14.6	-10.9	-11.2 ± 0.4

^a predicted to be unstable

Of the monomeric complexes, N₂ was the weakest ligand while the diazo and azide ligands were observed to be marginally stronger. This ordering can be rationalized by examining the σ donating abilities of the ligands. Using gas phase proton affinity (N₂ = 118 kcal mol⁻¹; N=N=N-H = 180 kcal mol⁻¹; N=N=CH₂ = 205 kcal mol⁻¹)¹¹¹ as an estimate for σ basicity it can be seen that N₂ by far has the smallest thermodynamic basicity of the set. The azide has a lower proton affinity than that of the diazo compound which reciprocates to an approximate 25 kcal mol⁻¹ reduction in thermodynamic basicity for the azide relative to the diazo. This trend most likely explains reason for the ordering of ligand bond strength as N₂ < N₃Ad < N₂CHSiMe₃.

Experimental displacement of N₂ is exothermic by 3.5 kcal mol⁻¹ for N₂CHSiMe₃. This reaction may be viewed as a carbene transfer (Figure 4.9). Similarly displacement of the N₂ ligand by N₃Ad corresponds to formal nitrene transfer. Transfer of the N-Ad nitrene corresponds to $\Delta H = -0.9$ kcal mol⁻¹. The relatively small value derived for nitrene transfer may be a consequence of the nitrene fragment being inherently more stable than that of a corresponding carbene.

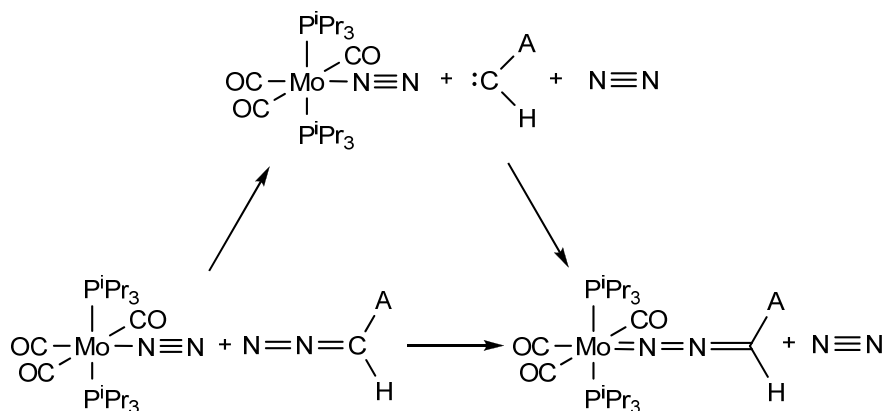


Figure 4.9. Ligand substitution viewed as carbene transfer.

Spectroscopic changes of the complexes can be used to probe alterations in back-bonding between the metal and ligands.^{xxii,112} Table 4.6 summarizes changes in ν_{CO} and ν_{NN} as compared to unsaturated $\text{Mo}(\text{P}^i\text{Pr}_3)_2(\text{CO})_3$ and free ligand determined.

Table 4.6. Experimental stretching frequencies (cm^{-1}) of Mo-NNX complexes in toluene solution as determined by FTIR.

	$\Delta\nu_{\text{NN}}^a$	$\Delta\nu_{\text{CO}}^a$	
$\text{Mo}(\text{P}^i\text{Pr}_3)_2\text{CO}_3$ (free)		1954	1848 1813
N_2	-148	5	2 1
NNNAd	? ^b	-2	-4 17
NNCHSiMe ₃	-46	-2	-1 12

^a $\Delta\nu_{\text{NR}} = \nu_{\text{NR}}(\text{free}) - \nu_{\text{NR}}(\text{bound})$ (R = N,C); ^b Peak intensity was too weak to be assigned.

N_2 displayed a large bathochromic shift in ν_{NN} while simultaneously hypsochromic shifts occurred in all three carbonyl stretches. This indicates that while N_2 is the weakest σ donor of the lot, it is inversely the most able back-bonder.

^{xxii} Carbonyl ligands have long been viewed as a means of evaluating an introduced ligand's ability donate/withdraw electron density from a metal center. As electron density is donated through the sigma bond the electron density about the metal increases thus causing it to back-donate electrons into the π^* orbitals of the coordinated carbonyls. This back donation causes a weakening in the bond strength of the carbonyl and generally this is accompanied by a shift to lower frequencies in its characteristic ν_{CO} stretches. This relationship is reversed when the introduced ligand is a strong π acceptor. (see reference 112)

Complexation of the diazo resulted in a smaller change in ν_{NN} . This signifies less back bonding from the metal in comparison to N_2 . Attempts to identify the NN stretch for the azide proved unfruitful. The azide and diazo showed similar changes in ν_{CO} . Thus, comparing the order of back bonding ability ($\text{N}_2 > \text{N}_3\text{Ad} \approx \text{N}_2\text{CHSiMe}_3$) to the order of exothermicity of the binding enthalpies ($\text{N}_2\text{CHSiMe}_3 > \text{N}_3\text{Ad} > \text{N}_2$) it can be seen that there is an offset that occurs due presumably to the increased σ basicity of the diazo and azide ligands.

NCR Ligands. Experimental nitrile binding enthalpies remained strikingly constant (Table 4.7). As previously discussed, the absolute bond strengths are on the order of $\sim 25 \text{ kcal mol}^{-1}$ due to the displaced agostic bond. It seems that bonding of nitriles to the $\text{Mo}(\text{P}^i\text{Pr}_3)_2(\text{CO})_3$ fragment is only slightly sensitive to changes in the π -bonding ability of the nitrile ligand. In spite of the small changes in bond energy, spectroscopic character shows up in shifts in the FTIR data in both ν_{CO} and ν_{CN} , as well as changes in color and λ_{max} in UV-vis spectra for these complexes.

As shown in Table 4.8, aromatic nitriles exhibit bathochromic shifts of ν_{CN} as electron withdrawing groups are added from 2225 (for bound AdCN) to 2177 cm^{-1} (for bound $\text{F}_5\text{C}_6\text{CN}$), indicating greater π back-donation. When we consider a difference of ν_{CN} before and after the binding of nitriles, the values of -9 , -10 , -24 , -26 , -45 , -48 , and -68 cm^{-1} are obtained for AdCN, 4-NMe₂C₆H₄CN, 2,4,6-Me₃C₆H₂CN, C₆H₅CN, 4-CF₃C₆H₄CN, 2,6-F₂C₆H₃CN and F₅C₆CN, respectively. These values are much smaller compared to the corresponding $\Delta\nu_{\text{NN}}$ of -148 cm^{-1} for N_2 binding to $\text{Mo}(\text{P}^i\text{Pr}_3)_2(\text{CO})_3$.

Table 4.7. Experimental and computed binding enthalpies of NCR ligands (kcal mol⁻¹) in toluene solution.

	ΔH_{BSSE}	$\Delta H_{\text{BSSE, lg, sp}}$	ΔH_{BSSE}	ΔH_{Expt}
	Mo(PMe ₃) ₂ CO ₃		Mo(P ⁱ Pr ₃) ₂ CO ₃	
	-28.9	-30.3	-21.1	-29.0 ± 0.3
	-17.2	-17.6	-9.9	-16.7 ± 0.5
	-17.6	-17.9	-10.6	-15.5 ± 1.8 ^a
	-18.8	-19.2	-12.2	-16.3 ± 0.6
	-18.8	-19.2	-12.2	-16.3 ± 0.6
	-17.3	-17.8	-8.9	-16.6 ± 0.4
	-19.1	-19.6	-12.5	-17.6 ± 0.3
	-18.6	-19.2	-11.3	-16.7 ± 0.6
	-19.7	-20.1	-13.5	-16.7 ± 0.6
	-20.5	-20.7	-13.5	-17.1 ± 0.6
	-21.3	-20.6	-15.3	-16.4 ± 0.6

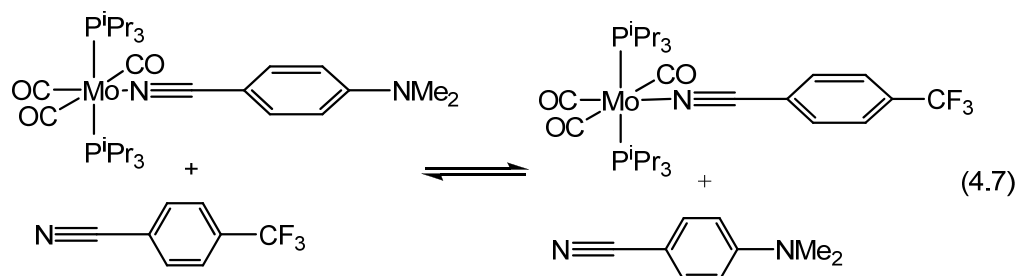
^a based on K_{eq} measurements with AdCN**Table 4.8.** Experimental (UV-vis and FTIR) data on nitrile complexes (ν_{CR} in cm⁻¹; λ_{max} in nm)

	λ_{max}	ν_{CN}	$\Delta\nu_{\text{CN}}^{\text{a}}$	$\Delta\nu_{\text{CO}}^{\text{a}}$		
Mo(P ⁱ Pr ₃) ₂ (CO) ₃				1954	1848	1813
AdNC		2089	-41	-11	-7	1
AdCN		2225	-9	-13	-19	-1
Me ₂ NCN		- ^b	- ^c	-14	-22	-7
p-Me ₂ NPhCN	454, 396	2207	-10	-15	-19	0
MeCN		- ^b	- ^c	-12	-16	2
PhCN	518, 444	2203	-26	-12	-16	3
MesitylCN	497, nr ^d	2195	-24	-12	-16	4
F ₂ PhCN	575, 488	2194	-48	-10	-11	11
p-CF ₃ PhCN	594, 502	2189	-45	-11	-11	12
F ₃ PhCN	618, 515	2177	-68	-8	-4	20

^a $\Delta\nu_{\text{CR}} = \nu_{\text{CR}}(\text{free}) - \nu_{\text{CR}}(\text{bound})$ (R= N, O) ^b Peak intensity too low to be identified. ^c $\Delta\nu_{\text{CN}}$ was unable to be calculated due to the lack of identification of the ν_{CN} bound complexes. ^d not resolved.

In the case of weaker σ donor $\text{N}\equiv\text{N}$ ligand, an electron density by π back-donation from both metal d_{xy} and d_{xz} orbitals is localized on $\text{N}\equiv\text{N}$ to stabilize the M-N bond. In the cases of $\text{N}\equiv\text{C}-\text{R}$ larger electron density on $\text{N}\equiv\text{C}$ was observed with stronger electron withdrawing groups, however, smaller $\Delta\nu_{\text{CN}}$ clearly indicate that σ donation ability of $\text{N}\equiv\text{C}-\text{R}$ is much stronger than that of $\text{N}\equiv\text{N}$. Analogous bathochromic ν_{CN} shifts have been reported for $[\text{Ru}(\text{NH}_3)_5(\text{RCN})]^{2+}$, -23 to -59 cm^{-1} .¹¹³

Since steric factors can also play a role, it is instructive to compare 4- $\text{NMe}_2\text{C}_6\text{H}_4\text{CN}$ and 4- $\text{CF}_3\text{C}_6\text{H}_4\text{CN}$ as ligands since the group in the *para*-position it should not alter the steric interactions significantly. It was found that 4- $\text{CF}_3\text{C}_6\text{H}_4\text{CN}$ bound more exothermically yielding a derived value of $\Delta H^\circ = -0.8 \pm 0.2 \text{ kcal mol}^{-1}$ for the reaction shown in eqn. 4.7.



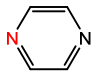
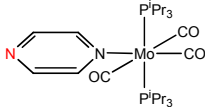
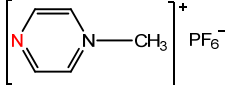
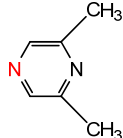
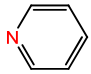
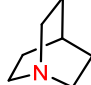
FTIR spectroscopic studies showed that at $20 \text{ }^\circ\text{C}$ in toluene solution $K_{\text{eq}} = 0.3 \pm 0.2$ for reaction 13 which corresponds to a value of $\Delta G^\circ = +0.7 \pm 0.3 \text{ kcal mol}^{-1}$. This generates an estimated value of $\Delta S^\circ = -5 \pm 2 \text{ cal mol}^{-1} \text{ K}^{-1}$ for the nitrile substitution reaction. A low value for the entropy of exchange would be expected and is observed. There is an apparent increase in backbonding to the nitrile ligand since as shown in Table 3, the difference between coordinated nitrile and free nitrile changes from 10 cm^{-1} for the 4- $\text{NMe}_2\text{C}_6\text{H}_4\text{CN}$ ligand to 45 cm^{-1} for the 4- $\text{CF}_3\text{C}_6\text{H}_4\text{CN}$ ligand. Concomitant with that change, however, there is a rise in average CO frequency of about 10 cm^{-1} . A simple

interpretation would be that the gain in backbonding to the nitrile is offset by a loss in backbonding to the CO ligand.

In order to explain UV-vis spectra of $\text{Mo}(\text{P}^i\text{Pr}_3)_2(\text{CO})_3(\text{nitrile})$ complexes, TD-B3LYP calculations were carried out. The calculations universally identified d_{xz} as the HOMO and π^*_{ligand} as the LUMO, and provided λ_{max} (Appendix C Table C.2) that were fairly consistent with experimentally determined values (Table 4.8.) Aromatic nitriles exhibit bathochromic shifts in λ_{max} as electron withdrawing groups are added, causing color darkening. This is consistent with stabilization of the LUMO (ligand CN π^*) and greater π back-donation to the ligand. On the other hand, the electron donating group Me_2N on the aromatic benzonitrile serves to destabilize the LUMO causing a hypsochromic shift in λ_{max} . The experimental UV-vis spectra were similar to those previously reported for $[\text{Ru}(\text{NH}_3)_5(\text{RCN})]^{2+}$ complexes.¹¹⁴

N-Heterocyclic Ligands. Quinuclidine does not bind to the P^iPr_3 complex, but computation says that it *should* bind to the cropped $\text{Mo}(\text{PMe}_3)(\text{CO})_3$ complex (Table 4.9). This is keeping with the already reported fact that the $\text{M}(\text{PR}_3)_2(\text{CO})_3$ complex does not bind tertiary amines due to sterics.¹⁰⁸ There was close agreement between mononuclear pyrazine and 2,6-dimethylpyrazine, which, as mentioned earlier, does not bind in a bridging fashion. The apparent conformity between stretching frequencies and heats of binding would be expected due to the similar electronics between the two ligands.

Table 4.9. Computed and experimental binding enthalpies (kcal mol⁻¹) of pyrazine-like ligands in toluene solution.

	Mo(PMe ₃) ₂ CO ₃		Mo(P ⁱ Pr ₃) ₂ CO ₃	
	$\Delta H_{\text{BSSE small}}$	$\Delta H_{\text{BSSE large sp}}$	ΔH_{BSSE}	ΔH_{expt}
	-17.7	-16.6	-8.6	-14.9 ± 0.9
	-13.5	-13.0	8.3	-19.3 ± 2.5
	-23.6	-23.2	-16.7	-17.5 ± 0.8 ^a
	-17.9	-16.8	-8.7	-14.8 ± 0.6
	-17.9	-16.7	-8.5	-17.0 ± 0.4
	-7.9	-5.9	11.2	NR ^b

^avalues measured in THF solution; ^b no reaction.

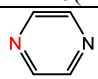
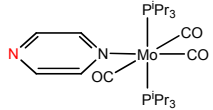
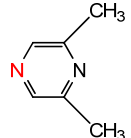
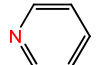
The bridging pyrazine is preferred by 4.4 kcal mol⁻¹. This is in contrast to the bridging N₂ complex in which the monomer is preferred by 1.5 ± 0.3 kcal mol⁻¹. This may be due to sufficient spacing between the metals in the pyrazine dimer, as compared to the N₂ dimer which holds the two halves too close together. Computational results did not estimate this well, but did a somewhat less-worse job on the PMe₃ molecules.

Binding of the Me-N₂C₄H₄⁺ ligand was determined to be the most exothermic of the monomeric pyrazine-like complexes. This is most likely due to the fact that the ligand is electron deficient and consequently will be a more efficient π acceptor. The increased binding of the C₅H₅N and Mo(PⁱPr₃)₂(CO)₃(C₄H₄N₂) over that of 2,4-Me₂C₄H₄N₂ and free C₂H₂N₂ can be accounted for by the two former's increased basicity. Taube has

noted the increased basicity pyrazine upon coordination to $[\text{Ru}(\text{NH}_3)_5]^{2+}$ ($[\text{Ru}(\text{NH}_3)_5(\text{C}_4\text{H}_4\text{N}_2)]^{2+}$ $pK_a = 2.5$; $\text{C}_4\text{H}_4\text{N}_2$ $pK_a = 0.6$ in aqueous solutions.)^{104b}

Experimental carbonyl stretching frequencies (Table 4.10) echo the previously discussed similarity between complexes involving the pyrazine and 2,6-dimethylpyrazine as ligands. Binding of all of the N-heterocyclic ligands generally result in bathochromic shifts in ν_{CO} as compared to the free $\text{Mo}(\text{P}^i\text{Pr}_3)_2(\text{CO})_3$. This implies that ligands' σ donation is much stronger than their respective back-donating acidity.

Table 4.10. Experimental (FTIR) ν_{CO} stretching frequencies (cm^{-1}) of N-heterocyclic complexes, in toluene solution.

Mo(P^iPr_3) ₂ CO ₃ (free)	$\Delta \nu_{\text{CO}}^a$		
	1954	1848	1813
	-14	-26 ^b	-2 ^b
	-24	-18	4
	-15	-23	0
	-18	-27	-8

^a $\Delta \nu_{\text{CO}} = \nu_{\text{CO}}(\text{free}) - \nu_{\text{CO}}(\text{bound})$ ^b Due to the large amount of pyrazine needed to make only the monomer, assignment of these band was with the dimer present. These stretches are unresolved from the monomer and tentatively assigned.

Geometries. Tables 4.3 and 4.5 recapitulate the highlighted bond distances and angles of the X-ray crystal structures, against computational results. In agreement with the solution calorimetric data, the R group of RCN did not introduce large differences in the length of $\text{N}\equiv\text{C}$. The largest difference was observed between the tungsten and molybdenum analogs of $\text{M}(\text{P}^i\text{Pr}_3)_2(\text{CO})_3(\text{AdCN})$ (1.153(6) Å [W]; 1.140(4) Å [Mo]).

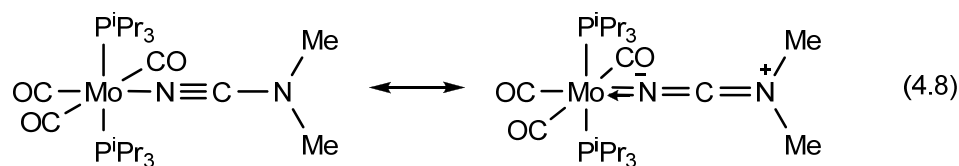
Comparison of the structures of bound nitriles to the X-ray structures of the free nitriles reveals only a minute lengthening of $\text{N}\equiv\text{C}$. Solid state structures report 1.139 Å for AdCN^{115} (bound 1.140(4) Å [Mo] and 1.153(6) [W]) and 1.145 Å for 2,6- $\text{F}_2\text{C}_6\text{H}_3\text{CN}^{116}$ (bound 1.145(6) Å [W]). Similar observations of only slight elongation of the $\text{N}\equiv\text{N}$ bond for $\mu\text{-(N}_2\text{)[W(CO)}_3\text{(P}^i\text{Pr}_3\text{)}_2$ ($\text{W-N}\equiv\text{N-W} = 1.136$ Å) have been noted. It was determined that electron donation into π^*_{NN} was minimal.¹¹⁷ This was explained in terms of resonance structures in which the $\text{W-N}\equiv\text{N-W}$ (not $\text{W}\equiv\text{N-N}\equiv\text{W}$) dominated. In the case of free 2,4,6- $\text{Me}_3\text{C}_6\text{H}_2\text{CN}$ the $\text{N}\equiv\text{C}$ bond length is 1.160 Å.¹¹⁸ The bound $\text{N}\equiv\text{C}$ bond length is 1.145(6) Å; a 0.015 Å shorting upon binding. The reason for this apparent strengthening of the $\text{N}\equiv\text{C}$ bond is unknown and is contrary to the FTIR spectral data in that ν_{CN} decreases by 30 cm^{-1} upon being coordinated.

Steric interactions with the phosphines seem to not play a large role in nitrile binding. The NC may be thought of as a “spacer” between two bulky groups. In fact, the shortest W-N bond lengths were observed for benzonitriles with substituents in the *ortho*-position, those being electron-withdrawing fluorines. The W-N distance was 2.130(6) Å for 2,6- $\text{F}_2\text{C}_6\text{H}_2\text{CN}$ and 2.166(4) Å for 2,4,6- $\text{Me}_3\text{C}_6\text{H}_2\text{CN}$, but 2.192(5) Å for NCNMe_2 . This is consistent with an increased donation to the π^*_{NC} by the electron-withdrawing fluorines. The M-N bond distances for the complexes with nitrile adducts are consistent with literature values: 2.190(5) Å in *fac*- $\text{W(dppm)(CO)}_3\text{(MeCN)}$,¹¹⁹ 2.227(12) and 2.204(12) Å (the two values are the result of the unit cell containing 2 molecules) in $\text{W(CO)}_5\text{(AdCN)}$,¹²⁰ and 2.21 Å in $\text{W(CO)}_3\text{(MeCN)}_3$.¹²¹

Structures of the isonitrile complexes are shown in Appendix C Figures C.3 and C.4. As expected, the M-C bonds (2.139(3) Å Mo; 2.113(6) Å W) are much shorter than

the M–N (2.220(3) Å Mo; 2.195(4) Å W) bond of the nitrile complexes. This reflects increased σ -donation from the isonitrile, as C is a weaker electrophile than N, and thus a stronger electron donor. Both the W–C bond and the C \equiv N bond are consistent with similar literature values: CpW(CO)₃(μ -PPh₂)W(CO)₄(^tPrNC)¹²² (W–C = 2.144(11) Å, C \equiv N = 1.139(13) Å), *cis*-W(η^1 -dppm)(CO)₄(C₆H₅NC)¹²³ (W–C = 2.133(8) Å, C \equiv N = 1.117(10) Å), Mo(CO)₃(^tBuNC)₃¹²⁴ (Mo–C = 2.140(4), 2.148(4), and 2.156(4) Å, C \equiv N = 1.159(5), 1.162(5), and 1.146(6) Å).

The most remarkable feature of W(PⁱPr₃)₂(CO)₃(NCNMe₂) is that the amide N exhibits trigonal planar geometry. This behavior has been previously reported for other complexes such as Cr(CO)₅(NCNEt₂),¹²⁵ *trans*-[Fe(Et₂PCH₂CH₂PEt₂)₂(NCNEt₂)₂][BF₄]₂,¹²⁶ and *trans*-Mo(Ph₂PCH₂CH₂PPh₂)₂(NCNEt₂)(N₂).¹²⁷ The planar configuration indicates significant contribution for the cumulene resonance (eqn. 4.8) and accounts for the weak ν_{CN} stretch of the bound Mo(PⁱPr₃)₂(CO)₃(NCNMe₂) complex. Structural data of the free ligand has been determined by gas phase electron diffraction.¹²⁸ The free NCNMe₂ ligand exhibits the conventional pyramidal geometry about the amine group. Bond distances appear to be very similar between the uncoordinated and coordinated ligands.



¹H NMR resonances for pyrazine protons are very sensitive to coordination to metal fragments. The aromatic protons of free pyrazine and 2,6-dimethylpyrazine resonate at $\delta(\text{C}_6\text{D}_6) = 8.04$ and 7.72 ppm. Pyrazine derivatives with $6\pi e^-$ show a normal

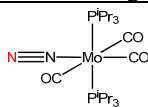
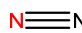
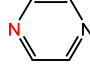
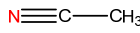
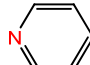
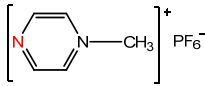
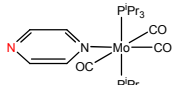
downfield shift.¹²⁹ In $\text{Mo}(\text{P}^i\text{Pr}_3)_2(\text{CO})_3(2,6\text{-Me}_2\text{C}_4\text{H}_2\text{N}_2)$ and $\mu\text{-}(\text{C}_4\text{H}_4\text{N}_2)[\text{M}(\text{P}^i\text{Pr}_3)_2(\text{CO})_3]_2$ resonances at $\delta = 8.76$ and 7.82 ppm (in C_6D_6) respectively were located for the pyrazine protons. The small paratropic shifts in the complexes, $\Delta\delta = -0.72$ and -0.22 ppm respectively, seem to indicate small changes in the pyrazine structure upon coordination to the $\text{Mo}(\text{P}^i\text{Pr}_3)_2(\text{CO})_3$ fragment. A similar downfield shifts of $\Delta\delta = -0.32$ ppm ($\mu\text{-}(\text{C}_4\text{H}_4\text{N}_2)[\text{Ru}(\text{NH}_3)_5]_2^{4+}$),¹³⁰ -0.59 ppm (H3 and H5 protons of $\text{Mo}(\text{CO})_5(\text{C}_4\text{H}_4\text{N}_2)$),¹³¹ -0.70 ppm (H2 and H6 protons of $\text{Mo}(\text{CO})_5(\text{C}_4\text{H}_4\text{N}_2)$),¹³¹ and -0.39 ppm ($\text{Mo}(\text{CO})_5(2,6\text{-Me}_2\text{C}_4\text{H}_4\text{N}_2)$)¹³¹ have been previously reported for other related complexes. Analogously, the resonances of the pyrazine protons of the free pyrazine and 2,6-dimethylpyrazine shift -0.59 and -0.40 ppm respectively upon protonation.¹³⁰ However, all of these values are clearly smaller than the large upfield shifts observed when the ligand is formally reduced by $2 e^-$ upon coordination to form the “antiaromatic” 1,4-dihydropyrazine system with $8 \pi e^-$.¹³²

Kaim et. al. have reported the structure of $[\text{W}(\text{PCy}_3)_2(\text{CO})_3(\text{N-MeC}_4\text{H}_4\text{N}_2)][\text{PF}_6]$. The W–N bond was reported as $2.101(10)$ Å.¹³² This bond length is greatly reduced from that which was determined in $\text{W}(\text{P}^i\text{Pr}_3)_2(\text{CO})_3(2,6\text{-Me}_2\text{C}_4\text{H}_2\text{N}_2)$ ($2.257(4)$ Å). This difference in bond length can be attributed to the higher degree of π -backdonation from the metal fragment to the pyrazinium ligand compared to neutral 2,6-dimethylpyrazine due to the stronger π -acid character of the cationic acceptor. It is also worth noting that Tutt and Zink have reported¹³³ a W–N bond length of $2.26(1)$ Å for the structure of $\text{W}(\text{CO})_5(\text{C}_5\text{H}_5\text{N})$ which is nearly identical to the W–N distance in the 2,6- $\text{Me}_2\text{C}_4\text{H}_2\text{N}_2$ structure. A single crystal x-ray structure has also been reported for the free

2,6-dimethylpyrazine ligand.¹³⁴ Binding of the 2,6-Me₂N₂C₄H₂ does not significantly alter the geometry of the ligand.

Comparison of binding of N-atom donor ligands to the Mo(PⁱPr₃)₂(CO)₃ and Ru(NH₃)₅²⁺ fragments. Data summarized in Table 4.11 include comparison of ligand displacement reactions for these two d⁶ isoelectronic complexes.

Table 4.11. Experimental and computational enthalpies (kcal mol⁻¹) of binding of N-donor ligands to Mo(PⁱPr₃)(CO)₃ (in toluene) and experimental heats of binding for N-donor ligands to [Ru(NH₃)₅(H₂O)]²⁺ in aqueous solution.

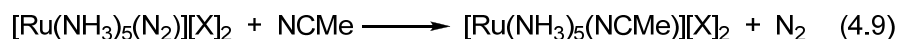
Ligand	ΔH_{exp}	ΔH_{calc}	$\Delta H_{\text{exp}}^{\text{a}}$
	-8.8 ± 1.2	unstable ^b	-11.2 ± 1.4
	-10.3 ± 0.6	-12.4	-10.1 ± 1.4
	-14.9 ± 0.9	-8.6	-16.8 ± 0.1
	-16.6 ± 0.4	-8.9	-9.2 ± 0.2
	-17.0 ± 0.4	-8.5	-12.7 ± 1.0
	-17.5 ± 0.8 ^d	-9.4	-18.0 ± 0.3
	-19.3 ± 2.5	unstable ^b	-13.8 ± 0.8

^aData for the ion [Ru(NH₃)₅(H₂O)]²⁺ taken from reference 104, see text for additional discussion; ^bcomputation predict this complex is endothermic and unstable; ^c based on K_{eq} with AdCN; ^d value measured in THF solution; ^e based on K_{eq} with PhCN.

For the Mo system, an agostic bond is displaced and the reactions are studied in toluene solution. The Ru²⁺ system were studied in aqueous solution and consequently, bound water is displaced by the incoming ligand. In spite of this, the measured enthalpies of binding of N₂ overlap within experimental error. The enthalpies of binding of pyrazine and MeC₄H₂N₂⁺ are also close for both systems. However, those of MeCN and pyridine are much lower for Ru²⁺.

For the Ru^{2+} system, bridging N_2 is preferred over the monomeric form, and monomeric pyrazine configuration is preferred over bridging. This scenario is exactly opposite that of Mo^0 . However, hydration energies and ion pairing are expected to play an important role for the Ru^{2+} system in aqueous solution. In fact, strong H-bonding between water molecules and the N of the pyrazine not coordinated to the Ru^{2+} fragment might be expected for the mononuclear complex. The stabilizing effect is not possible in the bridging species. Tellingly, coordination to the Ru^{2+} center makes pyrazine nearly two orders of magnitude more basic ($\text{p}K_{\text{a}}([\text{Ru}(\text{NH}_3)_5(\text{C}_4\text{H}_4\text{N}_2)]^{2+}) = 2.5$ vs $\text{p}K_{\text{a}}(\text{C}_4\text{H}_4\text{N}_2) = 0.6$).^{104b} For the Mo complexes, in toluene solution, solvation effects are presumed to be much smaller.

The large difference between the heats of binding for the NCMe ligand may also be the result of solvation energies. The enthalpy of solution of acetonitrile in water is itself a complex process¹³⁵ which Marcus and Migron have studied in terms of micro inhomogeneity.¹³⁶ Thus considering the ligand substitution in reaction 4.9, a significant contribution to the energy could be the differences in solvation energy of the nitrile and dinitrogen cationic complexes in aqueous solution.



In addition, this might depend on the nature of the counter ion. The position of the $\nu_{\text{N}=\text{N}}$ IR stretch in solid $[\text{Ru}(\text{NH}_3)_5(\text{N}_2)][\text{X}]_2$ depends on the nature of X and ranges from 2105 cm^{-1} for $\text{X} = \text{Cl}^-$ to 2167 cm^{-1} for $\text{X} = \text{PF}_6^-$.¹³⁷

In spite of some surprising similarities in bonding, detailed understanding of the Ru^{2+} system in aqueous solution and its comparison to the Mo^0 system in toluene solution

is a challenging but potentially important area, in particular in terms of phase transfer catalysis where differing solvation effects could be of practical utility.

4.4 Conclusions

The enthalpies of binding of a range of $\text{Mo}(\text{P}^i\text{Pr}_3)_2(\text{CO})_3(\text{NX})$ ($\text{NX} = \text{N}_2$, nitriles, N_3Ad , $\text{N}_2\text{CHSiMe}_3$, pyradine, pyrazines) complexes were examined. Heats of binding spanned a range of $\sim 10 \text{ kcal mol}^{-1}$. Spectroscopic analysis of these compounds was also utilized. Generally an increase in back bonding to the N-X ligand resulted in a decrease in the backbonding to the CO ligands.

Remarkably, most nitrile complexes were clustered within a 1 kcal mol^{-1} range, despite dramatic color changes and mild variation of ν_{CN} . This was in agreement to the several X-ray crystal structures that were determined in that only minute geometric changes were seen between the complexes with different nitrile ligands. The introduction of electron withdrawing groups to the nitrile ligands tended to increase back bonding however, this was generally counterbalanced by a decrease in backdonation to the CO ligands.

Binding of the N-heterocyclic compounds varied primarily on the intrinsic basicity of the ligand. The NNX ligands tended have a greater ability to back bond compared to both the N-heterocyclic compounds and the nitriles however, they also tended to be weaker σ donors. This translated into smaller heats of binding for the NNX ligands compared to the other classes of N-donors. In many cases, computation adequately approximated experimental data which enabled an increased interpretation of the data.

4.5 Experimental

General Considerations. Unless stated otherwise, all operations were performed in a drybox under an atmosphere of purified argon. Toluene, THF, benzene, heptane and octane were distilled over sodium metal before use. Distilled solvents were transferred under an out-flow of argon into vacuum-tight vessels and degassed before being transferred into the drybox. C_6D_6 was purchased from Sigma-Aldrich. $M(P^iPr_3)_2(CO)_3$ ($M = W, Mo$),¹³⁸ $Mo(P^iPr_3)_2(CO)(L)$ ($L = N_2$,¹³⁸ $[Me-N_2C_4H_4][PF_6]$,¹³² N_3Ad (see chapter 5)) and $AdNC$ ¹³⁹ were prepared following literature methods. $AdNC$ was crystallized from a CH_2Cl_2 /heptane mixture and sublimed at ≈ 85 °C before use. All other compounds were used as received. 1H NMR spectra were recorded on Bruker AVANCE-400 spectrometer at $T = 20$ °C. Chemical shifts are reported with respect to internal solvent: 7.16 ppm (C_6D_6). FTIR spectra were obtained using a Perkin Elmer 2000 FTIR/Microscope system that has been described elsewhere.¹⁴⁰ UV-vis spectra were recorded on a Perkin Elmer Lambda 900 spectrophotometer.

Synthesis of $Mo(P^iPr_3)_2(CO)_3(L)$ ($L = 2,6-Me_2C_4H_2N_2, Me_2NCN, 4-Me_2NC_6H_4CN, C_6F_5CN, NCM_e, NCA_d, 2,4,6-MeC_6H_2CN, 2,6-F_2C_6H_3CN, N_2CHSiMe_3, NC_5H_5, 4-CF_3C_6H_4CN, [Me-N_2C_4H_4][PF_6], C_6H_5CN, CNAd$.) All synthesis were performed in a similar manner. In a representative preparation a 20 mL scintillation vial was charged with 0.20 mmol of $Mo(P^iPr_3)_2(CO)_3$ and an equimolar amount of NCA_d . 5.0 mL of toluene was added. The reaction solution instantaneously turns from brown to yellow. The solution was then removed under reduced pressure the solid was then washed twice with a minimal amount of heptane to remove excess ligand

and $M(\text{P}^i\text{Pr}_3)_2(\text{CO})_4$. 0.114 g (86% yield) of yellow crystalline $M(\text{P}^i\text{Pr}_3)_2(\text{CO})_3(\text{CNAd})$ was recovered. All products except the $\text{N}_2\text{CHSiMe}_3$ and $\text{N}_2\text{CHCOOEt}$ complexes were recovered with >75% yields. $\text{N}_2\text{CHSiMe}_3$ and $\text{N}_2\text{CHCOOEt}$ complexes decomposed to unknown products upon concentration. Yields for these two were based on NMR data and were determined to be >95%. The products were characterized by FTIR and NMR. FTIR See Table C.3 in Appendix C. ^1H NMR shifts (C_6D_6) ppm: **2,6-Me₂C₄H₂N₂** 1.23 36H(q), 2.12 6H(m), 8.76 2H(s), 2.00 6H(s); **Me₂NCN** 1.39 36H(q), 2.36 6H(m), 1.79 6H(s); **4-Me₂NC₆H₄CN** 1.45 36H(q), 2.44 6H(m), 7.13 2H(d), 6.04 2H(d) 2.21 6H(s); **C₆F₅CN** 1.39 36H(q), 2.41 6H(m); **NCMe** 1.35 36H(q), 2.32 6H(m), 0.67 3H(s); **NCAd** 1.40 36H(q), 2.40 6H(m), 1.59 6H(d), 1.50 3H(m), 1.24 6H(m); **2,4,6-MeC₆H₂CN** 1.38 36H(q), 2.39 6H(m), 6.36 2H(s), 2.28 6H(s), 1.83 3H(s); **2,6-F₂C₆H₃CN** 1.40 36H(q), 2.42 6H(m), 6.28 1H(m), 6.04 2H(t); **NC₅H₅** 1.25 36H(q), 2.11 6H(m), 8.90 2H, 6.15 2H, 6.61 1H; **4-CF₃C₆H₄** 1.37 36H(q), 2.38 6H(m), 6.92 2H, 6.89 2H; **N₂CHSiMe₃** 1.27 36H(q), 2.22 2.38 6H(m), 2.78 1H(s) 0.03 9H(s); **C₆H₅CN** 1.38 36H(q), 2.38 6H(m), 7.04 2Hd, 6.84 2H(t), 6.74 1H(t); **N₂CHC(=O)OC₂H₅** 1.23 36H(q), 2.24 6H(m), **CNAd** 1.38 36H(q), 2.39 6H(m), 1.75 6H(d), 1.68 3H(m), 1.28 6H(m).

Synthesis of $W(\text{P}^i\text{Pr}_3)_2(\text{CO})_3(\text{L})$ (L = 2,6-Me₂C₄H₂N₂, Me₂NCN, NCAd, 2,4,6-MeC₆H₂CN, 2,6-F₂C₆H₃CN, CNAd.) Syntheses were the same as the Mo analogs. All yields were > 75%. ^1H NMR shifts (C_6D_6) ppm: **2,6-Me₂C₄H₂N₂** 1.22 36H(q), 2.23 6H(m), 8.89 2H(s), 1.97 6H(s); **Me₂NCN** 1.37 36H(q), 2.43 6H(m), 1.81 6H(s); **2,4,6-MeC₆H₂CN** 1.36 36H(q), 2.47 6H(m), 6.36 2H(s), 2.28 6H(s), 1.82 3H(s); **2,6-F₂C₆H₃CN** 1.38 36H(q), 2.48 6H(m), 6.28 1H(m), 6.03 2H(t); **NCAd** 1.39 36H(q),

2.47 6H(m), 1.60 6H(d), 1.51 3H(m), 1.26 6H(m); **CNAd** 1.37 36H(q), 2.45 6H(m), 1.75 6H(d), 1.68 3H(m), 1.29 6H(m).

Calorimetric Measurement of Displacement of L from Mo(PⁱPr₃)₂(CO)₃L by AdNC. In the glove box, a solution of the target compound was prepared in 5 mL of freshly distilled toluene, and transferred *via* syringe into the calorimeter cell. A few milligrams of freshly sublimed AdNC was loaded into the solid sample holder of the calorimeter cell. The cell was sealed, taken from the glove box, and loaded into a Setaram C-80 calorimeter. After thermal equilibration, the reaction was initiated and followed to completion at 30 °C. Following return to baseline, the cell was taken back into the glove box and its contents examined by FTIR to confirm complete conversion. The reported average values are based on four to six independent determinations for the enthalpy of reaction based on solid AdNC. From the measured values and the enthalpy of solution of AdNC in toluene ($\Delta H = 3.1 \pm 0.1 \text{ kcal mol}^{-1}$), a value with all species in solution was determined.

K_{eq} for Binding of N₂ to Mo(PⁱPr₃)₂(CO)₃. A thermostated medium pressure FTIR cell fitted with CaF₂ windows (obtained from Harrick Scientific) was fitted with a 40 ml stainless steel bomb, valves, pressure sensor and a thermistor probe inserted directly into the solution. This assembly was loaded in the glove box with 0.3050 g (0.6100 mmol) Mo(PⁱPr₃)₂(CO)₃ and 20.0 mL of a 4.0 mM solution of Mo(CO)₆ in toluene. The Mo(CO)₆ ν_{CO} stretch at 1984 cm⁻¹ was used in data analysis as a calibration standard to correct for increased path lengths under the higher pressures of N₂. Initially the cell was pressured to ~280 psi N₂ at room temperature to obtain a maximum value for the absorbance due to the Mo(PⁱPr₃)₂(CO)₃(N₂). This maximum value was then utilized

to calculate the relative concentrations by means of difference. The pressure was released to ~ 15 psi and the temperature was varied in incremental steps from 336 to 284 K. Values for K_{eq} were interpreted in units of atm^{-1} . Corrections in the observed pressure of N_2 due to an increase in the vapor pressure of toluene at higher temperature were made. At the end of the experiment the cell was re-pressured to ~ 280 psi at room temperature and the sample was again examined by FTIR spectroscopy. The resultant spectrum was ultimately compared to the spectrum taken in the beginning of the experiment indicating no decomposition of the reactive $\text{Mo}(\text{P}^i\text{Pr}_3)_2(\text{CO})_3$ complex. Variable temperature FTIR spectral data are shown in Appendix C Figure C.1. Three independent experiments were performed. The results of all the experiments were used in the final determination of $\Delta H = -10.3 \pm 0.6 \text{ kcal mol}^{-1}$ and $\Delta S = -32.3 \pm 2.0 \text{ cal mol}^{-1} \text{ K}^{-1}$ for the binding of N_2 to $\text{Mo}(\text{P}^i\text{Pr}_3)_2(\text{CO})_3$ to form $\text{Mo}(\text{P}^i\text{Pr}_3)_2(\text{CO})_3(\text{N}_2)$.

Calorimetric Measurements of the heat of binding $\text{W}(\text{P}^i\text{Pr}_3)_2(\text{CO})_3(\text{N}_2)$ to $\text{W}(\text{P}^i\text{Pr}_3)_2(\text{CO})_3$. In an representative experiment 19.3 mg of crystalline $(\mu\text{-N}_2)[\text{W}(\text{P}^i\text{Pr}_3)_2(\text{CO})_3]_2$ was loaded into the solid compartment of a calorimeter cell. The cell was then loaded with 5 mL of toluene then sealed under a nitrogen atmosphere. The cell was sealed, taken from the glove box, and loaded into a Setaram C-80 calorimeter. After thermal equilibration, the reaction was initiated and followed to completion at 30 °C. Following return to baseline, the cell was taken back into the glove box and its contents examined by FTIR to confirm complete conversion to $\text{W}(\text{P}^i\text{Pr}_3)_2(\text{CO})_3(\text{N}_2)$. The reported average values are based on three independent experiments. From the measured values and the enthalpy of solution of $(\mu\text{-N}_2)[\text{W}(\text{P}^i\text{Pr}_3)_2(\text{CO})_3]_2$ in toluene under an Ar atmosphere ($\Delta H = +6.7 \pm 0.3 \text{ kcal mol}^{-1}$), a value with all species in solution for the

reaction of $(\mu\text{-N}_2)[\text{W}(\text{P}^i\text{Pr}_3)_2(\text{CO})_3]_2$ with N_2 to form $\text{W}(\text{P}^i\text{Pr}_3)_2(\text{CO})_3(\text{N}_2)$ was determined to be $\Delta H = -1.5 \pm 0.6 \text{ kcal mol}^{-1}$.

K_{eq} for Binding of Pyrazine to $\text{Mo}(\text{P}^i\text{Pr}_3)_2(\text{CO})_3$. A thermostated medium pressure FTIR cell fitted with CaF_2 windows (obtained from Harrick Scientific) was fitted with a 40 ml stainless steel bomb, valves, and a thermistor probe inserted directly into the solution. This assembly was loaded in the glove box with 0.1939 g (0.4 mmol) $\text{Mo}(\text{P}^i\text{Pr}_3)_2(\text{CO})_3$, 0.5025 g (6.3 mmol) pyrazine, and 12 ml C_6D_6 . The concentration of pyrazine was considered not to change since any changes due to reaction were small compared to experimental error. Relative concentrations of the organometallic complexes were determined by band shape analysis of the spectra. Representative spectral data are shown in Appendix C Figure C.2. The absorbance maxima of the major and minor bands were measured. Assuming a symmetrical band shape, it was determined that the absorbance of the major band at the peak maximum position of the minor band was 0.19 times the major band height. This was done by measuring the absorbance equidistant on the low-wave number side. From this the ratio of the two bands was determined.

Crystallographic Analyses for $\text{Mo}(\text{P}^i\text{Pr}_3)_2(\text{CO})_3(\text{L})$ ($\text{L} = \text{AdCN}$, AdNC) and $\text{W}(\text{P}^i\text{Pr}_3)_2(\text{CO})_3(\text{L})$ ($\text{L} = \text{AdCN}$, $2,4,6\text{-Me}_3\text{C}_6\text{H}_2\text{CN}$, $2,6\text{-F}_2\text{C}_6\text{H}_2\text{CN}$, $2,6\text{-Me}_2\text{C}_4\text{H}_2\text{N}_2$.) Yellow single crystals of $\text{Mo}(\text{P}^i\text{Pr}_3)_2(\text{CO})_3(\text{AdNC})$, $\text{Mo}(\text{P}^i\text{Pr}_3)_2(\text{CO})_3(\text{AdCN})$ and $\text{W}(\text{P}^i\text{Pr}_3)_2(\text{CO})_3(\text{AdNC})$; orange single crystals of $\text{W}(\text{P}^i\text{Pr}_3)_2(\text{CO})_3(2,4,6\text{-Me}_3\text{C}_6\text{H}_2\text{CN})$ and maroon single crystals of $\text{W}(\text{P}^i\text{Pr}_3)_2(\text{CO})_3(2,6\text{-F}_2\text{C}_6\text{H}_2\text{CN})$ suitable for x-ray diffraction analyses were obtained by evaporation of a mixture of benzene and octane at 21°C under an inert atmosphere of argon. Blue single crystals of $\text{W}(\text{P}^i\text{Pr}_3)_2(\text{CO})_3(2,6\text{-Me}_2\text{C}_4\text{H}_2\text{N}_2)$, yellow single crystals of

$W(\text{P}^i\text{Pr}_3)_2(\text{CO})_3(\text{NCAd})$ were grown from a layered solution of heptane/toluene that was placed in a $-20\text{ }^\circ\text{C}$ freezer for 1 month. Once separated from the mother liquor the solid crystals were observed to be relatively air stable. Each crystal was glued onto the end of a thin glass fiber. No decomposition was observed during the data collection period.

X-ray intensity data were measured and interpreted by Burjor Captain from the University of Miami with a Bruker SMART APEX2 CCD-based diffractometer using $\text{Mo K}\alpha$ radiation ($\lambda = 0.71073\text{ \AA}$).¹⁴¹ The raw data frames were integrated with the SAINT+ program by using a narrow-frame integration algorithm.¹⁴¹ Corrections for Lorentz and polarization effects were also applied with SAINT+. An empirical absorption correction based on the multiple measurement of equivalent reflections was applied using the program SADABS. All structures were solved by a combination of direct methods and difference Fourier syntheses, and refined by full-matrix least-squares on F^2 , by using the SHELXTL software package.¹⁴² All non-hydrogen atoms were refined with anisotropic displacement parameters. Hydrogen atoms were placed in geometrically idealized positions and included as standard riding atoms during the least-squares refinements. Crystal data, data collection parameters, and results of the analyses are listed in Appendix C Tables C.4 and C.5.

All the complexes studied crystallized in the monoclinic crystal system. The systematic absences in the intensity data were consistent with the unique space groups $P2_1/n$ for $\text{Mo}(\text{P}^i\text{Pr}_3)_2(\text{CO})_3(\text{AdNC})$, $\text{Mo}(\text{P}^i\text{Pr}_3)_2(\text{CO})_3(\text{AdCN})$ and $\text{W}(\text{P}^i\text{Pr}_3)_2(\text{CO})_3(2,6\text{-F}_2\text{C}_6\text{H}_2\text{CN})$; $P2_1/c$ for $\text{W}(\text{P}^i\text{Pr}_3)_2(\text{CO})_3(2,4,6\text{-Me}_3\text{C}_6\text{H}_2\text{CN})$; $P2_12_12_1$ for $\text{W}(\text{P}^i\text{Pr}_3)_2(\text{CO})_3(\text{AdNC})$; and $Pbca$ for $\text{W}(\text{P}^i\text{Pr}_3)_2(\text{CO})_3(2,6\text{-Me}_2\text{C}_4\text{H}_2\text{N}_2)$.

For $W(P^iPr_3)_2(CO)_3(AdNC)$, there is minor disorder present in the Adamantyl group (atoms C51-C59) which was not modeled due to satisfactory low R factors, $R_1 = 3.45\%$, in the final stages of the refinement. The carbon atoms of the disordered Adamantyl group were refined with isotropic displacement parameters.

$Mo(P^iPr_3)_2(CO)_3(AdNC)$ and $Mo(P^iPr_3)_2(CO)_3(AdCN)$ are both isomorphous and isostructural. With $Z = 8$, there are two formula equivalents of the molecule present in the asymmetric crystal unit for compounds $Mo(P^iPr_3)_2(CO)_3(AdNC)$, $Mo(P^iPr_3)_2(CO)_3(AdCN)$ and $W(P^iPr_3)_2(CO)_3(2,6-F_2C_6H_2CN)$. With $Z = 16$, there are two formula equivalents of the molecule present in the asymmetric crystal unit for $W(P^iPr_3)_2(CO)_3(2,6-Me_2C_4H_2N_2)$.

Crystallographic Analyses for $W(P^iPr_3)_2(CO)_3(L)$ ($L = NCNMe_2$ and $CNAd$). Yellow single crystals of $W(PiPr_3)_2(CO)_3(NCNMe_2)$ and $W(PiPr_3)_2(CO)_3(CNAd)$ were crystallized from saturated solutions of a mixture of toluene and heptane stored at $-20\text{ }^\circ\text{C}$ for on month. Once the single crystals were separated from the mother liquor they were sent off site for X-ray analysis. X-ray intensity data were measured were measured by collaborators at Los Alamos National Laboratory. Data collection details are reported in literature.¹⁴³

Computational Details. Calculations included in this chapter were provided by Patrick Achord and Etsuko Fujita from Brookhaven National Laboratory and James T. Muckerman from Los Alamos National Laboratory. All electronic structure calculations used the B3LYP hybrid density functional method as implemented in the Gaussian 03 suite of programs. Structures were optimized using the LANL2DZ basis: LANL2DZ ECP and basis for the transition-metal centers and P atoms, the Dunning-Huzinaga D95V basis

for all other atoms. Optimizations were first carried out in the gas phase in order to obtain the basis set superposition error (BSSE) using counterpoise calculations. The structures were then reoptimized and vibrational frequencies calculated in “toluene solution” (or “THF solution”) using a polarizable continuum model (PCM) and UAHF radii.

Computed electronic energies were corrected for zero-point energy, thermal energy, and entropic effects to obtain the corresponding thermodynamic properties H° and G° in solution. Adding gas-phase BSSE corrections to H° provided the binding enthalpies. Full details on computational methods can be found in the manuscript that results from the work presented in this chapter.¹⁴³

CHAPTER 5: Conversion of 1-Adamantyl Azide to 1-Adamantyl Isocyanate by $[\text{Cr}(\text{CO})_3\text{Cp}]_2$, Hydrogenation to 1-Adamantyl Amine by $\text{HMo}(\text{CO})_3\text{Cp}$ and Reaction with $\text{Mo}(\text{CO})_3(\text{P}^i\text{Pr}_3)_2$ to Form $\text{Mo}(\kappa^2\text{-}^i\text{Pr}_3\text{P}=\text{N}-\text{N}=\text{N}-\text{Ad})(\text{CO})_3(\text{P}^i\text{Pr}_3)$.

5.1 Background.

Azides have a very diverse chemistry in both main group and organometallic chemistry. The focus of this chapter will predominately be on the reactivities of an alkyl azide's with low valent, group 6, organometallic complexes. Analogous to Chapter 2 in which diazoalkanes ($\text{N}=\text{N}=\text{CR}_2$) can be viewed as sources of carbenes, azides ($\text{N}=\text{N}=\text{N}-\text{R}$) can be viewed as the dinitrogen adducts of highly reactive nitrene fragments.¹⁴⁴ Chapter 2 discussed carbonylation of $\text{N}=\text{N}=\text{CHSiMe}_3$ by the metal radicals $\bullet\text{Cr}(\text{CO})_3\text{C}_5\text{R}_5$ ($\text{R} = \text{H}, \text{CH}_3$).⁵⁰ The net observed reaction based on $[\text{Cr}(\text{CO})_3\text{Cp}]_2$ (precursor to $\bullet\text{Cr}(\text{CO})_3\text{Cp}$ ($\text{Cp} = \eta^5\text{-cyclopentadienyl}$)) is shown in eqn. 5.1.



In addition, Chapter 3 discussed the reaction of $\text{N}_2\text{CHSiMe}_3$ with the metal hydrides $\text{HMo}(\text{CO})_3\text{C}_5\text{R}_5$ ($\text{R} = \text{H}, \text{CH}_3$) as a function of solvent and also prior coordination of the diazoalkane to $\text{Mo}(\text{P}^i\text{Pr}_3)_2(\text{CO})_3$ ($^i\text{Pr}_3 = \text{isopropyl}$).⁷⁷ This chapter extends those investigations to analogous reactions of N_3Ad ($\text{Ad} = 1\text{-adamantyl}$).

5.2 Results and Discussion

Reaction of $[\text{Cr}(\text{CO})_3\text{Cp}]_2$ with N_3Ad . The reaction of $[\text{Cr}(\text{CO})_3\text{Cp}]_2$ (a source of $\bullet\text{Cr}(\text{CO})_3\text{Cp}$ in solution) was shown to proceed cleanly as in shown in eqn. 5.2 under an Ar atmosphere.



When the reaction is executed under an atmosphere of CO, there is only minor production of $[\text{Cr}(\text{CO})_2\text{Cp}]_2$ and the chromium complex acts as a catalyst for carbonylation of the azide. Product distribution was determined by quantitative FTIR analysis (see Figures 5.1-5.3 for FTIR spectra). Shown in Appendix D Figure D.1 is the comparison of the consumption of $[\text{Cr}(\text{CO})_3\text{Cp}]_2$ under these two atmospheres.

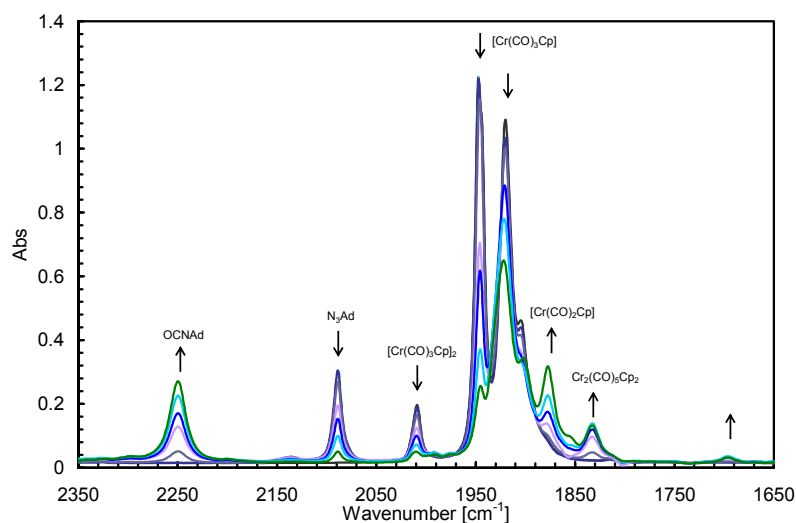


Figure 5.1 FTIR of first phase of the reaction of $[\text{Cr}(\text{CO})_3\text{Cp}]_2$ with N_3Ad in toluene under an Ar atmosphere. There is an initial induction period in which an intermediate is formed which in turn converts the N_3Ad to OCNAd .

Under an Ar atmosphere the reaction is best viewed as a “two part” reaction process.^{xxiii} The first “part” of the reaction is shown in Figure 5.1. From this FTIR it can be seen that initially there is an induction period. This is then followed by a build up of intermediates and a large drop in the starting materials $[\text{Cr}(\text{CO})_3\text{Cp}]_2$ and N_3Ad with the concurrent production of OCNAd . Also there is a small build up of the final unreactive $[\text{Cr}(\text{CO})_3\text{Cp}]_2$ complex. Continuing into the second “part” of the reaction (Figure 5.2),

^{xxiii} The reaction being viewed in two parts is completely arbitrary and only used as a means of interpreting the spectral data. There reaction, in reality, is one continuous reaction.

residual amounts of N_3Ad are converted into OCNAd and the intermediate $[\text{Cr}_2(\text{CO})_5\text{Cp}_2]$ loses CO to form $[\text{Cr}(\text{CO})_2\text{Cp}]_2$.

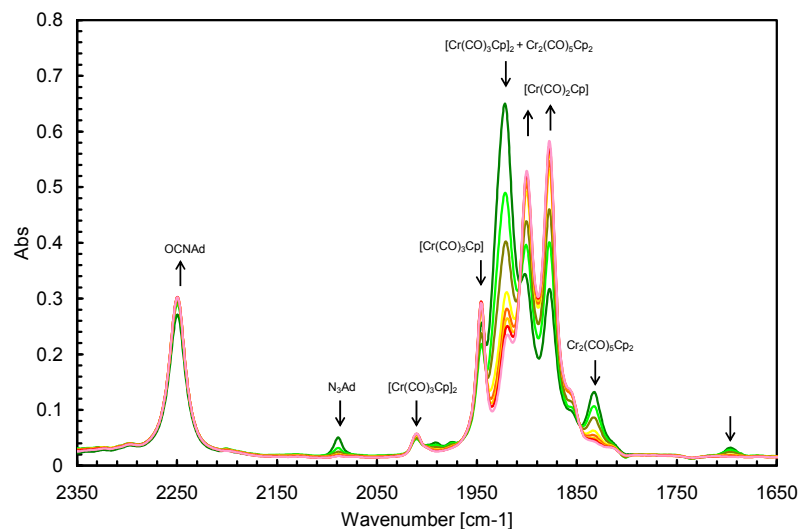


Figure 5.2. FTIR of the second phase of reaction of $[\text{Cr}(\text{CO})_3\text{Cp}]_2$ with N_3Ad in toluene under an Ar atmosphere. The maximum concentration of the intermediate has been reached and as it decays there is a significant buildup of the final unreactive species $[\text{Cr}(\text{CO})_2\text{Cp}]_2$. (spectra overlap with Figure 5.1 at dark green spectra)

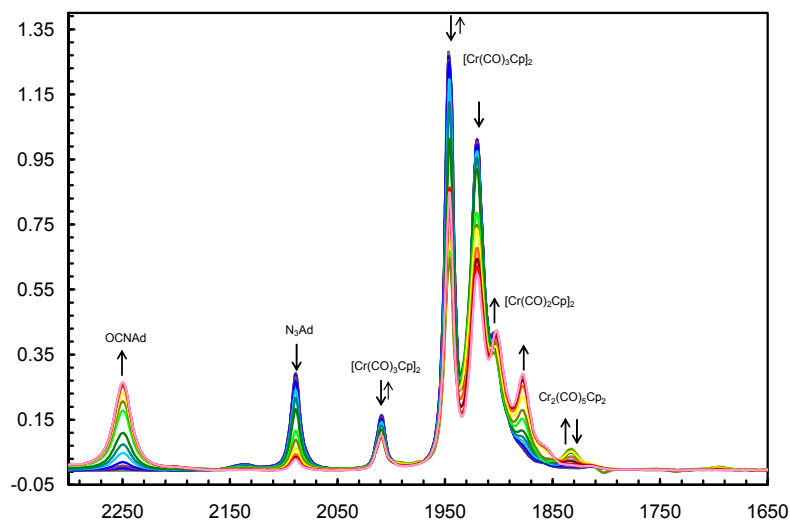


Figure 5.3. FTIR of the reaction of $[\text{Cr}(\text{CO})_3\text{Cp}]_2$ with N_3Ad in toluene under a CO atmosphere. The significant differences under the CO atmosphere is the there is significantly less $[\text{Cr}(\text{CO})_3\text{Cp}]_2$ consumed during and there is a visible increase in the resolved absorbance peaks assigned to this starting material in the end of the reaction.

Under CO atmosphere (Figure 5.3) there is also an induction period followed by a rapid increase in the rate of carbonylation of the azide. The intermediate $[\text{Cr}_2(\text{CO})_5\text{Cp}_2]$ is mostly converted back to the starting material $[\text{Cr}(\text{CO})_3\text{Cp}]_2$. Only approximately 1/3 of the starting $[\text{Cr}(\text{CO})_3\text{Cp}]_2$ is consumed (See Appendix D Figure D.1).

ESR study of eqn. 5.2 (see Figure 5.4) shows buildup and decay of an intermediate at $g = 2.004$. The observed signal is tentatively assigned to the intermediate $[\text{Cr}(\text{CO})_2(\text{OCNAd})\text{Cp}]$ which will be discussed later. Support for the assignment of the ESR signal to the aforementioned intermediate originates from isotopic experiments. Labeling studies using $[\text{Cr}({}^{13}\text{CO})_3\text{Cp}]_2$ (see Figure 5.5) display a partially resolved doublet of triplets consistent with formulation as $\bullet\text{Cr}({}^{13}\text{CO})_2(\text{O}^{13}\text{CNAd})\text{Cp}$, in analogy to earlier reported $\bullet\text{Cr}({}^{13}\text{CO})_2(\text{O}^{13}\text{CC}(\text{H})(\text{SiMe}_3))\text{Cp}$ in Chapter 2. Production of free O^{13}CNAd was confirmed by its IR ν_{CO} shift from 2250 cm^{-1} to 2192 cm^{-1} .

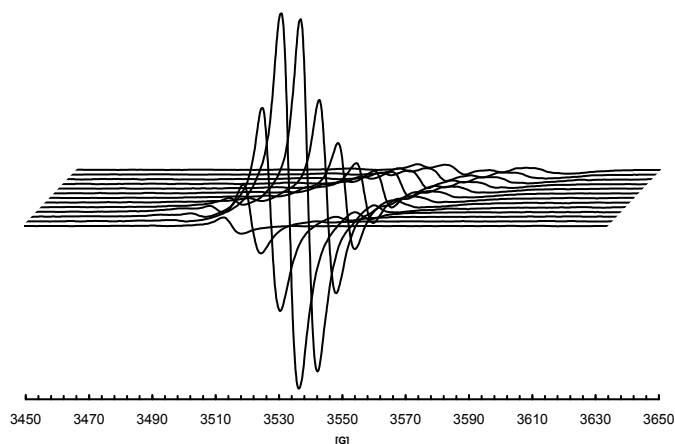


Figure 5.4. Sequential ESR (approximately every 50 seconds) of reaction of $[\text{Cr}(\text{CO})_3\text{Cp}]_2$ with N_3Ad . ($g_{\text{iso}} = 2.004$, $A({}^{53}\text{Cr}) = 44.9\text{ Hz}$)

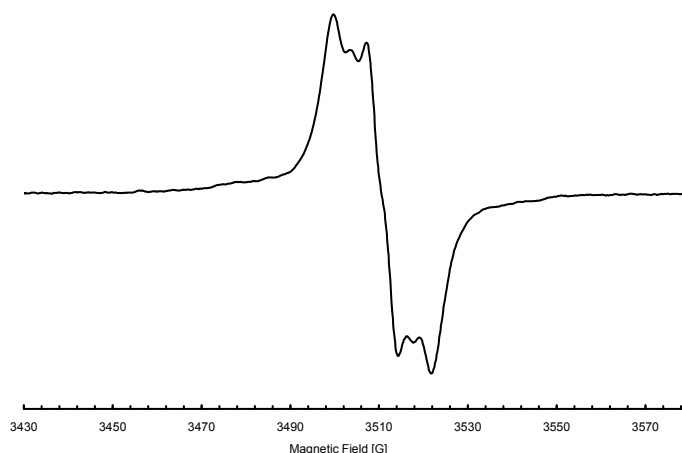


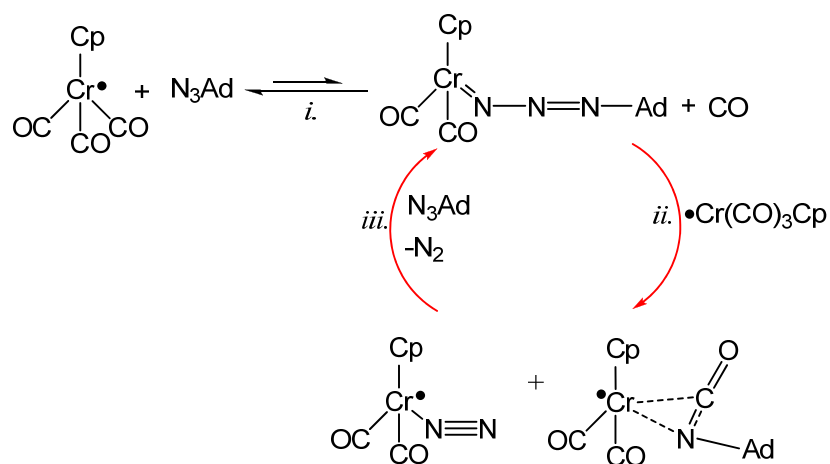
Figure 5.5. ESR of the paramagnetic intermediate involved in the reaction of N_3Ad with $[Cr(^{13}CO)_3Cp]_2$ showing an unresolved doublet of triplets due to additional splitting from the ^{13}CO .

A second intermediate is the metastable complex $Cr_2(CO)_5Cp_2$ which was identified by characteristic FTIR bands (See Figures 5.1 and 5.2). This intermediate was also produced in reaction of $N_2CHSiMe_3$ and $[Cr(CO)_3Cp]_2$. The reaction of $[Cr(CO)_3Cp]_2$ with N_3Ad and $N_2CHSiMe_3$ possess many parallel characteristics which include: (a) an induction period prior to reaction, (b) production of $Cr_2(CO)_5Cp_2$ as a reactive intermediate, (c) production of an ESR detectable intermediate which parallels the course of the reaction and (d) catalytic behavior under a CO atmosphere. These observations are in keeping with the proposed initial reaction mechanism as shown in Scheme 5.1.

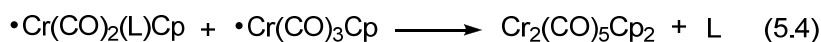
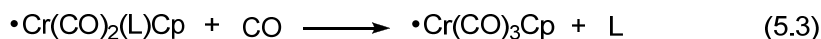
The first step involves reversible displacement of CO by N_3Ad to form the substituted radical $\bullet Cr(CO)_2(N_3Ad)Cp$. This equilibrium is unfavorable since CO is a better ligand than N_3Ad . The reversible nature of this initial step is supported by the observed lengthening of the induction period when reactions are carried out under a CO atmosphere. In step 5.1.ii., the substituted radical $\bullet Cr(CO)_2(N_3Ad)Cp$ is attacked by $\bullet Cr(CO)_3Cp$ to produce $\bullet Cr(CO)_2(N_2)Cp$ and $\bullet Cr(CO)_2(OCNAd)Cp$. The proposed

intermediate $\bullet\text{Cr}(\text{CO})_2(\text{N}_2)\text{Cp}$ is not detected and is expected to be highly reactive. Displacement of N_2 by N_3Ad (step 5.1.iii.) accounts for the induction period in the reaction since this step presents a more facile route to $\bullet\text{Cr}(\text{CO})_2(\text{N}_3\text{Ad})\text{Cp}$ than does displacement of CO as a ligand as shown in step 5.1.i.

Scheme 5.1. Proposed initial phase of reaction of $\bullet\text{Cr}(\text{CO})_3\text{Cp}$ with N_3Ad .

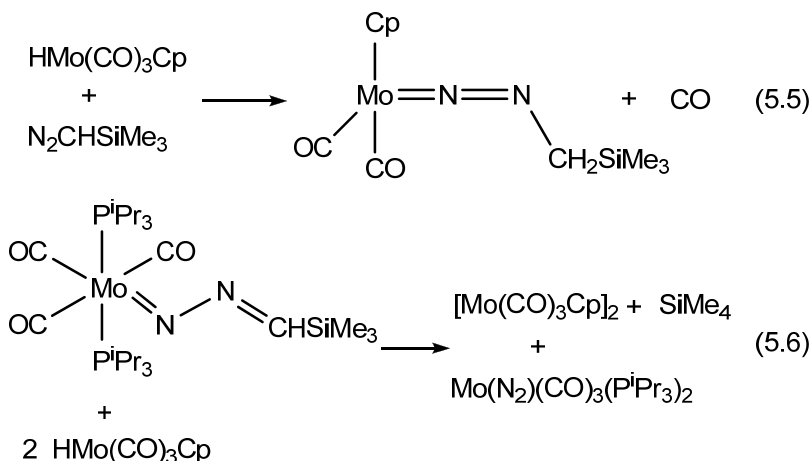


In the presence of CO , carbonylation of the two proposed intermediate radicals in Scheme 5.1 ($\bullet\text{Cr}(\text{CO})_2(\text{L})\text{Cp}$ ($\text{L} = \text{N}_2$ or OCNAd)) would be expected to occur as shown in eqn. 5.3, and reaction with $\bullet\text{Cr}(\text{CO})_3\text{Cp}$ as shown in eqn. 5.4.

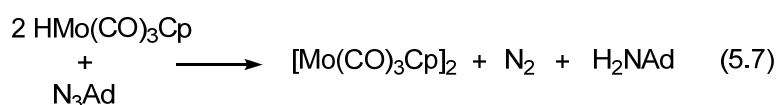


As was found for reaction of $\text{N}_2\text{CHSiMe}_3$, $\text{Cr}_2(\text{CO})_5\text{Cp}_2$ generated in eqn. 3, loses CO under argon to form $[\text{Cr}(\text{CO})_2\text{Cp}]_2$ and adds CO under a carbon monoxide atmosphere to reform the initial starting material $[\text{Cr}(\text{CO})_3\text{Cp}]_2$. In summary there is a very strong similarity between carbonylation of the diazoalkane, $\text{N}_2\text{CHSiMe}_3$ and the azide, N_3Ad by $\bullet\text{Cr}(\text{CO})_3\text{Cp}$ which is indicative of the similar mechanism proposed here.

Reaction of $\text{HMo}(\text{CO})_3\text{Cp}$ with N_3Ad . In contrast, there was little similarity found between the reaction of the metal hydride $\text{HMo}(\text{CO})_3\text{Cp}$ and N_3Ad when compared to earlier studies of its reaction with $\text{N}_2\text{CHSiMe}_3$. The free diazoalkane was shown to react cleanly in THF as shown in eqn. 5.5 and the bound diazoalkane to undergo clean hydrogenation as shown in eqn. 5.6 (see Chapter 3.)



Under comparable conditions, N_3Ad and $\text{HMo}(\text{CO})_3\text{Cp}$ in THF were observed to react cleanly at a greatly diminished rate according to eqn. 5.7.



A possible explanation for the decreased rate of reaction is the lower basicity of the azide compared to the diazo compound. The gas phase proton affinity of $\text{N}=\text{N}=\text{CH}_2$ is $858.9 \text{ kJ mol}^{-1}$ compared to a value for $\text{N}=\text{N}=\text{N}-\text{H}$ of 756 kJ mol^{-1} .¹¹¹ This reciprocates to an approximate 103 kJ mol^{-1} (25 kcal mol^{-1}) reduction in thermodynamic basicity for the azide relative to the diazo. The proposed first step in eqn. 5.5 is protonation at C of $\text{N}=\text{N}=\text{C}(\text{H})(\text{SiMe}_3)$ which may be less likely favorable than protonation of $\text{N}_1=\text{N}_2=\text{N}_3$ -Ad at N_3 .

Prior coordination of $\text{N}_2\text{CHSiMe}_3$ to $\text{Mo}(\text{P}^i\text{Pr}_3)_2(\text{CO})_3$ was shown to greatly alter the rate and product yield in reaction with $\text{HMo}(\text{CO})_3\text{Cp}$.⁷⁷ Similar inquest of the reaction of the terminally bound $\text{Mo}(\text{N}_3\text{Ad})(\text{CO})_3(\text{P}^i\text{Pr}_3)_2$ with $\text{HMo}(\text{CO})_3\text{Cp}$ led to a complex set of products and are under additional investigation. Reaction of $\text{HMo}(\text{CO})_3\text{Cp}$ and $\text{Mo}(\text{N}_3\text{Ad})(\text{CO})_3(\text{P}^i\text{Pr}_3)_2$ was relatively rapid and produced $[\text{Mo}(\text{CO})_3\text{Cp}]_2$, and other products. A large amount of $\text{Mo}(\text{P}^i\text{Pr}_3)_2(\text{CO})_4$ was produced indicating some unknown additional reaction. The product would potentially be 1-adamantyl amine however $\text{Mo}(\text{CO})_3(\text{P}^i\text{Pr}_3)$ is known to react with primary amines.¹⁰⁸ Overall the reaction was not clean, produced a number of side products and is under further investigation.

Formation of a metal stabilized phosphazide. During attempts to grow single crystals of $\text{Mo}(\text{P}^i\text{Pr}_3)_2(\text{CO})_3(\text{N}_3\text{Ad})$ for structural determination, insertion of N_3Ad into the $\text{Mo}-\text{P}^i\text{Pr}_3$ bond of $\text{Mo}(\text{P}^i\text{Pr}_3)_2(\text{CO})_3$ was accidentally observed. Over the course of approximately a week the compound converted slowly to the κ^2 -bound phosphazide complex in Figure 5.6. (Table 5.1 contains selected bond lengths and angles.) Single-crystal X-ray analysis was performed by Burjor Captain at the University of Miami for a collaborative project.

Table 5.1. Selected bond length and angles for the single crystal x-ray structure of $(\kappa^2\text{-}^i\text{Pr}_3\text{PN}_3\text{Ad})\text{Mo}(\text{P}^i\text{Pr}_3)_2(\text{CO})_3$.

Bond Lengths (Å)			
Mo(1)-N(1)	2.443(2)	N(1)-N(2)	1.385(3)
Mo(1)-N(3)	2.186(2)	N(2)-N(3)	1.263(3)
N(1)-P(1)	1.641(2)	N(3)-C(1)	1.486(3)
Bond Angles (deg)			
N(1)-N(2)-N(3)	107.22(18)	N(2)-N(3)-C(1)	115.01(19)
N(1)-Mo(1)-N(3)	54.54(7)	N(2)-N(3)-Mo(1)	107.21(15)
N(2)-N(1)-P(1)	108.80(15)	C(1)-N(3)-Mo(1)	160.17(12)
N(2)-N(1)-Mo(1)	91.01(13)	P(1)-N(1)-Mo(1)	137.75(15)

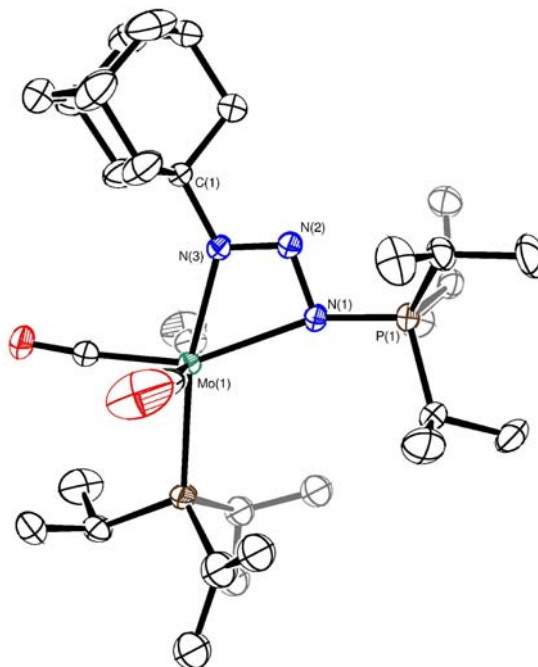


Figure 5.6. ORTEP diagram of $(\kappa^2\text{-}^i\text{Pr}_3\text{PN}_3\text{Ad})\text{Mo}(\text{P}^i\text{Pr}_3)_2(\text{CO})_3$ with ellipsoids drawn at 35% probability.

Three other structures of chelating phosphazides complexes have been reported, and all are for metals in higher formal oxidation states: $\text{WBr}_2(\text{CO})_3(p\text{-CH}_3\text{C}_6\text{H}_4\text{N}_3\text{PPh}_3)$,¹⁴⁵ $\text{RuCl}_3(\text{P}^i\text{Pr}_3)(\text{N}_3(\text{mes})\text{P}^i\text{Pr}_3)$,¹⁴⁶ and $[\text{tBuPCH}_2\text{SiMe}_2\text{NSiMe}_2\text{CH}_2\text{P}^i\text{Bu}_2\text{N}_3\text{Ph}]\text{FeCl}$.¹⁴⁷ The phosphazide is bound in the *s-trans* configuration. The N(1)-P(1) (1.641(2) Å) bond is in the range of the other complexes with other N-P multiple bonds reported. Somewhat surprisingly, this bond was found to be slightly shorter than the value of 1.653(4) reported for the free phosphazide $\text{Cy}_3\text{P}=\text{N}_3\text{Ad}$ (Cy = cyclohexyl). (See Appendix D Figure D.2)¹⁴⁸ This may imply that coordination to the metal in the *s-trans* confirmation serves to strengthen the P=N bond in the phosphazide by reducing the steric environment around the tertiary phosphine. The N(1)-N(2) (1.385(3) Å) and N(2)-N(3) (1.263(3) Å) bonds of the complexed phosphazide are both slightly longer than those for $\text{Cy}_3\text{PN}_3\text{Ad}$ where N(1)-

$N(2) = (1.345(2) \text{ \AA})$ and $N(2)-N(3) (1.261(2) \text{ \AA})$. The PNNN backbone is essentially planar with a torsion angle of 0.02° . The Mo is also included in this plane. The bite angle of the phosphazide ligand is $54.54(7)^\circ$.

There are several possible mechanisms for formation of the chelating phosphazide complex. The simplest, reaction of a pre-formed free phosphazide R_3PN_3Ad and $Mo(P^iPr_3)_2(CO)_3$, was ruled out since such a reaction was shown to merely rapidly reform $Mo(P^iPr_3)_2(CO)_3(N_3Ad)$ as shown in Figure 5.7.

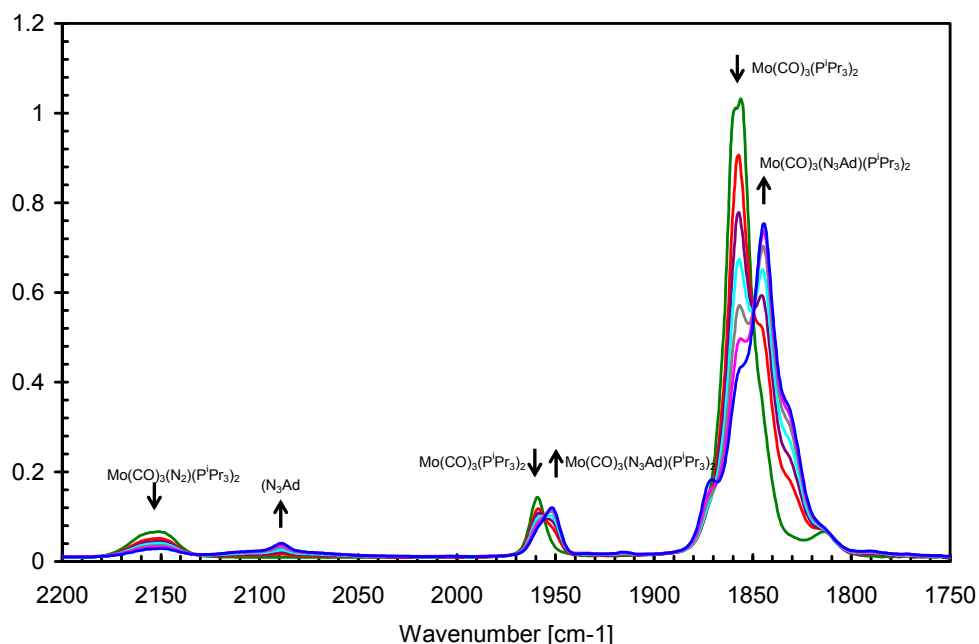


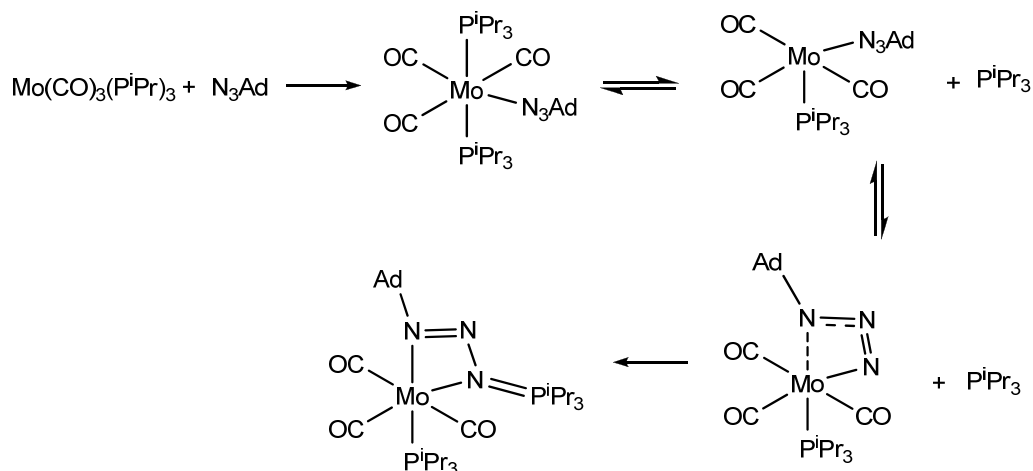
Figure 5.7. FTIR of the reaction of $Mo(P^iPr_3)_2(CO)_3$ with $^iPr_3P=N_3Ad$ under an atmosphere of 1.7 atm N_2 in toluene at 295 K. Depicted is the decrease in $Mo(P^iPr_3)_2(CO)_3(N_2)$ ($\nu_{NN} = 2153 \text{ cm}^{-1}$), an increase in unbound N_3Ad a decrease in coordinatively unsaturated $Mo(P^iPr_3)_2(CO)_3$ and an increase in $Mo(P^iPr_3)_2(CO)_3(N_3Ad)$

This is speculated to occur as a result of the equilibrium that is established between free iPr_3PN_3Ad and its components P^iPr_3 and N_3Ad .¹⁴⁸ Which is then quickly followed by the reaction of $Mo(P^iPr_3)_2(CO)_3$ with the free azide. Attempts to measure the rate of reaction

of the N_3Ad with $\text{Mo}(\text{P}^i\text{Pr}_3)_2(\text{CO})_3$ proved futile in that the reaction occurred too rapidly to be measured

Accordingly, the bound phosphazide complex is suspected to form with at least one of the components still in contact with the metal. NMR study of the reaction showed the presence of trace amounts of free P^iPr_3 present during the reaction. A mechanism in keeping with this is shown in Scheme 5.2. The azide is initially bound to form the terminally bound $\text{Mo}(\text{P}^i\text{Pr}_3)_2(\text{CO})_3(\text{N}_3\text{Ad})$. The rate determining step is dissociation, or at least loosening of one $\text{Mo}-\text{P}^i\text{Pr}_3$ bond to allow coordination of N_3Ad at the N(3) position. The free phosphine ligand would then attack the N(1) position in a Staudinger like reaction. The *s-trans* configuration of the bound phosphazide would prevent further loss of N_2 as is classical in the Staudinger reaction.²⁹

Scheme 5.2. Proposed mechanism for formation of the κ^2 -phosphazide ligand.



The formation of phosphazides is known to be equilibrium processes^{148,149} and thusly there is no sizable thermodynamic distinction between $\text{R}_3\text{PN}_3\text{Ad}$ and $\text{R}_3\text{P} + \text{N}_3\text{Ad}$. The fact that $(\kappa^2\text{-}^i\text{Pr}_3\text{PN}_3\text{Ad})\text{Mo}(\text{P}^i\text{Pr}_3)(\text{CO})_3$ is more stable than isomeric $\text{Mo}(\text{P}^i\text{Pr}_3)_2(\text{CO})_3(\text{N}_3\text{Ad})$ implies a reasonably strong bond between Mo and the chelating

phosphazide ligand as the driving force for the observed net insertion of azide into the bound phosphine.

5.3 Conclusions

This work reports preliminary comparison of reactivity of $\text{N}_2\text{CHSiMe}_3$ and N_3Ad with a metal radical, metal hydride, and coordinatively unsaturated metal phosphine complex. Reaction with the metal radical $\bullet\text{Cr}(\text{CO})_3\text{Cp}$ results in catalytic carbonylation under CO in a manner strictly analogous to that reported earlier for $\text{N}_2\text{CHSiMe}_3$. Reaction of N_3Ad with $\text{HMo}(\text{CO})_3\text{Cp}$ was found to be extremely slow and to give only hydrogenation in marked contrast to reaction of the diazoalkane reported earlier. Finally, the coordinated azide complex $\text{Mo}(\text{P}^i\text{Pr}_3)_2(\text{CO})_3(\text{N}_3\text{Ad})$ was found to undergo spontaneous isomerization at low temperature to form the novel low valent cyclic phosphazide complex $(\kappa^2\text{-}^i\text{Pr}_3\text{PN}_3\text{Ad})\text{Mo}(\text{P}^i\text{Pr}_3)(\text{CO})_3$. More detailed thermodynamic and kinetic studies of these and related reactions are planned.

5.4 Experimental

General Considerations. Unless stated otherwise, all operations were performed in a Vacuum Atmospheres glove box under an atmosphere of purified argon or utilizing standard Schlenk tube techniques under argon. Toluene and THF were purified by distillation under argon from sodium benzophenone ketyl into flame dried glassware. Heptane was purchased as anhydrous from Sigma-Aldrich and degassed before use. $[\text{Cr}(\text{CO})_3\text{Cp}]_2$,³⁶ $[\text{Cr}(\text{CO})_3\text{Cp}]_2$,⁵⁰ $\text{Mo}(\text{P}^i\text{Pr}_3)_2(\text{CO})_3$,¹³⁸ and $^i\text{Pr}_3\text{PN}_3\text{Ad}$ ¹⁵⁰ were prepared as described in earlier publications. 1-adamantyl azide, 1-adamantyl amine and

1-adamantyl isocyanate were obtained from Sigma-Aldrich and used without further purification. FTIR data were obtained on a Perkin Elmer Spectrum 400 FT-IR/FT-NIR spectrometer. NMR spectra were obtained on a Bruker AVANCE 400 MHz spectrometer. ESR spectra were taken with a Bruker EMX ESR Spectrometer.

Kinetic experiments of the reaction of $[\text{Cr}(\text{CO})_3\text{Cp}]_2$ with N_3Ad . Reactions were carried out at 295 K. In a typical experiment 25.0 mL of a 0.01275 M P^iPr_3 (3.187×10^{-4} mol) toluene solution was added to a temperature controlled reactor that was sealed under an atmosphere of nitrogen. The reactor also contained a stir bar to ensure proper mixing was achieved. A CaF_2 cell FTIR was attached directly to the reactor via Teflon tubing. On the “downstream” of the FTIR cell was a valve that was used to introduce fresh sample (via positive pressure from the N_2 atmosphere) from the reactor for each subsequent FTIR spectrum taken. After temperature equilibration of the Cr solution, 1.0 mL of 0.6398 M N_3Ad (6.398×10^{-4} mol) solution was added to the reactor with a Hamilton gas tight syringe. (Note to reader: *azides are explosive compounds that are shock sensitive. Care should be taken when using concentrated solutions of these compounds.*) Sequential FTIR spectra were recorded with time. Similar reactions were carried out so that the concentrations of N_3Ad and $[\text{Cr}(\text{CO})_3\text{Cp}]_2$ were equal. Also reactions in which the atmosphere was CO were examined. Reaction reagents and products were followed by characteristic IR stretches (see Table D.1.)

ESR Measurements of the Reaction of $[\text{Cr}(\text{CO})_3\text{Cp}]_2$ with N_3Ad . In a representative experiment a 0.0124 M $[\text{Cr}(\text{CO})_3\text{Cp}]_2$ solution in toluene was prepared under Schlenk techniques. The $[\text{Cr}(\text{CO})_3\text{Cp}]_2$ solution (0.5 mL, 6.2×10^{-3} mmol) was

syringe filtered into a Pyrex NMR tube.^{xxiv} The end of the NMR tube was sealed with a screw on cap with a septa and taken for ESR analysis. To the tube 250 μL of a 0.050 M (1.25×10^{-3} mmol) solution N_3Ad was added. The tube was inverted several times to ensure proper mixing. The ESR spectra were then taken sequentially approximately every 50 seconds. The reaction of $[\text{Cr}(\text{CO})_3\text{Cp}]_2$ with N_3Ad leads to an intense signal at $g = 2.004$; $A(^{53}\text{Cr}) = 44.9$ Hz) Experimental conditions: T , 298 K; microwave power, 0.630 mW; microwave frequency, 9.832 GHz; modulation amplitude, 1.00 G. The reaction of $[\text{Cr}(^{13}\text{CO})_3\text{Cp}]_2$ with N_3Ad leads to an intense signal at $g = 2.004$; $A(^{53}\text{Cr}) = 44.9$ Hz) Experimental conditions: T , 298 K; microwave power, 0.631 mW; microwave frequency, 9.842 GHz; modulation amplitude, 1.00 G.

Reaction of $\text{HMo}(\text{CO})_3\text{Cp}$ with N_3Ad . A 20 mL scintillation vial was charged with 0.0502 g (0.203 mmol) $\text{HMo}(\text{CO})_3\text{Cp}$ and 1 equivalent of N_3Ad . Both solids were dissolved in 8 mL of toluene. The reaction vial was left in the glove box and the reaction was followed via FTIR for the course of approximately 1 week. The products $[\text{Mo}(\text{CO})_3\text{Cp}]_2$ and H_2NAd were characterized by characteristic FTIR and NMR signals that were determined by separately prepared ($[\text{Mo}(\text{CO})_3\text{Cp}]_2$; see Chapter 3) or purchased (H_2NAd) samples.

Synthesis of $(\kappa^2\text{-}^i\text{Pr}_3\text{PN}_3\text{Ad})\text{Mo}(\text{P}^i\text{Pr}_3)(\text{CO})_3$. A 20 mL scintillation vial was charged with 0.2064 g (4.128×10^{-4} mol) $\text{Mo}(\text{P}^i\text{Pr}_3)_2(\text{CO})_3$ and 0.0729 g (4.11×10^{-4} mol) N_3Ad . Both solids were then dissolved in approximately 5 mL toluene. The immediate product was characterized by NMR and FTIR. FTIR data listed in Table D.1.

^{xxiv} Initial studies were made using quartz ESR tubes. It was found that 5mm screw cap NMR tube fitted with a teflon coated silicone septum showed no significant signal that overlapped with the signal for the Cr complex for these concentrated solutions.

^1H NMR(C_6D_6) δ (ppm): 1.31 (m, 36H, ^iPr CH_3), 1.37 (m, 6H, Ad CH_2), 2.29 (m, 6H, ^iPr CH), 1.70 (m, 6H, Ad CH_2), 1.80 (m, 3H, Ad CH), ^{31}P NMR (C_6D_6) δ (ppm): 41.2. FTIR (toluene) (cm^{-1}): ν_{CO} 1952, 1844, 1830 cm^{-1} .

The vial was capped and left to sit in the glove box for a week. The solvent was then removed under reduced atmosphere. The crude product produced an oily red solid. Two heptane extractions followed by an extraction with toluene produced a bright orange powder in 43 % yield. ^1H NMR (C_6D_6) δ (ppm): 1.04 (m, 18H, ^iPr CH_3), 1.72 (m, 6H, Ad CH_2), 2.01 (m, 3H, ^iPr CH), 2.07 (m, 6H, Ad CH_2), 2.12 (m, 3H, Ad CH), ^{31}P NMR (C_6D_6) δ (ppm): 41.9. 33.42. FTIR (toluene) (cm^{-1}): ν_{CO} 1915, 1803, 1786 cm^{-1} .

Kinetic experiments of the reaction of $\text{Mo}(\text{P}^i\text{Pr}_3)_2(\text{CO})_3$ with $^i\text{Pr}_3\text{PN}_3\text{Ad}$.

Reactions were completed in an analogous manner as that stated in the previous section on the kinetics of the reaction of $[\text{Cr}(\text{CO})_3\text{Cp}]_2$ with N_3Ad . In a typical reaction 20.0 mL of a 9.75×10^{-3} M (1.95×10^{-4} mol) solution of $\text{Mo}(\text{P}^i\text{Pr}_3)_2(\text{CO})_3$ in toluene would be reacted with 2.5 mL of a 0.0801 M (2.00×10^{-4} mol) solution of $^i\text{Pr}_3\text{PN}_3\text{Ad}$ in toluene. Reaction reagents and products were followed by characteristic IR stretches (see Table D.1.) The initial product formed in this reaction was $\text{Mo}(\text{P}^i\text{Pr}_3)_2(\text{CO})_3(\text{N}_3\text{Ad})$. This is presumably the result of the dissociation of the phosphazide to P^iPr_3 and N_3Ad .

Crystallographic Analyses: Crystallographic analysis was performed by Burjor Captain at the University of Miami. Orange single crystals of $(\kappa^2\text{-}^i\text{Pr}_3\text{PN}_3\text{Ad})\text{Mo}(\text{P}^i\text{Pr}_3)(\text{CO})_3$ suitable for x-ray diffraction analyses obtained by slow crystallization from a layered solvent mixture of heptane and toluene at 253 K. The data crystal was glued onto the end of a thin glass fiber. X-ray intensity data were measured by using a Bruker SMART APEX2 CCD-based diffractometer using Mo $\text{K}\alpha$ radiation (λ

= 0.71073 Å).¹⁴¹ The raw data frames were integrated with the SAINT+ program by using a narrow-frame integration algorithm.¹⁴¹ Corrections for Lorentz and polarization effects were also applied with SAINT+. An empirical absorption correction based on the multiple measurement of equivalent reflections was applied using the program SADABS. The structures were solved by a combination of direct methods and difference Fourier syntheses, and refined by full-matrix least-squares on F^2 , by using the SHELXTL software package.¹⁴² Hydrogen atoms were placed in geometrically idealized positions and included as standard riding atoms during the least-squares refinements. Crystal data, data collection parameters, and results of the analyses are listed in Table D.2.

$(\kappa^2\text{-}^i\text{Pr}_3\text{PN}_3\text{Ad})\text{Mo}(\text{P}^i\text{Pr}_3)(\text{CO})_3$ crystallized in the monoclinic crystal system. The systematic absences in the intensity data were consistent with the unique space group $P2_1/n$. All non-hydrogen atoms were refined with anisotropic displacement parameters. Two of the isopropyl groups (C33-C38) are disordered over two orientations which were refined in the ratio 50/50. Atoms of this group were refined with isotropic displacement parameters.

Appendix A. Supporting Information for Chapter 2.

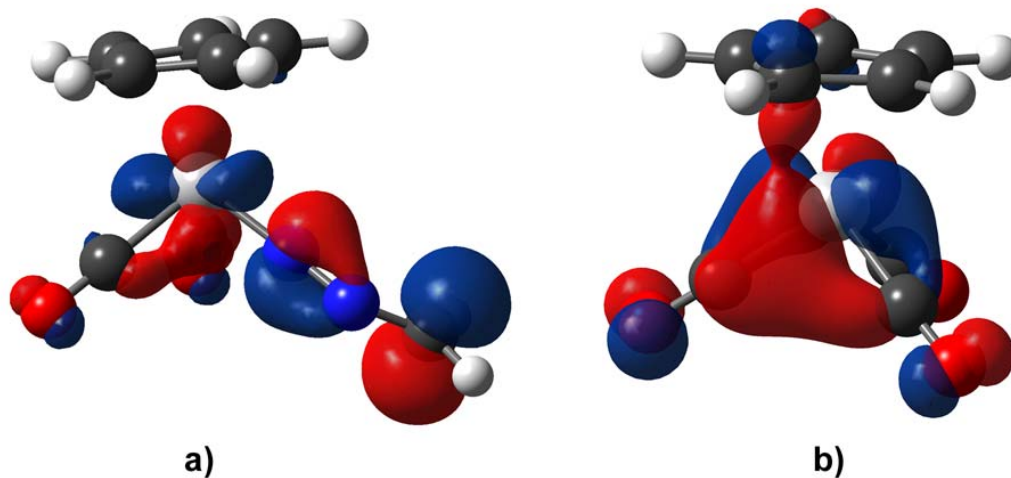


Figure A.1. Drawing of the calculated SOMO for (a) $\bullet\text{Cr}(\text{CO})_2(\text{NNCH}_2)(\text{C}_5\text{H}_5)$ and (b) $\bullet\text{Cr}(\text{CO})_3(\text{C}_5\text{H}_5)$

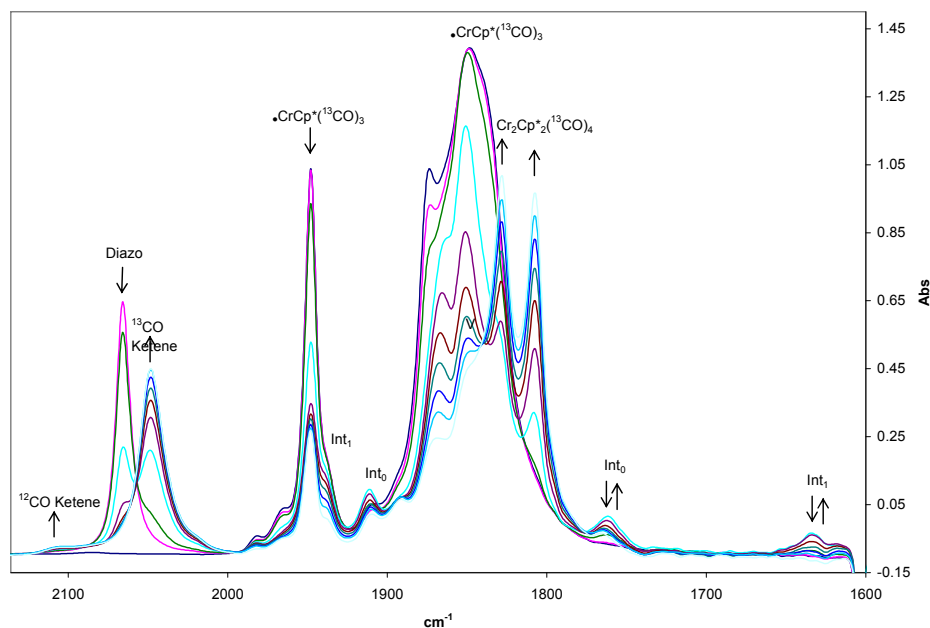


Figure A.2. Reaction of $\bullet\text{Cr}(^{13}\text{CO})_3(\text{C}_5\text{Me}_5)$ and $\text{N}_2\text{CHSiMe}_3$ run under conditions comparable to those shown in Figures 2.1 and 2.2 for $\bullet\text{Cr}(^{12}\text{CO})_3(\text{C}_5\text{Me}_5)$ and $\text{N}_2\text{CHSiMe}_3$. This figure shows the combined reactions stages for the ^{13}CO substituted complexes. Complete band assignments are found in Table A.1, however of particular note is the shift in $\nu\text{-CO}$ of the coordinated ketene from 1672 to 1634 cm^{-1} .

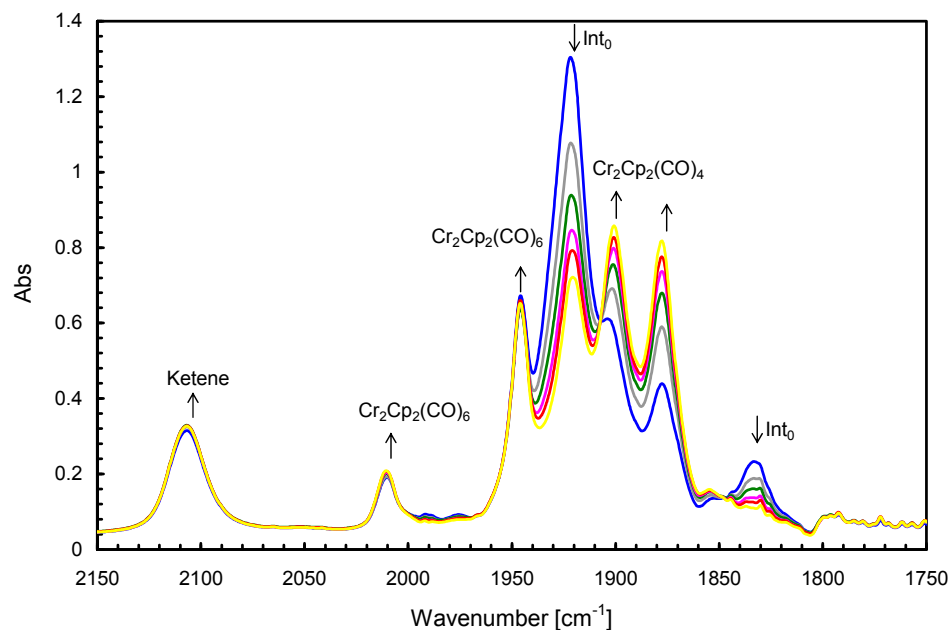


Figure A.3. Spectra run in phase two of reaction shown in Figure 2.7 of text. Subsequent runs showing decrease bands assigned to $\text{Cp}_2\text{Cr}_2(\text{CO})_5$ and major increase in bands assigned to $\text{Cp}_2\text{Cr}_2(\text{CO})_4$ according to eqn 2.8 and minor increase in bands assigned to $\text{Cp}_2\text{Cr}_2(\text{CO})_6$ according to eqn 2.9.

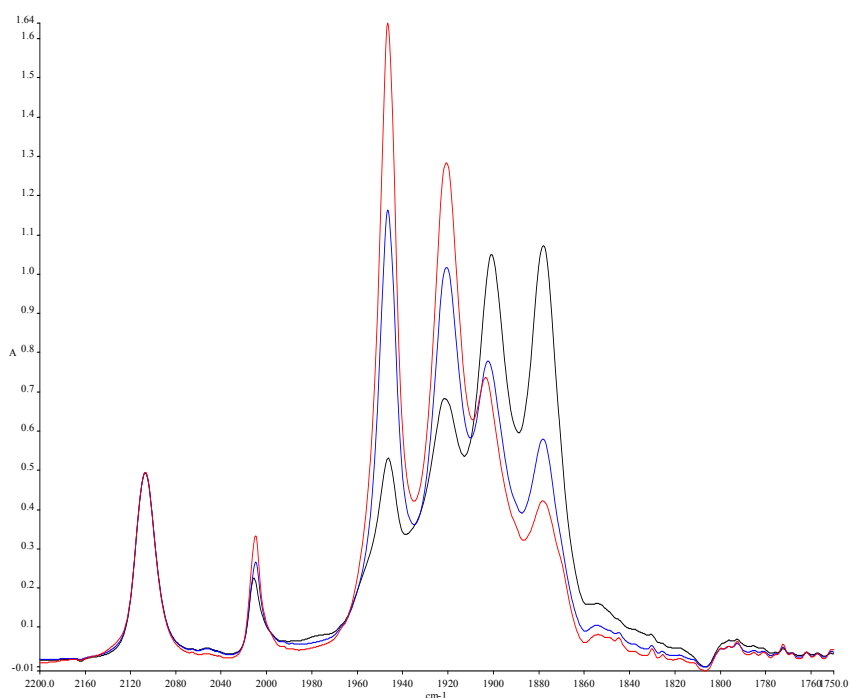


Figure A.4. Normalized spectra showing product distribution of intermediate complex as a function of CO pressure. Black spectrum is under argon, blue spectrum under 9 psi CO, and red spectrum under 45 psi CO. Reactions done under 200 psi CO (not shown) led to production of only traces of $\text{Cr}_2(\text{CO})_4\text{Cp}_2$.

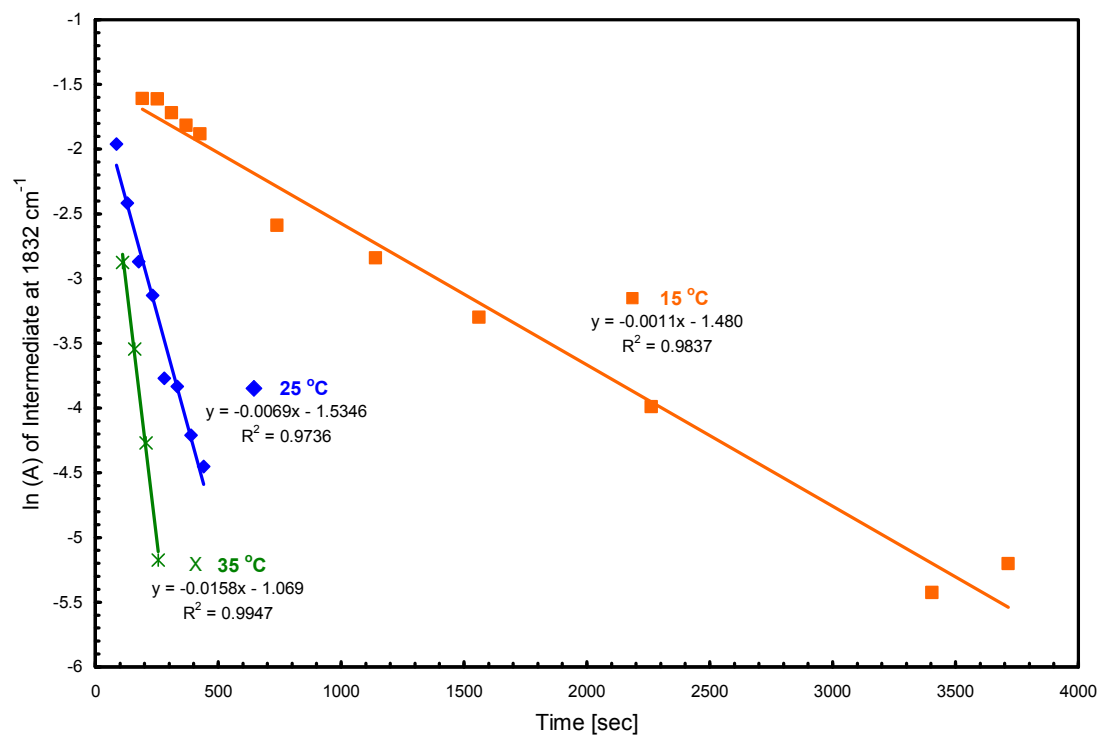


Figure. A.5. Kinetic plots as a function of time for decay of $\text{Cp}_2\text{Cr}_2(\text{CO})_5$, showing first order rate constants of 0.0011 s^{-1} at 15 °C, 0.0069 s^{-1} at 25 °C, and 0.0158 s^{-1} at 35 °C.

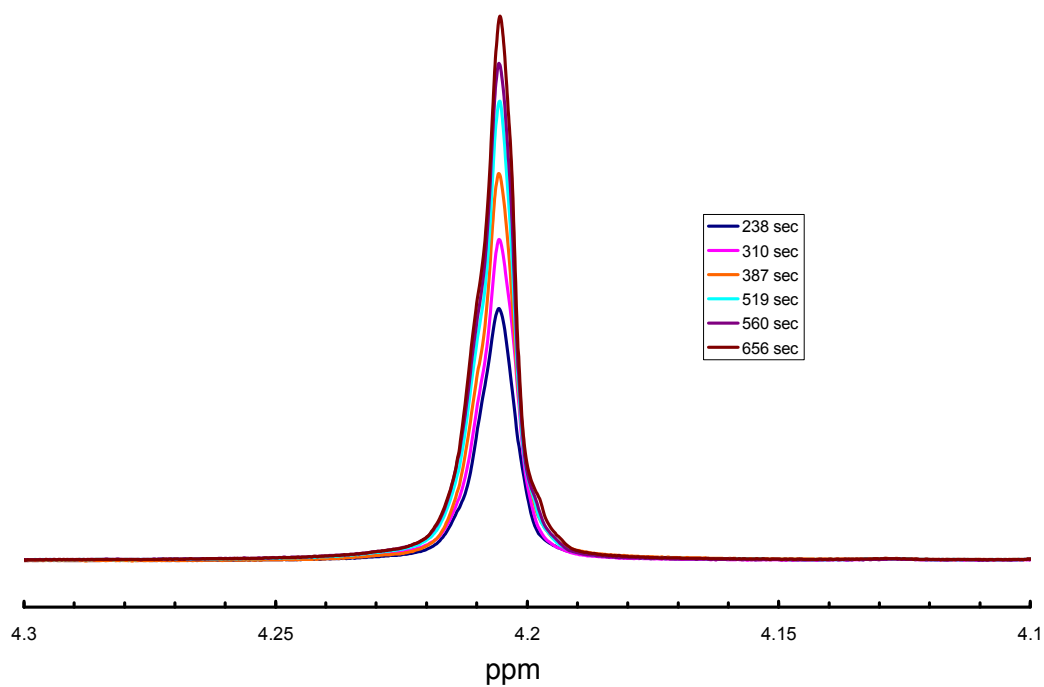


Figure A.6. ^1H NMR showing growth of signal due to $\text{Cr}_2(\text{CO})_4\text{Cp}_2$ "from nowhere" due to absence of an NMR signal due to $\text{Cr}_2(\text{CO})_5\text{Cp}_2$.

Table A.1. FTIR Data for selected compounds and intermediates in toluene solution.

Compound	FTIR Data (cm⁻¹)		
●Cr(CO) ₃ Cp*	1994	1893	1919 ^a
●Cr(¹³ CO) ₃ Cp*	1947	1850	1873 ^a
[Cr(CO) ₃ Cp] ₂	2009	1946	1920
[Cr(¹³ CO) ₃ Cp] ₂	1963	1901	1876
•Cr(CO) ₂ Cp*(OCCHSiMe ₃)	1984	1908	1672
•Cr(CO) ₂ Cp*(O ¹³ CCHSiMe ₃)	1940	1871	1634
•Cr(CO) ₂ Cp(OCCHSiMe ₃)	? ^b	? ^b	? ^b
Cr ₂ (CO) ₅ Cp* ₂	1957	1984	1799
Cr ₂ (¹³ CO) ₅ Cp* ₂	1912	1854	1768
Cr ₂ (CO) ₅ Cp ₂	2006 ^c	1922	1832
[Cr(CO) ₂ Cp*] ₂		1871	1851
[Cr(¹³ CO) ₂ Cp*] ₂		1828	1807
[Cr(CO) ₂ Cp] ₂		1901	1878
[Cr(¹³ CO) ₂ Cp] ₂		1855	1834
Na ⁺ [Cr(CO) ₃ Cp] ⁻	1897 ^d	1794 ^d	1744 ^d
N ₂ CHSiMe ₃	2066		
OCCHSiMe ₃	2107		
O ¹³ CCHSiMe ₃	2048		

^a. Shoulder band due to dimer [Cr(CO)₃(C₅R₅)]₂ (R = H, Me) ^b. Band could not be reliably assigned due to overlap with stronger bands of other species present and due to the apparent low concentration of Cr(CO)₂(OCCHSiMe₃)Cp. ^c. Band assigned based on peak intensity. Peak is partially obscured by a similar peak of Cr₂Cp₂(CO)₆ at 2009. Value here based on computer subtraction estimate. ^d. FTIR data obtained in THF.

Appendix B. Supporting Information For Chapter 3.

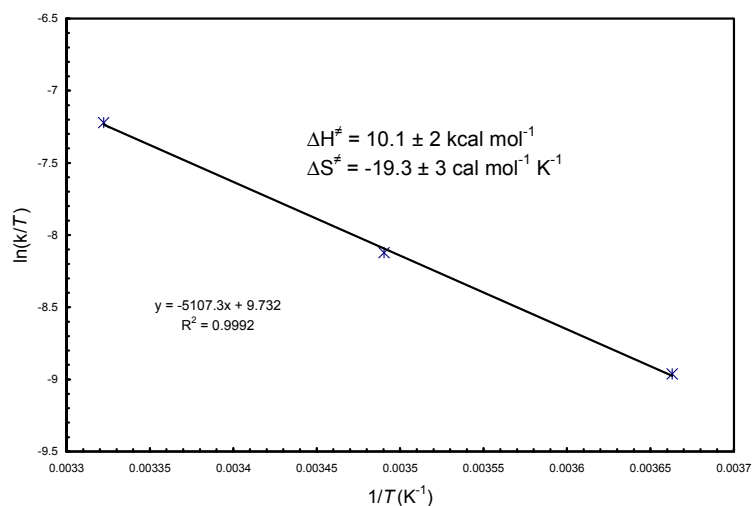


Figure B.1. Eyring plot for the reaction of $\text{HMo}(\text{CO})_3\text{Cp}$ with $\text{N}_2\text{CHSiMe}_3$ in heptane. Reactions were carried out at temperatures ranging from 273 K to 301 K.

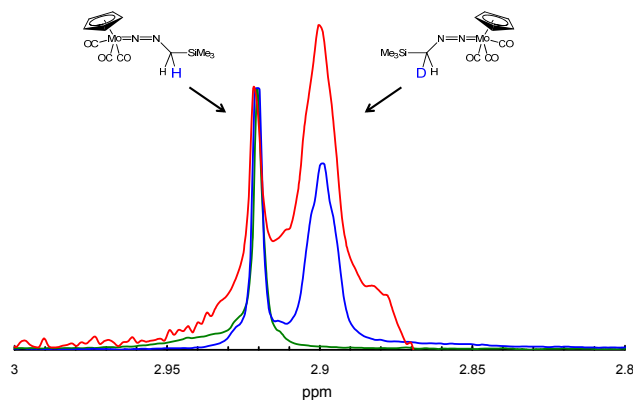


Figure B.2. ^1H NMR data showing peaks near 2.92 ppm assigned to $\text{Mo}(\text{CO})_2(\text{N}_2\text{C}(\text{H})_2\text{SiMe}_3)\text{Cp}$ and at 2.90 ppm assigned to $\text{Mo}(\text{CO})_2(\text{N}_2\text{C}(\text{H})\text{DSiMe}_3)\text{Cp}$. (—) product from reaction with $\text{HMo}(\text{CO})_3\text{Cp}$, showing 100 % H; (—) product from $\text{DMo}(\text{CO})_3\text{Cp}$ (85 % D, 15 % H) with approximately 10 fold excess N_2CHMe_3 ; (—) product from $\text{DMo}(\text{CO})_3\text{Cp}$ (85 % D, 15 % H) with a deficiency of $\text{N}_2\text{CHSiMe}_3$ (approximate ratio of $\text{Mo}/\text{N}_2\text{CHSiMe}_3$ 10/1). The red spectrum was multiplied by 7 to place it on a comparable scale to the other spectra. Note that since only the H signal of the H, D complex is seen, the actual integrated concentration must be multiplied by two—so the red spectrum shows a predominance of the H,D complex above the visible integral. The presence of $\text{Mo}(\text{CO})_2(\text{N}_2\text{CD}_2\text{SiMe}_3)\text{Cp}$ was inferred based on the integral ration of the C_5H_5 protons to the signals resulting from the $\text{N}_2\text{CH}_x\text{D}_{2-x}\text{SiMe}_3$ ligand.

Table B.1. Infrared data for complexes in different solvents.^a

Hydrides	Heptane	Toluene	THF
HMo(CO) ₃ Cp	2030 1946	2024 1935	2022 1932
HMo(CO) ₃ Cp*	2015 1931	2010 1922	2009 1921
HW(CO) ₃ Cp	2027 1939	2020 1926	2018 1924
Alkyls			
Me ₃ SiCH ₂ Mp	2021 1938	2016 1927	2015 1925
Me ₃ SiCH ₂ Mp*	2008 1923		
Me ₃ SiCH ₂ Wp	2019 1928		
Diazo complexes			
Mo(CO) ₃ (N ₂ CH ₂ SiMe ₃)Cp	1981 1905 1645	1972 1892 1644	1970 1889 1643
Mo(CO) ₃ (N ₂ CH ₂ SiMe ₃)Cp*	1965 1890 1628		
W(CO) ₃ (N ₂ CH ₂ SiMe ₃)Cp	1973 1895 1637		
Dimers			
[Mo(CO) ₃ Cp] ₂	2023 1962 1921	2015 1956 1912	2012 1956 1912
[Mo(CO) ₃ Cp*] ₂	2021 1933 1898		
[W(CO) ₃ Cp] ₂	2011 1952 1904	2008 1953 1904	

^a. All values in cm⁻¹ and Cp = η⁵-C₅H₅, Cp* = η⁵-C₅Me₅.

Table B.2. Crystal data and structure refinement for $W(CO)_2(N_2CH_2SiMe_3)Cp$.

Empirical formula	$C_{11} H_{16} N_2 O_2 Si W$	
Formula weight	420.20	
Temperature	203(2) K	
Wavelength	0.71073 Å	
Crystal system	triclinic	
Space group	P1	
Unit cell dimensions	$a = 6.3928(7)$ Å	$\alpha = 100.632(2)^\circ$.
	$b = 10.6551(12)$ Å	$\beta = 96.245(2)^\circ$.
	$c = 10.8766(12)$ Å	$\gamma = 93.510(2)^\circ$.
Volume	$721.32(14)$ Å ³	
Z	2	
Density (calculated)	1.935 Mg/m ³	
Absorption coefficient	8.083 mm ⁻¹	
F(000)	400	
Crystal size	0.14 x 0.10 x 0.08 mm ³	
Theta range for data collection	1.92 to 25.33°.	
Index ranges	-7<=h<=7, -12<=k<=12, -13<=l<=11	
Reflections collected	5327	
Independent reflections	2405 [R(int) = 0.0160]	
Completeness to theta = 25.00°	91.5 %	
Max. and min. transmission	0.5641 and 0.3974	
Refinement method	Full-matrix least-squares on F ²	
Data / restraints / parameters	2405 / 0 / 157	
Goodness-of-fit on F ²	1.114	
Final R indices [I>2sigma(I)]	R1 = 0.0311, wR2 = 0.0752	
R indices (all data)	R1 = 0.0326, wR2 = 0.0764	
Largest diff. peak and hole	2.841 and -2.644 e.Å ⁻³	

Appendix C. Supporting Information for Chapter 4.

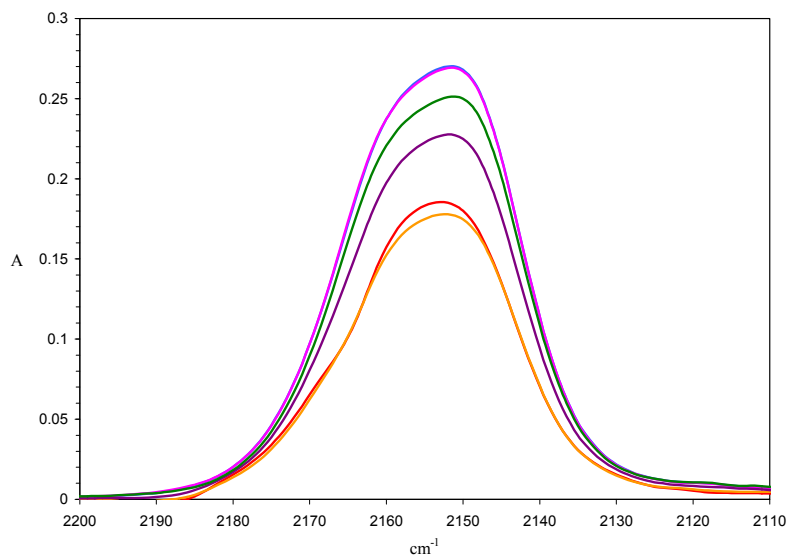


Figure C.1. Variable temperature FTIR data on reaction of $\text{Mo}(\text{P}^i\text{Pr}_3)_2(\text{CO})_3 + \text{N}_2 \rightarrow \text{Mo}(\text{P}^i\text{Pr}_3)_2(\text{CO})_3(\text{N}_2)$. The band shown is the ν_{NN} stretch of the $\text{Mo}(\text{P}^i\text{Pr}_3)_2(\text{CO})_3(\text{N}_2)$ complex. The spectra shown are at $T = 337.7$ (orange), 316.6 (red), 301 (purple), 284.1 K (green). The blue and pink spectra correspond to spectra that were taken at a pressure of 237 psi N_2 at 290 K.

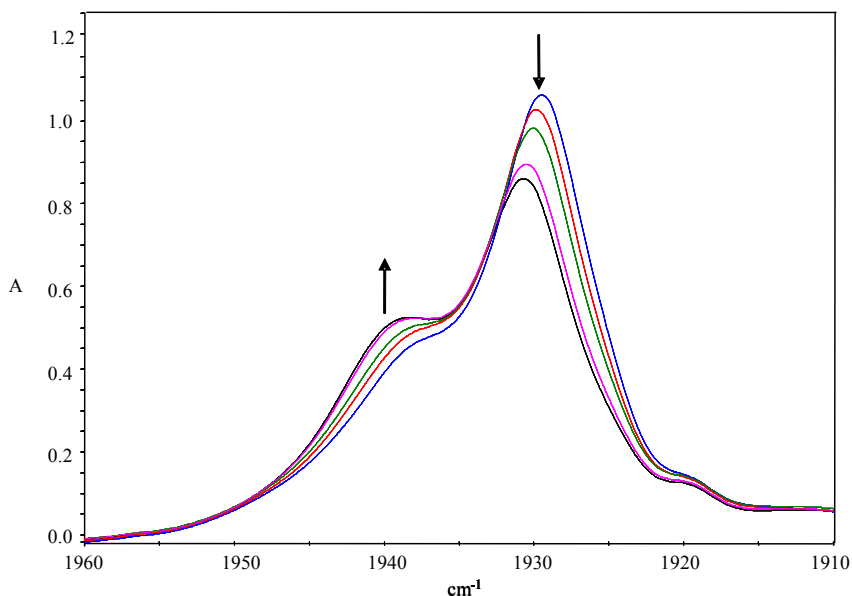


Figure C.2. Variable temperature FTIR data on reaction $(\mu\text{-C}_4\text{H}_4\text{N}_2)[\text{Mo}(\text{P}^i\text{Pr}_3)_2(\text{CO})_3]_2 + \text{pyrazine} \rightarrow 2 (\text{C}_4\text{H}_4\text{N}_2)\text{Mo}(\text{P}^i\text{Pr}_3)_2(\text{CO})_3$. The band near 1930 cm^{-1} is due to the bridging species and the band near 1940 cm^{-1} is due to the monometallic complex. The bands have been normalized so that the maximum absorbance is 1. The band near 1940 cm^{-1} increases in size as the temperature increases. Temperatures shown are at $T = 275.8$ (blue), 283.5 (red), 292.8 (green), 306 (pink) and 312.9 (black) K.

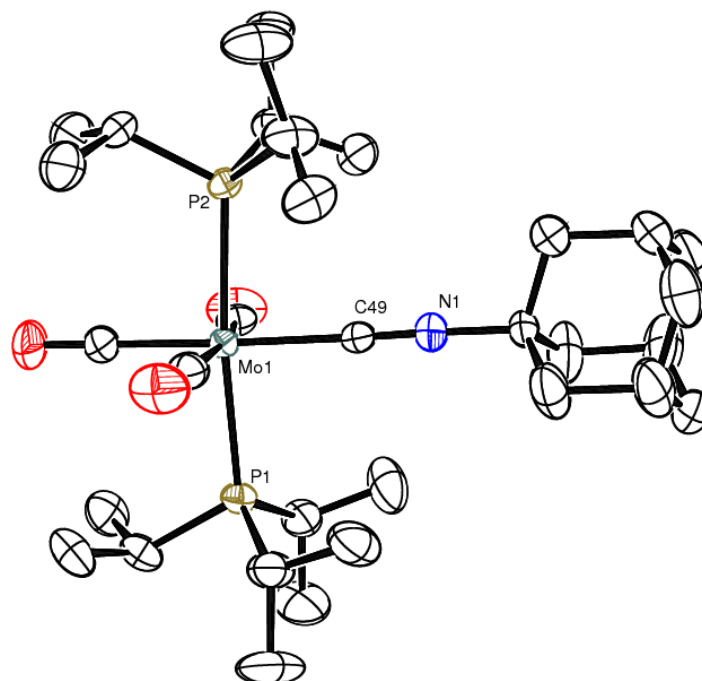


Figure C.3. ORTEP diagram of Mo(PⁱPr₃)₂(CO)₃(CNAd) showing 35 % probability thermal ellipsoids.

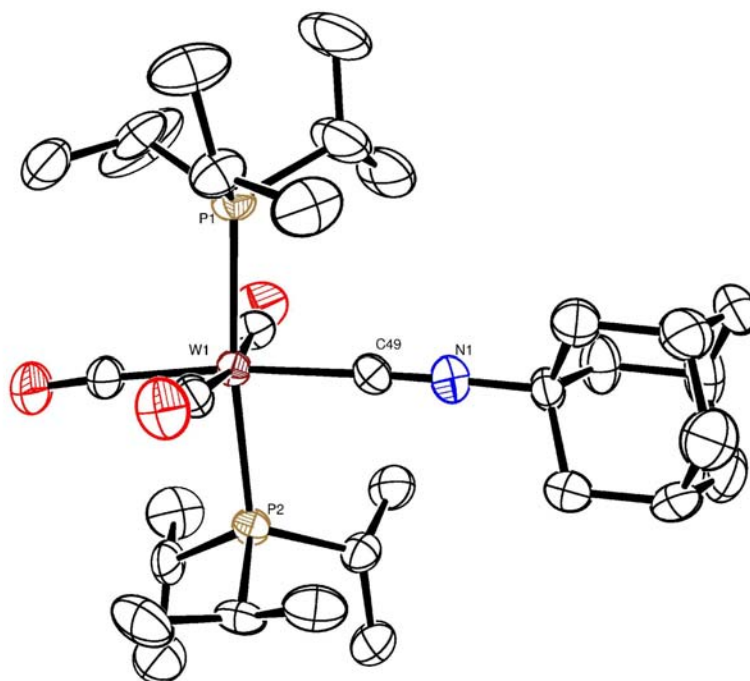


Figure C.4. ORTEP diagram of W(PⁱPr₃)₂(CO)₃(CNAd) showing 35 % probability thermal ellipsoids.

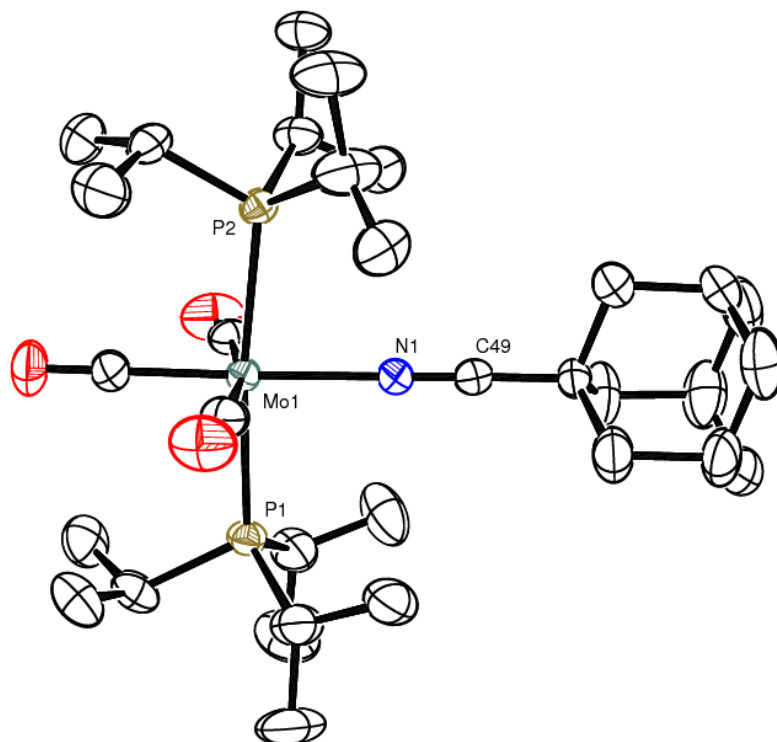


Figure C.5. ORTEP diagram of Mo(PⁱPr₃)₂(CO)₃(NCAd) showing 35 % probability thermal ellipsoids.

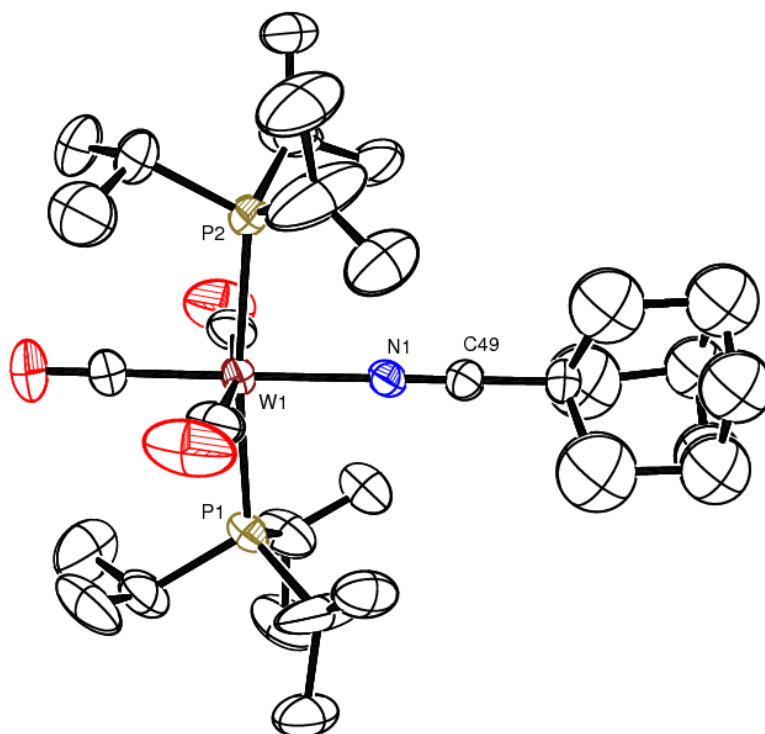


Figure C.6. ORTEP diagram of W(PⁱPr₃)₂(CO)₃(NCAd) showing 35 % probability thermal ellipsoids.

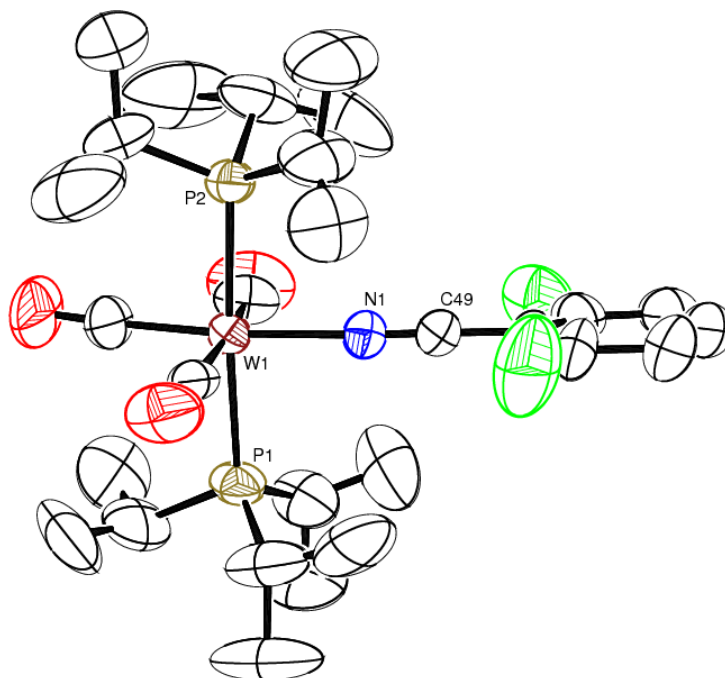


Figure C.7. ORTEP diagram of $W(P^iPr_3)_2(CO)_3(2,6-F_2C_6H_2CN)$ showing 35 % probability thermal ellipsoids.

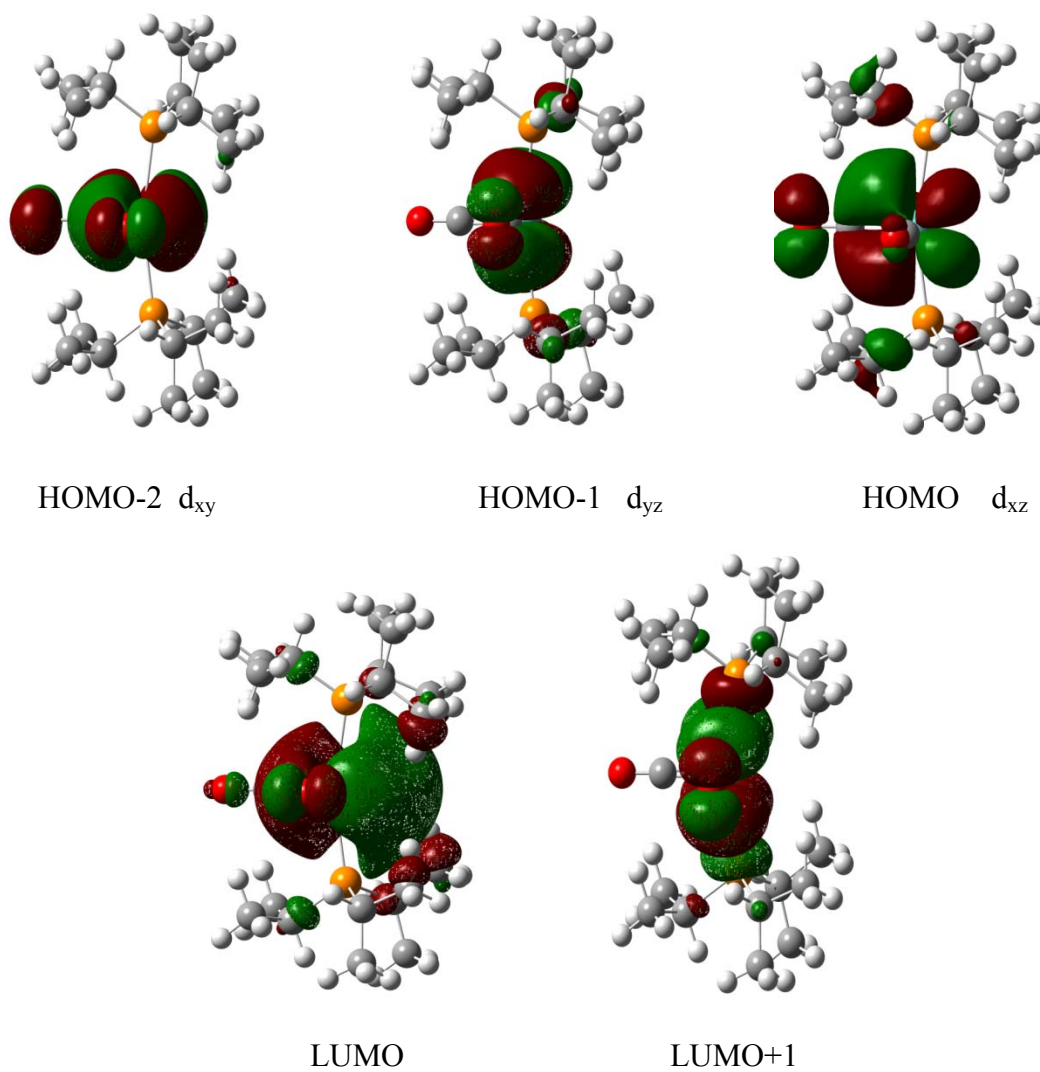
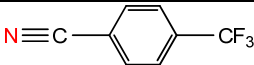
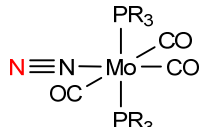
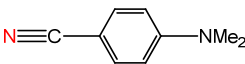
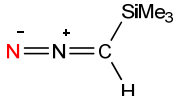
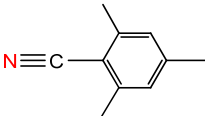
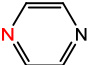
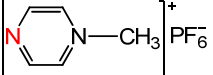
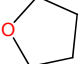
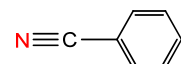
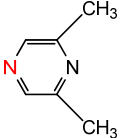
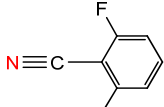
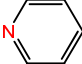
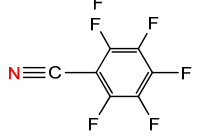
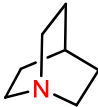
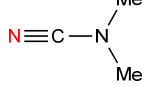


Figure C.8 TD-DFT calculated HOMO and LUMO orbitals of $\text{Mo}(\text{P}^i\text{Pr}_3)_2(\text{CO})_3$.

Table C.1. Table of experimentally and theoretically determined ΔH of binding to $\text{Mo}(\text{P}^i\text{Pr}_3)_2(\text{CO})_3$

Ligand	ΔH_{BSSE}	ΔH_{Expt}	Ligand	ΔH_{BSSE}	ΔH_{Expt}
	$\text{Mo}(\text{P}^i\text{Pr}_3)_2\text{CO}_3$			$\text{Mo}(\text{P}^i\text{Pr}_3)_2\text{CO}_3$	
$\text{N}\equiv\text{N}$	-12.4	-10.3 ± 0.6			
	+ 6.0 ^a	-8.8 ± 1.2		-12.2	-16.3 ± 0.6
	-11.9	-13.8 ± 0.5		-11.3	-16.7 ± 0.6
$\text{N}^-\text{=N}^+\text{-Ad}$	-10.9	-11.2 ± 0.4		-8.6	-14.9 ± 0.9
$\text{C}^-\equiv\text{N}^+\text{-Ad}$	-21.1	-29.0 ± 0.3		+ 8.3 ^a	-19.3 ± 2.5
$\text{N}\equiv\text{C}\text{-Ad}$	-9.9	-16.7 ± 0.5		-16.7 ^d	-17.5 ± 0.8^d
$\text{N}\equiv\text{C}\text{-CH}_3$	-8.9	-16.6 ± 0.4		-0.7 ^d	NM ^c
	-12.5	-17.6 ± 0.4		-8.7	-14.8 ± 0.6
	-13.5	-16.7 ± 0.6		-8.5	-17.0 ± 0.4
	-15.3	-16.4 ± 0.6		-11.2	NR ^f
	-10.6	-15.5 ± 1.8^e			

^a computation predict this complex is endothermic and unstable; ^b based on K_{eq} with PhCN; ^c based on K_{eq} with AdCN; ^d values measured/computed in THF solution. ^e value was not measured experimentally; ^f no reaction.

Table C.2. Computed and experimental λ_{\max} (nm) of bound benzonitriles $\text{Mo}(\text{P}^i\text{Pr}_3)_2(\text{CO})_3(\text{L})$.

L	Comp λ_{\max}	Expt. λ_{\max}
PhCN	545	518, 444
F ₂ PhCN	593	575, 488
F ₅ PhCN	624	618, 515
p-CF ₃ PhCN	628	594, 502
p-Me ₂ NPhCN	491	454, 396
MesitylCN	525	497, nr ^d

Table C.3. FTIR ν_{CO} of $\text{Mo}(\text{P}^i\text{Pr}_3)_2(\text{CO})_3(\text{L})$. (cm^{-1})

$\text{Mo}(\text{P}^i\text{Pr}_3)_2\text{CO}_3(\text{L})$	ν_{CO}		
none	1848	1813	1954
N ₂	1850	1814	1959
NNAd	1844	1830	1952
NNCHSiMe ₃	1847	1825	1952
AdCN	1829	1812	1941
AdNC	1841	1814	1943
MeCN	1832	1815	1942
PhCN	1832	1816	1942
F ₂ PhCN	1837	1824	1944
F ₅ PhCN	1844	1833	1946
p-CF ₃ PhCN	1837	1825	1943
p-Me ₂ NPhCN	1829	1813	1939
MesitylCN	1832	1817	1942
Me ₂ NCN	1826	1806	1940
N ₂ C ₄ H ₄	1822	1811	1940
$\text{Mo}(\text{P}^i\text{Pr}_3)_2(\text{CO})_3(\text{N}_2\text{C}_4\text{H}_4)$	1830	1817	1930
2,6 Me ₂ N ₂ C ₄ H ₄	1825	1813	1939
NC ₅ H ₅	1821	1805	1936

Table C.4. Crystallographic data for compounds Mo(PⁱPr₃)₂(CO)₃(AdNC), Mo(PⁱPr₃)₂(CO)₃(AdCN) and W(PⁱPr₃)₂(CO)₃(AdNC).

	Mo(P ⁱ Pr ₃) ₂ (CO) ₃ (AdNC)	Mo(P ⁱ Pr ₃) ₂ (CO) ₃ (AdCN)	W(P ⁱ Pr ₃) ₂ (CO) ₃ (AdNC)
Empirical formula	MoP ₂ O ₃ NC ₃₂ H ₅₇	MoP ₂ O ₃ NC ₃₂ H ₅₇	WP ₂ O ₃ NC ₃₂ H ₅₇
Formula weight	661.67	661.67	749.58
Crystal system	Monoclinic	Monoclinic	Orthorhombic
Lattice parameters			
<i>a</i> (Å)	20.3075(6)	20.3024(5)	11.8293(4)
<i>b</i> (Å)	13.3565(4)	13.3604(3)	14.0455(4)
<i>c</i> (Å)	27.8468(9)	27.8332(6)	21.2863(7)
β (deg)	110.393(1)	110.7249(3)	90
V (Å ³)	7079.7(4)	7061.2(3)	3536.7(2)
Space group	P2 ₁ /n (# 14)	P2 ₁ /n (# 14)	P2 ₁ 2 ₁ 2 ₁ (# 19)
Z value	8	8	4
ρ _{calc} (g / cm ³)	1.242	1.245	1.408
μ (Mo Kα) (mm ⁻¹)	0.490	0.492	3.386
Temperature (K)	296(2)	296(2)	296(2)
2Θ _{max} (°)	52.00	57.00	57.98
No. Obs. (I > 2σ(I))	10187	12946	8209
No. Parameters	727	727	320
Goodness of fit	1.014	1.003	1.020
Max. shift in cycle	0.003	0.003	0.001
Residuals*:R1; wR2	0.0420; 0.1282	0.0402; 0.1082	0.0345; 0.0906
Absorption Correction, Max/min	Multi-scan 0.9903/0.8668	Multi-scan 0.9525/0.8911	Multi-scan 0.7282/0.4730
Largest pk in Final Diff. Map (e ⁻ / Å ³)	0.952	1.170	0.869

*R = $\sum_{hkl} (|F_{obs}| - |F_{calc}|) / \sum_{hkl} |F_{obs}|$; $R_w = [\sum_{hkl} w(|F_{obs}| - |F_{calc}|)^2 / \sum_{hkl} w F_{obs}^2]^{1/2}$,
 $w = 1/\sigma^2(F_{obs})$; $GOF = [\sum_{hkl} w(|F_{obs}| - |F_{calc}|)^2 / (n_{data} - n_{vari})]^{1/2}$.

Table C.5. Crystallographic data for compounds $W(P^iPr_3)_2(CO)_3(2,6-(CH_3)_2C_4H_2N_2)$, $W(P^iPr_3)_2(CO)_3(2,4,6-(CH_3)_3C_6H_2CN)$ and $W(P^iPr_3)_2(CO)_3(2,6-F_2C_6H_2CN)$.

	$W(P^iPr_3)_2(CO)_3(2,6-(CH_3)_2C_4H_2N_2)$	$W(P^iPr_3)_2(CO)_3(2,4,6-(CH_3)_3C_6H_2CN)$	$W(P^iPr_3)_2(CO)_3(2,6-F_2C_6H_2CN)$
Empirical formula	WP ₂ O ₃ N ₂ C ₂₇ H ₅₀	WP ₂ O ₃ NC ₃₁ H ₅₃	WP ₂ F ₂ O ₃ NC ₂₈ H ₄₅
Formula weight	696.48	733.53	727.44
Crystal system	Orthorhombic	Monoclinic	Monoclinic
Lattice parameters			
<i>a</i> (Å)	21.5280(5)	12.1011(5)	25.0970(9)
<i>b</i> (Å)	22.6636(5)	14.6865(6)	10.3565(4)
<i>c</i> (Å)	26.1787(6)	19.6431(7)	25.5892(9)
β (deg)	90	93.893(1)	95.290(1)
V (Å ³)	12772.6(5)	3483.0(2)	6622.7(4)
Space group	Pbca (# 61)	P2 ₁ /c (# 14)	P2 ₁ /n (# 14)
Z value	16	4	8
ρ _{calc} (g / cm ³)	1.449	1.399	1.459
μ (Mo Kα) (mm ⁻¹)	3.745	3.437	3.623
Temperature (K)	296(2)	296(2)	296(2)
2θ _{max} (°)	56.62	56.60	50.00
No. Obs. (I > 2σ(I))	11862	5803	8747
No. Parameters	658	358	667
Goodness of fit	1.002	1.008	1.037
Max. shift in cycle	0.003	0.002	0.002
Residuals*: R1; wR2	0.0269; 0.0878	0.0378; 0.0704	0.0418; 0.1036
Absorption Correction, Max/min	Multi-scan 0.7457/0.5812	Multi-scan 0.9664/0.4686	Multi-scan 0.9311/0.4303
Largest peak in Final Diff. Map (e ⁻ / Å ³)	0.789	0.760	2.360

$$*R = \sum_{hkl} (| |F_{obs}| - |F_{calc}| |) / \sum_{hkl} |F_{obs}|; R_w = [\sum_{hkl} w(|F_{obs}| - |F_{calc}|)^2 / \sum_{hkl} wF_{obs}^2]^{1/2},$$

$$w = 1/\sigma^2(F_{obs}); GOF = [\sum_{hkl} w(|F_{obs}| - |F_{calc}|)^2 / (n_{data} - n_{vari})]^{1/2}.$$

Add a similar table for the other two compounds determined

Appendix D. Supporting Information for Chapter 5

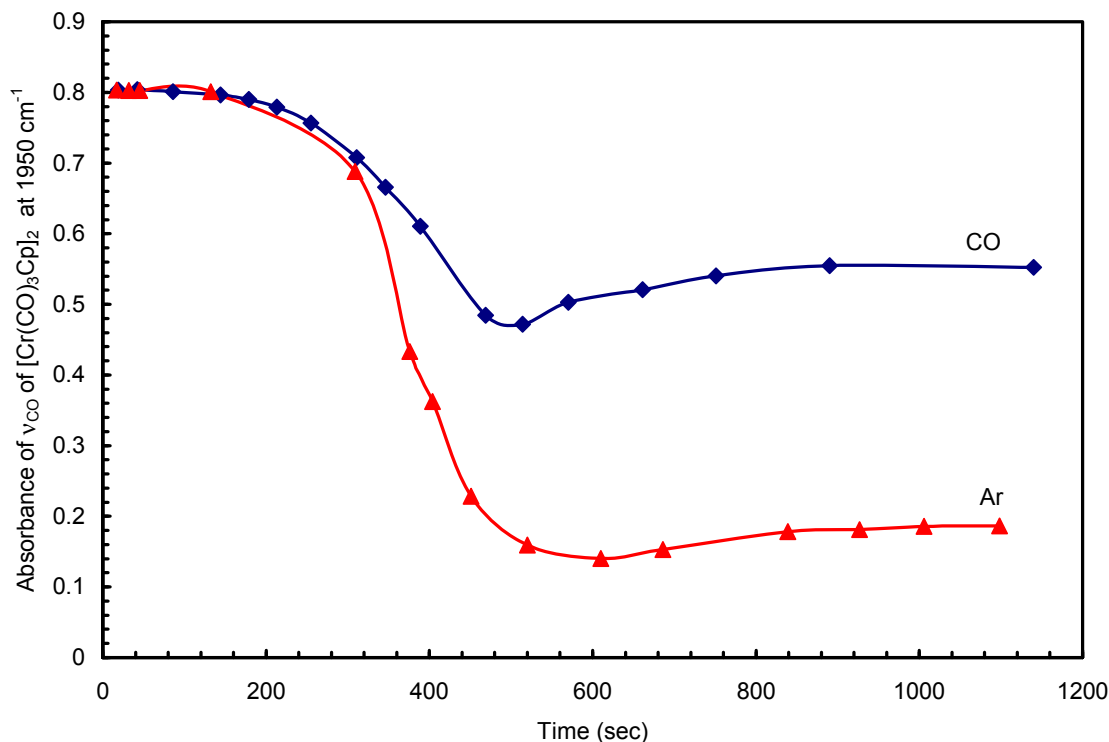


Figure D.1. Comparison of the reaction of the consumption of $[\text{Cr}(\text{CO})_3\text{Cp}]_2$ in the reaction with N_3Ad under CO and N_2 atmospheres.

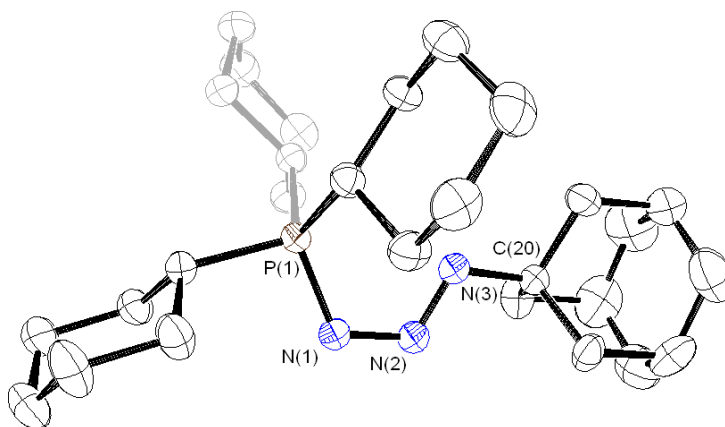


Figure D.2. ORTEP diagram of $\text{Cy}_3\text{PN}_3\text{Ad}$ in the *s-cis* conformation with ellipsoid probability of 35%. Selected bond lengths (Å) and angles (deg): P(1)-N(1) 1.6534(14); N(1)-N(2) 1.345(2); N(2)-N(3) 1.261(2); N(3)-C(20) 1.488(2); P(1)-N(3) 2.720(1) P(1)-N(1)-N(2) 118.62(11); N(1)-N(2)-N(3) 116.55(14); N(2)-N(3)-C(20) 112.17(13). The X-ray structure was determined by Bujor Captain from the University of Miami. For experimental details see ref. 148.

Table D.1. Identifying FTIR ν_{CO} stretches for species studied.

Compound	ν_{CO} (cm^{-1})		
Cr Compounds			
$[\text{Cr}(\text{CO})_3\text{Cp}]_2$	2010	1947	1920
$[\text{Cr}^{13}\text{CO}]_3\text{Cp}]_2$	1962	1901	1876
$\text{Cr}_2(\text{CO})_5\text{Cp}_2$? ^a	1922	1832
$[\text{Cr}(\text{CO})_2\text{Cp}]_2$		1900	1877
$[\text{Cr}^{13}\text{CO}]_2\text{Cp}]_2$		1856	1835
Mo Compounds			
$\text{Mo}(\text{CO})_3(\text{P}^i\text{Pr}_3)_2$		1959	1857
$\text{Mo}(\text{N}_3\text{Ad})(\text{CO})_3(\text{P}^i\text{Pr}_3)_2$		1952	1848
$\text{Mo}(\kappa^2\text{-N}_3\text{Ad})(\text{CO})_3(\text{P}^i\text{Pr}_3)_2$	1915	1803	1786
Organic Compounds			
N_3Ad		2137 ^b	2089 ^b
OCNAd			2250
O^{13}CNAd			2192

^a these bands for these stretches were unable to be assigned due their weak intensity in combination to overlap with other major bands. ^b bands assigned to ν_{NN}

Table D.2. Crystallographic data for Mo(κ^2 - i -Pr₃PN₃Ad) (CO)₃(P^{*i*}Pr₃).

	Mo(κ^2 - i -Pr ₃ PN ₃ Ad) (CO) ₃ (P ^{<i>i</i>} Pr ₃)
Empirical formula	MoP ₂ O ₃ N ₃ C ₃₁ H ₅₇
Formula weight	677.68
Crystal system	Monoclinic
Lattice parameters	
<i>a</i> (Å)	12.9113(3)
<i>b</i> (Å)	19.1140(5)
<i>c</i> (Å)	14.2556(3)
α (deg)	90
β (deg)	95.2725(6)
γ (deg)	90
<i>V</i> (Å ³)	3503.21(14)
Space group	P2 ₁ /n (# 14)
Z value	4
ρ_{calc} (g / cm ³)	1.285
μ (Mo K α) (mm ⁻¹)	0.499
Temperature (K)	296(2)
2 Θ_{max} (°)	56.00
No. Obs. (<i>I</i> > 2 σ (<i>I</i>))	7249
No. Parameters	371
Goodness of fit	1.036
Max. shift in cycle	0.001
Residuals*:R1; wR2	0.0406; 0.1112
Absorption Correction, Max/min	Multi-scan 0.9518/0.8813
Largest peak in Final Diff. Map (e ⁻ / Å ³)	1.653

$$*R = \frac{\sum_{\text{hkl}} (| | F_{\text{obs}} | - | F_{\text{calc}} | |)}{\sum_{\text{hkl}} | F_{\text{obs}} |}; R_w = \left[\frac{\sum_{\text{hkl}} w (| F_{\text{obs}} | - | F_{\text{calc}} |)^2}{\sum_{\text{hkl}} w F_{\text{obs}}^2} \right]^{1/2},$$

$$w = 1/\sigma^2(F_{\text{obs}}); \text{GOF} = \left[\frac{\sum_{\text{hkl}} w (| F_{\text{obs}} | - | F_{\text{calc}} |)^2}{(n_{\text{data}} - n_{\text{vari}})} \right]^{1/2}.$$

References

- (1) Toupadakis, A.; Kubas, G. J.; King, W. A.; Scott, B. L.; Huhmann-Vincent, J. *Organometallics* **1998**, *17*, 5315.
- (2) Griess, P. *Liebigs Ann. Chem.*, **1858**, *106*, 207.
- (3) (a) Doyle, M. P.; McKervey, M. A.; Ye, Tao In: *Moderen Catalytic Methods for Organic Syntheiss with Diazo Compounds: From Cyclopropanes to Ylides*, John Wiley and Sons, Inc. New York, **1998**. (b) Zollinger, H. In *Diazo Chemistry I & II*. VHC Publishing, New York, **1994**. (c) Smith, P. A. S. In *Derivatives of Hydrazine and Other Hydronitrogens Having N-N Bonds*. Benjamin/Cummings Publishing Company, Reading, MA, **1983**. (d) Ye, T.; McKervey A. *Chem Rev.* **1994**, *94*, 1091. (e) Zhang, Z., Wang, J. *Tetrahedron* **2008**, *64*, 6577.
- (4) (a) McDowell, L. J.; Khodaei, M. M.; Bethell, D. *Org. Biomol. Chem.* **2003**, *1*, 995. (b) Staudinger, H.; Meyer, J. *Helv. Chim. Acta.* **1912**, *2*, 619. (c) Wittig, B.; Haag, W. *Chem. Ber.* **1965**, *88*, 1654. (d) Laufer, R. S.; Dmitrienko, G. I. *J. Amer. Chem. Soc.* **2002**, *124*, 1854.
- (5) (a) Bug, T.; Hartnagel, M.; Schlierf, C.; Mayr, H. *Chem. Eur. J.* **2003**, *9*, 4068. (b)
- (6) (a) Meier, H.; Zeller, K.-P. *Angew. Chem. Int. Ed.* **1975**, *14*, 32. (b) Wong, F. M.; Wang, J.; Hengge, A. C.; Wu, W. *Org. Lett.* **2007**, *9* 1663. (c) Candeias, N. R.; Gois, M. P.; Veiros, L. F.; Afonso, C. A. M. *J. Org. Chem.* **2008**, *73*, 5926.
- (7) Regitz, M.; Heydt, H. *1,3-Dipolar Cycloaddition Chemistry* Padwa, A. Ed. Jon Wiley and Sons Inc., New York, 1984, *1*, Chapter 4.
- (8) Urry, W. H.; Eiszer, J. R. *J. Amer. Chem. Soc.* **1952**, *74*, 5822. (b) Schlenk, W.; Bornhardt, C. *Liebig's Ann. Chem.* **1912**, *394*, 183.
- (9) (a) Zollinger, H. In *Diazo Chemistry*. VHC Publishing, New York, **1994**, *2*, 421. (b) Sutton, D. *Chem. Rev.* **1993**, *93*, 955.
- (10) King, R. B.; Bisnette, M. B. *Inorg. Chem.* **1966**, *5*, 300.
- (11) Allen, A. D.; Semoff. C.V. *Chem. Comm.* **1965**, 621.
- (12) Kukushkin, V. Y.; Pombeiro, A. J. L. *Chem. Rev.* **2002**, *102*, 1771.
- (13) Scheele, K. W. *Opuscula* **1782**, *2*, 48.

-
- (14) Wohler, F.; Liebig, J. *Ann.* **1832**, *3*, 267.
- (15) Kukushkin, V. Y.; Pombeiro, A. J. L. *Inorg. Chem. Acta.* **2005**, *358*, 1.
- (16) Stephen, H. *J. Chem. Soc., Trans.* **1925**, *127*, 1874.
- (17) Moretto, A. F.; Zhang, H.-C.; Maryanoff, B. E. *J. Amer. Chem. Soc.* **2001**, *123*, 3157.
- (18) Griess, P. *Philos. Trans. R. Soc. London* **1864**, *13*, 375.
- (19) Bräse, S.; Gil, C.; Knepper, K.; Zimmerman, V. *Angew. Chem. Int. Ed.* **2005**, *44*, 5188.
- (20) Breslow, D. In *Azides and Nitrenes* Scriven, E. Ed. Academic Press, Inc. New York, **1984**, 491.
- (21) (a) Scriven, E. F.; Turnbull, K. *Chem. Rev.* **1988**, *88*, 297. (b) *Azides and Nitrenes* Scriven, E. Eds. Academic Press, Inc. New York, **1984**. (c) Smith, P. A. S. In *Derivatives of Hydrazine and Other Hydronitrogens Having N-N Bonds*. Benjamin/Cummings Publishing Company, Reading, MA, **1983**, 263.
- (22) (a) Kumar, H. M. S.; Reddy, B. V. S.; Anjaneyulu, S.; Yadav, J. S. *Tetrahedron Lett.* **1999**, *40*, 8305. (b) Maiti, S. N.; Singh, M. P.; Micetich, R. G. *Tetrahedron Lett.* **1986**, *27*, 1423. (c) Vaultier, M.; Knouzi, N.; Carrie, R. *Tetrahedron Lett.* **1983**, *24*, 763. (d) Knouzi, N.; Vaultier, M.; Carrie, R. *Bull. Soc. Chim. Fr.* **1985**, 81 5.
- (23) (a) Schneider, P.; Schomaker, J. H.; Deming, S.; Libbey, W. J.; Nowack, G. P. *J. Am. Chem. Soc.* **1965**, *87*, 306. (b) Nicholas, P. P. *J. Org. Chem.* **1975**, *40*, 3396. (c) Yang, C.-H.; Lee, L.-T.; Yang, J.-H. *Tetrahedron* **1994**, *40*, 12133.
- (24) (a) Freeze, S.; Norris, P. *Heterocycles* **1999**, *51*, 1807. (b) Moore, M.; Norris, P. *Tetrahedron Lett.* **1998**, *39*, 7027. (c) Kolb, H. C.; Finn, M. G.; Sharpless, K. B. *Angew. Chem. Int. Ed. Engl.* **2001**, *40*, 2004.
- (25) (a) Saalfrank, R. W.; Ackermann, E.; Fischer, M.; Wirth, U.; Zimmermann, H. *Chem. Ber.* **1990**, *123*, 115. (b) Lowe-Ma, C. K.; Nissan, R. A.; Wilson, W. S. *J. Org. Chem.* **1990**, *55*, 3755. (c) Onys'ko, P. P.; Proklina, N.V.; Prokopenko, V.P.; Gololobov, Y.G. *Zh. Obshch. Khim.* **1984**, *54*, 325. (d) Ponomarchuk, M.P.; Kasukhin, L.F.; Shevchenko, M.V.; Sologub, L.S.; Kukhar, V.P. *Zh. Obshch. Khim.* **1984**, *54*, 2468.

-
- (26) Horner, L.; Christmann, A. *Angew. Chem. Int. Ed. Engl.* **2003**, *2*, 599.
- (27) (a) Wu, H.; Hall, M. B. *J. Am. Chem. Soc.* **2008**, *130*, 16452. (b) Ciu, N.; Cheng, A.; Peng, H.; Gao, E.; He, M. *Struct. Chem.* **2007**, *18*, 43. (c) Cenini, S.; La Monica, G. *Inorg. Chim. Acta* **1976**, *18*, 279. (d) Guillemot, G.; Solari, E.; Floriani, C. *Organometallics* **2001**, *20*, 607.
- (28) Šima, J. *Coord. Chem. Rev.* **2006**, *250*, 2325.
- (29) Bebbington, W. P.; Bourissou, D. *Coord. Chem. Rev.* **2008**, (article in press) doi:10.1016/j.ccr.2008.08.009.
- (30) Tidwell, T. T. In *Ketenes*, Wiley and Sons Inc., New York, 1995.
- (31) (a) Ungvári, N.; Kégl, T.; Ungváry F. *J. Mol. Catal. A: Chem.* **2004**, *219*, 7 (b) Kégl, T.; Ungváry, F. *J. Organomet. Chem.* **2007**, *692*, 1825. (c) Tuba, R.; Ungváry F. *J. Mol. Catal. A: Chem.* **2003**, *203*, 59. (d) Fördös, E.; Ungvári, N. Kégl, T.; Ungváry F. *J. Eur. J. Inorg. Chem.* **2006**, 1875.
- (32) Zollinger, H. *Diazo Chemistry*, VCH, Weinheim, 1995.
- (33) (a) Grotjahn, D. B.; Collins, L. S. B.; Wolpert, M.; Bikzhanova, G. A.; Lo, H. C.; Combs, D.; Hubbard, J. L. *J. Am. Chem. Soc.* **2001**, *123*, 8260. (b) Grotjahn, D. B.; Lo, H. C. *J. Am. Chem. Soc.* **1996**, *118*, 2097. (c) Urtel, H.; Bikzhanova, G. A.; Grotjahn, D. B.; Hofmann, P. *Organometal* **2001**, *20*, 3938.
- (34) Grotjahn, D. B.; Bikzhanova, G. A.; Collins, L. S. B.; Concolino, T.; Lam, K. C.; Rheingold, A. L. *J. Am. Chem. Soc.* **2000**, *122*, 5222.
- (35) (a) Herrmann, W. A.; Plank, J. *Angew. Chem. Int. Ed. Engl.* **1978**, *17*, 525. (b) Herrmann, W. A.; Plank, J.; Ziegler, M. L.; Weidenhammer, K. *J. Am. Chem. Soc.* **1979**, *101*, 3133.
- (36) (a) Hoff, C. D. *Coord. Chem. Rev.* **2000**, *206*, 451. (b) Watkins, W. C.; Jaeger, T.; Kidd, C. E.; Fortier, S.; Baird, M. C.; Kiss, G.; Roper, G. C.; Hoff, C. D. *J. Am. Chem. Soc.* **1992**, *114*, 907. (c) McLain, S. J. *J. Am. Chem. Soc.* **1988**, *110*, 643. (d) Adams, R. D.; Collins, D. E.; Cotton, F. A. *J. Am. Chem. Soc.* **1974**, *96*, 749. (d) Curtis, M.D.; Butler, W. M. *J. Organomet. Chem.* **1978**, *155*, 131. (e) King, R. B.; Stone, F. G. A. *Inorg. Syn.* **1963**, *7*, 104.
- (37) Ehlers, A. W.; Frenking, G. *J. Am. Chem. Soc.* **1994**, *116*, 1514.

-
- (38) Delly, B.; Wrinn, M.; Lüthi, H. P. *J. Chem. Phys.* **1994**, *100*, 5785.
- (39) Li, J.; Schreckenbach, G.; Ziegler, T. *J. Am. Chem. Soc.* **1995**, *117*, 486.
- (40) Jonas, V.; Thiel, W. *J. Chem. Phys.* **1995**, *102*, 8474.
- (41) Barckholtz, T. A.; Bursten, B. E. *J. Am. Chem. Soc.* **1998**, *120*, 1926.
- (42) Niu, S.; Hall, M. B. *Chem. Rev.* **2000**, *100*, 353.
- (43) Macchi, P.; Sironi, A. *Coord. Chem. Rev.* **2003**, *238*, 383.
- (44) Carreon, J.-L.; Harvey, J. N. *Phys. Chem. Chem. Phys.* **2006**, *8*, 93.
- (45) Bühl, M.; Kabrede, H. *J. Chem. Theory Comput.* **2006**, *2*, 1282.
- (46) Schaefer, H. F., III; King, R. B. *Pure Appl. Chem.* **2001**, *73*, 1059.
- (47) King, R. B.; Xie, Y.; Schaefer, H.F.; Richardson, N.; Li, S. *Inorg. Chim. Acta.* **2005**, *358*, 1442
- (48) Wang, H.; Xie, Y.; King, R. B.; Schaefer, H. F., III *Inorg. Chem.* **2006**, *45*, 10849.
- (49) Li, Q.-S.; Zhang, X.; Xie, Y.; King, R. B.; Schaefer, H. F. *J. Am. Chem. Soc.* **2007**, *129*, 3433.
- (50) Fortman, G. C.; Kegl, T.; Li, Q.-S.; Zhang, X.; Schaefer, H. F., III; Xie, Y.; King, R. B.; Telser, J.; Hoff, C. D. *J. Am. Chem. Soc.* **2007**, *129*, 14388.
- (51) Nolan, S. P.; de la Vega, R. L.; Mukerjee, S. K.; Hoff, C. D. *Inorg. Chem.* **1986**, *25*, 1160.
- (52) (a) Rieger, P. H. *Coord. Chem. Rev.* **1994**, *135/136* 203. (b) Hoobler, R. J.; Hutton, M. A.; Dillard, M. M.; Castellani, M. P.; Rheingold, A. L.; Rieger, A. L.; Rieger, P. H.; Richards, T. C.; Geiger, W. E. *Organometal.* **1993**, *12*, 116. (c) Fortier, S.; Baird, M. C.; Preston, K. F.; Morton, J. R.; Ziegler, T.; Jaeger, T. J.; Watkins, C.; MacNeil, J. H.; Watson, K. A.; Hensel, K.; Page Y. L.; Charland, J. P.; Williams, A. J. *J. Am. Chem. Soc.* **1991**, *113*, 542.

-
- (53) (a) Cooley, N. A.; Baird, M. C.; Morton, J. F.; Preston, K. F.; Page, Y. L. *J. Magn. Res.* **1988**, *76*, 325. (b) Morton, J. R.; Preston, K. F.; Cooley, N. A.; Baird, M. C.; Krusic, P. J.; McLain, S. L. *J. Chem. Soc. Faraday Trans. I* **1987**, *83*, 3535.
- (54) Connelly, N. G.; Orpen, A. G.; Rieger, A. L.; Rieger, P. H.; Scott, C. J.; Rosair, G. M. *Chem. Comm.* 1992, 1293.
- (55) MacNeil, J. H.; Watkins, W. C.; Baird, M. C.; Preston, K. F. *Organometal.* **1992**, *11*, 2761.
- (56) Nolan, S. P.; de la Vega, R. L.; Hoff, C. D. *Inorg. Chem.* **1986**, *25*, 4446.
- (57) Curtis, M. D. *Polyhedron* **1987**, *6*, 759.
- (58) Lewis, K. E.; Golden, D. M.; Smith, G. P. *J. Am. Chem. Soc.* **1984**, *106*, 3905.
- (59) (a) Ginley, D. S.; Bock, C. R.; Wrighton, M. S. *Inorg. Chim. Acta.* **1977**, *85*. (b) Abrahamson, H. B.; Palazotto, M. C.; Reichel, C. L.; Wrighton, M. S. *J. Am. Chem. Soc.* **1979**, *101*, 4123.
- (60) Carreón-Macedo, J. L.; Harvey, J. N. *J. Am. Chem. Soc.* **2004**, *126*, 5789.
- (61) Herrmann, W. A. *Angew. Chem. Int. Ed. Engl.* **1975**, *14*, 355.
- (62) Herrmann, W. A.; Biersack, H. *Chem. Ber.* **1977**, *110*, 896.
- (63) Kling, M. F.; Cahoon, J. F.; Glascoe, E. A.; Shanoski, J. E.; Harris, C. B. *J. Am. Chem. Soc.* **2004**, *126*, 11414.
- (64) (a) Church, S. P.; Grevels, F. W.; Hermann, H.; Schaffner, K. *Inorg. Chem.* **1984**, *23*, 3830. (b) Hoff, C. D. *Prog. Inorg. Chem.* **1992**, *40*, 503. (c) Strohmeier, W.; Hellmann, H. *Chem. Ber.* **1964**, *97*, 1877.
- (65) Capps, K. B.; Bauer, A.; Sukcharoenphon, K.; Hoff, C. D. *Inorg. Chem.* **1999**, *38*, 6206.
- (66) Kiss, G.; Nolan, S. P.; Hoff, C. D. *Inorg. Chim. Acta.* **1994**, *227*, 285.
- (67) (a) Capps, K. B.; Bauer, A.; Sukcharoenphon, K.; Hoff, C. D. *Inorg. Chem.* **1999**, *38*, 6206. (b) Johnson, A. R.; Baraldo, L. M.; Cherry, J. P. F.; Tsai, Y. C.;

-
- Cummins, C. C.; Kryatov, S. V.; Rybak Akimova, V.; Capps, K. B.; Hoff, C. D.; Haar, C. M.; Nolan, S. P. *J. Amer. Chem. Soc.* **2001**, *123*, 7271.
- (68) Herrmann, W. A. *Angew. Chem.* **1975**, *87*, 358. *Angew. Chem. Int. Ed. Engl.* **1975**, *14*, 355.
- (69) Nolan, S. P.; Lopez de la Vega, R.; Mukerjee, S. K.; Hoff, C. D. *Inorg. Chem.*, **1986**, *25*, 1160.
- (70) Dixon, D. A.; de Jong, W. A.; Peterson, K. A.; McMahon, T. B. *J. Phys. Chem. A.* **2005**, *109*, 4073.
- (71) (a) <http://webbook.nist.gov> (b) Foster, M. S.; Beauchamp, J. L. *J. Am. Chem. Soc.* **1972**, *94*, 2425. (c) Hassler, J. C.; Setser, D. W. *J. Am. Chem. Soc.* **1965**, *87*, 3793.
- (72) Seyferth, D.; Dow, A. W.; Menzel, H.; Flood, T. C. *J. Am. Chem. Soc.* **1968**, *90*, 1080.
- (73) Lappert, M. F.; Poland, J. S. *Chem. Comm.* **1969**, 1061.
- (74) Ingleson, M. J.; Pink, M.; Caulton, K. G. *J. Am. Chem. Soc.* **2006**, *128*, 4248.
- (75) Polse, J. L.; Kaplan, A. W.; Andersen, R. A.; Bergman, R. G. *J. Am. Chem. Soc.* **1998**, *120*, 6316.
- (76) (a) Ungvári, N.; Kégl, T.; Ungváry F. *J. Molec. Catal. A.*; **2004**, *219*, 7. (b) Tuba, R.; Ungváry, F. *J. Molec. Catal. A* **2003**, *203*, 59.
- (77) Fortman, G. C.; Isrow, D.; McDonough, J. E.; Schleyer, P. v. R.; Schaefer; H. F.; Scott, B.; Kubas, G. J.; Kégl, T.; Ungváry, F.; Hoff, C. D. *Organometallics* **2008**, *27*, 4873.
- (78) Jones, W. D.; Bergman, R. G. *J. Am. Chem. Soc.* **1979**, *101*, 5447.
- (79) Bullock, R. M. *Transition Metal Hydrides* Dedieu, A., Eds; VCH Publishers: New York, 1991, 263.
- (80) Hillhouse, G. L.; Haymore, B. L.; Herrmann, W. A. *Inorg. Chem.* **1979**, *18*, 2423.
- (81) Landrum, J. T.; Hoff, C. D. *J. Organometal. Chem.* **1985**, *282*, 215.

-
- (82) Zollinger, H. *Diazo Chemistry*; VCH Publishers: New York, **1995**, 2, 303.
- (83) (a) Baer, T.; Bauer, S. H. *J. Am. Chem. Soc.* **1970**, 92, 4773. (b) More O'Ferrall, R. A.; Kwok, W. K.; Miller, S. I. *J. Am. Chem. Soc.* **1964**, 86, 24, 5553.
- (84) Cahoon, J. F.; Kling, M. F.; Schmatz, S.; Harris, C. B. *J. Am. Chem. Soc.* **2005**, 127, 12555.
- (85) Franz, J. A.; Linehan, J. C.; Birnbaum, J. C.; Hicks, K. W.; Alnajjar, M. S. *J. Am. Chem. Soc.* **1999**, 121, 9824
- (86) Kristjansdottir, S. S.; Norton, J. R. In *Transition Metal Hydrides*; Dedieu, A., Eds., VCH Publishers, New York, 1991, 322.
- (87) Nolan, S. P.; Lopez de la Vega, R.; Mukerjee, S. L.; Gonzalez, A. A.; Zhang, K.; Hoff, C. D. *Polyhedron*, **1988**, 7, 1491.
- (88) Suzuki, E.; Komuro, T.; Okazaki, M. Tobita, H. *Organometallics*, **2007**, 26, 4379.
- (89) (a) Steele, W. V. *J. Chem. Thermodynamics* **1983**, 15, 595. (b) Davalos, J. Z.; Baer, T. *J. Phys. Chem. A* **2006**, 110, 8572. (c) see ref 71a.
- (90) (a) A computed value of 3.8 kcal/mol for addition of $\bullet\text{H}$ to N_2 : Gu, J.; Xie, Y.; Schaefer, H. F. III *J. Chem. Phys.*, **1998**, 108, 8029. (b) A computed value of 8 kcal/mol for addition of $\bullet\text{H}$ to N_2 : Matus, M. H.; Arduengo, A. J. III, Dixon, D. A. *J. Phys. Chem.*, **2006**, 110, 10116.
- (91) Woodcock, C.; Eisenberg, R. *Organometallics* **1985**, 4, 4.
- (92) (a) Bruns, W.; Hausen, H. D.; Kaim, W.; Schulz, A. *J. Organomet. Chem.* **1993**, 444, 121. (b) Bruns, W.; Kaim, W.; Waldhoer, E.; Krejčík M. *Inorg. Chem.* **1995**, 34, 663.
- (93) King, R. B. *Organometallic Synthesis*; Academic Press: New York, **1961**, 1, 165.
- (94) Kubas, G. J.; Kiss, G.; Hoff, C. D. *Organometallics*, **1991**, 10, 2870.
- (95) Wasserman, H. J.; Kubas, G. J.; Ryan, R. R. *J. Am. Chem. Soc.* **1986**, 108, 2294.
- (96) Ju, T. D.; Capps, K. B.; Roper, G. C.; Hoff, C. D. *Inorg. Chim. Acta.* **1998**, 270, 488.

-
- (97) SMART-NT 4, **1996**, Bruker AXS, Inc., Madison, Wisconsin 53719.
- (98) SAINT-NT 5.050, **1998**, Bruker AXS, Inc., Madison, Wisconsin 53719.
- (99) SADABS, first release, George Sheldrick, University of Göttingen, Germany.
- (100) SHELXTL Version 6.10, **2001**, Bruker AXS, Inc., Madison, Wisconsin 53719.
- (101) Kubas, G. J. In *Metal Dihydrogen and π -Bond Complexes* Kluwer Academic/Plenum Publishers, New York 2001.
- (102) Kubas, G. J. *J. Chem. Soc., Chem. Comm.* **1980**, 61.
- (103) (a) McDonough, J. E.; Weir, J. J.; Sukcharoenphon, K.; Hoff, C. D.; Kryatova, O. P.; Rybak-Akimova, E. V.; Scott, B. L.; Kubas, G. J.; Mendiratta, A.; Cummins, C. C. *J. Am. Chem. Soc.* **2006**, *128*, 10295. (b) Lang, R. F.; Ju, T. D.; Kiss, G.; Hoff, C. D.; Bryan, J. C.; Kubas, G. J. *J. Am. Chem. Soc.* **1994**, *116*, 7917. (c) Torres, L.; Moreno, M.; Lluch, J. M. *J. Phys. Chem. A* **2001**, *105*, 4676. (d) Rattan, G.; Khalsa, K.; Kubas, G. J.; Unkefer, C. J.; Van der Sluys, L. S.; Kubat-Martin, K. A. *J. Am. Chem. Soc.* **1990**, *112*, 3855. (e) see ref. 106h. (e) see ref 106i.
- (104) (a) Armor, J. N.; Taube, H. *J. Am. Chem. Soc.* **1970**, *92*, 6170; (b) Wishart, J. F.; Taube, H.; Breslauer, K. J.; Isied, S. S. *Inorg. Chem.* **1984**, *23*, 2997.
- (105) Cases, M.; Frenking, G.; Durán, M.; Solà, M. *Organometallics* **2002**, *21*, 4182.
- (106) (a) McDonough, J. E.; Mendiratta, A.; Curley, J. J.; Fortman, G. C.; Fantasia, S.; Cummins, C. C.; Rybak-Akimova, E. V.; Nolan, S. P.; Hoff, C. D. *Inorg. Chem.* **2008**, *47*, 2133. (b) Weir, J. J.; McDonough, J. E.; Fortman, G.; Isrow, D.; Hoff, C. D.; Scott, B.; Kubas, G. J. *Inorg. Chem.* **2007**, *46*, 652. (c) Lang, R. F.; Ju, T. D.; Kiss, B.; Hoff, C. D.; Bryan, J. C.; Kubas, G. J.; *J. Am. Chem. Soc.* **1994**, *116*, 7917. (d) Kubas, G. J.; Burns, C. J.; Khalsa, G. R. K.; Van Der Sluys, L. S.; Kiss, G.; Hoff, C. D. *Organometallics* **1992**, *11*, 3390. (e) Zhang, K.; Gonzalez, A. A.; Mukerjee, S. L.; Chou, S. J.; Hoff, C. D.; Kubat-Martin, K. A.; Barnhart, D.; Kubas, G. J. *J. Am. Chem. Soc.* **1991**, *113*, 9170. (f) Gonzalez, A. A.; Hoff, C. D. *Inorg. Chem.* **1989**; *28*, 4285. (g) Gonzalez, A. A.; Hoff, C. D. *Inorg. Chem.* **1989**; *28*, 4295. (h) Gonzalez, A. A.; Zhang, K.; Nolan, S. P.; de la Vega, R. L.; Mukerjee, S. L.; Hoff, C. D.; Kubas, G. J. *Organometallics*, **1988**, *7*, 2429. (i) Gonzalez, A. A.; Mukerjee, S. L.; Chou, S. L.; Kai, Z.; Hoff, C. D. *J. Am. Chem. Soc.* **1988**, *110*, 4419.

-
- (107) Kubas, G. J.; Burns, C. J.; Khalsa, G. R. J.; Van Der Sluys, L. S.; Kiss, G.; Hoff, C. D. *Organomet.* **1992**, *11*, 3390.
- (108) Wasserman, H. J.; Kubas, G. J.; Ryan, R. R. *J. Am. Chem. Soc.* **1986**, *108*, 2294.
- (109) Afeefy, H. Y.; Liebman, J. F.; Stein, S. E. *Neutral Thermochemical Data in NIST Chemistry WebBook, NIST Standard Reference Database Number 69*, Linstrom, P.J.; Mallard, W.G. Eds. June 2005, National Institute of Standards and Technology, Gaithersburg MD, 20899 (<http://webbook.nist.gov>).
- (110) Gronert S.; Keeffe, J. R. *J. Org. Chem.* **2007**, *72*, 6343.
- (111) Hunter, E.P.; Lias, S.G. *J. Phys. Chem. Ref. Data* **1998**, *27*, 413.
- (112) Cotton, F. A. In *Chemical Applications of Group Theory* Wiley and Sons Inc., New York, 1990.
- (113) Clarke, R. E.; Ford, P. C. *Inorg. Chem.* **1970**, *9*, 227.
- (114) Ford, P. C.; Rudd, D. F. P.; Gaunder, R.; Taube, H. *J. Am. Chem. Soc.* **1968**, *90*, 1187.
- (115) Gibbons, C. S.; Trotter, J. *Can. J. Chem.* **1973**, *51*, 87.
- (116) Britton, D. *Acta Crystallogr., Sect.E* **2004**, *60*, 2189.
- (117) Butts, M.D.; Bryan, J. c.; Lou, X.-L.; Kubas, G. J. *Inorg. Chem.* **1997**, *36*, 3341.
- (118) Britton, D. *Cryst. Struct. Commun.* **1979**, *8*, 667.
- (119) Darensbourg, D. J.; Zalewski, D. J.; Plepys, C.; Campana, C. *Inorg. Chem.* **1987**, *26*, 3727.
- (120) Jefford, V. J.; Schriver, M. J.; Zaworotko, M.J. *Can. J. Chem.* **1996**, *74*, 107.
- (121) Hamilton, E. J. M.; Smith, D. E.; Welch, A. J. *Acta Crystallogr., Sect.C: Cryst. Struct. Commun.* **1987**, *43*, 1214.
- (122) Shyu, S.-G.; Singh, R.; Su, C.-J; Lin, K.-J. *Eur. J. Inorg. Chem.* **2002**, 1343.
- (123) Knorr, M.; Jourdain, I.; Lentz, D.; Willemsen, S.; Strohmam, C. *J. Organomet. Chem.* **2003**, *684*, 216.

-
- (124) Imhof, W.; Halbauer, K.; Donnecke, D.; Gorls, H. *Acta Crystallogr., Sect. E: Struct. Rep. Online* **2006**, *62*, m462.
- (125) Ohnet, M. -N.; Spasojevic-de Brie, A.; Dao, N. Q.; Schweiss, P.; Braden, M.; Fischer, H.; Reindl, D.; *J. Chem. Soc., Dalton Trans.* **1995**, 665.
- (126) Martins, L. M. R. D. S.; Fraústo da Silva, J. J. R.; Pombeiro, A. J. L.; Henderson, R. A.; Evans, D. J.; Benetollo, F.; Bombieri, G.; Michelin, R. A. *Inorg. Chim. Acta* **1999**, *291*, 39.
- (127) Cunha, S. M. P. R. M.; Guedes da Silva, M. F. C.; Pombeiro, A. J. L. *Inorg. Chem.* **2003**, *42*, 2157.
- (128) (a) Khaikin, L. S.; Vilkov, L. V.; Andruskaya, L. G.; Zenkin, A. A. *J. Mol. Struct.* **1975**, *29*, 171. (b) Li, Y. S.; Durig, J. R. *J. Mol. Struct.* **1973**, *16*, 433.
- (129) a) Willermann, M.; Mulcahy, C.; Sigel, R. K. O.; Morell Cerdà, M; Freisinger, E.; Sanz Miguel, P. J.; Roitzsch, M.; Lippert, B. *Inorg. Chem.* **2006**, *45*, 2093; b) Jude, H.; Krause Bauer, J. A.; Connick, W. B. *Inorg. Chem.* **2005**, *44*, 1211.
- (130) Lavalle, D. K.; Fleischer, E. B. *J. Am. Chem. Soc.* **1972**, *94*, 2583.
- (131) Stringfield, T. W.; Chen, Y.; Shepherd, R. E. *Inorg. Chim. Acta* **1999**, *285*, 157.
- (132) Bruns, W.; Hausen, H.-D.; Kaim, W.; Schulz, A. *J. Organomet. Chem.* **1993**, *444*, 12.
- (133) Tutt, L.; Zink, Z. I. *J. Am. Chem. Soc.* **1986**, *108*, 5830.
- (134) Kaiser-Morris, E.; Cousson, A.; Paulus, W.; Fillaux, F. *Acta Crystallogr., Sect. E* **2001**, *57*, 01116.
- (135) Catalán, J.; Díaz, C.; García-Blanco, F. *Org. Biomol. Chem.* **2003**, *1*, 575.
- (136) Marcus, Y.; Migron, Y. *J. Phys. Chem.* **1991**, *95*, 400.
- (137) Allen, A. D.; Bottomley, F.; Harris, R. O.; Reinsalu, V. P.; Senoff, C. V. *J. Am. Chem. Soc.* **1967**, *89*, 5595.

-
- (138) (a) Kubas, G. J. *Organomet. Synth.* **1986**, 3, 264. (b) Khaha, G. R. K.; Kubas, G. J.; Unkefer, C. J.; Van Der Sluys, L. S.; Kubat-Martin, K. A. *J. Am. Chem. Soc.* **1990**, 112, 3866.
- (139) Sasaki, T.; Nakanishi, A.; Ohno, M. *J. Org. Chem.* **1981**, 46, 5445.
- (140) Ju, T. D.; Capps, K. B.; Roper, G. C.; Hoff, C. D. *Inorg. Chim. Acta.* **1998**, 270, 488.
- (141) Apex2 Version 2.2-0 and SAINT+ Version 7.46A; Bruker Analytical X-ray System, Inc., Madison, Wisconsin, USA, 2007.
- (142) Sheldrick, G. M. SHELXTL Version 6.1; Bruker Analytical X-ray Systems, Inc., Madison, Wisconsin, USA, 2000.
- (143) A. Patrick; Fujita, E.; Muckerman, J. T.; Scott, B.; Fortman, G. C.; Temprado, M.; Xiaochen, C.; Captain, B.; Isrow, D.; Weir, J. J.; McDonough, E.; Hoff, C. D. *manuscript in preparation*.
- (144) (a) Jones, M. Jr.; Moss, R. A. In *Reactive Intermediate Chemistry*; Moss, R. A.; Platz, M. S.; Jones, M., Jr., Eds.; John Wiley & Sons, Inc. New York, 2005; p. 273. (b) Platz, M. S. In *Reactive Intermediate Chemistry*; Moss, R. A.; Platz, M. S.; Jones, M., Eds; John Wiley & Sons, Inc. New York, 2005; p. 501.
- (145) Hillhouse, G. L.; Goeden, G.V.; Haymore, B. L. *Inorg. Chem.* **1982**, 21, 2064.
- (146) Danopoulos, A. A.; Hay-Motherwell, R. S.; Wilkinson, G.; Cafferkey, S. M.; Sweet, T. K. N.; Hursthouse, M. B. *J. Chem. Soc., Dalton Trans.* **1997**, 3177.
- (147) Walstrom, A. N.; Fullmer, B. C.; Fan, H.; Pink, M.; Buschhorn, D. T.; Caulton, K. G. *Inorg. Chem.* **2008**, 47, 9002.
- (148) Fortman, G. F.; Captain, B.; Hoff, C.D. *Organometallics* **Manuscript accepted Jan 2009**.
- (149) (a) Albright, T. A.; Freeman, W. J.; Schweizer, E. E. *J. Org. Chem.* 1976, 41, 2716. (b) Leffler, J. E.; Temple, R. D. *J. Am. Chem. Soc.* 1967, 89, 5235.